THE UNIVERSITY *of* EDINBURGH

Instrumentation Development for Neutron Scattering at High Pressure

Junwei Fang

A thesis submitted in fulfilment of the requirements

for the degree of Doctor of Philosophy

to the

School of Engineering

University of Edinburgh

2012

Declaration

This thesis has been composed by myself and it has not been submitted in any previous application for a degree. The work reported within was executed by me, unless otherwise stated.

Junwei Fang

September 2012

Acknowledgements

In the first instance, I would like to express my sincere gratitude to Dr. Konstantin Kamenev who has supervised my work over the last four years. In this period, he has always been willing to devote time to me and offer guidance and support. Without these my PhD project and this thesis would not have been possible. Meanwhile, I also would like to thank him for his encouragement and patience in leading me through the technical difficulty in my project as well as introducing me to the field of high pressure science. I had a happy time working with him.

I also would like to thank my second supervisor Dr. John Loveday who is a knowledgeable scientist. He was very supportive of my work and kindly offered detailed answers when I was in doubt about the questions related to crystallography.

A special thank-you goes to Dr. Craig Bull who helped me with *in situ* testing of the rotator and with the advice on writing from publications to a variety of reports and technical notes. It is beyond doubt that his efforts were one of the key factors that drove me to learn how to do science. I also wish to thank Professor Richard Nelmes. Kindly he offered his precious time to support my academic study and research when I needed it most. I also would like to extend my gratitude to Dr. Hayrullo Hamidov who participated in the preliminary testing of the rotator.

In addition, over the years I was helped and supported by many people who offered assistance on different occasions and who my many thanks go to - Dr. Stefan Klotz, Dr. Mathias Gutmann, Dr. Geoffrey Bromiley, Mr. John Allibon and Mr. John Archer. While I was studying in the UK, my parents, uncle and brother have supported me throughout the whole period both mentally and financially. I wish I would be able to spend more time with them in future.

I am also grateful to my friends in CSEC. We are a very good team and provide full support for each other. Among them are Mr. Weiwei Wang, Mr. Xiao Wang, Dr. Artur Bocian, Dr. Suresh Narayanaswamy and Mr. Gaétan Giriat. The discussions and exchange of knowledge during our regular group coffee breaks are something I am going to miss in future.

I would also like to thank the technicians from the Physics workshop who have been very helpful through the manufacturing and testing stages of the work on the rotator. The time I spent with them was very enjoyable both professionally and personally. I especially wish to thank Mr. Paul Aitken and Mr. Andrew Downie for offering their professional expertise.

I am most grateful to my family. My parents are always very supportive and encourage me to do my best in the process. And finally, I love and thank my dear wife Linxi. We met, fell in love and got married while both of us were studying at the University. I would have never got this far without her.

Abstract

Neutron scattering at extremes of pressure is a powerful tool for studying the response of structural and magnetic properties of materials on microscopic level to applied stresses. However, experimental neutron studies require a relatively large sample volume, which makes it necessary to use rather large presses. One of the most commonly used high-pressure devices in neutron diffraction experiments is the Paris-Edinburgh (P-E) press. This compact hydraulic press has been successfully used at various neutron facilities across the world for over 20 years. However, there are some limitations imposed by the design of the press and this project addressed two of them.

The **first objective** of this research was to solve the problem of the spatial restriction on the scattered beam imposed by the tie-rods of the P-E press which results in the limited access to the reciprocal space of a single-crystalline sample. In order to overcome this challenge a rotating device has been designed and built to work with the existing P-E press mainframe. The purpose of the device is to rotate the anvils at a high load in a controlled fashion so that neutron diffraction data can be collected from the sample at particular angles. A number of technical challenges had to be overcome in the design process. One of the problems was caused by the significant friction in the commercially available thrust roller bearings at loads above 25 tonnes. To resolve this issue a set of custom-designed hydraulic bearings has been developed. In these bearings a thin layer of oil separates the two parts that can rotate with respect to each other.

The rotator is based on the mainframe of the existing V4 type of the P-E press and is given the name RV4 for 'rotating V4'. It has the central structure that incorporates an extended main-frame and rotational support components, and the side structure supporting the power supply and the gearing mechanism. The effective maximum torque that can be applied to rotate the anvils is 245 Nm. The RV4 has been shown to rotate at loads of up to 100 tonnes and has been used in experiments at the Institut Laue-Langevin (France) and ISIS spallation source (UK).

The **second objective** of this project was to look into the factors which limit the maximum pressure that can be achieved when the large-volume double-toroidal anvils are used with the Paris-Edinburgh press. The experimental data indicates that the anvils fail consistently at sample pressures of around 30 GPa, but the mode of failure was unknown. The behaviors of the anvils, the sample and the gasket that surrounds it have been modeled at high loads using finite element analysis (FEA). The comprehensive modeling was focused on calculating various stresses present in the anvil assemblies and was based on the available materials' properties and experimental deformation *vs.* load data. The model was shown to correlate well with available data on experimental pressure achieved as a function of the applied load.

The FEA analysis has shown that of all the stresses present in the anvils it is the tensile stress that leads to its failure. The location of the critical stress point at which the failure occurs has also been found. The validated model has then been used to indicate the possible avenues for improvements that can be followed in order to enhance the performance of the anvils and the gaskets. The simulation performed using the improved geometry shows the possibility of achieving pressures in excess of 30 GPa on a large-volume sample.

Contents

Chapter 1

Introduction

Over the past 50 years high-pressure crystallography has evolved as a powerful experimental technique for probing structure and dynamics of materials. To a large extent this has been a result of a number of instrumentation developments including high-pressure cells, large-scale diffraction facilities and measurement techniques. It is now possible to apply and control pressure delicately on a variety of samples (either in the form of powder or single crystal), to collect data from small sample volumes in reasonable time and analyse the data so as to determine the structure of a material.

Meanwhile there are still many technical challenges. In the case of neutron-diffraction experiments on large-volume samples, my PhD project aims to achieve (i) greater efficiency and (ii) higher pressure in these measurements. The former focuses on increasing the accessible reciprocal space in order to reduce the time it takes to complete a full data collection. The latter relies on the mechanical performance analysis and improvement of an anvil assembly to increase the pressure attainable.

The chapter introduces the subject of the PhD thesis – high-pressure crystallography, in particular neutron-diffraction experiments on large-volume single-crystal samples at large-scale facilities. Also it provides a brief outline of the technical challenges the PhD project intends to address.

1.1 High-Pressure Crystallography

1.1.1 Crystallography

Crystallography is the branch of science that investigates the structure of matter in the ordered solid state. Crystallographic studies reveal the crystal lattices (Figure 1.1), the three-dimensional arrangement of the smallest entities of matter – atoms – in molecules from minerals to complex proteins. In Greek, 'crystallon' means 'cold drop' or 'frozen drop' and 'grapho' means 'write'; however, the meaning of 'crystallography' nowadays extends to all solids and even liquids.

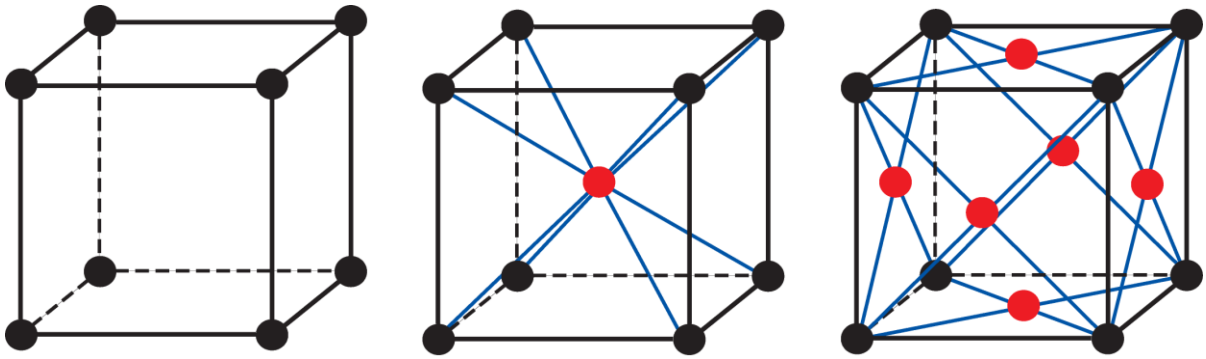

Figure 1.1 Three typical types of atomic arrangements in a matter. (a) Primitive cubic lattice; (b) Bcc cubic lattice; (c) Fcc cubic lattice.

Most of the crystallographic studies deal with solid samples with some degree of transparency to the electromagnetic radiation such as x-rays, electrons and neutrons. By passing an incident beam of the radiation through the crystal it is possible to obtain diffraction patterns which allow crystallographers to locate the individual entities in space that make up the crystal.

It is widely accepted that the crystal structures of a material very often explains its physical, chemical, biological and even pharmaceutical properties. Crystallography is thus essential to advances in the applied sciences & technology and the developments in all types of materials, including metals and alloys, ceramics, glasses and polymers. The most exciting application of crystallography today is helping to understand how life works at the molecular

level, which is leading to discoveries of new drugs for treating diseases. From 1901 to 2003, 21 Nobel prizes were awarded for research in crystallography.

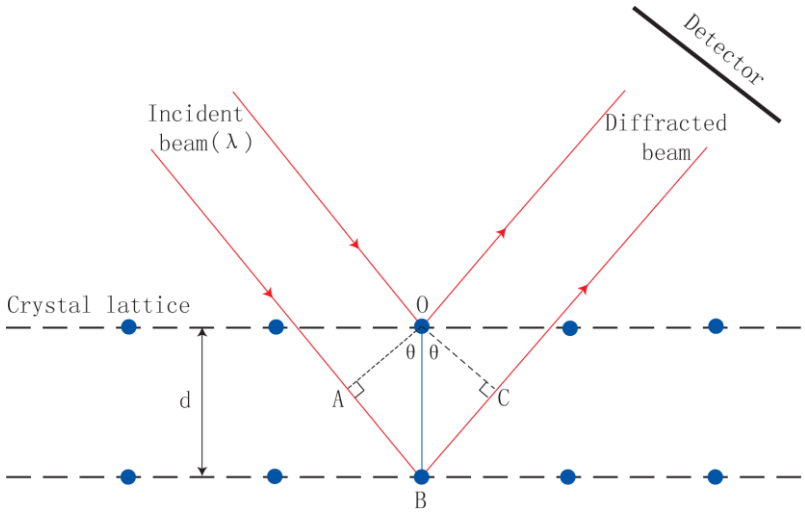

Figure 1.2 Illustration of an incident beam (red arrows) being scattered by two planes of crystal lattice and the diffracted beam being collected by the detector. θ is the diffraction angle; λ is the wavelength of the beam; d is the spacing of the crystal.

To explain how the atomic structure of crystals is revealed in a diffraction experiment, a single model with two lattice planes and an incident beam of single spectrum is illustrated in Figure 1.2. As the monochromatic beam is scattered by the crystal lattice, a detector covering a certain area in space is positioned to record the interference patterns of the diffracted beam. Based on the observed diffraction angle, the geometric information related to the crystal lattice is calculated through Bragg's Law which provides the condition for constructive interference:

$$n\lambda = 2d\ sin\theta \qquad (1.1)$$

where λ is the wavelength of the radiation, θ is the diffraction angle, n is the diffraction order (n = 1, 2, 3…) and d is the distance between atomic layers in the crystal (lattice plane).

When the crystal structure of the sample and the wave properties of the incident beam become more complicated, e.g. if the sample is polycrystalline or if the neutrons of different wavelengths are combined into the incident beam, sophisticated computing techniques may be required to determine the lattice parameters. Refinement software available to crystallographers simulates the physical phenomenon based on the existing knowledge or estimates of these parameters and generates a diffraction pattern. This simulation pattern, when compared with the observation patterns obtained in experiments, can be calibrated and then adjusted to get more accurate lattice parameters.

1.1.2 High Pressure

The crystal structure of matter is a variable, dependent on the experimental conditions including temperature, pressure and other thermodynamic parameters, such as applied magnetic or electrical field, etc.

Up to 2007, only 100 out of 404800 organic and organometallic structures deposited in the Cambridge Crystallographic Database Centre (CCDC) were determined at elevated pressure [1]. Although since then a larger number of elements, minerals and inorganic compounds were studied under pressure, a majority of known materials are yet to be investigated and their properties at extreme conditions are yet to be understood.

1.1.2.1 High Pressure as a Tool

While most studies are performed at ambient conditions or using temperature as a variable, the application of high pressure provides another thermodynamic dimension to crystal-structure studies. The high-pressure variable can induce significant changes in the structure of solids, and these could result in dramatic changes in properties. Scientists are thus equipped with a powerful tool for tuning in a controllable manner the volume of the sample and, therefore, the properties of the sample. The interesting effects of high pressure can be found in various areas of science including the following:

- Geosciences and astrophysics

  It is natural that geoscientists and astrophysicists are among those most interested in matter under pressure as a vast amount of the matter in the universe is at extreme conditions – high pressure and high temperature. For instance, the pressure at the centre of a neutron star is estimated to be 10^{26} GPa.

Inside the Earth (Figure 1.3), the pressure at the bottom of the crust is 0.5 GPa, that of the mantle is 135.2 GPa, that of the outer core is 328.1 GPa and that of the inner core is up to 361.7 GPa [2]. Geoscientists rely on high-pressure studies of the Earth's internal matters to extend the understanding of the formation of the natural minerals and carbon fuels, volcanoes and earthquakes, the continent and ocean, and the Earth itself.

For instance, a large amount of water on the Earth – possibly several times the oceans' mass – exists as H_2O or OH^- in water-containing minerals of the crust and upper mantle. Most of them are at pressures above 10 GPa [3]. It is very important to study the high-pressure behaviour of hydrogen and other light elements in these dense media, for instance the pressure dependence of the hydrogen bond length. It provides insights to how to predict physicochemical properties of hydrogenous compounds at extreme pressures and also provides direct determination of crucial parameters used in current models of the planetary interiors [4].

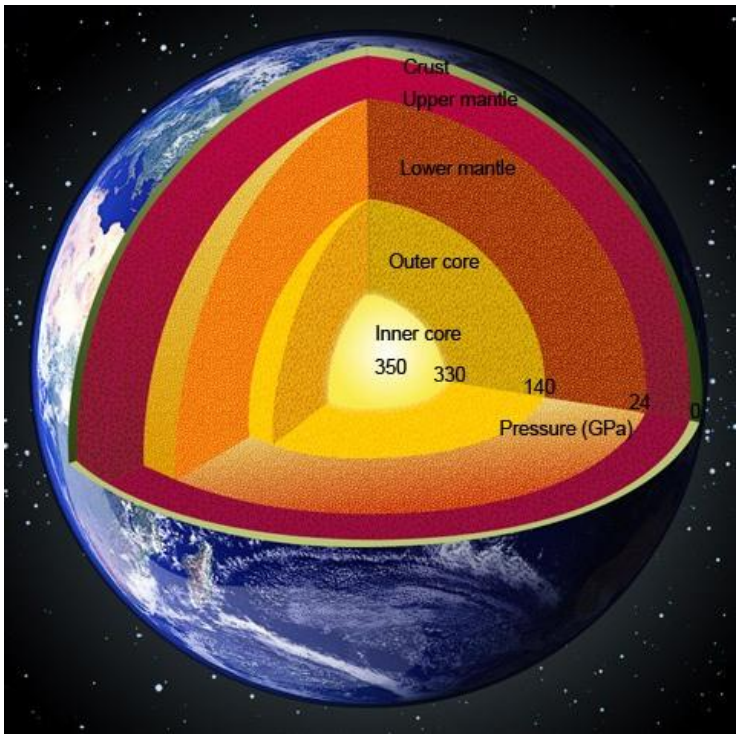

Figure 1.3 Illustration of the pressure range inside the Earth (from [5]). The pressure increases from nearly 0 GPa to 350 GPa as the depth increases from the crust to the mantle, and to the core of the earth.

- Chemistry, material science and engineering

  High-pressure synthesis and crystallography is a powerful method for the preparation and investigation of novel materials, for instance with high elastic modulus and hardness, or sometimes with interesting thermal, optoelectronic, semiconducting, magnetic, or superconducting properties.

  A recent example of the technologically important high-pressure synthesis is the creation at 24 GPa and about 2200 K of the diamond-like B-C (Boron-Carbide) phase with the highest boron content ever achieved [6]. The synthesized phase has low compressibility (bulk modulus of 335 GPa) and conductivity, and exhibits extreme Vickers hardness (71 GPa), fracture toughness (9.5 MPa $m^{1/2}$), and high thermal stability (up to 1900 K). This is unusual for superhard materials and makes B-C exceptionally superabrasive and also a promising material for the application in high-temperature electronics.

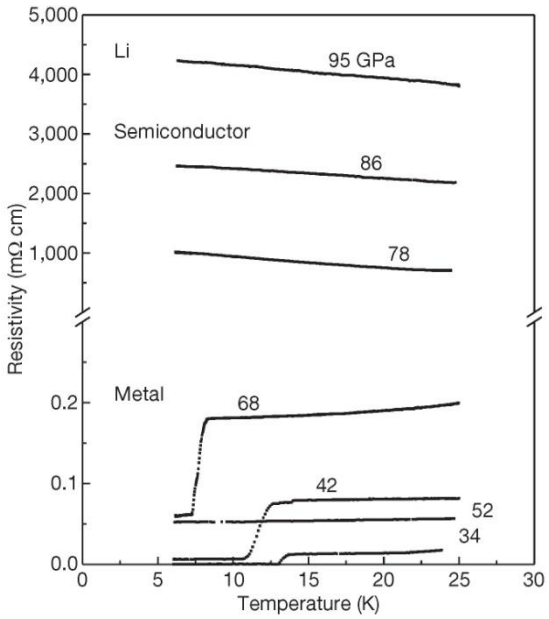

Figure 1.4 The resistance-temperature dependence for lithium at various pressure values (from [6]). This is a direct observation of a pressure-induced metal-to-semiconductor transition in lithium.

Pressure can be used to induce superconductivity in some materials [7, 8] and suppress it in others [9, 10]. For example, below 68 GPa lithium shows metallic character and indicates superconducting transitions (at pressure of 34 GPa at 13 K, 42 GPa at 11-12 K and 68 GPa at 7 K-8 K), it becomes semiconductor for pressures of 78 GPa and above [6] (Figure 1.4).

- Biology

High-pressure crystallography can now be applied to a variety of biological systems [11, 12]. Historically the pioneering work in high-pressure protein research was that of Bridgman who observed that a pressure of ~100 MPa would make egg's white look similar but not identical to that of a cooked egg.

Although more than half (approximately 62%) of the total volume of biosphere is at a depth in excess of 1000 m and subjected to a pressure higher than 10 MPa, biological systems are very vulnerable to high pressure [11, 13]. For this reason, it is an interesting discovery that some organisms such as bacteria not only survive but thrive in the deepest parts of the ocean where the pressure is as high as 100 MPa [14].

In addition, high-pressure treatment is used in food processing industry (Figure 1.5). High pressure induced changes in the taste or the flavour of food ingredients can be beneficial to the food industry [15]. Although freezing has long been regarded as a way of keeping food fresh, high-pressure 'pascalisation' is found to be an effective alternative.

Figure 1.5 Various food products manufactured with high-pressure processing (from [16]).

1.1.2.2 High Pressure Generation

Pressure is the thermodynamic parameter that processes probably the greatest range of magnitude – 60 orders[1] from the highest vacuum in space to the pressure in the centre of a neutron star. Today, the maximum static pressure obtainable in the laboratory is over 300 GPa while dynamic pressures as high as 10^{10} GPa has been created in thermonuclear explosions [17].

There are two methods of generating high pressure: static and dynamic. Shown in Figures 1.6 and 1.7 are two examples of generating high pressure in the laboratory. Figure 1.6 shows the setup and principle of the diamond anvil cell (DAC) [18] – a typical static pressure generation technique. Two diamonds are aligned to mate each other on the flat tip culet. A small sample (in red) and a gasket ring are inserted in between the anvils. When axial load is applied to the bottom surface of the diamond table, the sample enclosed by the diamonds and the gasket is compressed.

[1]Throughout this thesis, two units of pressure are used: GPa (10^9 Pascal) and MPa (10^6 Pascal). Another common unit in the high pressure field is bar (or kilobar/kbar or megabar). 1 bar = 1 atm (1 atmosphere = 0.1MPa), 1 kbar = 0.1GPa and 1 megabar = 100 GPa.

In the dynamic method, lasers, gas guns, and other dynamic high-pressure testing methods launch an instantaneous shock into a target generating high pressure on it. Figure 1.7 shows the setup and principle of the light gas gun [19] which works on the same principle as a spring piston air-gun, relying on the projectile impact to produce dynamic high pressure on a target specimen. When the gas in the left-hand chamber is heated very quickly and becomes hot in a short period of time, the piston in the pump tube slides toward the right hand side and pushes the hydrogen gas in the same direction. Because the barrel has a much smaller diameter than the pump tube, the impactor accelerates in the barrel to a very high speed and hits the target, creating an extremely high pressure lasting a very small fraction of time. During the short event, physical and chemical phenomena are observed.

The most popular technique to generate high-pressure shock nowadays is by using a laser which provides higher energy intensity and better control of the shocks. One problem with this method is when hit by the laser beam the target is rapidly heated and caused to melt. A new technique called laser-driven ramp compression hit the material with a carefully tailored laser shot [20]. Laser-driven ramping can achieve states of high compression while simultaneously keeping the target material relatively cool so scientists can examine the material under high pressures. The "loading" time of the laser ramp compression is just a few nanoseconds. To date, laser-ramp-compression experiments have achieved pressures up to 1,400 GPa.

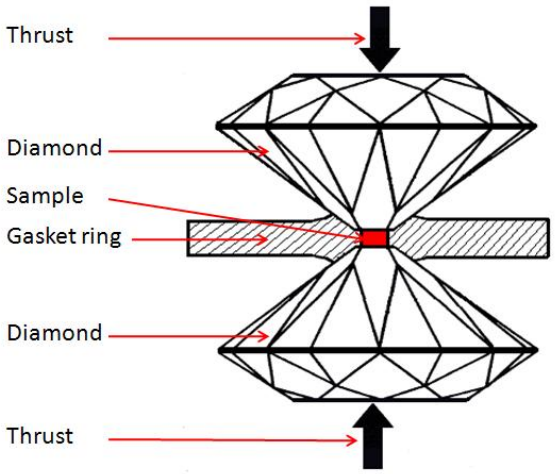

Figure 1.6 An example of static pressure generation – diamond anvil cell (DAC) (after [18]).The sample (in red) is surrounded by the gasket ring and placed between two mating diamonds. Large axial loads are applied to the bottom of the diamonds to compress the sample.

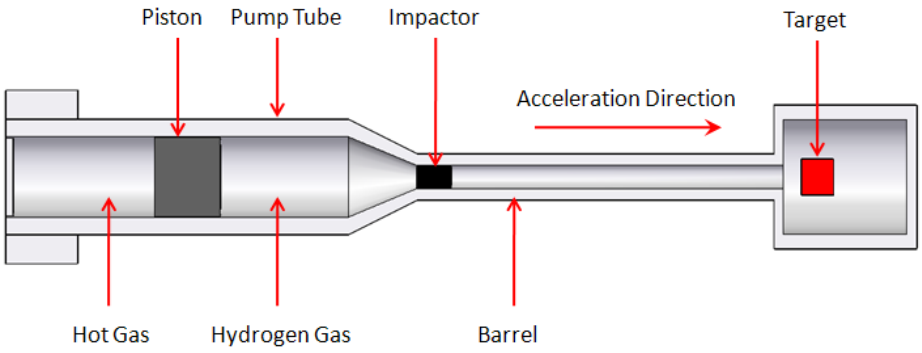

Figure 1.7 An example of dynamic pressure generation – light gas gun (after [19]). The impactor and the target are normally very small compared to the piston. Hot gas is created in a short period and expands to accelerate the piston and then the impactor.

1.2 Neutron Diffraction

Crystallographic study is an analysis of the diffraction patterns of a sample that is exposed to an incident beam, such as x-rays, electrons or neutrons. Being different types of waves, these three types of radiation are suitable as probes to the interior for certain types of materials. Neutron diffraction has the following characteristics:

- Neutron beam has a wavelength range between 0.1 Å and 1000 Å. Because of this, it is used to probe a wide range of materials - both atomic and molecular structures.

- Neutrons are scattered by the atomic nuclei through the strong nuclear forces while x-rays interact with the spatial distribution of the valence electrons and electrons as negatively charged particles interact with matter through the Coulomb forces.

- The magnetic moment of neutrons is non-zero, which means that they can be scattered by magnetic fields.

As a consequence of its unique way of interaction with the sample materials, neutron diffraction has several advantages compared to x-rays and electrons. Some of the advantages are listed below:

- Neutron diffraction is capable of precisely locating protons and light atoms (low Z), while heavier ones are at presence. To date, neutron diffraction is the most successful technique for determining the structure of hydrogen bonds.

- It can be used to distinguish neighbouring elements in the periodic table, when the elements have a similar number of electrons, but sufficiently different scattering cross sections for neutrons.

- Isotopes of the same element have significantly different scattering lengths for neutrons. Neutron scattering techniques thus can be used, together with isotopic substitution technique for marking up different parts in material structures.

- Neutron beams are electrically-neutral and thus non-destructive even when they penetrate deep into the matter. They are therefore ideal for biological materials and medical application.

- Neutrons have a magnetic dipole moment and thus are sensitive to magnetic fields. For this reason, neutrons going through materials with unpaired electrons which generate magnetic fields will indicate the structure of the materials.

The Group of Extreme Condition Physics at the Centre for Science at Extreme Conditions (CSEC) [17], University of Edinburgh, led by Prof. Richard Nelmes, is currently tackling a number of interesting and exciting areas of high-pressure science across its research programs. In a majority of the research, neutron diffraction is used as the main technique [17].

- Ices (H_2O, NH_3 and CH_4 etc.)

  These are model systems for studies of hydrogen bonding as a function of bond strength and geometry. It is hoped that the research will provide fundamental insight into the transition between amorphous forms of H_2O ice and the structural changes in very dense water at high pressure-temperature (P-T).

- Diatomic molecules (N_2, H_2 etc) and hydrocarbons

  The studies of the interplay in molecular solid under high pressure can reveal information needed for classical molecular modelling, e.g. by modelling the high-pressure behaviour of the simplest diatomic system – H_2.

Although the neutron diffraction can provide significant complementary information in many structural problems, its application is not as wide as x-ray diffraction mainly due to the limited access to neutron sources around the world. Two large neutron sources located in Europe are ISIS (Rutherford Appleton Laboratory, Oxfordshire, UK) [21] and the Institut Laue-Langevin (ILL, Grenoble, France) [22]. ISIS and ILL facilities are used for research areas such as energy, nanotechnology, materials processing, drug design and pharmaceuticals, bio-technology and green technology for a clean environment.

ISIS is a spallation source producing pulsed neutrons and muons with the time-of-flight (ToF) techniques being used [21] while the reactor at ILL delivers monochromatic neutrons [22]. They are both among the most powerful neutron sources, with very intense beams of neutrons and a suite of high performance instruments. The two diffractometers used in this PhD project are among these instruments and their specifications are described in detail in Chapter 2.

The main challenge in neutron scattering experiments is the low intensity of the neutron beam. Neutron radiation sources have low brightness – both continuous beam reactors and spallation sources are intrinsically much weaker than synchrotrons or even the x-rays from a conventional laboratory x-ray source. Besides, the scattering of neutrons by most materials is very low because neutrons scatter from the nucleus which is much smaller than the electron cloud. In order to obtain precise structural refinement of atomic positions and thermal motion and collect the diffraction patterns in a reasonable amount of time, samples of large-volume are required. Usually the samples to be studied using neutron-diffraction techniques are a few mm^3 if it is single crystal and a few cm^3 if it is powder [1, 4].

This poses a challenge for high-pressure neutron scattering – when the sample volume is large the pressure that can be generated on it is not as high as that on a smaller sample. To date, high pressure of about 30 GPa can be produced on large-volume sample in neutron scattering experiments using sintered diamond toroidal anvils [4] – this pressure is less than 1/10 of that using x-ray and DAC [23, 24].

1.3 Powder and Single-Crystal Diffraction

Another important aspect of any diffraction experiment is the type of the sample – poly-crystalline (powder) or single crystal.

In powder diffraction, an x-ray, neutron, or electron beam is pointed at powder samples to generate a diffraction pattern for structural characterization of materials. Figure 1.8a is an example of the powder diffraction rings produced in an x-ray experiment. In practice, a powder sample is easy to prepare in laboratory conditions. Powder is relatively robust compared to single-crystal sample at high pressure, requiring less control of its conditions during the experiments. For these reasons, it is widely used around the world [1, 4].

X-ray diffraction on powder samples is a popular characterisation technique that can be done not only at synchrotrons but also in laboratory conditions [23]. At synchrotrons, very intense x-ray beams can be collimated to a few micrometres thus allowing efficient and quick experiments to be performed on a small sample as well as provide for reduced background noise in the measurements. Some arrangements, e.g. using very short wavelengths, and extending the distance between the sample and the detector, can also be made to improve the resolution and increase the completeness of the accessible structural data.

Although, powder diffraction has been dominant in high-pressure structural analysis in the past several decades, it has reached the stage at which its natural limitation as a one-dimensional measurement becomes obvious and critical to many studies [1]. The overlapping Bragg peaks can be so close that they are not distinguishable and recognisable. This is more obvious in the lattice with low symmetry and/or small d-spacings but can be made even worse by the background noise.

In this case the intense diffracted beam in single-crystal diffraction becomes valuable as the diffraction pattern gives extra information of the lattice structure. Single-crystal diffraction produces sharp diffraction spots on a two-dimensional position-sensitive detector. Much more intense diffracted beams are obtained compared to that produced by powdered sample which is ‘isotropic’ and scatters the diffracted neutron beam over a greater area. Figure 1.8b gives the diffraction patterns obtained by scattering neutrons on single-crystal samples.

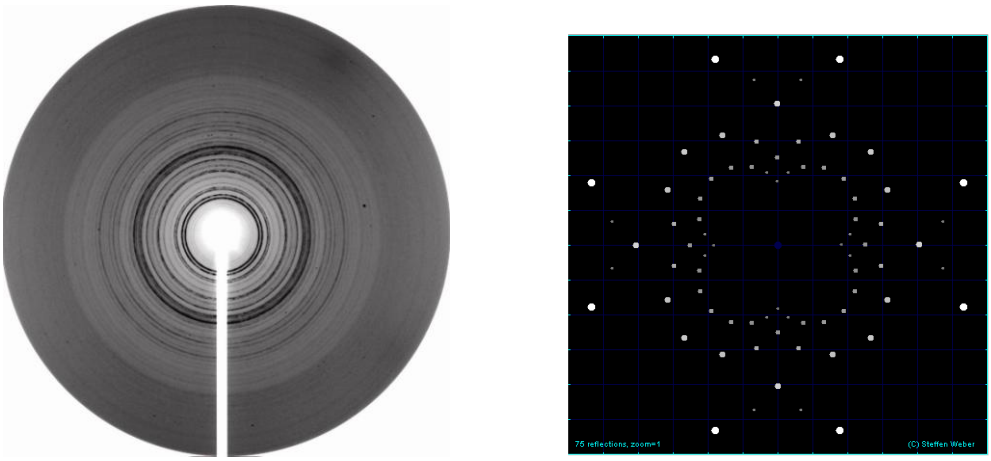

(a) *(b)*

Figure 1.8 Examples of diffraction patterns produced by powder sample and single-crystal sample.

(a): Powder diffraction image obtained for the ζ-form of CL-20 (Formula: $C_6H_6N_{12}O_{12}$) at a pressure of 1.4 GPa (from [25]).

(b): Diffraction pattern of single crystals with primitive lattice in simulation [26].

The application of single-crystal diffraction in high-pressure research for a long time has been hindered by a few technical difficulties. The primary one is maintaining hydrostatic conditions in the sample at high pressure. Single crystals are very fragile and can be damaged or destroyed upon pressure change or phase transitions. For instance, shear stress that occurs at high pressure can easily break the crystal. Another difficulty is associated with the growth of single crystal. The crystal sample is normally prepared in advance and then loaded into the cell. Now it is also possible to grow crystals *in situ* [27]. Either method requires very delicate control of the reaction conditions to grow large crystals.

1.4 Technical Challenges

There are a number of technical challenges in the rapidly developing field of high-pressure neutron scattering. The research presented in this thesis deals with two of them: the limited access to the reciprocal space of the single crystal imposed by the parts of the pressure cell and the operational pressure limit set by the geometry of the anvils and the materials used in their construction.

1.4.1 Background – Paris Edinburgh Press and Toroidal Anvil Cell

This section provides a brief introduction to the Paris-Edinburgh press and cell. Its detailed description is presented in Chapter 2.

Paris-Edinburgh press (P-E press) is a compact high-pressure device designed to apply pressure to large samples studied by means of neutron scattering. Now one of the most widely used devices for high-pressure neutron scattering, P-E press was developed in early 1990s as a result of collaboration between the groups of scientists and engineers from *Université Pierre et Marie Curie, Paris, France* and *University of Edinburgh, Edinburgh, UK* [28, 29, 30, 31 and 32].

The Paris-Edinburgh cell consists two parts: the press and the cell.

- The press
  The Paris-Edinburgh press (P-E press) press provides axial thrust to the cell for compression by a hydraulic ram (see more details in Section 2.1.1). The P-E press is one of the most compact devices for its given load capabilities and can be found at many large-scale neutron and synchrotron facilities around the world. A standard V4 variant of the P-E press (Figure 1.9a) has a loading capacity of 250 tonnes and the weight of only 60 kg. With this load it is possible to compress samples of 100 mm^3 to 10 GPa, or samples with 35 mm^3 to 25 GPa [4].

- The cell
  The cell is an assembly of anvils, gaskets and sample. Figure 1.9b shows the components in a toroidal anvil cell that encloses the sample between the anvils and gaskets. When a large load provided by the press pushes the anvils and concentrates on their top surfaces, these gaskets and sample are compressed. The sample volume thus attains high pressure (see more details in Section 2.3.2).

(a) *(b)*

Figure 1.9 The V4 variant of Paris-Edinburgh press and anvil cell components. The layout and assembly of the press is included in Appendix A.

a) The V4 variant of Paris-Edinburgh press;

b) Four toroidal anvils and four small gaskets enclosing the sample.

1.4.2 Limitation on the Access to the Reciprocal Space Imposed by the Tie Rods

One intrinsic disadvantage associated with the design of the standard Paris-Edinburgh press is its limited aperture access. In the V4 variant of the standard P-E press four tie rods separate the equatorial aperture into four 67.5˚ windows (Figure 1.10a). In the vertical plane, the azimuthal window is less than ±7 degrees (Figure 1.10b).

These aperture openings provide paths for the scattered neutrons that form diffraction patterns in the detector. While a restricted angular aperture generally poses no major limitations in powder neutron-diffraction measurements on instruments like HiPr at the ISIS spallation neutron source, the tie rods significantly obstruct access to the reciprocal space for single-crystal diffraction and inelastic techniques at pulsed and constant wavelength sources. Therefore, it is important to develop and new system for full or at least improved access to the reciprocal space of the sample.

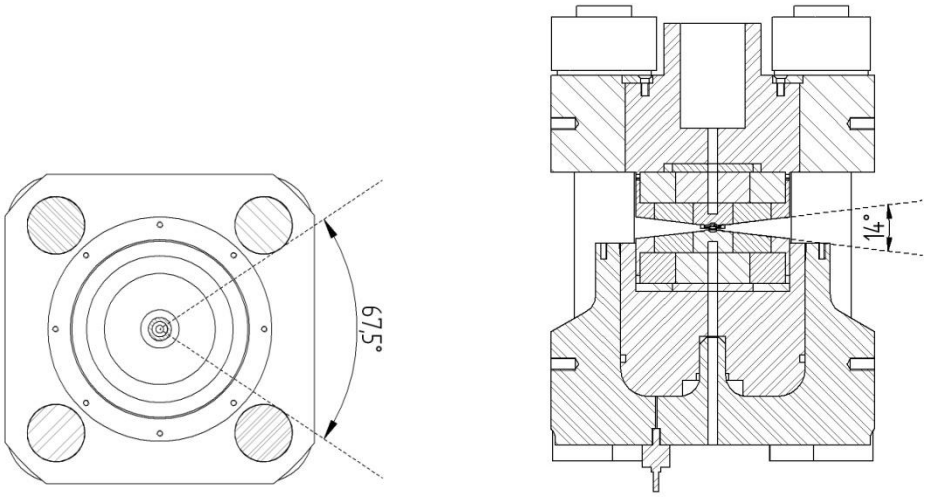

a) *b)*

Figure 1.10 The restricted aperture windows in the standard V4 variant of the Paris-Edinburgh press.

a) The aperture access windows in the equatorial plane;

b) The aperture access window in the azimuthal plane. If 7° anvils are used, the window angle is 14°. If 20° anvils are used, the window angle is 40°.

1.4.3 Failure Investigation of Double-Toroidal Anvils

As a core part of the Paris-Edinburgh cell, the toroidal anvils are its most critical component for generating high pressure. Based on the concept of the Bridgman anvils [33], the cell comprises of two identical coaxial dies with mutually facing surfaces which have toroidal recess, and a set of compressible gaskets enclosing the sample. Toroidal anvils were pioneered in Russia [35, 36], and proved to be a simple and efficient design for generating high pressure on large-volume samples.

The double-toroidal variant of these anvils has two grooves around the central sample chamber on the anvil surface. A pressure of approximately 30 GPa can be produced on samples with a volume of ~35 mm^3 when double-toroidal anvils made of sintered diamond are used [4].

However, at approximately 30 GPa (which corresponds to an applied load of around 240 tonnes) the double-toroidal anvils fail routinely. On examination they exhibit the cracks on the top surface. Figure 1.11 shows the pictures of two broken double-toroidal anvils with the characteristic damage.

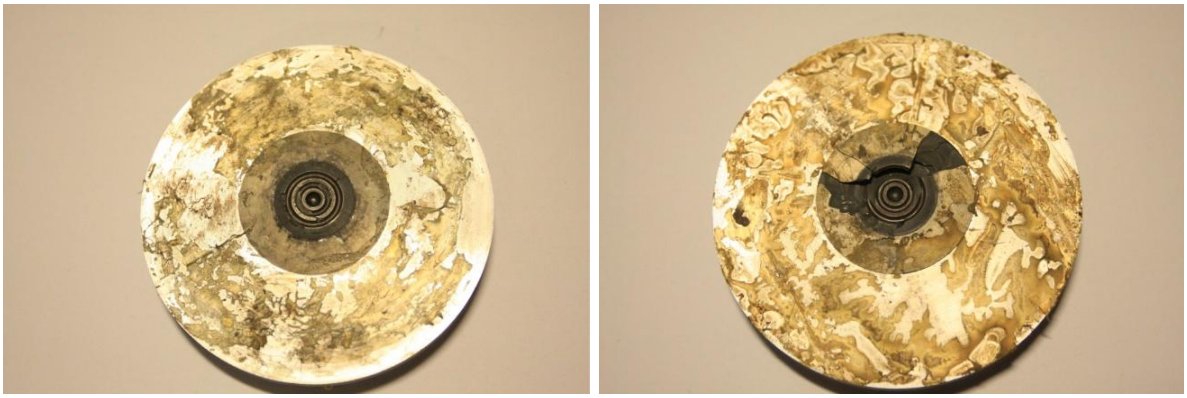

Figure 1.11 Photos of two broken double-toroidal anvils with binding rings. The dark core in the centre is the anvil made of sintered diamond and WC; the binding ring outside is made of maraging steel.

In order to understand the mechanism of the failure and to achieve higher pressure, a mechanical engineering investigation is required. As the traditional analysis by experimental procedure can be costly, time-consuming and also may not be able to provide precise and direct mechanical data for key quantities such as stress, strain and deformation, computer based Finite Element Method (FEM) is used to simulate the experimental conditions. A theoretical model for the multi-component assembly is established with multiple parameters and verified by the data observed experimentally. It is also used to optimize the design in order to improve the mechanical performance and to achieve higher pressure.

1.5 Thesis Layout

Chapter 1: Introduction

The chapter is an introduction to the subject of the PhD thesis – high-pressure crystallography, in particular neutron-diffraction experiments on large-volume single-crystal samples at large-scale facilities.

Section 1.1 outlines the general aspects of high-pressure crystallography, mainly its principles and application in a variety of scientific and engineering fields.

Section 1.2 and 1.3 provide insight into a specific high-pressure crystallography technique: neutron-diffraction measurements on single-crystal samples. The merits of the technique as a structural probe into materials are discussed.

Section 1.4 provides a brief outline of the technical challenges the PhD project intends to address.

Chapter 2 Literature review

The chapter is a review of the literatures relevant to the PhD project. It includes publications and past projects that are related to:

- The widely-used high-pressure experimental equipment for neutron-diffraction measurements, in particular high-pressure rotational instruments.

- The methods and techniques available for failure investigation and optimization of the opposed anvil cells.

Section 2.1 describes the history and application of the Paris-Edinburgh press – a compact and powerful instrument for high-pressure experiments at large-scale neutron facilities.

Section 2.2 describes two existing rotational apparatuses for high-pressure research. A comparison is made between them and the proposed rotator based on the V4 Paris-Edinburgh press.

Section 2.3 describes the background of the mechanical analysis for the double-toroidal anvil cells. Publications in which similar numerical techniques were used for analysis of high-pressure devices are discussed.

Chapter 3 The RV4 system – a high-pressure rotational apparatus

This chapter presents the design of a modified high-pressure rotational V4 Paris-Edinburgh press for single-crystal experiments (RV4). The new type of press capable of rotating an anvil assembly under load is described in detail. It is designed and built to work for high-pressure single-crystal studies on neutron diffractometers where an increased equatorial angular aperture is beneficial.

Section 3.1 outlines the general specifications of the RV4 as a high-pressure instrument for single-crystal neutron scattering experiments on large-volume single-crystal sample. Technical specifications and the requirements it was designed to meet are discussed.

Section 3.2 describes the mechanical structure of two versions of the RV4 design. The RV4 consists of two major assemblies – the central structure and the side structure. It is shown how the structures and key components are integrated.

Section 3.3 looks at individual components of the structures. The key aspects such as the materials used, mechanical performance and also the finite element analysis performed on them are specified in detail.

Section 3.4 gives a brief description of the components from a dynamic control's perspective with the most relevant here being the control, electronics and the operation of the motor.

Chapter 4 Testing and use of the RV4 system

This chapter presents the results of testing and use of the RV4 in the workshop and at large-scale neutron facilities along with the process of refining of the RV4 system.

Section 4.1 describes the experiment and use of the 1st version of the RV4 system at the D9 single-crystal diffractometer, ILL.

Section 4.2 describes the technical problems encountered in the 1st version of the RV4 system and relevant mitigations. The corresponding testing and subsequent modifications made led to the 2nd version of the RV4 system.

Section 4.3 describes the experiment and use of the 2nd version of the RV4 system on the single-crystal diffractometer SXD at ISIS.

Chapter 5 Finite element analysis of double-toroidal anvils

The chapter describes the numerical work on the mechanical performance of the double-toroidal anvil cell. The background of the analysis is that these anvil cells have seen repeated failure on the anvils when the applied load approaches 240 tonnes.

Section 5.1 describes the background details of the work. The problem encountered in the experiments is explained and illustrated.

Section 5.2 describes the finite element model. The components of the modelling include the geometry, the materials' properties, and the load conditions. The description of the modelling also includes the analysis settings, such as the assumptions, the mesh and the calculation methods. This is followed by the explanation of the analysis procedure using this model and the validation process. The two major material properties crucial to the analysis are then determined.

Section 5.3 describes the results of the analysis. They include the direct model outputs such as the stress and deformation as well as the rationale (based on these results) to explain what is observed in experimental tests.

Section 5.4 describes the paths for optimizations of the existing anvil configuration. In order to improve the mechanical performance of the anvil cell under very large applied load. Future work and some discussions on this issue are also included.

Chapter 6 Conclusions and future developments

The chapter is the summary of the thesis with conclusions on the work so far. In addition it provides a review of future developments that could be undertaken to address the current issues.

Section 6.1 is the final overview of the content of this thesis.

Section 6.2 considers future developments. The results of the current work are extrapolated.

Chapter 2

Literature Review

This chapter provides a review of the commonly-used high-pressure experimental equipment for neutron-diffraction measurements and also the numerical techniques for design and mechanical analysis of high-pressure devices. The items of equipment described are the Paris-Edinburgh press (P-E press) and toroidal anvil cell. This part is relevant to the first part of my PhD project – the development of a modified Paris-Edinburgh press with rotation capability. The numerical methods and techniques used to improve high-pressure devices are described. This is used throughout my PhD project – failure investigation and optimization of the double-toroidal anvil cells.

Section 2.1 describes the history and current application of the Paris-Edinburgh press in high-pressure experiments at large-scale neutron facilities. The need to develop a rotational version of the high-pressure press is explained in detail.

Section 2.2 describes two existing rotational instruments in the area of high-pressure research. A comparison is made between the two and the proposed rotator based on the V4 Paris-Edinburgh press.

Section 2.3 describes the background of the mechanical analysis for the double-toroidal anvil cells. As one of the modern techniques for numerical simulation of structural performance, the applications of Finite Element Analysis (FEA) in high-pressure engineering are reviewed.

2.1 Paris-Edinburgh Press for Neutron Diffraction Measurements at High Pressure

2.1.1 Paris-Edinburgh Press

The Paris-Edinburgh press (P-E press) was first reported in two papers in the early 1990s by J. M. Besson *et al.* [28, 29]. The press is designed to provide very large load on large-volume samples for neutron-diffraction experiments. This is mainly because of the fact that most diffractometers in neutron sources have a small experimental platform, or in some cases a small tank used for providing cryogenic and/or high vacuum sample environment. A conventional large-capacity press would not fit onto these platforms and tanks. In the case of the powder diffractometer *POLARIS*[2] at the ISIS pulsed source [36] – the instrument that the P-E press was initially designed for, the tank had a diameter of only 40 cm (Figure 2.1).

For this reason, the press had to be compatible with the hutch – its size less than 40 cm in any dimensions and its weight in the order of ~50 kg. This press however, was to be a compact yet a large-capacity press. Shown in Figure 2.2a is the standard V4 variant of the Paris-Edinburgh press that is capable of providing the load of 250 tonnes. It has a size and weight that is only a fraction of a conventional commercially available hydraulic press with the same load capacity (Figure 2.2b).

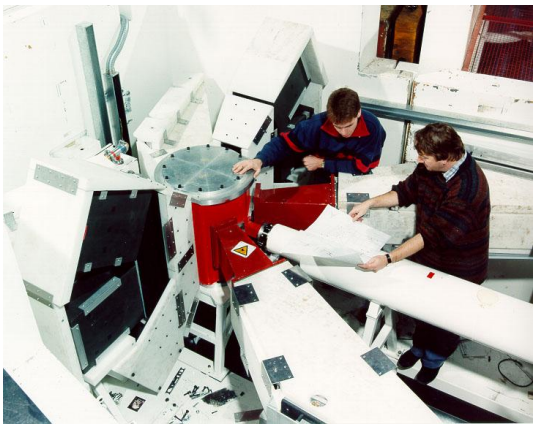

Figure 2.1 A photo of the powder diffractometer POLARIS, ISIS (from [36]).

[2] POLARIS has been redesigned since the Paris-Edinburgh press was developed in the early 1990s. Refer to the ISIS website for more updates on the station.

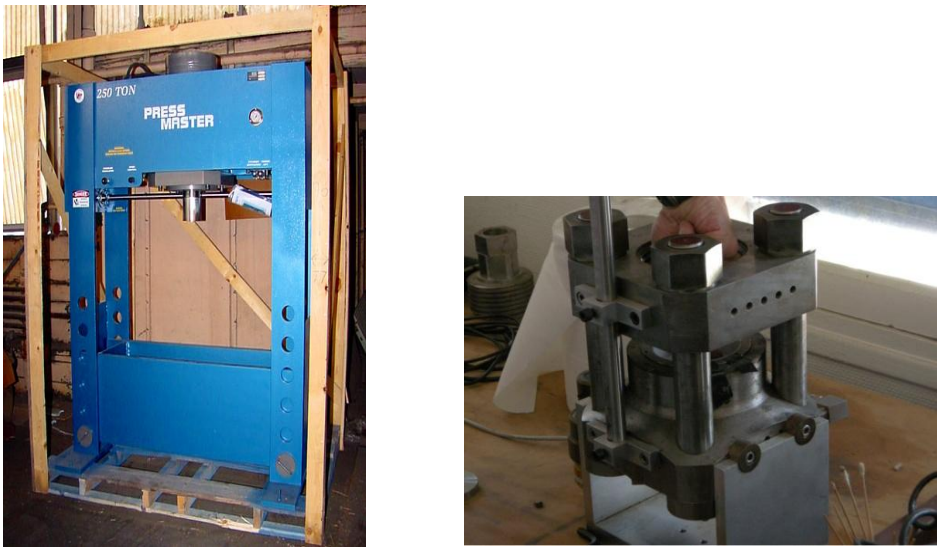

(a) *(b)*

Figure 2.2 A comparison of the size and load capacity between a typical conventional large capacity hydraulic press and the V4 variant of the Paris-Edinburgh press.

a) Conventional H-frame hydraulic press.

Weight: *3,100 kg*

Size: *441 cm × 193 cm × 147 cm*

Load capacity: *250 tonnes*

b) Standard V4 variant of the Paris-Edinburgh press

Weight: *60 kg*

Size: *30 cm × 20 cm × 20 cm*

Load capacity: *250 tonnes*

The main structure of the V4 variant of Paris-Edinburgh press consists of the top platen, the bottom platen, four mounting tie rods and a small hydraulic ram as the actuator (Figure 2.3). The basic idea behind the design is to construct a small frame with a ram incorporated into its body and the removable tie rods as the pillar connecting the bottom and top platens. The reduction in mass and size is achieved by use of high-strength maraging steels in the

construction of the press and optimization of the design with finite element analysis (FEA). Section 3.3 describes in more detail the function and specifications of these components.

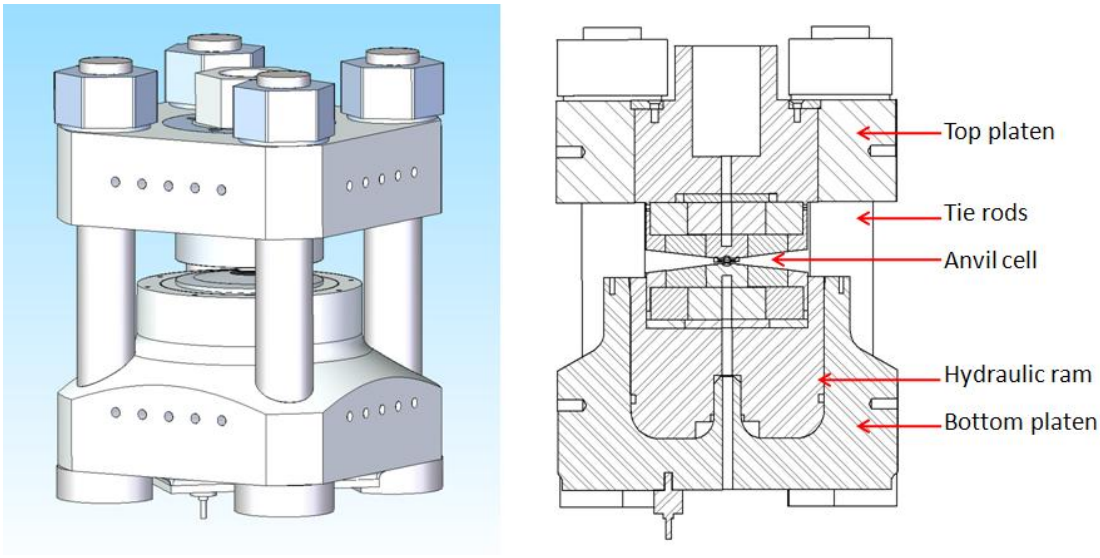

Figure 2.3 3D view (left) and sectional drawing (right) of the standard V4 variant of Paris-Edinburgh press (after [28, 29]). The main structure has the top platen, the bottom platen, four tie rods and a hydraulic ram. The anvil assembly is mounted in the centre of the press.

2.1.2 Paris-Edinburgh Press on SXD and D9

When the P-E press was developed it was initially used for powder diffraction experiments at ISIS the spallation neutron source at the Rutherford Appleton Laboratory, primarily on the *POLARIS* powder diffractometer. High-pressure neutron-diffraction measurements and full structure refinements were performed above 10 GPa on samples such as lithium deuteride, deuterated ices VII and VIII and Fe [28, 29 and 30].

Despite the fact that the press from the outset was designed for neutron powder diffraction in the energy-dispersive mode, it is now routinely used in both elastic and inelastic single-crystal neutron scattering experiments in the angle-dispersive mode [37, 38]. With the advances in relevant techniques that provide improved delicate sample environment, it has been used in inelastic neutron scattering experiments on single crystals of germanium and Fe_3Pt to 7 GPa [39] and also in measurements of phonon dispersion curves of simple solids

at pressures up to 10 GPa [40]. Most recently it was used to extract high quality structural data for single crystals of hydrogen rich materials such as KDP and squaric acid ($H_2C_4O_4$ or H_2SQ) in Time-of-Flight (ToF) neutron diffraction measurements [42] and monochromatic measurements at D9 [43]. It has also been used for low-temperature high-resolution neutron single-crystal diffraction studies of ice VI sample grown at very high pressure [27].

On a regular basis the high-pressure crystallography science group based at *the Centre for Science at Extreme Conditions* and *the School of Physics & Astronomy, University of Edinburgh* [17] uses the Paris-Edinburgh press for single-crystal studies on two diffractometers: *SXD* at *ISIS* and *D9* at *ILL*.

2.1.2.1 Single-crystal Diffractometer – SXD

The Single-Crystal Diffractometer (SXD) is designed for experiments which exploit the large continuous coverage of volumes of reciprocal space [42, 44]. High-pressure experiments for structure determination (e.g. hydrogen atom location) and phase transition observation (e.g. the changes of symmetry, and super-lattice reflections) have been carried out on SXD. The SXD instrument operates in angular dispersive mode and uses the Time-of-Flight Laue diffraction technique[3]. Besides large area position-sensitive detectors are employed. As a result it is possible to access larger reciprocal space in a single measurement. Technical specifications of the SXD are given in Appendix C.

The SXD's area detectors cover a large amount of 3D reciprocal space (the layout of the detectors is shown in Figure 2.4a). However, when the Paris-Edinburgh press is installed in the sample tank on the experimental platform (Figure 2.4b), the tie rods of the press come between the sample and the detectors. The diffracted beams in the direction of the tie rods are absorbed by the tie rods and cannot be detected by the detectors behind the tie rods. This obstructs a significant part of the scattered beam and reduces the effective amount of the scattered neutrons.

As shown in Figure 2.5 the tie rods create four 'blind spots' in the reciprocal space where the neutron reflections are not accessible. These 'blind spots' each obscure an angular sector of

[3] Time-of-Flight Laue technique uses white beam – a continuous spectrum (instead of constant wavelength beam) to irradiate the crystal in order to reduce the time of neutron data set collection. Monochromatic neutron beam only uses a small fraction of the white beam and takes very long time to collect data. Because the wavelength/energy corresponds to the velocity of neutrons; hence for neutron beam with a spectrum of different wavelengths, it is possible to work out the wavelength of each reflection by recording the time of the neutron scattered beam travelling from the sample to the detector – the so-called 'Time of Flight' method.

~22.5º, separating the equatorial aperture of the press into four ~66.5º windows. The diffraction pattern is thus restricted and incomplete and this can be critical to the structure measurements of single crystals as some valuable reflections may fall into the 'blind spots' and may not be observed.

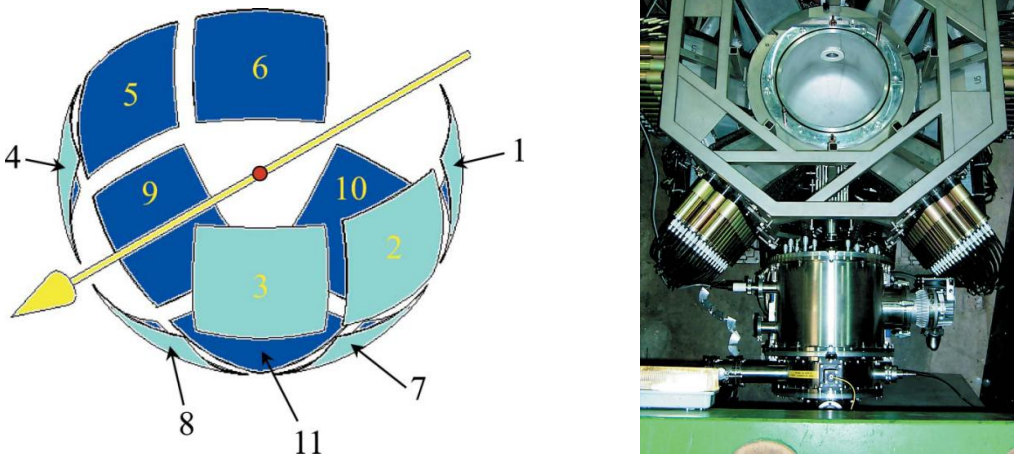

(a) *(b)*

Figure 2.4 The layout of the SXD's area detectors relative to the beam and a photograph of the SXD platform (from [42]).

a) The layout of the 11 area detectors surrounding the incident beam. They cover a large 3D area in space. The red circle in the center is the sample position. The yellow arrow is the direction of the incident beam.

b) A photo of the SXD instrument taken from above the platform. The incident neutron beam comes in from the bottom of the view. The octagonal frame supports the sample tank and surrounding detectors.

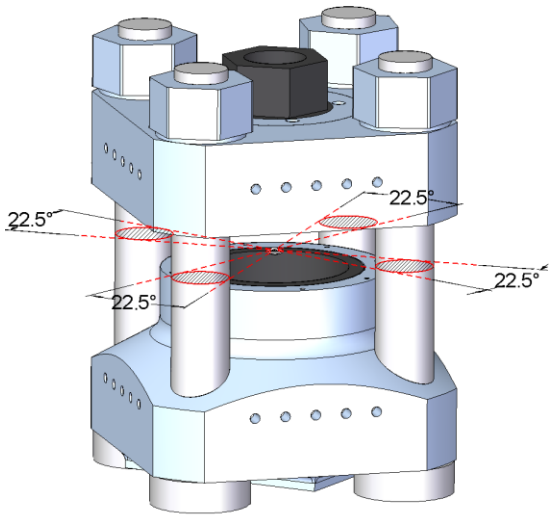

Figure 2.5 Illustration of the four tie rods obstructing the scattered beam each by a sector of 22.5˚. Four 'blind spots' are as a result created in the detectors (not shown) behind the tie rods.

2.1.2.2 Monochromatic Single-crystal Diffractometer – D9

The monochromatic single-crystal diffractometer D9 in ILL, Grenoble is used for accurate measurements of Bragg intensities [45, 46]. One of the most important features of D9 is that it allows a continuous choice of wavelengths in the range 0.35 - 0.85 Å. The wavelength of the neutrons on D9 is among the shortest available at any reactor in the world and very small atomic displacements can be resolved with the accuracy typically to 0.001 Å. With high-resolution nuclear density, it is ideal for structural refinements beyond the determination of average atomic positions.

D9 (Figure 2.6) is equipped with a small 2D area detector. The detector covers 8˚×8˚ in 32×32 pixels and is rotatable around the sample position. When the Paris-Edinburgh press is used on D9, it is mounted on the top of the rotatable ω table, which allows the whole press to rotate in the horizontal plane.

On D9 the Paris-Edinburgh press also has restricted access in the equatorial plane. Only limited observation of the diffracted pattern of reciprocal space can be observed. This is because the tie rods' positions remain the same relative to the sample inside the press, and the positioning flexibility created by the rotation of the detector and the whole press is not sufficient to solve the problem.

While theoretically it is possible to change the wavelength of the incident beam to offset the diffracted pattern and to move the blocked reflections out of the shadow of the tie rods, there are however further issues which need to be addressed with this approach. First of all, it is not convenient to change the wavelength. Adjusting the monochromator during an experiment takes a significant amount of time, especially when the operation intends to bring all the obstructed reflections in front of the detectors. Also changing the wavelength of the monochromatic incident beam would result in different resolutions and change in the intensities during the measurements. This has to be dealt with in the data processing later. For instance, the intensity and resolution recorded by the detector is lower at shorter wavelengths. At 0.5 Å the intensity is only approximately 1/4 of that at 0.8 Å while there is also significant sacrifice in the resolution as in the monochromator the take-off angle of the beam becomes smaller [45].

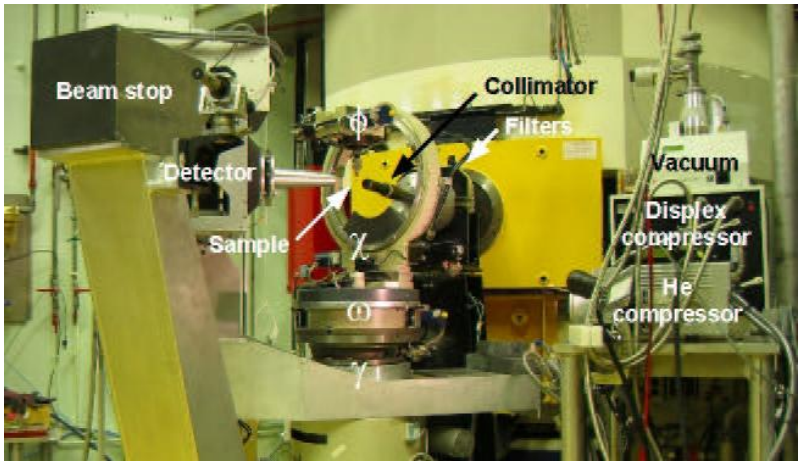

Figure 2.6 The layout of the monochromatic single-crystal diffractometer – D9 (from [45, 46]). The beam comes out from the collimator and points at the beam stop. The detector and the ω table are rotatable. The platform can rotate in the directions of γ, ϕ and χ as well.

2.1.3 VX type of Paris-Edinburgh Press

In an effort to increase the reciprocal space access of the Paris-Edinburgh press, Stefan Klotz *et al.* developed a VX variant of P-E press, which is also referred to as 'Panoramic P-E press' [47]. A typical VX2 P-E press is a compact hydraulic press with the capacity of 200 tonnes and the mass of 60 kg.

The VX P-E press only has two webs and hence has two large openings of 140˚ (equatorial aperture) × 60˚ (azimuthal aperture) (Figure 2.7). It was designed in such a way that it can partly overcome the restriction in reciprocal space posed by the tie rods in the V4 variant. This is most important when both incident and diffracted beams are close to the equatorial plane in inelastic neutron scattering experiments and angle-dispersive neutron powder scattering at continuous neutron sources [46]. Having larger angular apertures it is also useful for single-crystal neutron diffraction [46].

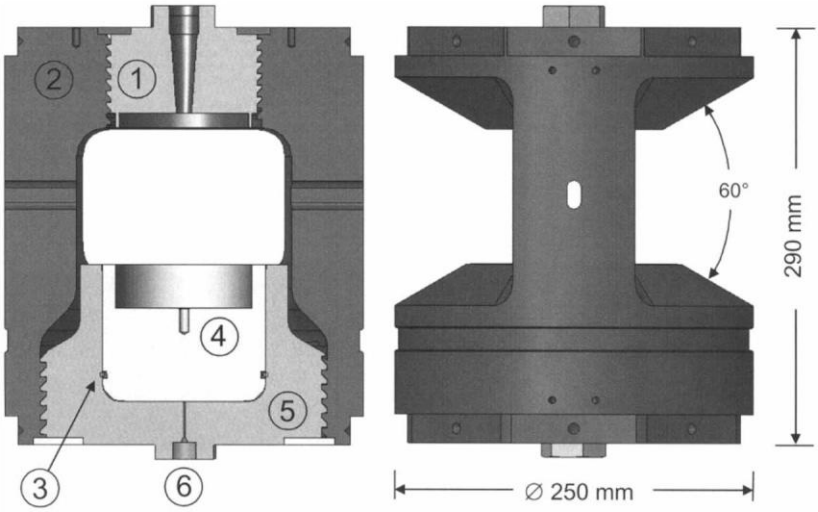

Figure 2.7 Cross section (left) and side view (right) of the VX2 PE press with an azimuthal window of 60˚ and two equatorial apertures of 140˚ (from [47]). The mass is 60 kg. The capacity is 200 tonnes. The size is 290 mm in length and 250 mm in diameter. The components are ① breech; ② press body; ③ O-ring seal; ④ piston; ⑤ cylinder; ⑥ hydraulic fluid inlet.

Nevertheless, with the design of the VX type of Paris-Edinburgh press two pillars still hinder access to reciprocal space. Angular 'blind' sectors of a total of 80˚ (2×40˚) still exist as shown in Figure 2.8. This is critical to single-crystal diffraction measurements.

Since the 'blind spots' are associated with the stationary sample and the tie rods surrounding it inside the press, and it is impossible to entirely remove the tie rods or pillars from the press frame in the structural design, one possible solution is to rotate the single-crystal sample relative to the tie rods. By doing this, the diffraction reflections can be moved out of the

shadow of the tie rods or pillars, and collected into the detectors. The critical element of the solution is that the sample needs to rotate whilst the applied load and the hydrostatic conditions in the sample are maintained.

It was decided to design a rotational apparatus which is capable of rotating the sample and anvils under load for single-crystal neutron diffraction measurements at high pressure. The rotational apparatus was expected to be based on the V4 standard variant of Paris-Edinburgh press in order to fit into the existing diffractometer facilities. We called the new press 'the RV4' (Section 3.1 details the naming convention with regard to the RV4).

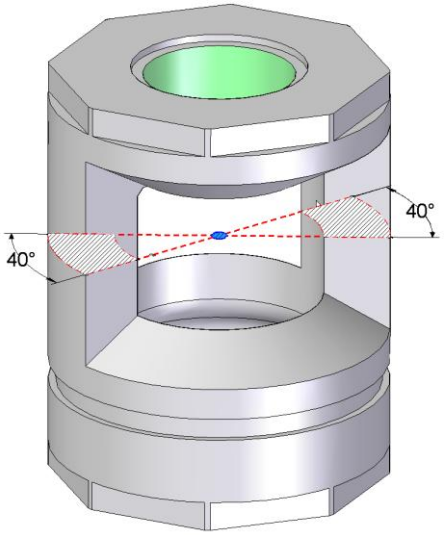

Figure 2.8 Illustration of the sectors imposed by the two pillars in the VX P-E press. Two sectors are both 40˚, resulting in the equatorial aperture being two windows of 140˚.

2.2 Existing Rotational Instruments for High-pressure Studies

While it is impossible to entirely get rid of the tie rods or pillars in the press frame, the mechanism of rotating the sample (around the vertical axis) inside the press under applied load has been explored in the past. To our knowledge there are two existing instruments providing rotation the sample at high pressure and we review them below.

2.2.1 The Cambridge roPEC apparatus

At *the University of Cambridge* Geoffrey D. Bromiley *et al.* developed a portable high-pressure stress cell based on the V7 Paris-Edinburgh apparatus [48] for torsional testing of materials. The press is called the roPEC apparatus.

In the roPEC apparatus, highly-compressed samples can be deformed using simple shear geometry between opposed anvils. As is shown in Figure 2.9, simple shear of the sample is achieved by rotating the lower anvil, with respect to an upper, stationary anvil. The sample is encased in a deformable gasket made of amorphous-boron epoxy and loaded between the opposed anvils.

The high-pressure loading frame is based on a modified V7 (450 tonne capacity) Paris-Edinburgh apparatus. A 50% elongation of the four tie rods provides the additional space between the platens required to accommodate the rotation components. The principal components of the press include two conical anvils, a central piston, a high-ratio harmonic gearbox [49], a conical spacer and two spherical thrust roller bearings [50]. A stepper motor is also installed and provides torque to a timing belt which is coupled to the Harmonic Drive™ gearbox and an encoder for position monitoring.

It is possible to achieve the rotation with an applied load of ~35 tonnes. With this load capacity, torsional deformation experiments have been performed in the roPEC at pressures up to 7 GPa which is extendable to 15 GPa if a different sample and anvil/gaskets assembly is adopted.

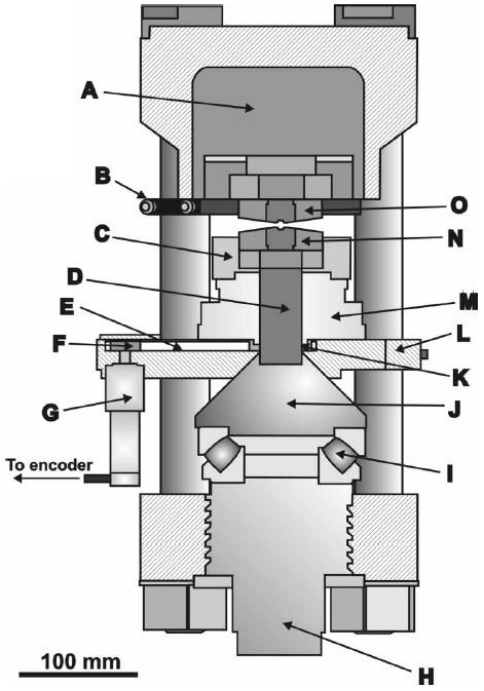

Figure 2.9 Cross-sectional view of the rotatable Paris-Edinburgh Cell (roPEC) (from [48]).

The apparatus is based on a modified V7 450-tonne press frame and developed for high-pressure torsional testing. The components in the structure are (A) hydraulic ram, (B) plate preventing rotation of upper (stationary) anvil, (C) housing for the lower (rotating) anvil, (D) central piston, (E) 3:1 steel-reinforced timing belt, (F) gear-head on externally-mounted servo, (G) externally mounted servo with Harmonic Drive© 100:1 reduction gearing on output, and lined to digital encoder, (H) breech with artillery thread, (I) spherical roller thrust bearings, (J) conical spacer, (K) input gear for reduction gearing, (L) support plate for servo and housing to reduction gearing, (M) 160:1 Harmonic Drive© reduction gearing, (N) lower (rotating) carbide anvil, and (O) upper (stationary) carbide anvil. Descriptions are after [48].

2.2.2 High pressure X-ray microtomography (HPXMT) device

The high pressure x-ray microtomography (HPXMT) device [51] is a rotational cell developed by a group of researchers from *the University of Chicago* and *the University of California at Davis* in 2005. The cell is used for experiments on magnesium silicate glasses and supercooled liquid [52]. Pressures up to 8 GPa have been generated with a hydraulic load of 25 tonnes using two opposed anvils and modified containment rings.

The apparatus uses the modified Drickamer anvil cell[4]. As shown in the schematic diagram of the apparatus (Figure 2.10) [48], the sample is compressed by a pair of Drickamer anvils (A) and supported by steel columns (B) through WC spacers (C). The columns (B) above and below the sample in turn are supported by steel disks (D) that spread the load onto two concentric low-profile thrust bearings (E1, E2). The load support columns (B) and the Drickamer anvil are attached to the passive rotating members or flexspline of the Harmonic Drive™ units [49] (F) driven by the active member of the upper and lower units (wave generator G) through coupler plates (H). The wave generators are attached to large precision gears (I) driven by smaller gears (J) through right-angle gear boxes (K) and stepper motors (L).

The axial dynamic and static load specifications of the apparatus are approximately 14 tonnes and 102 tonnes, respectively, and 9.1 tonnes and 56 tonnes, respectively, for the smaller thrust bearings. The frictional coefficient is expected to be 0.05 when grease lubricant is used while the calculated working torque for rotation is 745 Nm at a motor speed of 2000 rpm delivered through the harmonic gearbox.

A series of tests have been conducted with this system, including pressure generation, pressure measurements, and the investigation of high-pressure tomography operational features such as spatial resolution, shear deformation and volume measurement. The technical development has potential applications in imaging microstructure evolution of composite materials under varying physical conditions – high pressure, temperature, and during deformation and other areas.

[4] Drickamer anvil cell is a well-known and widely used device for high pressure experimentation using opposed anvils similar to the Bridgman anvil apparatus and the diamond anvil cell [50].

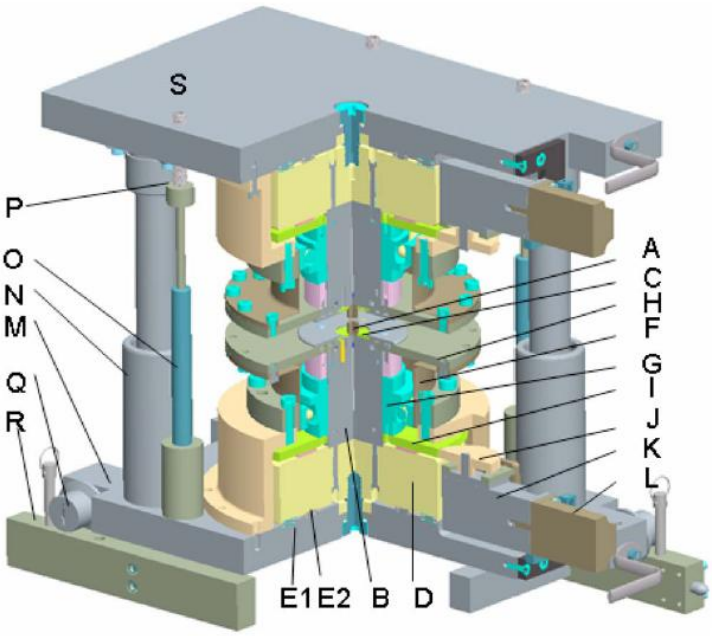

Figure 2.10 Colour cutaway view of the high-pressure tomography apparatus – the HPXMT device from ([51]).

A) a pair of Drickamer anvils, B) a steel column, C) WC spacer, D) a steel disk; E1, E2: two concentric low profile thrust bearings on each end of the cell, F) the passive rotating member – flexspline of the Harmonic Drive™ unit, G) the active member (wave generator) of the gearbox unit, H) coupler plate, I) a large precision gear, J) a smaller gear, K) a right-angle gear box, L) a stepper motor. M) hardened steel die plate of the die set on which the apparatus is mounted, N) ball-bearing die posts, O) four gas springs, Q) rollers for rolling the entire apparatus in and out of the hydraulic press, R) transport rails, S) screws. Descriptions are after [51].

2.2.3 Comparison of the specifications of roPEC and HPXMT devices with the expected performance of RV4

The roPEC apparatus and the HPXMT device are both compact high-pressure rotational systems which incorporate some features that would be relevant to the rotator for single-crystal neutron diffraction experiments. There are, however, major issues that make them different from the proposed RV4 and unsuitable for use in single-crystal diffractometers.

Below is a general discussion on some technical aspects of the desired features for a rotational Paris-Edinburgh press for neutron scattering experiments on single crystals at high

pressure compared to the operational features and technical specifications of the roPEC and HPXMT devices.

- **Anvils**

  For neutron-diffraction measurements using the Paris-Edinburgh cell, toroidal-profile anvils are required in order to accommodate large-volume samples so that an intense diffracted beam can be achieved. Anvils with round shape of the outer edge of the binding ring are traditionally used to provide good support to the centre-pieces of the anvil made of WC or sintered diamond.

  Ideally the RV4 should be compatible with the standard toroidal anvils. The roPEC apparatus uses anvils with a hexagonal hollow profile in the components that support and hold the anvils. The HPXMT device uses Drickamer anvils. In both cases the rotational devices are used with the synchrotron radiation or with an x-ray beam and therefore the anvils accommodate smaller samples than those required for neutron-diffraction measurements.

- **Rotation mode**

  The roPEC apparatus only rotates one (upper) anvil relative to the stationary (lower) anvil in order to give a shearing effect on the sample for torsional deformation. In the RV4 the requirement is that the sample and anvils are rotated simultaneously without relative rotational movements between the anvils as these movements would result in shearing the sample between the anvils under applied load. Any shearing of the single-crystal sample could result in the significant damage to its integrity or change the orientation or to the loss of homogeneity of the pressure distribution across the sample [53]. The relative movement also makes the measurements less accurate, possibly to the extent that the measurements could become invalid due to non-hydrostaticity of the pressure medium.

  The HPXMT device uses two motors and separate transmission power train to rotate the upper and lower anvils. It is very useful for x-ray microtomographic experiments as it provides the flexibility to rotate the anvils in different directions and at different speeds. Although, theoretically it is possible to rotate them in the same direction – clockwise or counter clockwise – at the same speed, it is very difficult in practice to start the rotation of both shafts simultaneously and control the rotating speed of the

anvils with a satisfactory precision to allow use in single-crystal diffraction measurements. The difference comes from:

1) The different execution time for commands to start the motors. It has to be at exactly the same time which can be achieved by setting up the software and electronics and thus synchronising their steps.

2) The differences in losses in the mechanical transmissions from the motors to the anvils. There are many components in the power train that can introduce different positioning errors and backlashes.

The goal is to design the transmission structure such that one motor drives a single shaft which in turn drives both anvils. This approach provides better synchronization of the rotation of the two anvils. This design is adopted in the RV4.

- **Load capacity**

The load capacity of the roPEC apparatus and the HPXMT device is in the range of 25 to 35 tonnes. The roPEC applies the load to compress samples typically with a thickness of 2 mm and a diameter of 3.5 mm up to 5 GPa. Torsional testing of material has been performed on the system at pressures up to 7 GPa. The HPXMT device has been used to compress Mg_2SiO_4 sample of 0.8 mm diameter sphere to 1 GPa. Pressures up to 8 GPa were generated in the cell with a hydraulic load of 25 tonnes.

Although the load capacity of 35 tonnes can produce high enough pressure for tomography and x-ray microtomography studies which normally uses small-volume sample, the load is not sufficient for neutron-diffraction measurements and full structure refinements for crystallographic study as a much larger sample is required because of the intrinsically low flux of neutron beams. Using an arrangement of single-toroidal anvils made of tungsten carbide, it is possible to routinely achieve pressures in excess of 10 GPa under applied load of at least 100 tonnes. Using double-toroidal anvil cell made of sintered diamond, it is possible to achieve nearly 30 GPa under applied load of 240 tonnes. It is intended that the RV4 should be capable of rotating under the applied load of at least 100 tonnes.

- **Size, weight and sample position**

  To fit onto the existing single-crystal diffractometers such as SXD and D9, there are strict requirements as to the dimensions of the RV4. These restrictions include the overall dimensions in any direction of the body, and also the distance between the sample position and the top side of the press as this is related to the beam position with respect to the tank or the table of the diffractometers on which the press is mounted. Besides, the RV4 should also be light so that it can be lifted by a portable crane and supported by the infrastructure of the diffractometers.

  On SXD the vacuum tank surrounding the RV4 has the inner diameter of 395 mm and the distance from the centre of the beam to the bottom of the tank is around 210 mm. On D9, the RV4 is to be mounted on top of the ω table (Figure 2.6) and the allowed distance between the sample position in the RV4 and the top surface of the table is determined by the beam to be less than 208 mm. The dimensions of the RV4 in the equatorial plane are also limited as both the detector and the collimator have fixed and close distance to the RV4.

  The roPEC apparatus is too big with a height of ~580 mm and the distance between the top of the press and the sample being 380 mm (although its weight is less than 150 kilos and it is light enough for being lifted on the experimental platform). The HPXMT device is also very big with the dimensions in any direction over 400 mm. Because it is designed to be used on the fixed x-ray experimental platform and does not need to be lifted often, it is heavy and not suitable for mounting on neutron diffractometers.

- **Dynamic characteristics**

  One of the desired features of the RV4 is that the rotation of the anvils under load has reasonable rotational speed and positioning precision. It is roughly estimated that the time taken to rotate the anvils by an angle less than one turn (360°) needs to be no longer than several minutes. Ideally, the faster the rotation is completed, the better the experiments can make use of the beam time. In practice the increase in rotational speed can lead to an increase of the positioning error and possible damage to the sample integrity during the rotation. It also results in a decrease in the drive power for rotation as the motor has an inverse relationship between its output torque and speed. The higher the speed the motor is running at, the lower its output torque.

The requirement on the rotation positioning error is mainly determined by the coverage of the detectors and the strategy is to make sure the angular error is no greater than a certain portion of the coverage angle. When there is a certain amount of error – which cannot be eliminated entirely from a technical point of view – it can always be checked by analysing the diffraction pattern and corrected in the software. The SXD diffractometer has very large detector coverage of reciprocal space while the area detector of the D9 instrument covers a sector of ~15 ºof the equatorial plane of the reciprocal space. In order to ensure the accuracy of the positioning, the required precision of the rotation is set to be better than 0.5 º.

As discussed above both the roPEC apparatus and the HPXMT device are not suitable as an alternative to the RV4 for application in neutron-diffraction experiments on single crystals. They however have relevant features that can be used in the development of the RV4. The major technical difficulties associated with this kind of heavy duty rotational system and the solutions for them are similar. The most important parts that are used in all of these devices are the thrust bearings and the gearbox. These two components in such types of devices are discussed below.

2.2.3.1 Thrust bearings

Inside the rotational Paris-Edinburgh cell, the core module for pressure generation – the anvil assembly and its support components – needs to be supported by axial thrust bearings so that the entire cell can be rotated under load. There are two main types of the commercially available products that meet the requirements in terms of their size and load capacity. Both of them are manufactured by SKF bearings – designated parts numbers being 29412E and 89412TN, respectively. Except for these two types of the roller bearings, other existing bearings are not suitable for use in the RV4. For instance, the low profile bearings used in the HPXMT device are too big.

- 29412E spherical roller thrust bearing

  29412E [50] is a spherical roller thrust bearing with tapered washer and housing. In the spherical roller thrust bearing the axial load is transmitted from one raceway to the other at an angle to the bearing axis, giving tapered support to the load in the axial directions.

29412E is 42 mm in height and has an outer diameter of 130 mm which fits into the space between the four tie rods of a V4 Paris-Edinburgh press (Figure 2.11). According to the specifications, the bearing is capable of sustaining static load of up to 91.5 tonnes and dynamic load up to 39 tonnes. As the RV4 is expected to be running at a very low speed, less than 1 revolution/min, the operation condition is similar to that of a static application, and thus it is hoped that 29412E can be used with an axial load of around 90 tonnes inside the RV4.

Another important characteristic of the spherical roller thrust bearings is their self-aligning capability. This makes the bearing insensitive to shaft deflection and misalignment of the shaft relative to the housing even when it is running at high speed.

29412E is used in the roPEC apparatus for low speed torsional deformation tests and in the 1st version of the RV4 (the two versions of design of the RV4 are described in Chapter 3). In the 1st version of the RV4 the frictional resistance in the 29412E bearings however was later found to be significantly larger than in other types of bearings such as plain or cylindrical roller bearings (see Chapter 4 for more information).

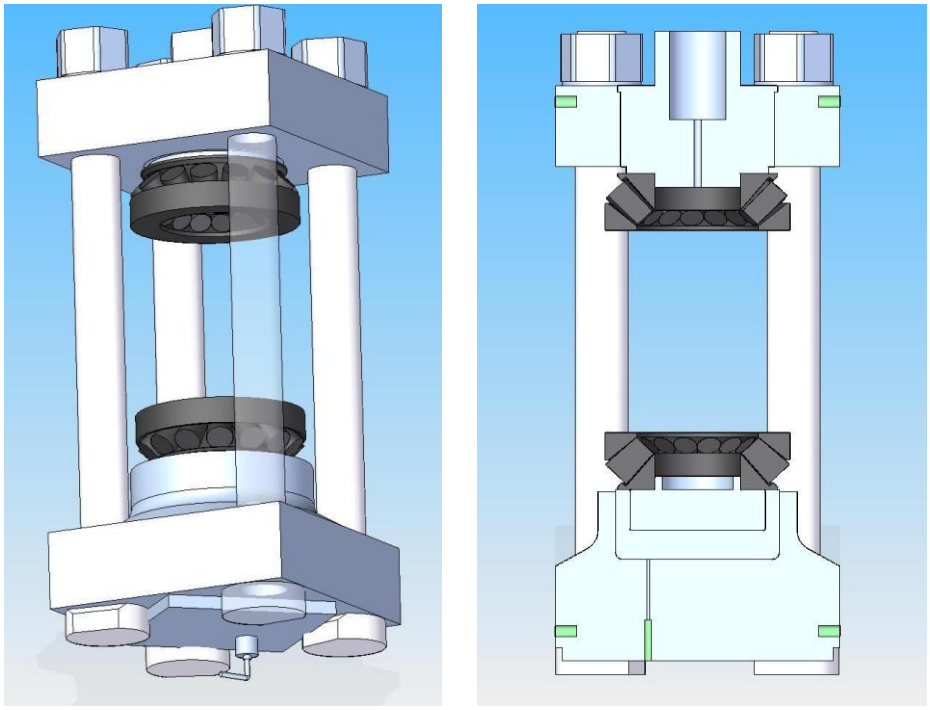

Figure 2.11 The spherical roller thrust bearings SKF 29412E [49] inside an extended frame of the V4 variant Paris-Edinburgh press. The bearings are 42 mm in height and 130 mm in outer diameter.

- 89412TN cylindrical roller thrust bearings

  Cylindrical roller thrust bearings are suitable for arrangements that have to support heavy axial loads with good stiffness and little axial space. The 89412TN [54] bearing also has a height of 42 mm and an outer diameter of 130 mm. With a simple shape and design, it is possible to accommodate a static load of up to 118 tonnes and a dynamic load of up to 31 tonnes. The disadvantage of the bearings is that they are not self-aligned during rotation which could pose a danger to the integrity of the sample and the effectiveness of the measurements. Figure 2.12 shows the SKF 89412TN inside an extended frame of the V4 variant Paris-Edinburgh press.

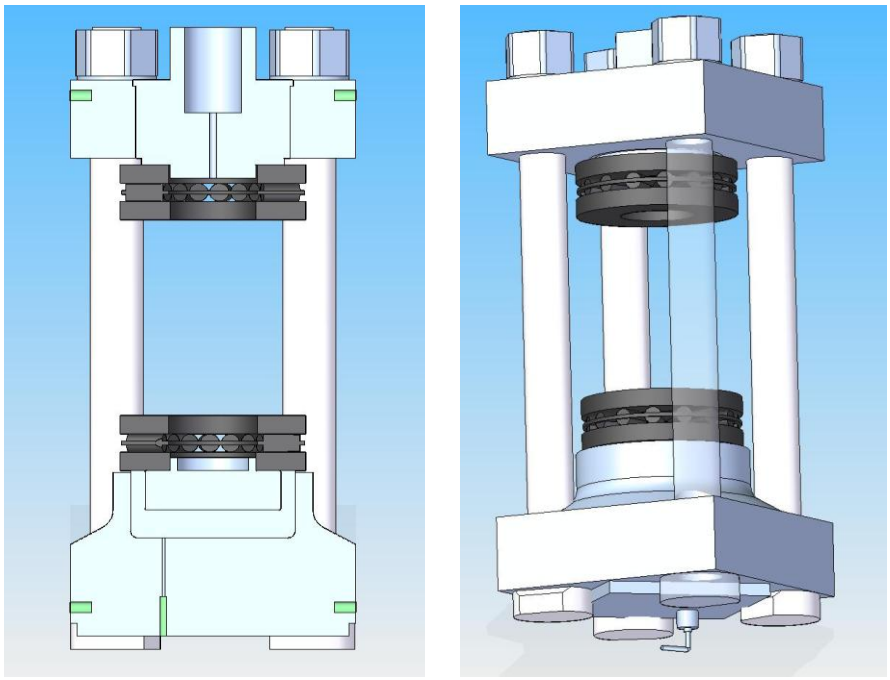

Figure 2.12 The cylindrical roller thrust bearings SKF 89412TN [54] inside an extended frame of the V4 variant Paris-Edinburgh press. The bearings are 42 mm in height and 130 mm in outer diameter.

2.2.3.2 Gearbox

The gearbox is the second most important component in the power transmission of the heavy-duty rotational system. Most of them, when designed for large power transmission with a high reduction ratio are very large in size. Taking into account the constrained space allowed for mounting the gearbox in the V4 most of them are not suitable.

The drive torque is needed to overcome the frictional resistant moment on the thrust bearings under applied load. Rotating the anvil shafts requires a torque that is far more than the output torque of a compact motor. The compactness here means the motor is small enough to be installed inside the RV4. Based on the calculations (details in Section 3.2.3) performed as part of the design process, only harmonic gearbox can meet these requirements.

A harmonic gearbox is a compact gearbox that allows high reduction ratios with concentric shafts. It has a very simple mechanism that utilizes the elasto-mechanical property of the metallic components. Shown in Figure 2.13 are three key components of a harmonic gearbox: the flexspline (passive rotating member connected to the output shaft), the wave generator (active rotating member connected to the input shaft) and the circular spline (stationary mainframe). The reduction ratio (K:1) is determined by the number of the teeth in the flexspline (K) and the circular spline (K-1). It operates in such a way that when the input shaft is rotated with a small torque at a relatively high speed, the output shaft rotates at a low speed (1/K of that of the input shaft) with a large output torque (K times that of the input torque).

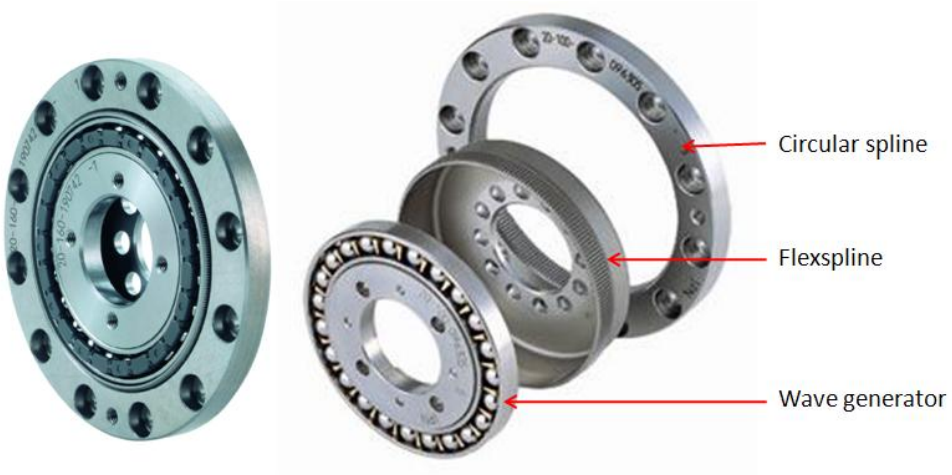

Figure 2.13 The assembly and components of a typical harmonic gearbox (from [49]). The flexspline is the passive rotating member connected to the output shaft. The wave generator is the active rotating member connected to the input shaft. The circular spline is a stationary mainframe.

Both the roPEC apparatus and the HPXMT device use a harmonic gearbox module for power transmission and magnification. In the roPEC apparatus, an HFUS-32-160-2UH module manufactured by Harmornic Drive^{TM} [49] is used to gear up the output torque of the servo (linked to gearbox via a timing belt). HFUS series of harmonic gearboxes are units that have high torsional stiffness and a large hollow shaft. HFUS-32-160-2UH has the reduction radio of 160:1 (K=160) and the maximum output of 314Nm. In the HPXMT device, the harmonic gearbox also has the reduction ratio of 160:1.

As the RV4 has less room for installing the motor and the gearbox, the CSD series of harmonic gearboxes from Harmornic Drive^{TM} are suitable. It is a compact gearbox with small axial length and a very large gear ratio and allowable output torque. More details of the design of CSD and its application in the RV4 are described in Section 3.3.9.

2.3 Finite element analysis of double-toroidal anvil cells

Engineering simulation has long proven to be a cost-effective way of developing innovative design of instruments. One of the simulation techniques – Finite Element Method (FEM) – is often used for designing high-pressure devices, in particular the pressure generating components. As part of this project, the technique is used to simulate the stress distribution and the deformations in the parts of the rotator as well as to probe the failure mechanism of double-toroidal anvil cells under excessive load. Relevant research on similar high-pressure devices and/or using the same technique is presented and discussed here.

2.3.1 Finite Element Analysis (FEA)

Finite Element Analysis (FEA) is a numerical method of analysis for studying continuous physical systems and used to solve a variety of engineering problems in structural mechanics, in systems exposed to thermal gradients and electrical field, fluid dynamics and in recent years increasingly multi-physical phenomena.

As a method of approximate solutions to a wide range of problems the Finite Element Method (FEM) originates from a mathematical concept in structural analysis. A number of discrete structural elements are created mathematically to represent a continuum. These elements can be either 1D, 2D or 3D and various shapes have been used (Figure 2.14). In an FEA model, the properties of each of these elements, such as the mechanical strength, the boundary conditions, etc. can be determined according to the macro-physical information.

They are then combined to form a series of algebraic equations for the entire structure. There is a technical issue with solving for a large number of equations as a very high calculation capability is required. In modern times these equations are solved using the computer with which the solution of the large-order systems of equations is possible.

A number of prewritten commercial codes compatible with machines from microcomputers to supercomputers are available. Among these FEA programs, ANSYS [55] is one of the most mature and widely used in the application of computational methods to solve the engineering design challenges. ANSYS has a broad spectrum of capabilities that cover a range of analysis types, elements, contact, materials and solvers. ANSYS Workbench package is extensively used for mechanical analysis of components and assemblies in this PhD project.

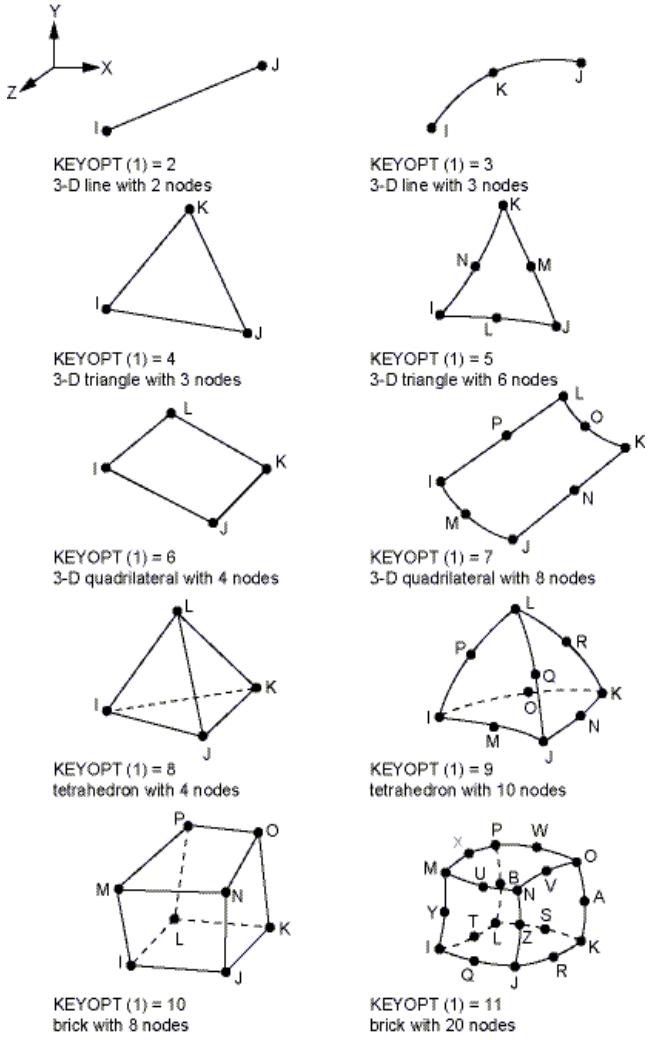

Figure 2.14 Different types of elements that are used in ANSYS for structural analysis (from [55]).

2.3.2 Toroidal Anvils

In the Bridgman anvils the compression of the sample occurs as the gasket material is compressed and extruded. The deformation of the anvils under pressure and excessive extrusion of the gasket material hinder high-pressure generation in all high-pressure anvil devices. In the toroidal anvil cell, a new method of supporting the gaskets materials surrounding the sample is used so as to produce higher pressure in the sample chamber.

Developed in Russia several decades ago, the toroidal device [34, 35] proved an efficient design for generating high pressure on large-volume sample. These anvils combined with the Paris-Edinburgh press have since become popular among the researcher in high pressure research worldwide particularly in the field of neutron diffraction [4, 28, 27, 28, 29, 30, 31, 32, 37, 38 and 41]. Currently the Paris-Edinburgh press with toroidal anvils made of tungsten carbide (WC) is used to routinely produce pressure around 10 GPa.

The design of the toroidal anvil, like other types of anvils, is based on the principle of massive support [33, 56]. A typical assembly of the toroidal device (Figure 2.15) comprises of two coaxial anvil dies with mutually facing surfaces that have one or more toroidal recesses, and a set of solid compressible gaskets between the surfaces with the sample to be studied enclosed. The toroidal groove in the anvil supports the gasket and restricts the flow of the gasket material when it is in the plastic deformation regime. This allows a large starting volume of the sample and keeps the gap between the anvils reasonably wide for neutron scattering once the anvils are under the load.

When the axial load is applied to the back surface, the anvils are brought together against the gaskets and the sample. The gaskets then undergo significant plastic deformation – flatten and expand outward as soon as the stress exceeds the yield strength of the gasket material. The thrust load compresses the pressure medium[5] thus generating high pressure on the sample.

The original design of the toroidal anvils has only one recess and a tapered angle of 7 degrees (Figure 2.16a). In order to increase the azimuthal aperture and thus the accessible reciprocal space, single-toroidal anvil with 20 ° taper angle has also been developed [37] (Figure 2.16a).

[5] Pressure medium is the substance surrounding the sample inside the sample chamber formed by the gaskets as to transmit the compression load uniformly and thus improve the pressure distribution in the sample.

In order to increase the pressure range of the anvils the double-toroidal type with two grooves around the central sample chamber on the anvil's surface has also been developed (Figure 2.16b). When the double-toroidal anvils are made of sintered diamond, it is possible to use them to generate pressure in the range of 30 GPa on powdered samples of a volume of ~35 mm^3 [4].

There are two types of gaskets used with the toroidal anvils – standard gasket and encapsulated gasket. The standard type is the original design of the gasket that is a ring(s) positioned in the toroidal groove(s). It provides radial support for the sample. The soft-metal-encapsulated (SME) gasket (Figure 2.15) was developed by W. G. Marshall and D. J. Francis to attain near-hydrostatic compression conditions at high pressure [57]. As the name suggests, in the SME gaskets the sample is enclosed by two flanged hemispherical cups (Figure 2.15 and 2.16). The SME gaskets can contain fluids as samples and as pressure-transmitting medium. With standard gaskets it is difficult to contain hydrostatic medium at high pressure.

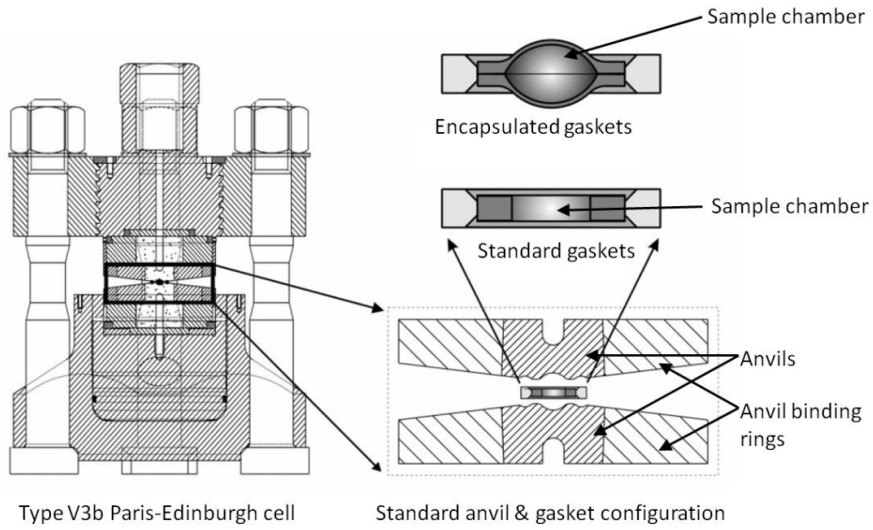

Figure 2.15 A typical assembly of the single-toroidal anvil cell with encapsulate gaskets (from [57]). Two types of gaskets are shown: standard gasket and encapsulated gasket. The standard type is the original design with two flat circular rings, providing radial support for the sample.

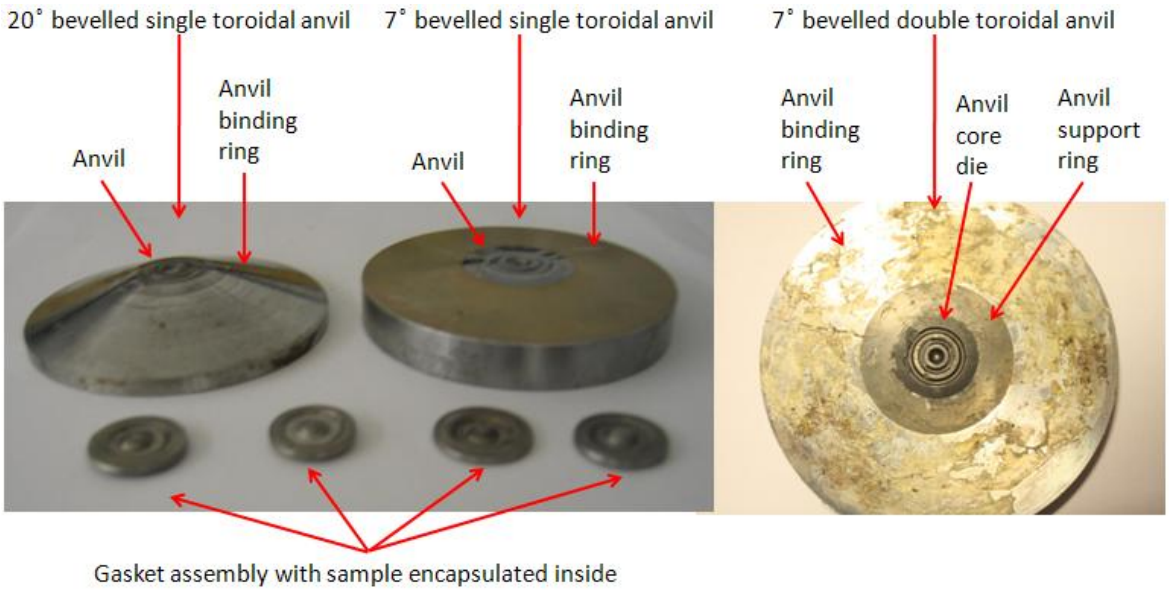

Figure 2.16 Different types of toroidal anvils and the gasket assemblies. Single-toroidal anvils have a 7˚ tapered variant and a 20˚ tapered variant [37] (more details about 20˚ can be found in Section 2.3.5). The double-toroidal anvil exists in 7˚ tapered angle variant only.

a) *A photo of the single-toroidal anvils and gasket assemblies. The anvils are made of tungsten carbide and the surfaces are polished. They are surrounded by an anvil binding ring made of high-strength maraging steel. The gasket assemblies in the photo were previously used in experiments and have been deformed with the sample encapsulated.*

b) *A photo of the double-toroidal anvil with an anvil binding ring. As is seen in the picture, from the centre outward the dark piece is the core part of the anvil made of polycrystalline diamond (PCD), the medium dark ring is the tungsten carbide (WC) supporting ring of the anvils and the outer ring is the anvil binding ring made of high-strength maraging steel.*

2.3.3 FEA in Mechanical Analysis of High-Pressure Devices

Finite Element Analysis (FEA), as a fast, inexpensive and non-destructive method for finding the mechanical quantities such as the stress, strain or deformation distributions, has since 1980s been used for evaluating the mechanical performance of high-pressure devices. In general, there are three approaches to the analysis.

1) The first one is to calculate these quantities to determine if they are too large in any part of the design and thus can cause failure of the anvils or other components. This

method requires the availability of precise strength and modulus data for the materials used in the construction of the cell. However, this data is usually not available or very difficult to determine for gasket materials and diamonds. Gaskets experience significant deformation in high-pressure experiments and their properties in the plastic deformation regime are not well known. For the anvil made of diamond, the quality of the gem-stone diamond largely affects its properties and it is nearly impossible to predict its strength and the modulus theoretically.

2) When the materials' properties are not available or not known accurately enough for use in finite element models, a range of values for the properties are applied and the best fit data is verified later by the experimental results. This method requires enhanced computational resources as one needs to assume a wide range of the starting values for each quantity that is unknown. To assist the modelling, some assumptions normally have to be applied as well. For instance, in many studies it is assumed that there is no premature brittle failure of diamond before it reaches its elastic limit [58].

3) Another method used when there's a lack of the material property data is, instead of trying to predict when and where the anvil cell will fail under a specific load, to compare different experimental configurations using nominal or simplified representative strength and modulus data. This allows the determination of the optimum configuration which can potentially achieve higher pressure. This method does not give direct prediction of the maximum pressure attained for a particular cell but by doing a comparative study, it provides valuable information about how the device should be constructed and how to improve the performance of the device.

2.3.4 Diamond Anvil Cell (DAC)

Most of the finite element studies in the high-pressure science are focused on improving the reliability of the Diamond Anvil Cell (DAC) in order to achieve the highest possible pressure. In many cases, brittle failure of the diamond before the plastic deformation is found to be accountable for failure in the anvils, and the causes are identified as excess of shear stress or tensile stress at the critical locations [58, 59, 60, 61 and 62]. There are a number of design parameters that can be tuned in order to minimize these destructive stresses/strains in the anvils, and eventually to increase their working lifetime and the sample pressure attainable.

1) Bruno *et al.* in [58] describe the results of the finite element analysis performed on an assembly of a brilliant cut diamond anvil and a metal gasket up to 21 GPa. The investigation of the stress distribution included compressive vertical stress, compressive radial stress, compressive hoop stress and octahedral shearing stress. It demonstrated that chipping at the edge of the anvil face as a result of high shear stress was the most likely cause of the failure. The use of a bevelled angle tended to reduce the high shear stress near the edge and an optimised bevelled angle of 15 degrees gave the optimum stress distribution. In the model, it was assumed that there was no premature brittle failure of diamond before it reached its elastic limit and a perfectly cohesive interface was applied between the diamond and metal.

2) Two publications by W. C. Moss [59, 63] between 1986 and 1987 reported on a finite element analysis of the diamond anvil cell that allowed the researchers to achieve 4.6 Mbar experimentally. It was the highest static pressure at the time. The model shows double bevelling can improve the results and maintain the stability of the sample and high yield strength and good ductility of the gasket material are desirable in order to reduce the shear stress and avoid fracture at the same time. In the simulations, there is significant 'cupping' of the diamond anvil face, the diamond tips come into contact in an annulus at the outer edge of the tips and failure probably initiates as a result. By optimizing the anvil tip geometry and the gasket material properties, it is possible to make sure ultimate failure of the DAC occurs in the diamond by tensile fracturing or plastic flow instead of the contact of the opposing diamond tips.

3) In [61] David Adams and Andrea Shaw carried out a computer-aided design study of stress patterns in diamond anvils in high-pressure optical and x-ray cells. In the model, the largest compressive and shear stresses are near the working face of the anvil where the plastic flow begins and they limit the performance of the anvils. In another report by D. M. Adams *et al.* [62], the author calculates the maximum principal tensile stresses in the lower half of the diamond anvil with Young's modulus, Poisson's ratio and some geometrical parameters varied. The basal tension appears to be accountable for many experimental failures as diamond is an extremely brittle material and liable to failure by cleavage in tension. Theoretically, brittle failure can occur well before the onset of plastic deformation. However, the stress concentration can be minimized if the conical light port is made with the semi-angle between 25 and 30 degrees.

4) S. Merkel *et al.* present a model of the diamond anvil cell (DAC) at megabar pressures [64]. It uses different curves to represent the pressure dependence of the

yield stress of the gaskets and the results show a strong dependence on the assumed properties of the gaskets. The plastic-elastic finite element model proves to be sufficient for understanding the behaviour of the anvils in diamond cells. It is possible to use the model to reveal the origin of the remarkably large elastic tensor strains in diamond observed at multi-megabar pressures. This explains some x-ray observations that image the deformation of the diamond tip.

5) As discussed above, gasket materials have long been recognized as a crucial factor in the performance of the anvil cells. In [65] by V. I. Levitas, the deformation of a gasket in diamond anvils is investigated in great detail, taking into account the effect of high pressure and large elastoplastic strains for the material. A procedure is developed and implemented in a finite element method to look into the properties of the gasket with a stepwise iteration algorithm. Hardened stainless steel T301 and pressed lithographic limestone are considered and evaluated as the material for the gaskets. The study simulates T301 in compression by a factor of eight (pressure ~24 GPa) and lithographic limestone by a factor of 5.8 (pressure ~50 GPa). The results provide insights into the material properties with deformation by pressure in the megabar range and were used to optimize conditions for generating ultrahigh quasistatic pressures.

6) In another publication by V. I. Levitas [66], stress distribution in deformable gaskets of high-pressure toroidal dies is studied by using a so called 'Ductility' program. The program is developed for mechanical analysis by means of constructing slip line fields instead of finite element calculation.

   The model has four components: reactive charge, container, die and deformable gaskets (Figure 2.17) and it is assumed that the gaskets are entirely in ductile state and the dies are perfectly rigid. The cylindrical system of coordinates *rθz* has four equations for determining the components(σ_z , σ_r , σ_θ , $\tau = \tau_{rz}$) of the stress tensor$\bar{\sigma}$: two equilibrium equations, the Coulomb ductility condition, and the complete ductility condition. By solving the equation matrix in the program by the slip line method, results are obtained for a container made of pressed lithographic stone. Figure 2.18 illustrated the slip line field in the container for a one-recess system. It concludes that the contact friction is largely dependent on the geometry of the plastic deformation centre and not just the surface quality and this friction in turn could affect the established pressure. An increased friction results in increased pressure. However, the model fails to observe qualitative differences in the model for multiple-recess systems.

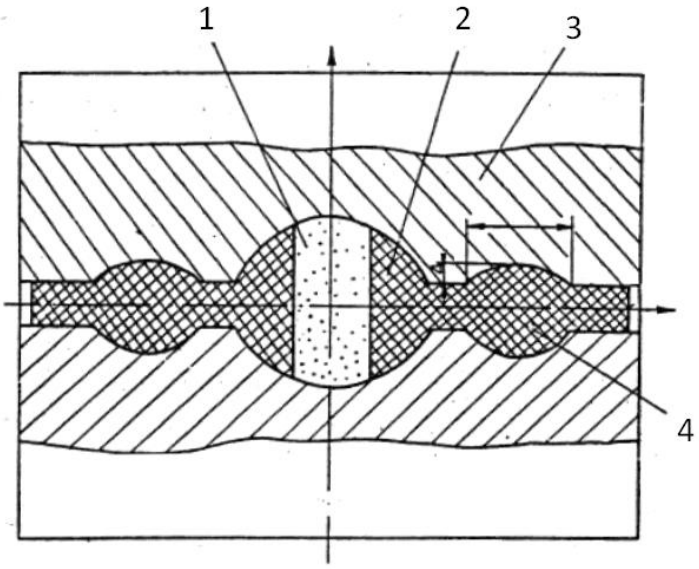

Figure 2.17 The diagram of the toroidal high-pressure arrangement used in the simulation (from [66]): 1) reactive charge; 2) container; 3) die; 4) deformable gaskets.

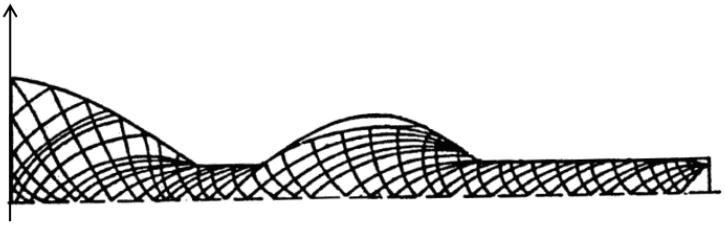

Figure 2.18 The slip line field in the container for a one-recess system (from [66]). Only a quarter of the geometry is shown.

2.3.5 Other Studies

Compared to the analysis of the DAC, the finite element analysis of the double-toroidal anvil assembly features large-volume sample enclosed between soft gaskets, large anvils made of sintered diamond and/or tungsten carbide, and much more complex geometry profile on the anvil surface. Some of the previous simulations performed on systems of similar scale and complexity are summarised below:

1) Standard/Modified Paris-Edinburgh Press and components

In terms of the finite element calculations of large components in the high-pressure field, the Paris-Edinburgh press is a structure that has been extensively studied. Most of these theoretical studies are focused on the press frame [4, 28, 29 and 31] in order to make the cell as compact as possible for use in time-of-flight neutron scattering facilities. The analysis includes calculation of the extension of the tie rods, the deformation of the bottom platen (to ensure the hydraulic ram was to work properly), the strength of the artillery threads, to name but a few. Unfortunately, publications systematically reporting finite element modelling at the development stage of the design process are not available.

Finite element analysis was later also used for further developments of the Paris-Edinburgh press and relevant experimental techniques. In 2004, [47] by S. Klotz *et al.* reports on the design of a two-column compact hydraulic press provided with large window openings for observation. The use of finite element calculation was crucial in designing the cell. Proper choices of mesh and element types in the codes are carefully made to refine the solution and ensure convergence.

In 2005, [37] by C. L. Bull *et al.* reports a modified design of toroidal anvils based on standard Paris-Edinburgh cells to achieve greater angular access for single-crystal neutron scattering. Finite element calculations were performed on the design and showed that the inward pressure of the binding ring is able to maintain the integrity of the anvil when the proper bevel angle is used. As a result, the total accessible aperture is increased from 14 degrees up to 40 degrees for pressure up to ~8 GPa when WC single-toroidal anvils are used.

2) Large anvil/gasket assembly with enclosed sample.

There are several reports on finite element analysis of the large-volume Cubic-anvil High-pressure Apparatus (CHPA) in recent years. Listed below are three of them related to a commercial design of the apparatus for the synthesis of diamond in China. They have focused on either the pressure distribution, shear stress or the holistic design with the view to increase the diamond production. The CHPA is an assembly of six anvils and pyrophyllite gaskets with the sample contained inside. The 3D FEA models in these papers are applied to one-eighth of the apparatus to reduce calculation requirements (Figure 2.19).

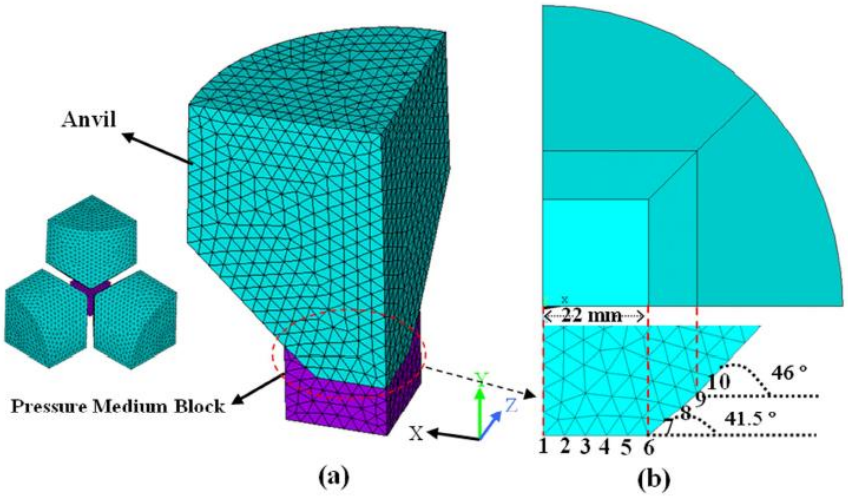

Figure 2.19 The finite element model uses an eighth of the apparatus for simulation in order to reduce computing demand (from [67]).

(a) Assembly of the anvils and the pressure medium block.

(b) Zoom-in view of anvil and the local mesh.

R. Li *et al.* describe the pressure distribution in a pyrophyllite high-pressure cell in the range of 6 GPa and 1800K [67]. ANSYS/LS-DYNA [55] is used to simulate the plastic deformation and volume compression of pyrophyllite under load. In the cubic-anvil system, pyrophyllite powder is compressed to be a block with a size of 55 mm $\times$ 55 mm $\times$ 55 mm and serves as pressure-transmitting medium. The tungsten carbide anvils have a size of 44 mm $\times$ 44 mm $\times$ 44 mm with the elastic modulus of 650 GPa and Poisson's ratio of 0.3. The model uses non-linear contact with a frictional coefficient of 0.7, and penalty method algorithm with contact stiffness of 0.6 and contact surface penetration of 4. Also, non-linear geometry and material properties are applied. Tetrahedron and hexahedron elements are applied to the anvils and the pressure medium respectively when the mesh is generated. The simulation results indicate almost 90% of the pressure in the pyrophyllite cell is isotropic hydrostatic pressure.

Q. G. Han *et al.* compute the limiting shear stress of cemented tungsten carbide anvil using the 3rd theory of mechanical strength [68]. In the model, cobalt cemented tungsten carbide is with a yield strength of 5.2 GPa and the Poisson's ratio is 0.185.

20-node brick elements are used in the mesh. The results show that the limiting shear stress is 2.65 GPa in tungsten carbide anvils. This is validated by experimental results.

In [69] Q. G. Han *et al*. focus on the design of the apparatus. Its objective is to achieve desirable pressure and temperature in the cubic chamber and therefore improve the quality and quantity of synthesized diamond. A double bevelled anvil of the large-volume CHPA is developed with several parameters tuned to give optimum performance. The new apparatus widens the zone of synthesis of high quality diamond crystals on the pressure – temperature phase diagram.

Chapter 3

The High-Pressure Rotational V4 Paris-Edinburgh Press for Single-Crystal Experiments (RV4)

In this chapter a new type of high-pressure device based on the V4 variant of Paris-Edinburgh press is described. It is capable of rotating an anvil assembly under an axial thrust load of 100 tonnes, and is referred to as the RV4 or the rotator. The state-of-the-art press is designed and built for high-pressure single-crystal studies on neutron diffractometers where an increased equatorial angular aperture is of particular benefit to the measurements. The structural design and key techniques are described in detail here while the off-line and on-line testing of the press will be presented in Chapter 4.

Section 3.1 outlines the general specifications of the RV4 as a high-pressure instrument for neutron scattering experiments on large-volume single-crystal sample. Its technical specifications and the requirements it was designed to meet are discussed.

Section 3.2 describes the mechanical structure of the two versions of the RV4 design. The RV4 consists of two major assemblies – the central structure and the side structure.

Section 3.3 looks at individual components. The key aspects such as the materials, mechanical performance and design calculation are specified in detail.

Section 3.4 gives a brief description of the components from a dynamic control's perspective. Most relevant is the control, electronics and the operation of the motor.

3.1 General Specifications

We have developed the RV4 system – a high-pressure device capable of rotating the two anvils simultaneously (Figure 3.1). The portable device is primarily designed for performing high-pressure experiments on the large-volume single-crystal samples at neutron-scattering facilities.

To clarify the naming convention, we refer to the rotational press that is developed with some modifications to the V4 Paris-Edinburgh press as the RV4 press. When the RV4 press is used with the anvil assembly, it is referred to as the RV4 cell. When the RV4 cell is connected to the hydraulic pump and the electronic control module, the whole assembly is referred to as the RV4 system.

This section gives an overall description of the RV4 system as a high-pressure rotational apparatus for use at neutron facilities. These functional aspects of the RV4 are discussed with the technical requirements it was designed to meet.

3.1.1 The RV4 system at a Glance

The RV4 press uses all the standard components of the V4 P-E press apart from the tie-rods which have been extended to accommodate the rotation mechanism. The rotation mechanism has a two-fold function – it provides the torque acting on the anvil assembly inside the press and supports it in order to preserve the alignment of the anvils during the rotation. The press is also connected the electronic controller and to the hydraulic pump (Figure 3.1).

Figure 3.1 The RV4 system on an assembly stand in the workshop. The system incorporates the RV4 press, the hydraulic pump and the electronic control.

The RV4 system is designed in such a way that its functional and technical aspects meet the requirements set out by the objectives of the project. To fulfil the need of providing a rotation at high-pressure for neutron-diffraction measurements at large-scale facilities, its general specifications are customised in terms of the load capacity, the compatible anvil types, the size and weight aspects, the rotation dynamics, the positioning precision etc. The rest of this section provides their detailed description. Some relevant information in the context can be found in Section 2.2.3 where the proposed design of the RV4 is compared with the existing high-pressure rotational systems with regards to the functional and technical requirements.

3.1.2 Load Capacity

The RV4 is designed to achieve a greater dynamic load capacity than the existing high-pressure rotational systems which have a load capacity in the range of 25 tonnes to 35 tonnes.

The rationale behind this is to attain higher pressure on larger-volume samples. As it has been mentioned already, the samples used in neutron-diffraction measurements are relatively large in size – mainly because of the intrinsically low brightness of the neutron source and the small scattering cross-sectional area of a material to the neutron beam. Ideally it should be capable of rotation at an applied load of at least 100 tonnes in order to match the load capacity of the single-toroidal anvils. This will allow the pressure in the range of 10 GPa to be produced on a sample of a reasonable volume.

To date, it has been demonstrated that the RV4 is capable of rotating simultaneously two full-size opposing toroidal anvils whilst maintaining an axial load of 100 tonnes.

3.1.3 Rotational Dynamics

The way the RV4 rotates the anvils is the most important factor in protecting the gasket and the sample. The RV4 system rotates the pair of anvils in the cell assembly simultaneously at the same rate. The two anvils have the same speed and run in the same direction (either clockwise or counter-clockwise).

The reason is to maintain the hydrostatic conditions in the sample and make sure that there are no significant shearing effects on the sample and the gasket assemblies. Single crystals are very fragile. Under very high load if the loadings are not homogeneous or the

surrounding pressure is non hydrostatic, the crystal can be twisted or damaged easily. If there is a difference in the rotation direction or speed between the upper and lower anvils, the crystal might be broken.

Even if the crystal is not damaged or destroyed, twisting to a certain extent due to the shearing stress between the horizontal cross section through the sample will introduce changes to the sample position and alter the matrix of the atomic lattice of the sample. This would compromise the accuracy of the measurement and the original motivation of these measurements.

In the RV4, *in situ* neutron-diffraction measurements showed that it maintained the integrity of sample after rotation under applied load (more details in Chapter 4).

In terms of the rotation pattern, the system is required to be able to complete a rotation of 180 degrees in a continuous run. A complete set of structural refinement measurement may require a series of repositioning moves for the sample. On D9 for instance it may need to complete about dozens of runs in 20 – 30 minute intervals. In each run the rotation is no greater than 180 degrees. Normally each run should be completed within a few minutes as to not waste the valuable beam time. At the moment, the RV4 is set to be rotating at a speed that takes approximately 2 minutes to turn by 180 degrees.

3.1.4 Anvil

The RV4 is expected to be compatible with various toroidal anvils including both single-toroidal anvils (Figure 3.2) and double-toroidal anvils (Figure 3.3).

The single-toroidal anvils can be bevelled to either 7 ° or 20 °. They are normally made of tungsten carbide (WC). The WC anvils are supported by a binding ring made of 819AW grade of maraging steel fretted around the anvil to provide hoop stress support. An anvil seat made of tungsten carbide is used on the back of the anvil to provide support in the axial direction. Figure 3.2 shows the setup of single-toroidal anvils with anvil seats and binding rings.

A sintered-diamond double-toroidal anvil consists of two parts: the core die made of polycrystalline diamond (PCD) and a supporting ring made of tungsten carbide (WC). Figure 3.3 shows the cross section of the double-toroidal anvil. In the anvil from the centre outward the dark piece is the PCD core of the anvil, the medium dark ring is the WC supporting ring of the anvils.

These types of anvils have been tested and are compatible with the RV4.

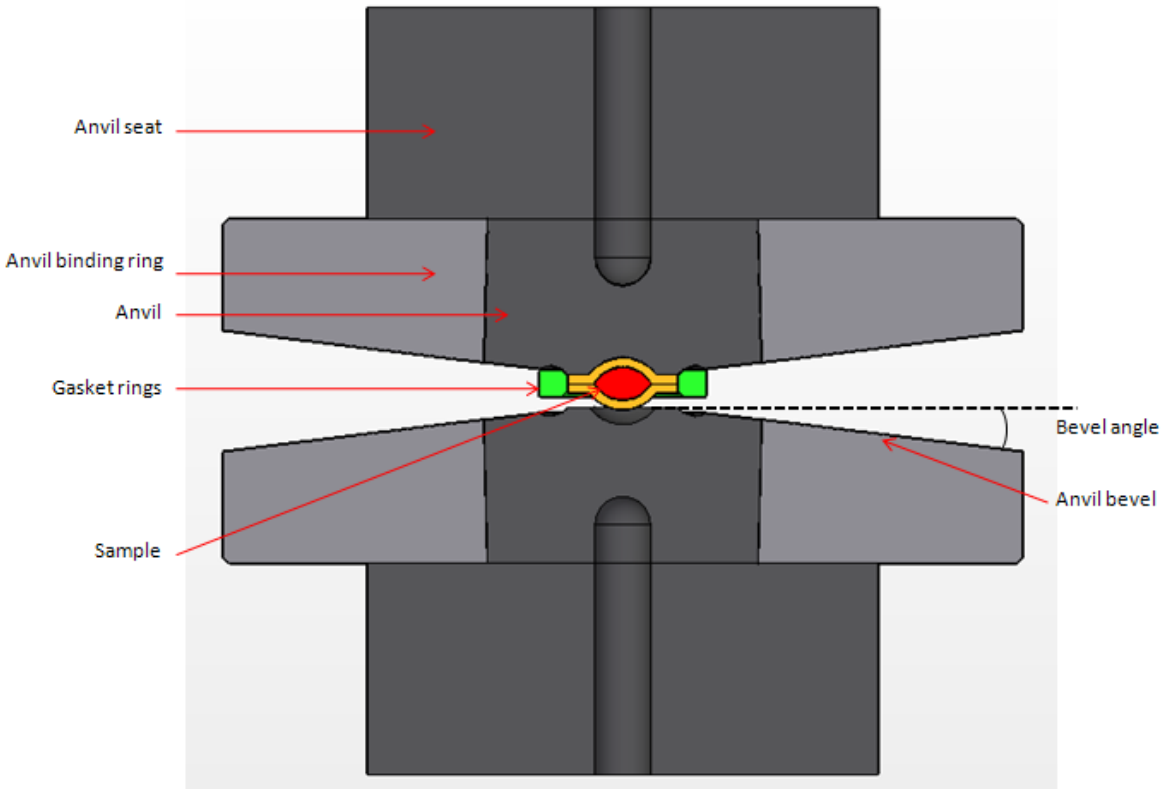

Figure 3.2 Cross-sectional view of the single-toroidal anvils with gaskets, sample, binding rings and anvil seats (after [37]). The anvils are surrounded by binding rings made of high-strength maraging steel. There are three pieces in the SME gasket.

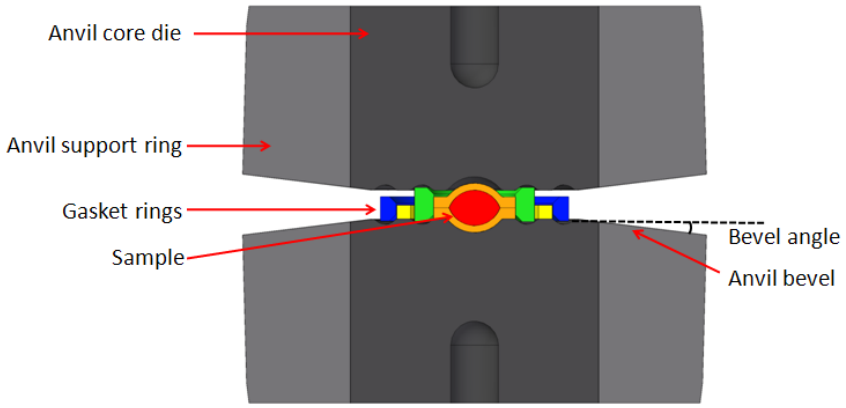

Figure 3.3 Cross-sectional view of the polycrystalline diamond double-toroidal anvil with gasket rings and sample (after [37]). The anvil has a 7° bevel. The core die is made of sintered diamond and the anvil support ring is made of tungsten carbide. There are five pieces in the SME gasket assembly. The anvil binding ring and anvil backing seat are not shown.

3.1.5 Size, Weight and Sample Position

The RV4 is required to fit into the sample tank on SXD (ISIS) and the mounting table on D9 (ILL) and should be light enough to be lifted by a small crane installed on site. For this reason, the RV4 press is based on the standard V4 Paris-Edinburgh press frame with extended tie rods and optimized using finite element analysis. Its mass is approximately 126 kg and the size is 479 mm × 267 mm × 200 mm (Figure 3.4).

In terms of the sample position, as the positions of the incident beam and sample environment support platform are fixed, the structure is also designed to ensure accurate alignment of the sample position relative to the incident beam. This requirement significantly constrains the size of the device and the layout of its structure. The distance between the sample and the top edge of the press should not be greater than 208 mm. This is the requirement for both the D9 and the SXD instrument platforms. In fact this distance in the RV4 is approximately 203 mm (Figure 3.4). The mounting position is such that the breech is at the bottom side and the ram is at the top side, as illustrated in Figure 4.10 in Section 4.3.

3.1.6 Positioning Precision & Resolution

The basic requirement in the positioning precision of the rotation in the RV4 is that it would not affect the effectiveness of collecting diffraction patterns and resolving the atomic structure in the high-pressure neutron scattering experiments.

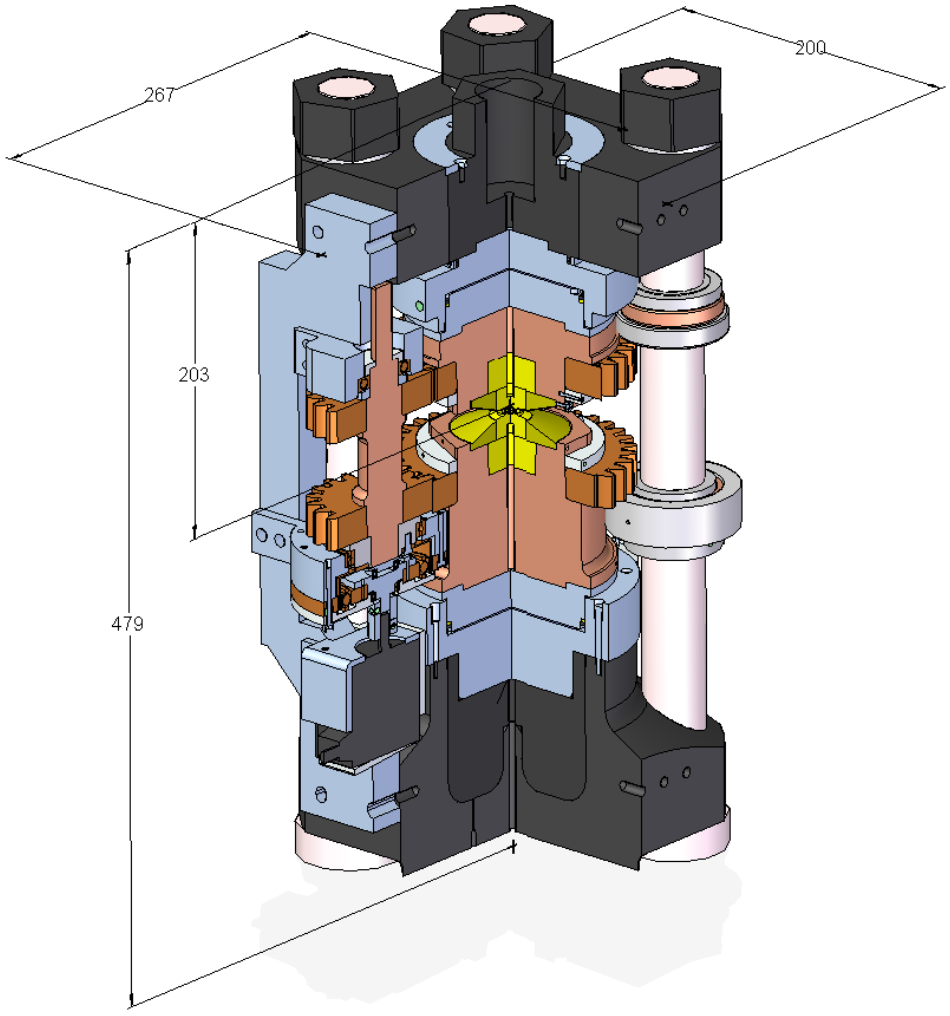

Figure 3.4 The dimensions of the RV4 press and the position of the sample relative to the press. The press is 479 mm in height, 267 mm in length and 200 mm in width. The sample position is 203 mm from the top end of the press.

As discussed in Section 2.2.3, the target error in the rotation should be limited to less than 0.5 º. In the proposed open-loop control mode, the positioning is controlled by the stepper motor's output and a home sensor is used as position reference. The positioning error is determined by the error in the various components along the power train. When the RV4 uses the home sensor as the reference starting point for each re-positioning move and only moves in the same direction (i.e. clockwise or counter-clockwise), it is estimated that the error is around 0.08˚. The major sources of the error originate from the twisting angular deformation of the side shaft, the hysteresis loss in the gearbox and the mating error in the

gears. However it is assumed that there are no misalignment and tilting in the central shaft (see Section 3.2.2 for the definition of the central shaft; more discussions on this issue are in Section 4.1 and 4.2). It has been demonstrated by neutron experiments that the rotation of the RV4 under applied load maintained the effectiveness of the neutron-diffraction measurements (more details in Section 4.3).

The RV4's rotation resolution is determined by the resolution of the stepper motor and the reduction gearing system. The stepper motor has a resolution of 0.36˚ per step which translates to 0.00135˚ in the anvils with the total reduction ratio of 800:3.

To improve the performance, a close-loop control with high-resolution feedback can be applied if an encoder is used (detailed in Section 6.2).

3.2 Mechanical Structure of the RV4

During the development of the RV4, there were two versions of the design.

The prototype – the 1st version was the original design developed by October 2008. It made use of the original calculation of the frictional resistance generated in the mechanical thrust bearings (SKF 29412E). The construction work of the 1st version including ordering of the components, manufacturing of parts and assembly started in October 2008 and was completed in June 2009. The RV4 was then tested in the workshop and used in an experiment on the D9 instrument at ILL. The tests and trials indicated a larger-than-expected frictional torque in the bearings when the applied load was above 25 tonnes. For this reason, some structural modifications were made to address this problem and the RV4 design evolved into the 2nd version.

The revised design – the 2nd version was built and tested between June 2009 and March 2010. The major modification compared to the 1st version was the use of two sets of custom-designed hydraulic thrust bearings in replacement of the mechanical roller bearings (detailed description of the design is in Section 3.2.5). Other changes were the enhancement in the anvil support mounted on the tie rods (Section 3.2.6) and a new solid coupling for the motor shaft which replaced the original flexible coupling. Detailed description of the testing and subsequent structural modification is presented in Chapter 4.

Pictures of the two versions of the RV4 assembly are shown in Figure 3.5 and sectional views of the two versions of the design are illustrated in Figure 3.6. A right-angle cut view of

the 2nd version of the RV4 is also presented in Figure 3.7. The components are labelled in the figures.

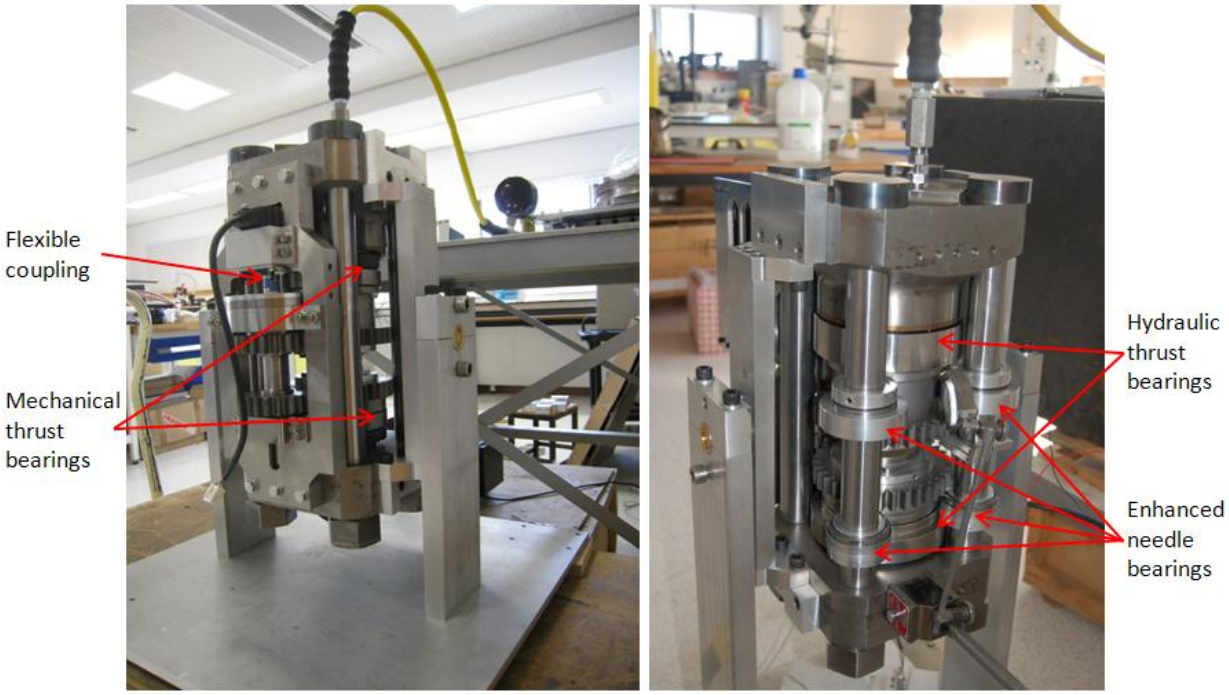

(a) *(b)*

Figure 3.5 Photos of the RV4 assembly in the workshop.

(a) The 1st version of the RV4 with spherical roller thrust bearings.

(b) The 2nd version of the RV4 with hydraulic bearings.

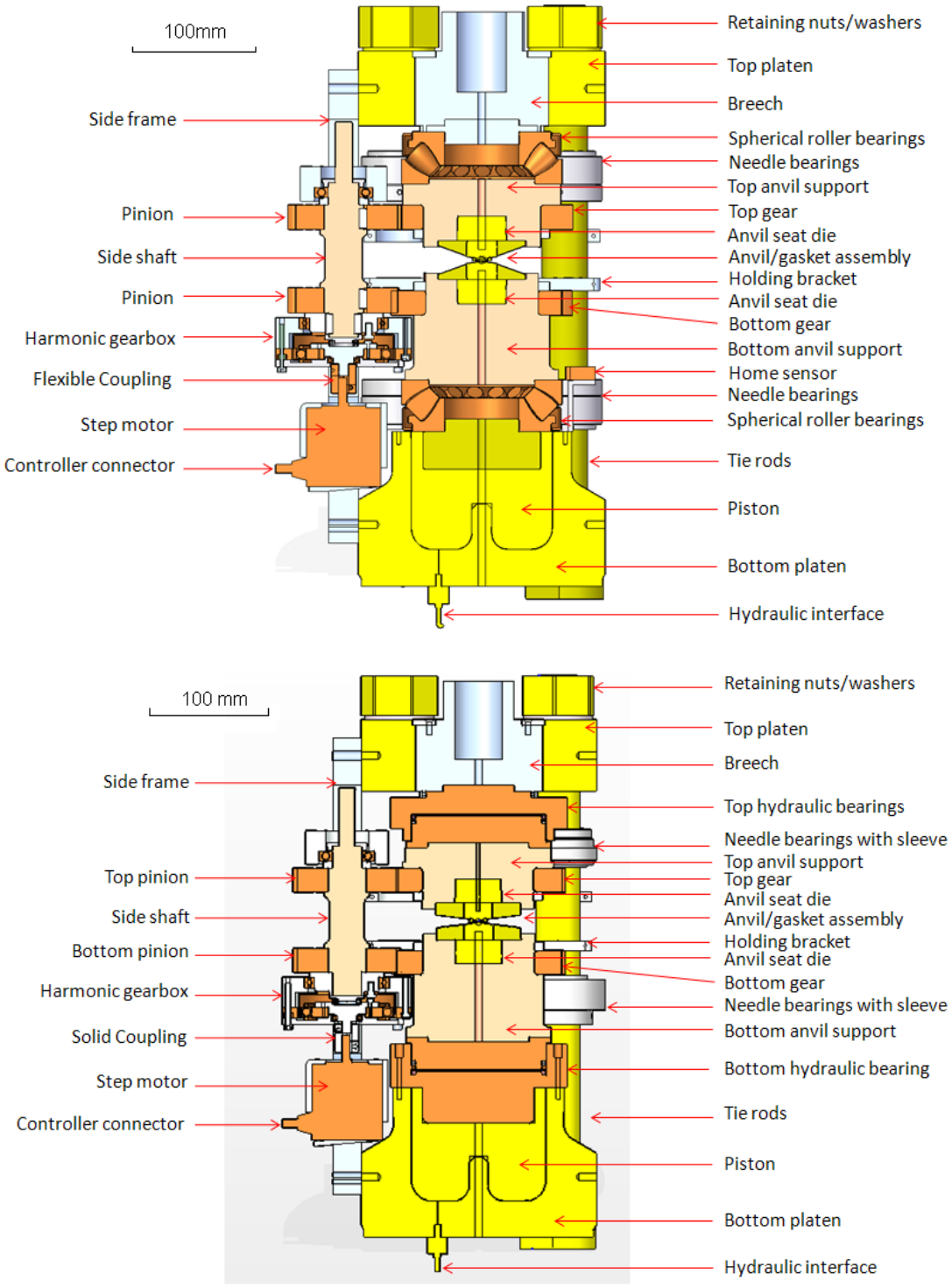

Figure 3.6 Sectional views of the two versions of the RV4 design.

TOP: the 1st version with spherical roller bearings (mechanical thrust bearings) and flexible couplings. BOTTOM: the 2nd version with hydraulic rotational bearings (thrust bearings), solid couplings and sleeve-encased needle bearings. Note the home sensor is not visible in this sectional view.

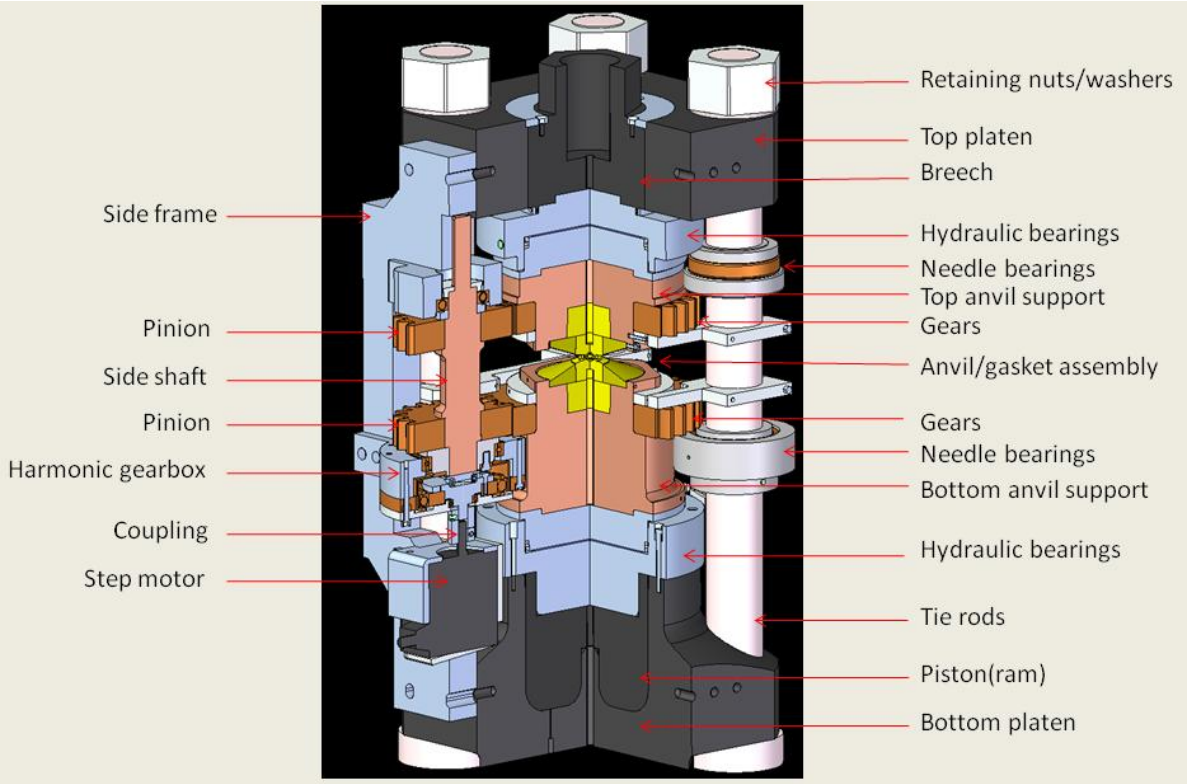

Figure 3.7 A right-angle cut view of the latest version (2nd version) of the RV4.

3.2.1 Sub-structures

For both versions, the RV4 design can be divided into three sub-structures. They are the central structure – a modified V4 Paris-Edinburgh press with rotational support module, the side structure that supports torque generation and gearing mechanism, and an assembly stand used for installation and off-line mechanical test of the press.

- The central structure. The central structure is the assembly that transfers the axial load generated by the hydraulic press and also rotates along with the anvil assembly under this load. To fulfil these functions, it consists of the mainframe (including the hydraulic ram), the rotational central shaft, the main rotational support bearings and the anvil assembly.

- The side structure. This is a gearing mechanism that provides large power torque for driving the rotation of the central shaft. It consists of a motor, a gearbox and a side shaft with two pinions that are coupled with gears on the central shaft.

- The assembly stand with wheels (Figure 3.8) is built to facilitate the assembly of the RV4 and other operations, such as sample preparation, off-line mechanical/electronic tests, the inspections and mobility of the RV4. The stand is a trolley with holding arms and other mounting elements. The RV4 press in the stand can be fixed and secured in position or rotate freely to switch between different positions such as normal position (top – bottom), reverse position (upside down) and horizontal position. In addition, a shielding plate is also made to protect users from potential hazards caused by a loaded press. Previous experience using the standard Paris-Edinburgh cell showed a possibility of the gasket and the sample assembly breaking and exploding under applied load, although it only happened on very rare occasions.

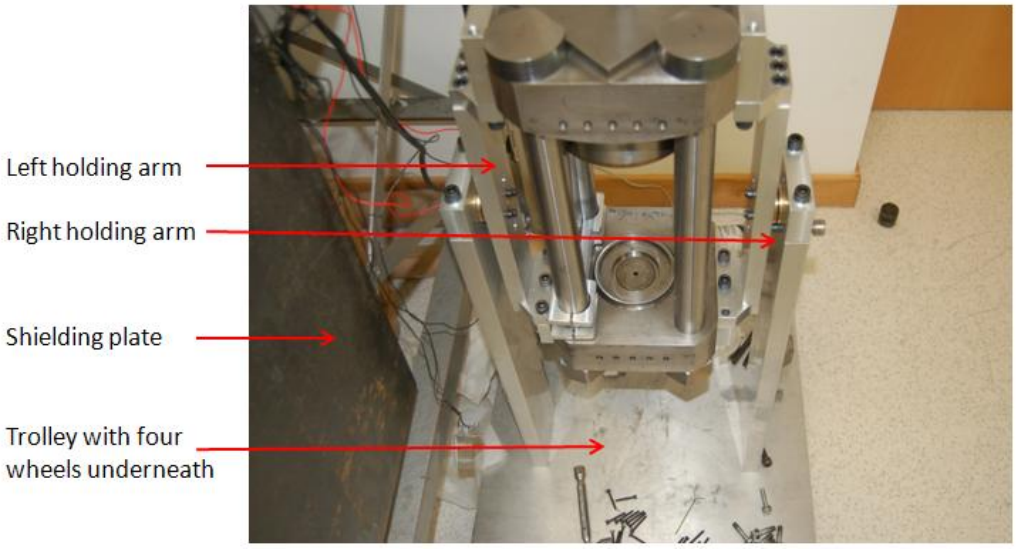

Figure 3.8 Photo of the assembly stand with the RV4's press frame. The stand is based on a wheeled trolley. A shielding plate on the left side of the picture is for protection of users during the tests and use of the press.

The following sections describe in full detail the central structure and the side structure. Then the power train through various components will also be discussed. Some discussions regarding the design process are presented towards the end, including the design of the hydraulic bearings, the alignment arrangements, etc.

3.2.2 The Central Structure

The central structure (Figure 3.9 and 3.10) incorporates rotational modules into the loading frame of the standard V4 P-E press. The modules incorporated into the frame are the thrust bearings and the gears. The bearings provide rotational support for the axial thrust. The gears transmit the torque from the pinions on the side shaft to the central shaft for rotation. In addition, some auxiliary components are also installed, such as the holding brackets, sensor assembly, etc.

- The frame

  The central structure (Figure 3.10) is based on an extended mainframe of the V4 variant of the standard Paris-Edinburgh press. The frame is the principal element of the standard press that allows large hydraulic loading capacity. It consists of the top platen (including the breech), the bottom platen (including the hydraulic ram) and the tie rods.

  To accommodate the extra height required for the thrust bearings, gears and shafts, the tie rods have been extended in length. The modified tie rods are made of heat-treated 819 AW steel and are 70% longer compared to the standard ones of the V4 press. Finite element analysis suggests that under 150 tonnes the tie rods will experience an axial elongation of less than 1 mm (the static structural analysis on the tie rods is included in Section 3.3).

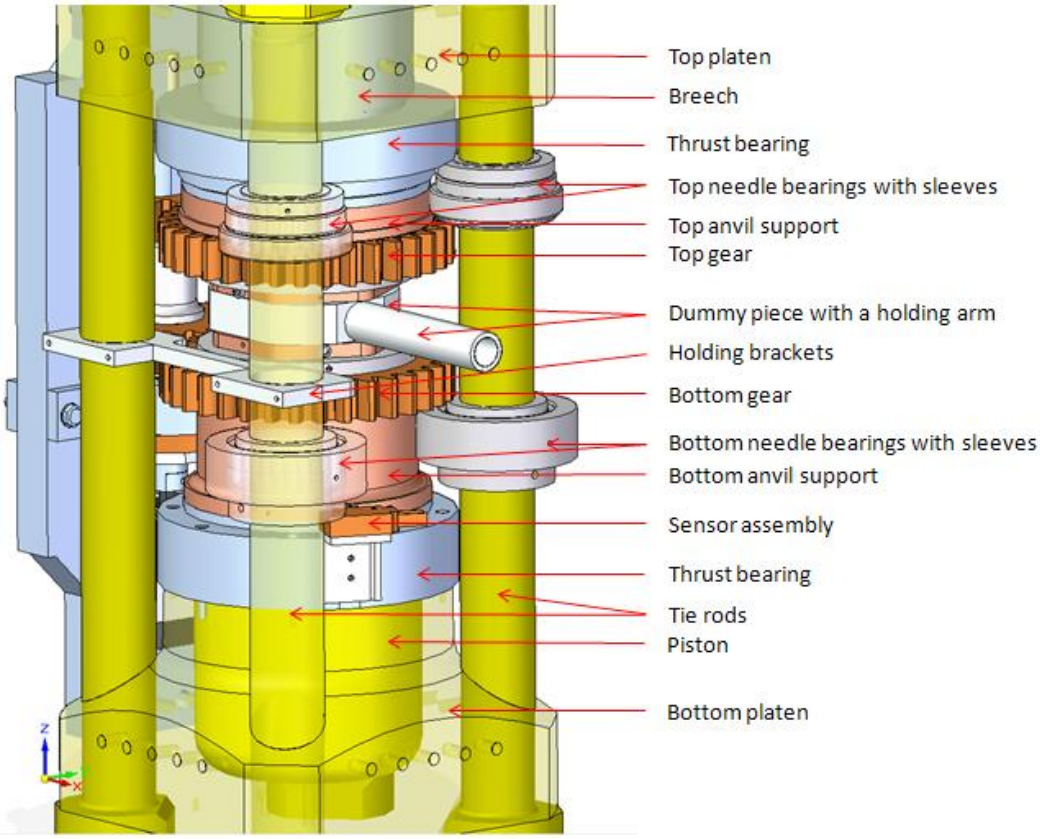

Figure 3.9 A view of the central structure and the components. The central shaft includes the top shaft and the bottom shaft with an anvil assembly (not shown) or a dummy piece (which was used in some off-line tests instead of the anvils) in between. Components such as the sensor assembly, the needle bearings and the holding brackets are also installed. The top and bottom platens, one tie rod, two needle bearings are made 'glass' in the figure for better view of other components. Only one out of the four holding bracket sets is shown as well.

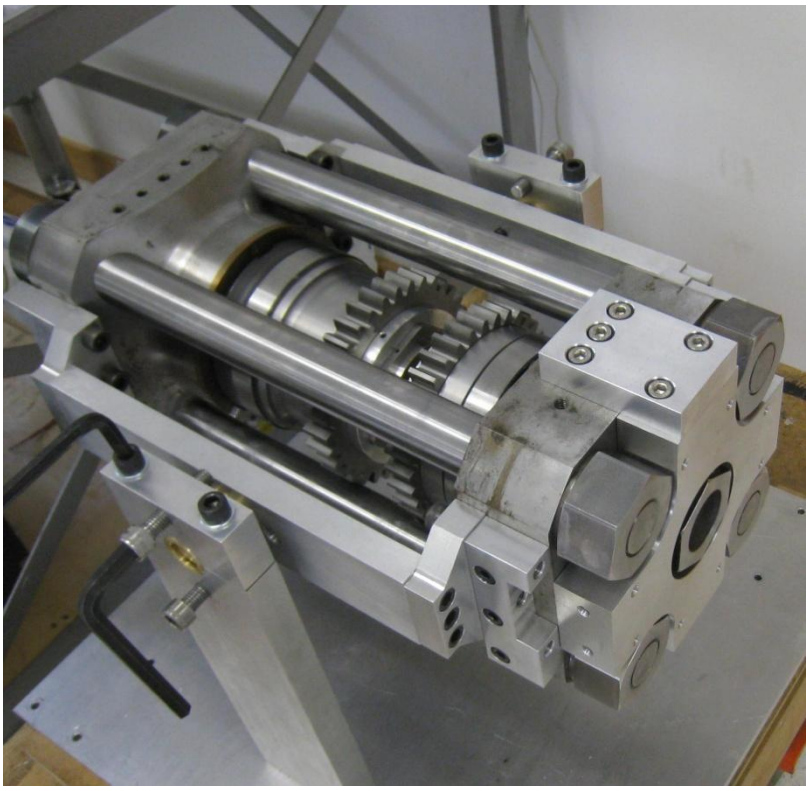

Figure 3.10 Photo of the central structure in horizontal position on the assembly stand. The press shown in the figure is the first version of the RV4 design.

- The central shaft

  As illustrated in Figure 3.11 attached to the breech on the top end of the press is a set of thrust bearing that carries the axial load. The thrust bearings mentioned above are mechanical spherical roller bearings – SKF 29412E in the first version of the RV4 and custom-made hydraulic bearings in the second version of the RV4. They are both compatible with the connecting parts in terms of the size and geometry. Details of the design and analysis of these bearings are presented in Section 3.3.5. Details of the test and use of these bearings are explained in Section 4.2.

  Below the thrust bearing is the anvil support. The anvil support is manufactured from high-performance maraging steel and has a complex shape (the simulation of its mechanical performance is described in Section 3.3.4). Also mounted on the anvil support are a gear, a gear guide ring and an anvil seat. The gear is a 35 teeth spur gear with a module of 4 mm (detailed in Section 3.3.7). It is mounted on the anvil support with a hexagonal profile and secured in the axial direction by the guide ring. The

anvil seat is fretted into a cylindrical cutout in the anvil support. This tungsten carbide (WC) piece is to sustain a very large axial load exerted on the contact surface by the anvils.

The anvil support and these components essentially form the top half of the central shaft or the anvil shaft and thus are sometimes referred to as the top shaft. Similarly, on the bottom side of the press the other set of hydraulic bearing is mounted on the top surface of the piston and connects to the other anvil support assembly. This anvil support assembly is referred to as the bottom shaft.

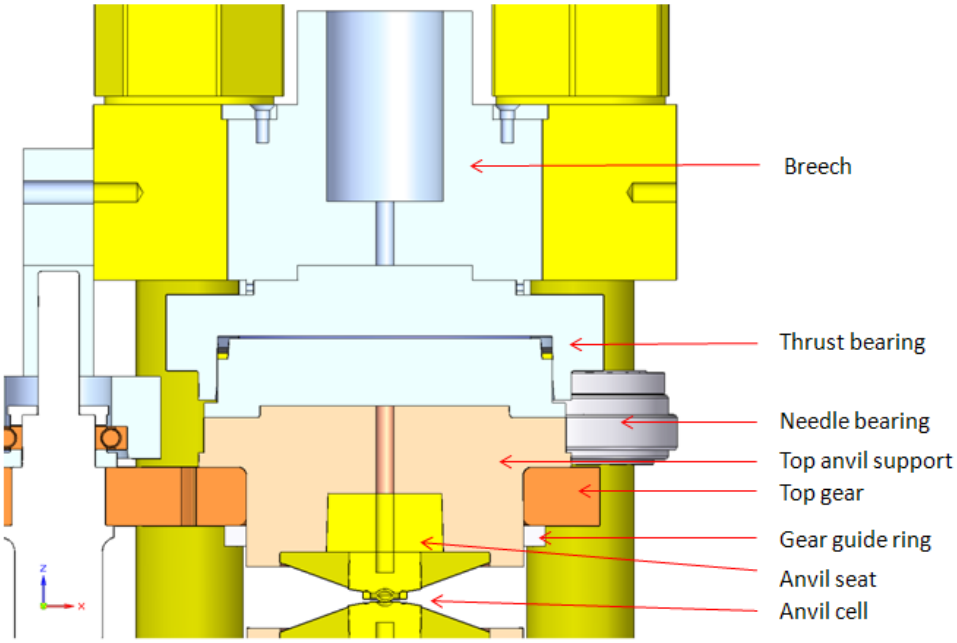

Figure 3.11 The drawing of the top shaft with adjacent components. The thrust bearing shown is a set of hydraulic bearing used in the 2nd version of the RV4 (a spherical roller bearing was used in the 1st version). The needle bearing installed on the tie rods is for radial support of the top shaft.

- Other modules.

  As illustrated in Figure 3.9, other components such as a dummy piece, the needle bearings, the sensor and the holding bracket are also installed in the central structure.

The anvil assembly is mounted between the top and bottom anvil supports. The space between the anvil supports is slightly larger than the anvil assembly in height to allow more space for the inserting of the anvils and gaskets. The gap is about 3.0 mm (more details with regard to the anvil, gasket and sample preparation are in Section 4.1 and 4.3). A dummy piece in thin 'pie' shape is inserted between the anvil supports in replacement of the anvils in some of the mechanical performance tests. The stainless steel piece is also used to help push the piston back to the starting position in the ram after the loading procedure. An extension holding arm is made to couple to the dummy piece for ease of handling, facilitating the insertion and extraction of the piece.

Needle bearings are mounted on the tie rods as radial constraints to the central shaft so that the misalignment between the top and bottom shafts can be reduced. It also helps stop the shaft tilting towards one side. More details on the design are in Section 3.3.6 and the misalignment and tilting issues are discussed in Chapter 4. In the first version of the RV4, there are eight needle bearings; in the second version, the needle bearings are enhanced by sleeves outside and only four of them are installed on the side opposite to the side structure.

The sensor is a Honeywell micro switch. It is installed on the bottom platen in the first version of the RV4 and on the stationary cylindrical housing of the hydraulic bearing in the second version. It is a constant-open-trigger-close mechanical switch. When a round stud on the rotational bottom anvil support passes by the switch, it triggers the switch and generates an electrical signal that can be read into the motor controller. The absolute position is thus established. The use of the sensor in the control operation is described in Section 3.4.

The holding brackets are made to hold the top shaft and the bottom shaft in place during the assembling of the cell. They are mounted on the tie rods and can be tightened by screwing. There are four sets, all of which are made of aluminium alloy.

3.2.3 The Side Structure

The side structure (Figure 3.12) is an independent assembly that can be mounted and removed from the central structure completely. It is designed to provide power for driving the central shaft to rotate in the press.

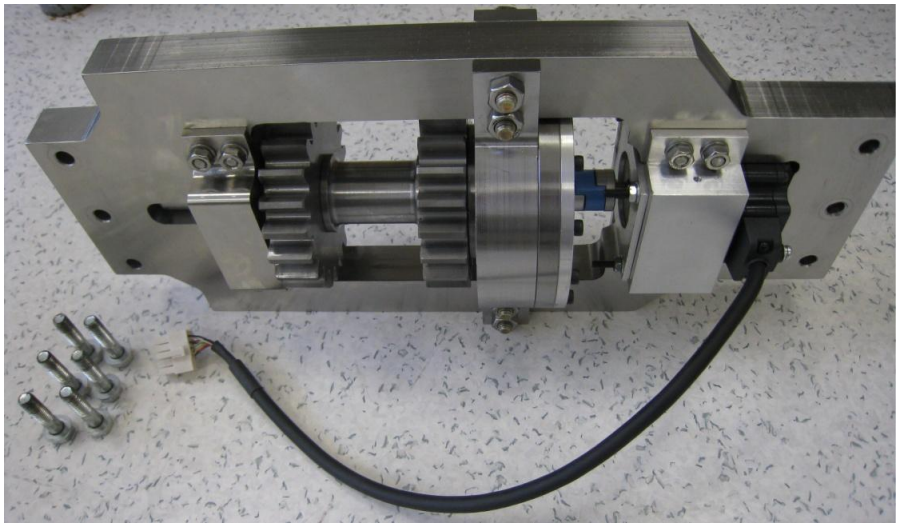

Figure 3.12 Photo of the stand-alone side structure. The side structure can be mounted on the central frame by six screws. Shown above is the first version of the design with a flexible coupling.

- Components

  The side structure transmits the power generated by the electric motor to drive two gears attached to the modified seats; meanwhile by applying a reduction mechanism, the power is increased along the power train while the rotation speed is reduced.

  The side structure is a flat frame with a series of power generation and gearing components mounted on it. The steel frame provides support for the motor, the gearbox, the side shaft, the pinions and accessional bearings. The AC stepper motor from *Oriental Motor Corp.* outputs a torque on its shaft which is linked by solid coupling to 160:1 ratio reduction gearbox by *Harmonic Drive AG* (the model's maximum output torque is 360 Nm). The resulting geared torque is then transmitted to the side shaft which has two pinions mounted on it and transmits the torque to the central hexagonally hollowed gears. These are two pairs of spur gears with the reduction ratio of 5:3. They are custom-made of EN36 steel and case hardened by *HPC Gears Ltd.* [71].

  It worth mentioning that in the first version of the RV4 a flexible coupling is used while the second version uses a custom-made solid coupling made. The original flexible coupling was a standard commercial product made up of three components,

but it did not provide sufficient rigidity, which resulted in excessive twisting under load and reduced efficiency.

- Torque generation and gearing.

  As shown above, the torque provided to drive the central shaft is supplied by the motor and then geared up by the gearbox and gear/pinion pairs. The motor provides no less than 1.3 Nm when turning up to 500 revolutions per minute. Conservatively taking into consideration the efficiency of various components along the mechanical transmission chain, it is estimated that the operational torque transmitted into the central shaft would be around 160 Nm. However when the motor is running at low speed or at the starting point, the maximum output torque is 245 Nm. If the case of no efficiency loss is considered, the maximum output torque is 373 Nm.

  The design calculation of the transmission train is included in Table 3.1:

	Motor	Gearbox	Side shaft	Pinions/Gears	Anvil shaft
Efficiency	100%	70%	90%	95%	98%
Transmission Ratio	1:1	160:1	1:1	5:3	1:1
Operational Input Torque(N)	1.0	1.0	112	108	171
Maximal Input Torque(N)	1.4	1.4	157	157	250
Operational Output Torque(N)	1.0	112	108	171	167
Maximal Output Torque(N)	1.4	157	157	250	245

Table 3.1 Estimated power input/output and efficiency of transmission components in the design.

3.3 Components, Materials & Mechanical Performance

In this section, the key components of the RV4 are described in full detail with the details of their function, materials and mechanical performance. There are four types of the components:

- Type 1: Original components in the standard Paris-Edinburgh press V4 variant, for example the top platen, the bottom platen, the breech, the hydraulic ram & piston. Some of them have been slightly modified for use in the RV4, such as the tie rods which have been extended. A view of the components in the V4 variant press is in Figure 3.13.

- Type 2: Integrated mechanical and electronic products purchased from the commercial suppliers, for example the stepper motor, the gearbox, the mechanical switch sensor, the radial bearings and the spherical roller bearings. Information on product specification is available in the Appendix B.

- Type 3: Components custom-made by outside suppliers, for instance the gears and pinions are made by *HPC Gears Ltd.* and the anvil supports are made by the *M.G. 63*. Components' mechanical calculations were carried out and the drawings with technical requirements were supplied to the companies for manufacture.

- Type 4: Workshop manufactured parts (drawings of key parts are available in Appendix D). Most of these components are made in the mechanical workshops of the Schools of Engineering and of Physics and Astronomy, University of Edinburgh. The technicians machined a number of parts, including the hydraulic bearings in the central structure, the side frame and supporting parts of the side structure, and most of the parts used in the assembly stand.

The major components in the RV4 are listed in Table 3.2 with general description of their functions. The following content describes these key components from a technical perspective. The exception is the anvil assembly which is fully described in Chapter 5 where its mechanical performance is investigated in depth. A full list of all the parts in the RV4 is in Appendix B with supplementary drawings in Appendix D and assembly instructions in Appendix E.

No	Part Name	Description and function
1	Top Platen/bottom platen	*Principal parts of the frame, connected to each other by the tie rods.*
2	Breech and breech centring rings	*Can be tightened to secure the central shaft and also provide locating centre reference.*
3	Tie Rods, nuts and washers	*Form the press frame with the platens.*
4	Anvils, gaskets and binding rings.	*This is the anvil assembly. It contains the experimental sample and transmits axial thrust to compress it to extremely high pressure. Descriptions of the assembly can be found in Section 2.3.2 and Section 3.1.4.*
5	Top anvil support Bottom anvil support	*Have multiple structural and dynamic functions as specified in Section 3.3.4.*
6	Thrust Bearings	*Provide main axial support for the central shafts in rotation.*
7	Needle bearings	*Help alignment of the central shaft and prevent the shaft from tilting towards one side*
8	Gears/pinions and keys	*Transmit and magnify the drive torque from the side shaft to the central shaft.*
9	Stepper motor	*Provide mechanical torque as a power source.*
10	Gearbox	*Magnify the torque from the motor and transmit to the side shaft*
11	Side shaft	*Transmit the drive torque from the gearbox to the pinions, support various transmission structural components*

Table 3.2 A list of the main components in the RV4 and their functions

3.3.1 Top and Bottom Platens

Both of the platens are original components of the V4 variant of the Paris-Edinburgh press manufactured by the company *M.G. 63* [72]. When assembled with the tie rods, the platens form the mainframe of the press body. They are made of maraging steel – 819AW alloy (35NiCrMo16 or BS: 835M30) which has a good dimensional stability and a high level of hardenability. The 819AW is supplied by *Aubert & Duval* [73] and heat-treated to full the hardness of 52 HRC. In the heat-treatment process, it is air cooled from 875 ℃, followed by sub-zero treatment at 80 ℃ for 2 hours and then tempered at 200 ℃ for 3 hours. After the

treatment, the material exhibits a yielding strength of 1500 MPa and an ultimate tensile strength of 1900 MPa.

The top platen has the dimensions of 200 mm (L) × 200 mm (W) × 60 mm (H) with a shape resembling a thick square plate. It has five through-body cut-outs between the top and bottom surfaces: four ∅34 mm holes for mounting the tie rods and the ∅108 mm hole in the centre for mounting the breech. The breech mounting hole has the artillery tapered threads (8 mm pitch) which are heat-treated to increase their strength so that they can retain the breech. The breech is subjected to large axial thrust generated by the hydraulic ram which passes through the central shaft. On each side of the top platen, there are five holes (M8, 15 mm deep) for mounting the press on the assembly stands.

The bottom platen has the dimensions of 200 mm (L) × 200 mm (W) × 125 mm (H). In order to accommodate the hydraulic ram and mount the tie rods, its shape is rather complex. At the top end, it is cylindrical with a hollow cylindrical cut-out for mounting the piston. In the middle section, it has a tapered profile. At the bottom end, it is square-shaped with a small cut-out for the hydraulic oil inlet. The inlet is connected through a small path to the hydraulic ram.

The hydraulic ram has a complex shape that has been calculated [28] to compensate for the strain under load. It is designed in such a way as that the deformation under load at the level of the sealing gaskets and at the top of the piston is negligible. Inside the hydraulic ram, the cylindrical piston is driven by the oil from the hydraulic pump to slide axially and provide axial thrust for the anvil assembly.

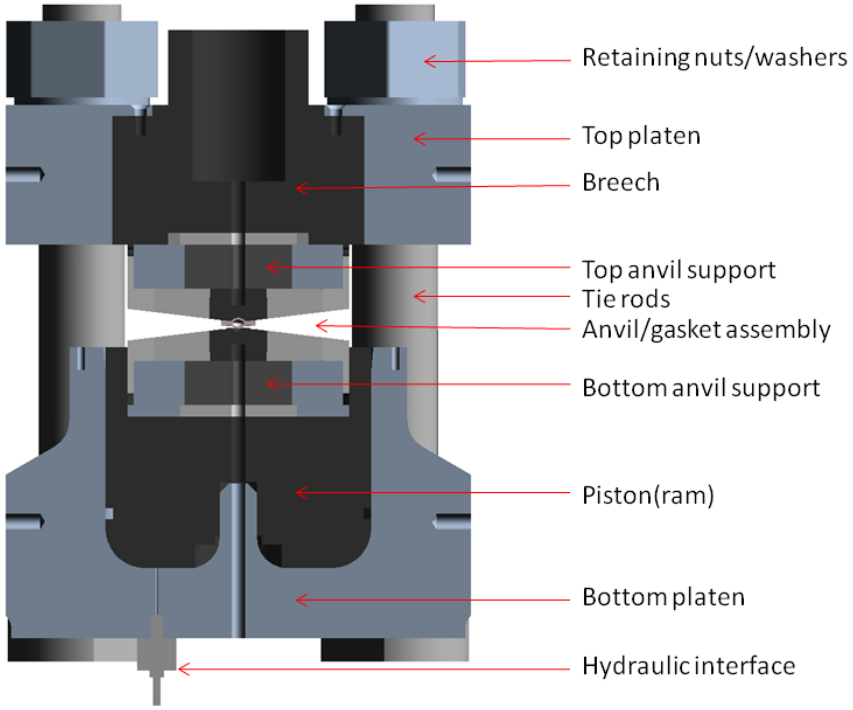

Figure 3.13 A cross-sectional view of the V4 variant of the standard Paris-Edinburgh press with its components (after [28], [29]).

3.3.2 Breech and Breech Centring Ring

The breech and breech centring rings are also original parts of the standard Paris-Edinburgh press. They are installed at the centre of the top platen to sustain the axial thrust. The breech has artillery threads that are 108 mm in diameter with a pitch of 8 mm. It is also made of 819 AW and heat-treated to 52 HRC following the process described above for the platens. Most of the features require very tight tolerances of ±0.05 mm. On the top surface of the breech, a centring ring is mounted with three screws uniformly positioned along the circumference. This bronze ring is used to mate it with the top platen for concentric alignment.

3.3.3 Tie Rods, Nuts and Washers

Four extended tie rods are used for the RV4 compared with the standard tie rods used in the V4 variant of the Paris-Edinburgh press. While the general profile on the ends remains the same, the middle section is increased from 159 mm to 362 mm, resulting in an extension of

the overall length of the tie rods from 282 mm to 479 mm. The 70% extension increases the space inside the mainframe so as to accommodate the thrust bearings and the anvil support on which the gears and anvil assembly are located. These tie rods come with specially made retaining nuts and washers. Similarly to the platen and breech, all of them are made of heat-treated 819AW.

Finite element calculation for the extended tie rods is needed for two reasons. The first is to determine if it is safe to apply axial loads of 150 tonnes to them. Previous calculations by the Paris group [28, 29] demonstrated that it was safe to use the standard tie rods in the V4 P-E press for loading up to 240 tonnes; these calculations still apply to the threads in the new tie rods as the threads and their load conditions remain unchanged. However, with extra length, the new tie rods need to be re-verified for the strength of the body section. Calculation shows that the mid-section of the four tie rods, each of which is subjected to an axial load of a quarter of the 150 tonnes, which is the figure 50% larger than the required operational load, is stressed in tensile with a magnitude of approximately 342 MPa. The safety factor is 4.4 if a yielding strength of 1500 MPa is applied. In the finite element model with 3D geometry (Figure 3.14a) statically distributed pulling forces are applied to the threaded area while at the other end a fixed support is assigned to the surface underneath the tie rod's cap. The calculated stress and deformation distribution are also shown in Figure 3.14 (b) and (c). There appears to be higher stress on the bottom surface of the cap. However the stress concentration area is extremely limited and its magnitude (a maximum stress of 1,447 MPa) is not convincing as the surrounding area generally has a stress less than 1 GPa. Provided that very localised plastic deformation does occur, it will redistribute the peak stress to a wide area and become a plain feature. Thus we are confident that it is within safety limit.

The second reason for running the simulation is to estimate the elongation of the tie rods under the load. Excessive elongation of the tie rods effectively increases the space between the top and bottom platens. As the side frame is mounted on the platens, it might become stretched. Each of its ends is attached to one platen using three M8 screws that go through a cut-out slot and engage with the threaded holes on the side surface of the platen (Figure 3.7). A distorted shape could compromise the alignment of the rotary elements to the side shaft, the pinions, the gearbox, the motor shaft and the coupling, and impose excessive stress on the supporting structures such as the bearings and mounting parts. It also changes the relative position of the mating gears and pinions on the horizontal plane. The FEA simulation shows that the tie rods with the current setting have an elongation of nearly 0.9 mm under a total applied load of 150 tonnes (a quarter of 150 tonnes on the assembly). Figure 3.14 (c) shows the displacements in axial direction – Z axis.

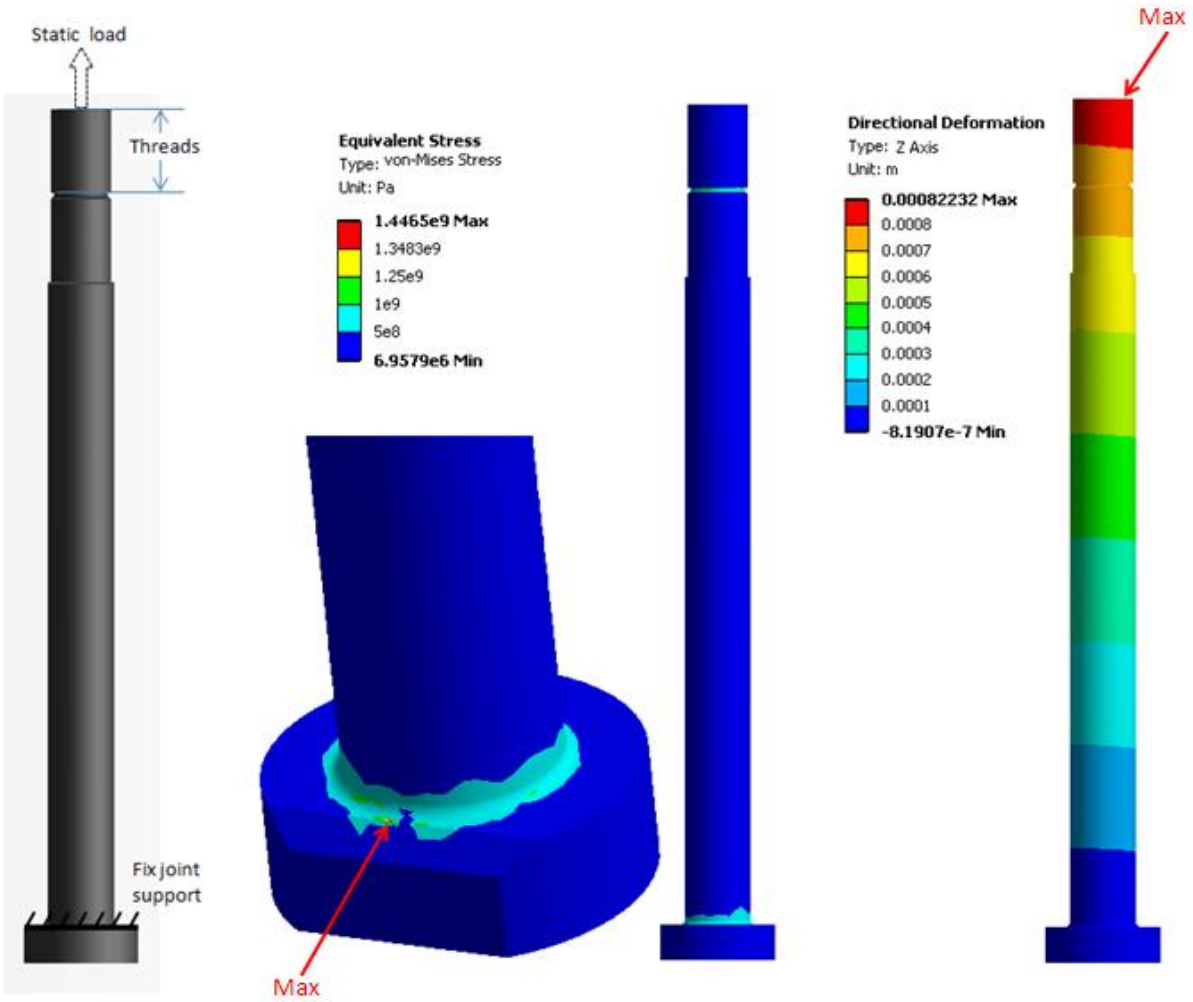

(a) (b) (c)

Figure 3.14 Finite element model of the tie rods and the simulation results.

(a) The geometry and loading conditions. The geometry consists of the cap, the mid-section body and the threaded section;

(b) The calculation stress results. The maximum equivalent stress is below 1.5 GPa. There is very localised peak stress on the cap's edge;

(c) The displacement calculation results. It shows that the maximum displacement in the axial direction exists on the threaded section and is around 0.822 mm in tensile.

To minimize the effect of the tie rods' deformation on the side structure, some optimizations are performed. On the bottom end of the side frame, the mounting slots for the fixing screws are designed to have 2 mm extra downward length in the axial direction (Figure 3.15) while the top end remains unchanged. When the tie rods stretch under load, the shaft together with the gears mounted on it move upward (in the view of Figure 3.7 and 3.8) and push the top platen in the direction opposite to the bottom platen. The top-end fixing screws and the side frame are to follow the top platen; the bottom-end fixing screws slide relatively downward inside the slot and prevent the side frame from stretching.

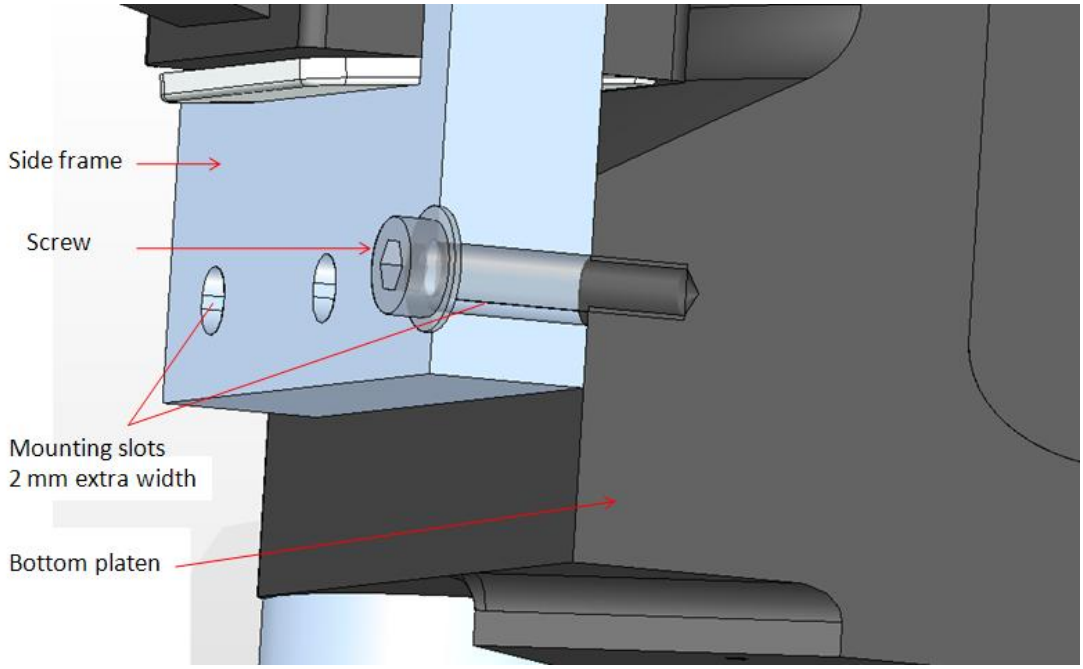

Figure 3.15 The optimized design of 2 mm longer screw slot at the bottom end of the side frame part.

3.3.4 Anvil Supports

The anvil supports are the main parts on the rotational central shaft. They couple the gears, the thrust bearings and the anvil assembly and form the top and the bottom halves of the shafts. For this reason, they are also referred to as the top or bottom shafts. The multiple structural functions of these supports are to:

1) *Hold the top and bottom shaft for rotation;*
2) *Couple the hydraulic bearings' piston to the anvil;*
3) *Maintain and support the anvil assembly;*
4) *Maintain the gears whilst they transmit rotational torque.*

In order to perform these functions within the limited space inside the press, the anvil supports have a complex shape. Figure 3.16 shows pictures of these manufactured anvil supports with the gears on them.

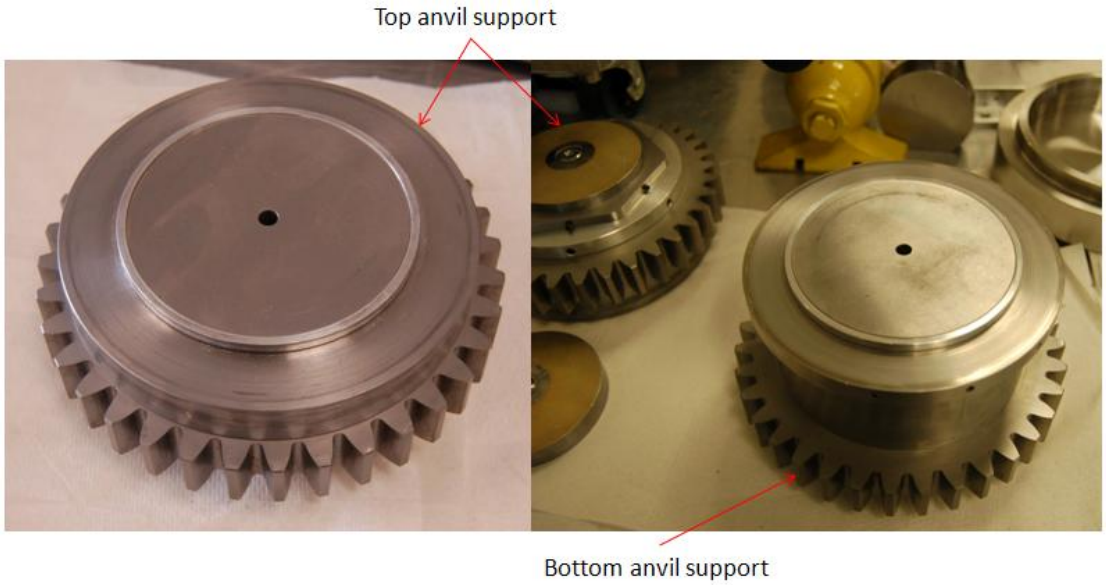

Figure 3.16 Photos of the top and bottom anvil supports with gears and locating rings on them

With regard to the loading conditions, the anvil supports are subjected to a combination of force, pressure, torque and boundary conditions. Figure 3.17 illustrates the load and constraints on the top anvil support in finite element models. The bottom anvil support is loaded in a similar manner but calculated to be relatively less stressed.

1) Axial load. The massive axial load on the top surface is dominant. The load is distributed to two areas: the annular area on the top surface where the anvil binding ring sits (Figure 3.17 B) and the flat circular area of the cut-out that mates the anvil die (Figure 3.17 A). In the FEA model, a total of 150 tonnes is applied to the areas.

2) Torque load. The gears have a rotary moment in the horizontal plane. It is much smaller compared to the axial load in magnitude. As the two anvil supports have a small length-to-radius aspect ratio, the resulting torsional effect is subtle. To simulate the torque, two forces are applied to a pair of opposite flat surfaces which are in contact with the gear (Figure 3.17 C and D). The forces are 2000 N on each side but in opposite directions. The forces represent a rotational moment of 180 Nm acting on each of the anvil support. This load is slightly pessimistic and is a compromise approach to account for possible machining clearance between the gear and the anvil support. It is possible to model this using conventional method of modelling the

hexagonal profile on screw driving tools which may produce a more accurate prediction of the stress levels.

3) The supports. The supports on the bottom side are provided by the hydraulic thrust bearings. It is simulated with displacement supports on two areas on the bottom surfaces (Figure 3.17 E and F).

4) Pressure load. The cylindrical cut-out in the anvil support is created slightly smaller than the volume of the anvil dies. This is to accommodate the anvil dies with a hoop stress. The cut-out thus has a pressure load on its internal surface (Figure 3.17 G).

The simulation results show that the anvil supports under the applied load have a few spots of high Von-Mises stress in the circular corner of the cut-out for the anvil die (Figure 3.18). Its magnitude is less than 1,000 MPa for the top anvil support which is made of maraging steel heat-treated to the strength of 1,900 MPa. The deformation in the axial direction is not significant (Figure 3.19).

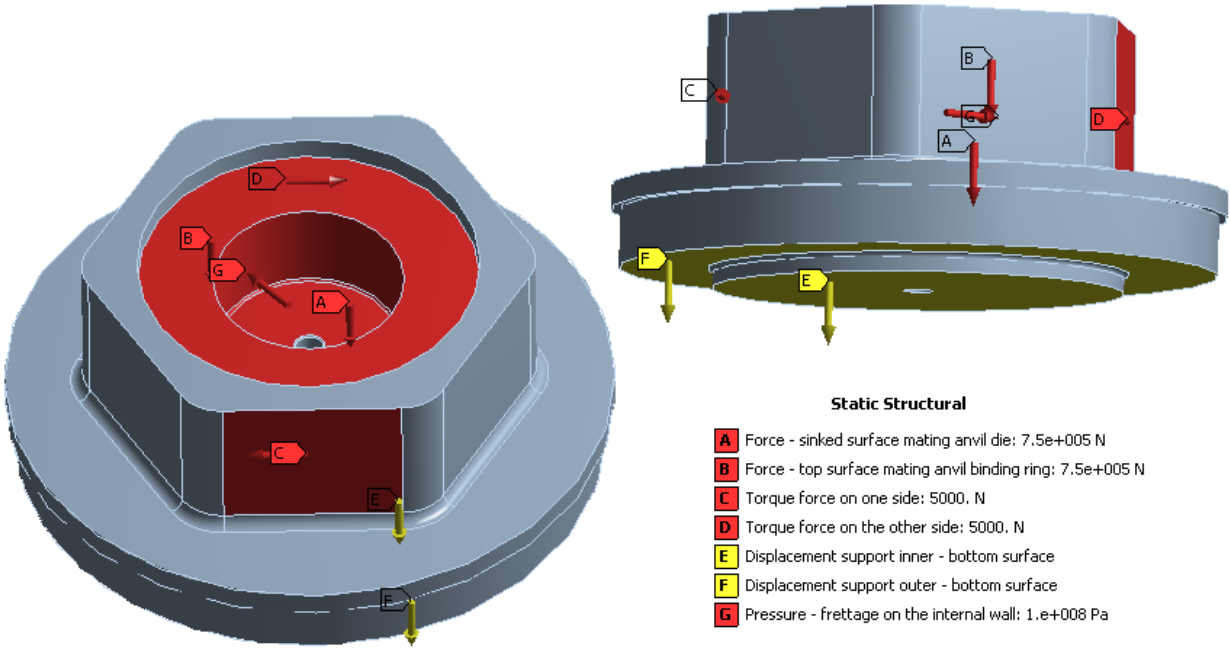

Figure 3.17 The simulation model of the top anvil support. The loading conditions are illustrated. The axial load is distributed to be A on the circular area on the top surface and B on the flat surface in the cut-out cylinder. C and D are the forces to simulate the rotational torque. E and F are the displacement supports on the bottom surfaces. G is the pressure that captures the hoop stress created by the frottage of the anvil die in the cut-out.

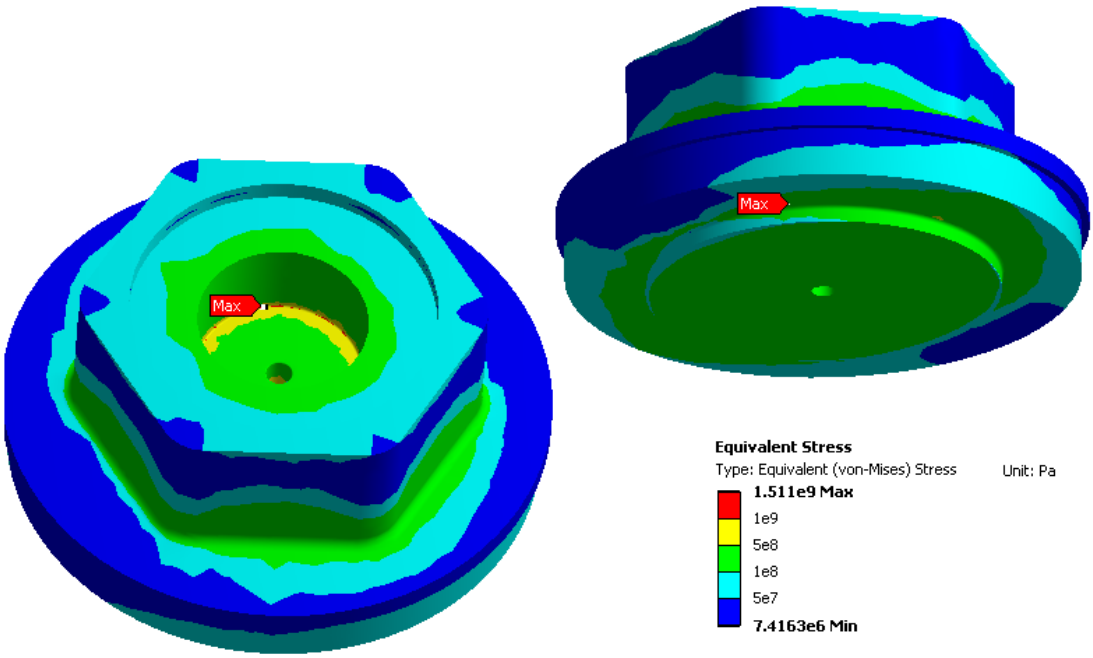

Figure 3.18 The resultant stress in the simulation of the top anvil support. There is stress concentration near the edge radius in the cut-out cylinder. The magnitude is nearly 1,000 MPa. Small spots with 1,511 MPa stress are not representative as their area is extremely limited and subject to calculation error.

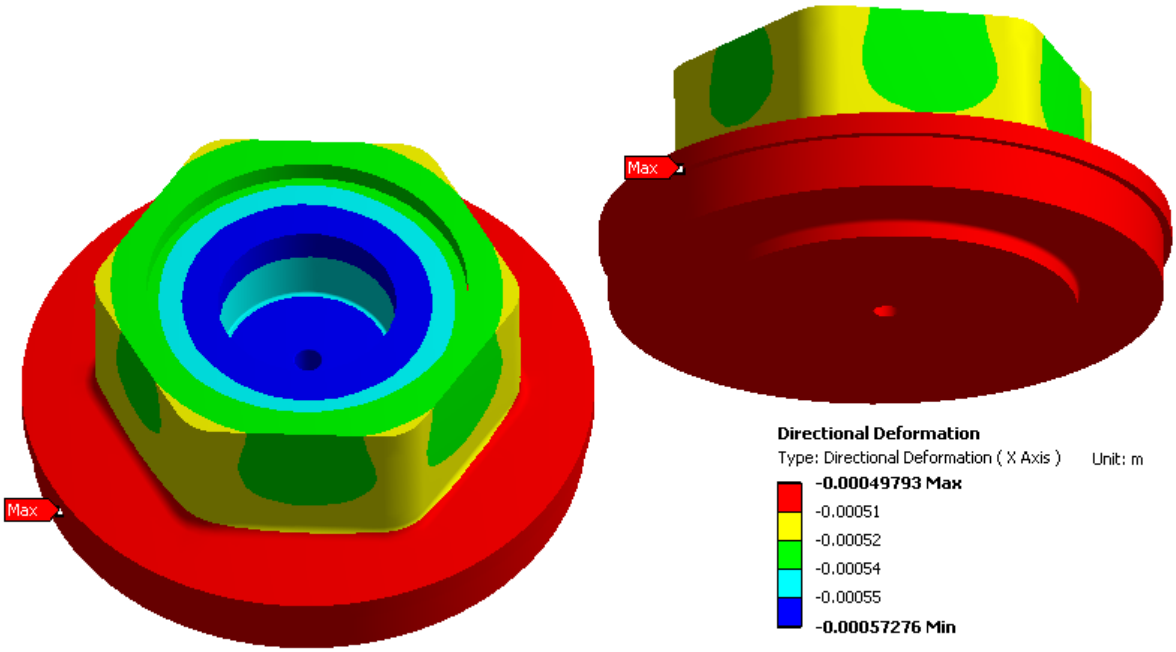

Figure 3.19 The resultant deformation in the simulation of the top anvil support. The maximum displacement in axial direction is about 0.5 mm.

3.3.5 Thrust Bearings

As mentioned in Section 3.2, there are two versions of the RV4. The main difference between them is in the design of the thrust bearings and the needle bearings (Figure 3.7). The 1st version employs mechanical spherical roller thrust bearings and simple needle bearings. The 2nd version employs custom-made hydraulic thrust bearings and enhanced needle bearing assemblies. The first modification is to overcome the frictional resistance, the second to improve the alignment of the central shaft. Here the structures and mechanical analysis are described. The design and testing process is described in Chapter 4.

3.3.5.1 The spherical roller thrust bearings

For the 1st version of the RV4, different types of the thrust bearings that are commercially available have been discussed in Section 2.2.3.1. The selected spherical roller bearings are SKF 29412E that have a taper profile in the vertical sectional view (Figure 2.11, Figure 3.7). The top roller bearing is mounted on the breech and connects to the top anvil support; the bottom roller bearing resides on the piston and connects to the bottom anvil support. They are 42 mm high and 130 mm in outer diameter. The basic loading capacity is 91.5 tonnes whilst static or – in the case of the RV4 – at low speed rotation.

3.3.5.2 The design of the hydraulic roller bearings

For the 2nd version of the RV4, the hydraulic thrust bearings are adopted. The design of the compact heavy-duty hydraulic bearings is based on the principle that the friction between two slipping surfaces with a thin layer of lubricant between them is small.

Each of these simple and precisely engineered bearing sets consists of a cylinder (cylindrical housing), a piston, a 1 mm-thick layer of hydraulic oil and two sealing rings made of PTFE and nylon, respectively (Figure 3.20). Essentially the piston rests (or "floats") on the layer of oil with a very low friction on the contact surface while the gap between the cylinder and piston is sealed by the plastic rings to prevent leakage of the pressurized oil.

Currently, hydraulic bearings made of stainless steel are used in the RV4 and a series of tests has been carried out (Section 4.2.1). They have been verified by a laboratory test to above 100 tonnes in the RV4 and have much less frictional moment than spherical roller bearings. It has also been shown that the PTFE rings are effective in sealing while exhibiting good resistance to wear.

The stainless steel bearings however showed significant deformation – 1 mm indentation on the bottom surface of the piston – after being loaded to the static load of 150 tonnes in 50% over-load safety tests. The bearing cylinder and piston made of maraging steel were calculated in finite element analysis to be capable of sustaining more than 150 tonnes (details of the calculation are shown in the next section). Two new sets of bearings made of maraging steel are being developed and are predicted to have better performance under load above 100 tonnes.

Figure 3.20 The structure of the hydraulic rotational bearing. The main parts of the bearing are the rotational piston (A) and the stationary cylinder (C). Between the piston and the cylinder, a 1 mm layer of hydraulic oil (F) is made to reduce the frictional resistance upon relative rotation between the two. The PTFE ring (D) and the rubber ring (E) are inserted to seal the gap between the piston and cylinder. In the body of the cylinder a small path is created to let the air out during the assembly process. The path is sealed by a screw (B).

Figure 3.21 Pictures of the components of the disassembled hydraulic bearing made of stainless steel.

3.3.5.3 The finite element simulation of the hydraulic bearings

This section focuses on the finite element simulation model of the hydraulic bearings and the calculation results regarding their mechanical performance.

The hydraulic thrust bearings have two main structural parts: the rotational piston and the static cylinder. Positioned above the top surface of the bearing's piston are the anvil support parts, and supporting underneath the bottom surface of the cylinder are the breech (for the top bearing) and the hydraulic ram (for the bottom bearing). Upon thrust loading of the press, the piston is subjected to axial load on its top surface (Figure 3.22). The force is transmitted through the piston's solid body and compresses the hydraulic oil layer between the piston and the cylinder. The oil is a fluid and exerts normal pressure to all the surrounding surfaces that enclose it. The cylinder thus has normal pressure inside its bore, mainly in the downward direction and partly in outward direction. On the bottom surface, it has solid support which is simulated with fixed joint support in the finite element model. The static structural analysis models the piston and cylinder separately and assumes that both are solids made of maraging steel.

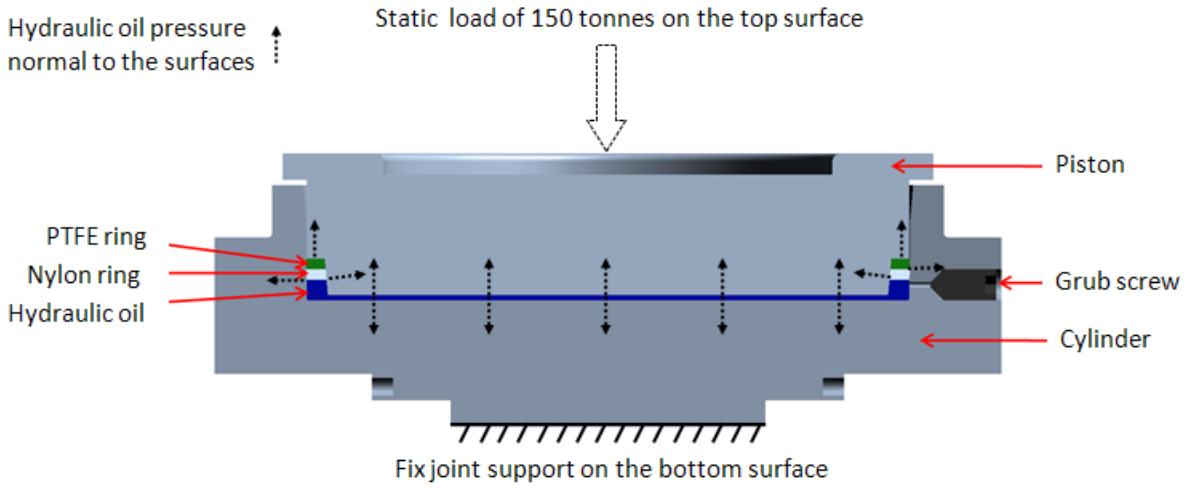

Figure 3.22 The loading conditions of the assembly of the hydraulic bearings. In the FEA simulation, the actual models apply these conditions to the piston and the cylinder separately instead of using the assembly. The material properties used in the models are those of maraging steel. The load is 150 tonnes and the bottom of the cylinder locked with fixed support.

The calculation results for the loaded hydraulic bearings are demonstrated in Figure 3.23. It shows in colour the Von-Mises stress and deformation distribution in the bearing body for loading up to 150 tonnes on the bearing piston and cylinder. A dimension scale is also included in the plot.

The maximum stress value is 0.61 GPa which occurs at the centre of the piston's bottom surface (circled area A). The stress on the cylinder is relatively low compared to the piston. However, the cylinder tends to open up on the internal wall of its bore and has high stress concentration near the corner of its step flanges on the bottom side (circled area B).

The maximum deformation is nearly 0.2×10^{-3} mm at the top of the piston's central section, though the whole central section shows a high level of deformation. The deformation direction is downward and outward. In general the piston tends to sink in the centre and becomes slightly U shaped in the axial cross-section. Static mechanical test up to 150 tonnes on stainless steel hydraulic bearings have seen excessive deformation in the axial downward direction on the piston's bottom surface.

3.3.6 Needle Bearing Assembly

The needle bearing assemblies are installed on the tie rods so as to hold the central shaft in position. They help the alignment between the top and bottom shafts and stop them from tilting towards one side when they are driven by the gears (details on this issue are provided in Chapter 4). Described below is the structure of the assembly in the 2nd version of the RV4. The 1st version has eight needle bearings with a similar design to this except that they do not have the outer sleeve that enhances the strength of the assembly. However due to the larger size of the hydraulic bearing assembly, the 2nd version of the RV4 has only four installed on the two tie rods on the side of the RV4 opposite the side shaft.

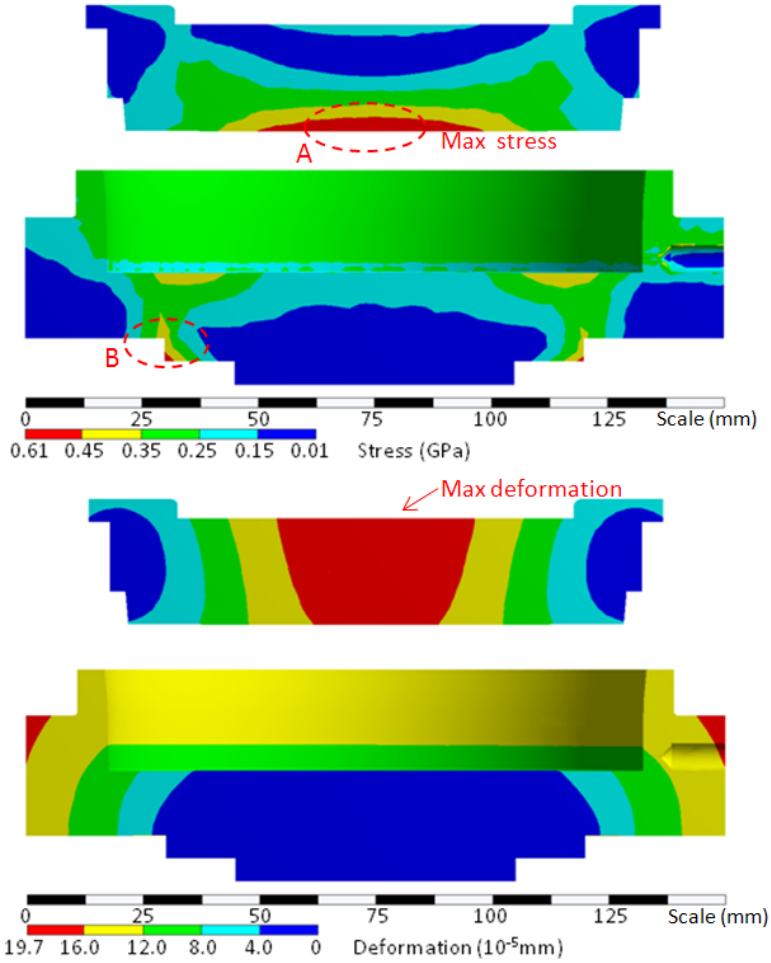

Figure 3.23 The stress and deformation of the piston and cylinder under applied load. It shows the maximum stress is in the centre of the piston's bottom surface – 0.61 GPa, the maximum deformation in the centre of the piston's top surface – only 0.2×10^{-3} mm.

The design of the assembly (Figure 3.24) mainly focuses on restricting the position of the central shaft to be in the centre of and equidistant from the four tie rods. The tie rods are used as the position reference, and a holder is designed to clamp the needle bearing on them. The holder consists of an inner ring and an outer ring. The cylinder of the bearing is held on the tie rod with grub screws. Outside the needle bearing casing, a sleeve is installed to make the bearing assembly more rigid against the central shaft.

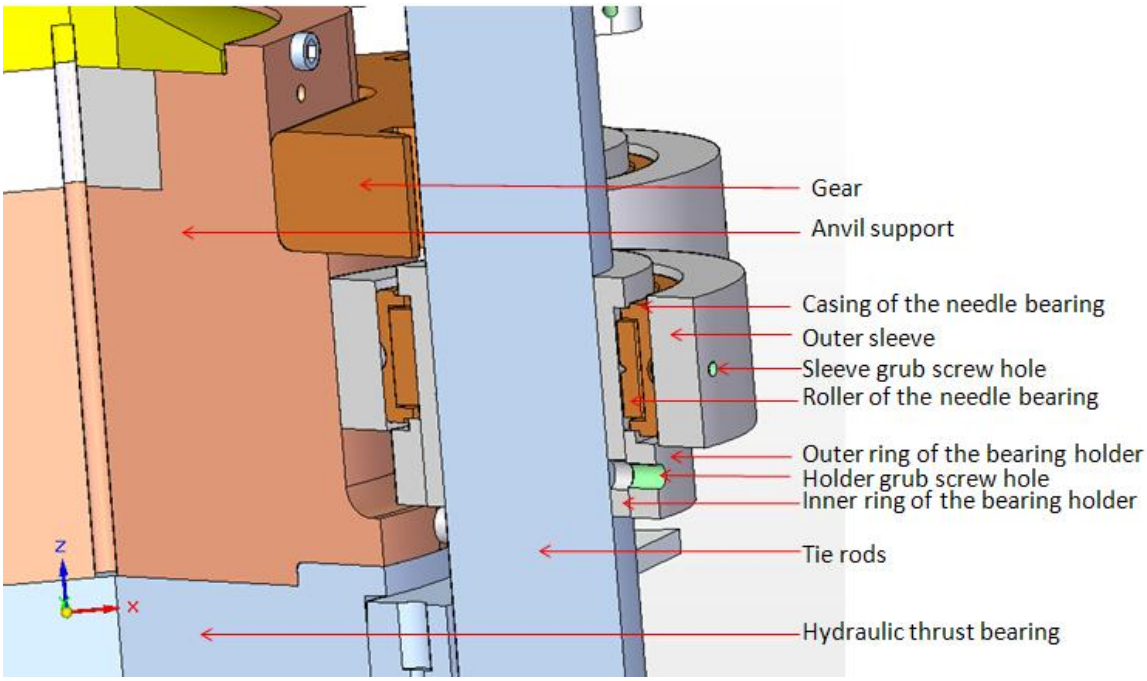

Figure 3.24 The assembly of the needle bearing with a sleeve outside as an enhancement. The assembly shown here is used on the bottom side in the 2nd version of the RV4, while a similar but smaller assembly is used on the top side. The sleeve as well as the bearing holder that supports the needle bearing on the tie rod is made of stainless steel. In the 1st version of the RV4, there is no sleeve outside the needle bearing.

3.3.7 Gears/Pinions and Transmission Keys

3.3.7.1 Gears/pinions

The gears and pinions that transmit power and torque from the side shaft to the central shafts are custom-made by a commercial supplier – *HPC gears Ltd.* They are expected to carry a load of at least 250 Nm at low speed. Their design has two main constraints:

1) Diameter. As the gears are installed inside the V4 frame, its max diameter allowance is around 150 mm. This limits the reduction ratio of the two gear/pinion pairs. Ideally with the same pinions that provide the input power, the larger the diameter of the gears, the larger the output torque that can be generated in the gears to drive the anvil shaft. To put the gears inside the mainframe, a module of 4 mm and a pitting diameter of 140 mm are employed.

2) Thickness. Ideally the thicker (taller) the gears and pinions are, the more power they are capable of transmitting. However, an increase in the thickness results in an extension of the distance between the sample position and the top of the press which is restricted tightly by the neutron facilities' beam position. It also adds to the overall weight of the press which makes handling of the unit more difficult.

These gears have to operate under certain conditions:

1) High transmission load. For the limited size of the gears and pinions, the average operational torque is expected to be above 162 Nm to a maximum of 250 Nm. However, in order to make a provision for potential application with even large torque, it was designed so that they have a large margin and can transmit over 1000 Nm before failure. In fact, the width of teeth was later changed from 25 mm to 20 mm in order to shorten the axial dimension; the stress on the teeth was thus increased and the gears can transmit over 800 Nm.

2) Low axial load. The gears are mounted on the anvil support parts. With a hexagonal profile to transmit the large torque on the horizontal plane, there is nearly no axial force acting on the gears. The gears are retained axially on the anvil support parts with retaining rings. They are made of aluminium alloy which is relatively soft and only give a small retaining force. The majority of the massive axial load to be provided to anvil for sample compression is taken by the anvil supports. Likewise, the pinions withstand small axial loads.

3) Low speed. Compared to conventional gear applications where the speed can be well beyond hundred and thousands of revolutions per minute, the RV4 press is to be used at very low speed, as a measure to protect the sample and improve the positioning precision. The speed is estimated to be between 0.2 rpm and 1 rpm on the anvil shaft.

4) Light duty. The RV4 is only needed for certain types of neutron experiments and as we know, beam time is normally very limited. The RV4 will be in operation for a maximum of a few weeks per year. Though a complete experiment may take two days, during each experiment the RV4's gears only rotate when a re-positioning of anvil shaft is executed which is to be done every 10-15 minutes. The re-positioning operation normally only takes a few minutes.

Taking into consideration the above factors, two pairs of gears and pinions are designed. They are involute spur gears and their specifications are listed in Table 3.3.

	Gears	Pinions
Teeth No	35	21
Material	EH36	EN36
Process	Case hardened	Case hardened
Module (mm)	4	4
Gear ratio	1.667	1.667
Face Width (mm)	20*	20
Pressure angle (˚)	20	20
Root Circle Diameter (mm)	129.68	74.32
Base Circle Diameter (mm)	131.56	78.93
Pitting Circle Diameter (mm)	140.00	84.00
Outside Circle Diameter (mm)	147.68	92.32
Power (W)	14.7	16.0
Speed (rpm)	1.2	2
Torque (Nm)	127.32	76.4

Table 3.3 The design and analysis parameters of the gears and pinions

* *Initial strength calculation used 25 mm for face width and the safety factor was around 10. It was subsequently changed to 20 mm to allow for more space for installing the thrust bearings.*

The strength and stress of the gears are calculated by the manufacturer to meet the loading conditions. The design has a safety factor of over 10 with respect to the operational torque of 250 Nm (the calculations provided by the supplier are presented in Appendix F) or a safety factor of 2 with respect to a heavy duty operation at 1000 Nm. Table 3.4 contains the calculation results and the corresponding safety factors. In the calculation of the duty conditions, the allowable tangential load at pitch radius is used to estimate the least load that can be taken by the teeth. For the allowable load at the pitch radius, both the wear and strength are calculated for the gears (35 teeth) and pinions (21 teeth) individually.

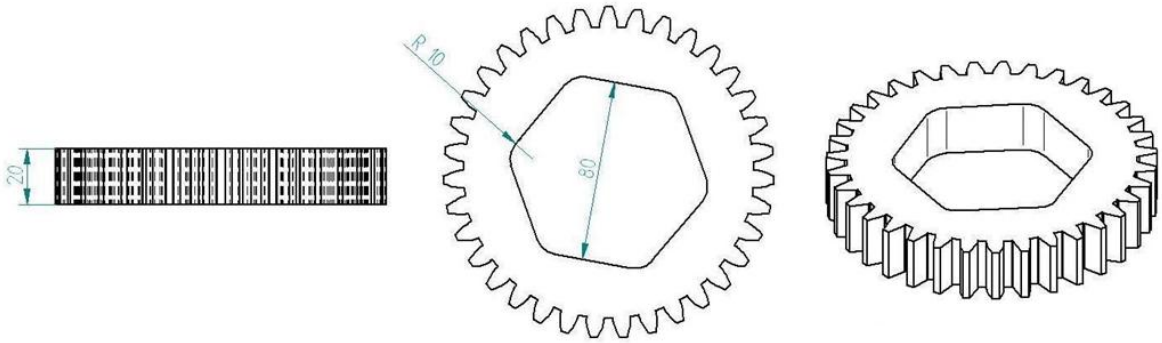

Gears (Module: 4 mm, 35 Teeth)

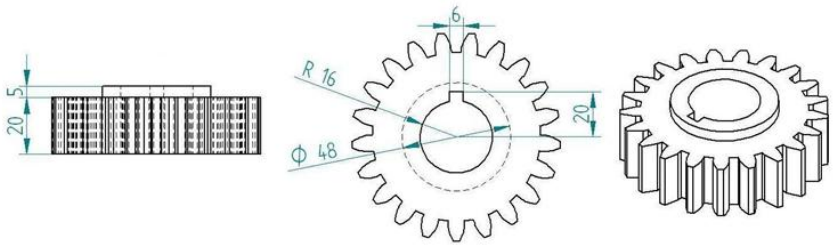

Pinions (Module: 4 mm, 21 Teeth)

Figure 3.25 The design of the gears and pinions for power transmission between the side shaft and the central shaft. They are involute spur gears with a module of 4 mm. The gears have 35 teeth. The pinions have 21 teeth. They are both made of EN36 case hardened steel.

			Tangential load at pitch radius (N)	Safety factor for normal operation (250Nm)	Safety factor for heavy duty operation (1000Nm)
Duty	Normal operation		408.9	-	-
	Heavy duty operation		1635.6	-	-
Strength	Wear	Pinion	6769	16.6	4.2
		Gear	7642	18.7	4.7
	Strength	Pinion	4474	10.9	2.7
		Gear	4169	10.2	2.5

Table 3.4 The mechanical calculation for the gears and pinions, provided by HPC Gears, Ltd.

3.3.7.2 Transmission keys

The gears mounting on the anvil support parts have a hexagonal profile to transmit the torque to the central shaft. Unlike the gears, the pinions couple with the side shaft with a circular profile and small square keys with round ends are used to transmit rotational torque from the side shaft to the pinions.

Illustrated in Figure 3.26 is the key between a shaft and a gear. The key has a profile of $l \times b \times h$ where l is the length (not shown in the figure), b is the width of the cross section and h is the height. The key is positioned between the shaft (with the diameter of d) and the gear. The side surfaces of the key will be in contact with the gears on the upper area with the length of k and with the shaft on the lower area with a length of t. In reality, the height h' of the key slot might be slightly larger than that of the key h, leaving a small gap at one end or at both ends: $t' \geq t$ or/and $k' \geq k$. To transmit a rotational torque of T, the key is subjected to normal force on both its sides. Assuming the direction of T is counter clockwise, a load of equal magnitude F acts on the upper area of the left side surface (height: k) and the lower area of the right side surface (height: t). They are both compressive pressures on the surfaces.

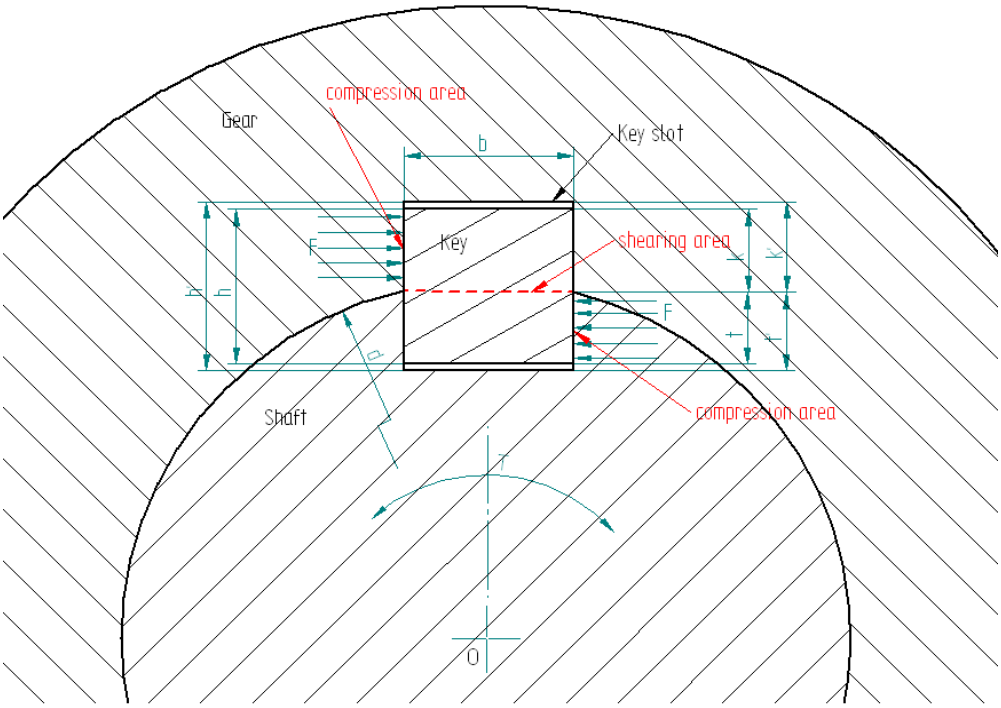

Figure 3.26 Illustration of the design and loading conditions for a key in a typical shaft and gear transmission case.

The key is thus subjected to both shearing stress and compressive stress (Figure 3.26). The stresses are calculated using the following formula:

Shearing stress:

$$\sigma_s = \frac{2T}{dbl} \tag{3.1}$$

Compressive stress:

$$\sigma_p = \max\left(\frac{2T}{dtl}, \frac{2T}{dkl}\right) \tag{3.2}$$

where *l* is the length of the key, *h* is the height of the key, *b* is the width of the key's the cross section, d is the diameter of the shaft, and T is the transmission torque.

With the current side shaft (d = 34 mm) and pinions design (T = 74.9 Nm), we chose a commercial product that is manufactured to DIN 6885 (364.0606.014). It has

l = 14 mm
h = 6 mm
b = 6 mm

and the tolerance grade is h9. Because the keys have round ends with a radius of 3 mm, a conservative length *l* of 8 mm is chosen.

The key slots are created with the following dimensions:

h' = 6.3 mm
t' = 3.5mm
k' = 2.8 mm

This yields a possible minimum of k = 2.5 mm and t = 3.2 mm.

Using Equation (3.1), the resulting shearing stress is: σ_s = 91.4 MPa.

Using Equation (3.2), the resulting contact pressure is: σ_p = 219.4 MPa.

3.3.8 Stepper motor

The stepper motor – AS65ACEP – from *Oriental Motor (UK) Ltd*. [74] is selected as the power source for the RV4 press. The package is a stand-alone unit consisting of a motor and a driver with built-in host controller function. It features non-misstep and low speed/low vibration operation. The motor uses a built-in rotor position sensor to monitor the speed and rotational displacement during use to avoid misstep due to an overload. The driver has a micro-step mechanism that enables operation at very small step angles so that it is running in a steady manner even at low speeds.

The letters of the designation ***AS66ACEP*** stand for (in sequence):

AS : Standard type of the αSTEP series
6 : Motor frame size is 60 mm.
6 : Motor case length is 60 mm
A : Standard with single shaft) without electromagnetic brake
C : Power supply voltage is single-phase 200 – 230 VAC (-15% to +10%) 50/60 Hz
E : Motor classification
P : The driver type is built-in controller package

The specifications are listed below:

Maximum output torque:	1.4 Nm
Maximum holding torque:	1.2 Nm
Revolution setting:	1000 pulses/turn or 0.36˚/pulse
AC power current output:	> 3 A

The selection of the motor largely focuses on the output torque and the dimensions. Other issues related to the electrical connection and the control system are described later in Section 3.4.

1) Output torque and speed.

   The target anvil shaft rotation speed is between 0.2 rpm and 1 rpm. This translates to a motor speed between 54 rpm and 270 rpm, respectively. The average maximum torque driving the anvil shaft is around 160 Nm, which translates to above 1.0 Nm with the discounts in component efficiency as discussed in Section 3.2.3. To provide maximum output torque of 250 Nm on the anvil shaft, the motor is required to provide the output of 1.4 Nm.

Figure 3.27 below is the torque-speed chart provided by the manufacturer. According to the chart, it provides up to 1.0 Nm when the speed is no greater than 1500 rpm. It can also provide nearly 1.4 Nm when it is at a very low speed, e.g. 54 rpm.

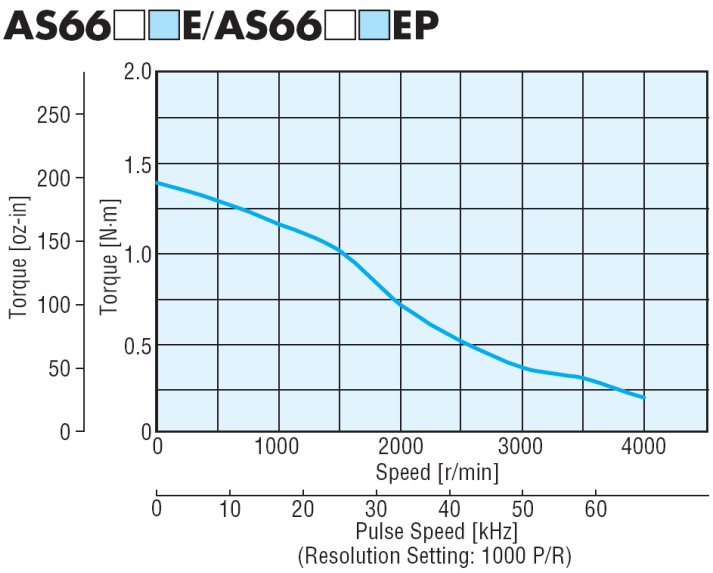

Figure 3.27 A chart illustrating the relationship between the output torque and speed of the stepper motor AS65ACEP (from [74]). The motor provides approximately 1.4 Nm at start.

2) Dimensions

It was intended that the motor could be accommodated in a position near the side shaft so that it would be coupled to the gearbox directly to improve the transmission efficiency and reduce the overall size of the RV4 press. A large motor also requires the side frame be made thicker and would add weight to the structure. The selected AS66ACEP has a length of 63.6 mm and the frame (cross section) is 60 mm by 60 mm. It is installed in the cut-out area on the bottom end of the side frame (Figure 3.28).

The built-in controller package is an electronic box with high control capability and multiple operational functions. A wired controlling system is created with the controller connecting the sensors, external signals, motor and power supply. More details about the controlling system are reported in Section 3.4.

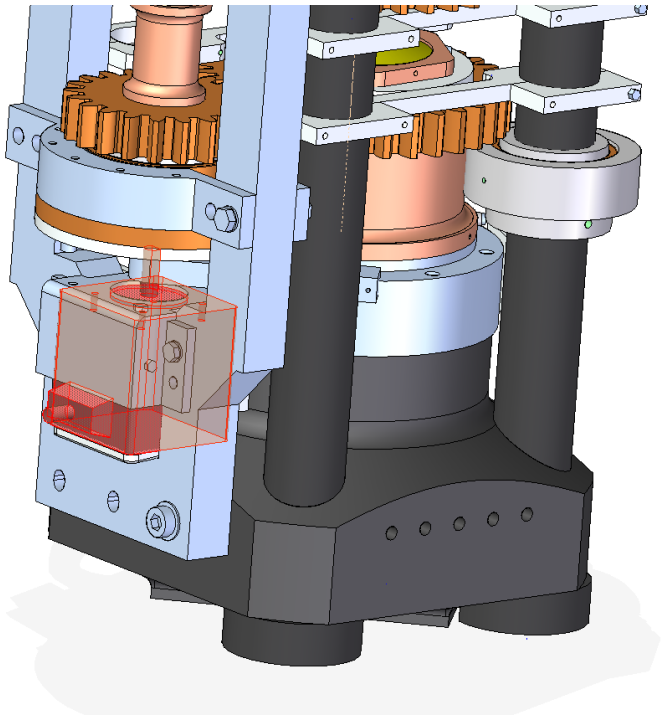

Figure 3.28 The design of the stepper motor on the side frame. Its dimensions are limited by the surrounding components.

3.3.9 Gearbox

The gearbox between the motor shaft and the side shaft is a harmonic gearbox with a very large reduction ratio. It is a CSD series component set sourced from Harmonic Drive Ltd [49].

Harmonic drive is also known as ‘Strain Wave Gearing’. The most exciting feature is its compactness and low mass. It is ultra flat with a very small axial length. Compared to traditional gearboxes with similar reduction ratios such as planetary gears and helical gears, the size and mass of the harmonic gearbox are only a fraction of a traditional one. It also features high accuracy and repeatability.

In the case of the selected CSD-32-160-2A-GR-Standard [49], the reduction ration is 160:1, the axial length is only 42 mm and the mass is only 0.51 kg. Both the transmission accuracy and hysteresis loss are less than 1 arc min. The repeatability is better than ±0.1 arc min.

However, the harmonic gearbox is not perfect in terms of its transmission efficiency, which typically is between 55% and 75% depending on the temperature and the supporting structure. In the RV4 press, the gearbox takes in a torque of 1.0 Nm from the motor and provides the side shaft with a torque of 112 Nm with 30% loss in efficiency when it is running at 20˚C. With sufficient input, it is capable of repeatedly outputting 261 Nm and momentarily outputting 361 Nm.

As shown in Figure 2.13, 3.29 and 3.30, the gearbox consists of three main components: the wave generator, the flexspline and the circular spline. The wave generator is a flat ring with a circular track of internal ball bearings. It is fixed to the input shaft piece with 4 screws, which connect to and are driven by the motor shaft via a stainless steel coupling. The flexspline is a thin and flexible cup-shape circular piece with 160 teeth on its outer surface. In the assembly, its top surface is fixed to the output shaft piece with 11 screws which connects to the side shaft and transmits the magnified torque via two opposite keys. The circular spline is a solid flat ring with 159 teeth on its internal surface. This spline mates with the gearbox flange and the holder. They are coupled together by 12 long strong screws to form a rigid assembly which is then mounted on the side frame. Lubricant grease is applied in the chambers between the flange, wave generator and the flexspline. It also has three structural ball bearings for radial support and axial positioning, including the input shaft bearing, the output shaft bearing and the positioning bearings (Figure 3.29).

When the wave generator turns it pushes the flexspline against the circular spline. Because there is a difference in the teeth number between the flexspline and the circular spline, the teeth on the flexspline shift relative to the circular spline in radial direction. The offset is very small – only 1 tooth when the wave generator rotates by one turn. An animation of the working principal can be found on [75].

The mechanism ratio R is dependent on:

$$R = \frac{Flexspline\ teeth\ number}{Flexspline\ teeth\ number - Circular\ spline\ teeth\ numbe} \qquad (3.3)$$

The setup in the CSD-32-160-2A-GR-Standard results in a ratio of 160:1. The speed of the flexspline and the side shaft is 1/160 of that of the wave generator and the motor shaft while theoretically it is possible to magnify the torque by a factor of 160.

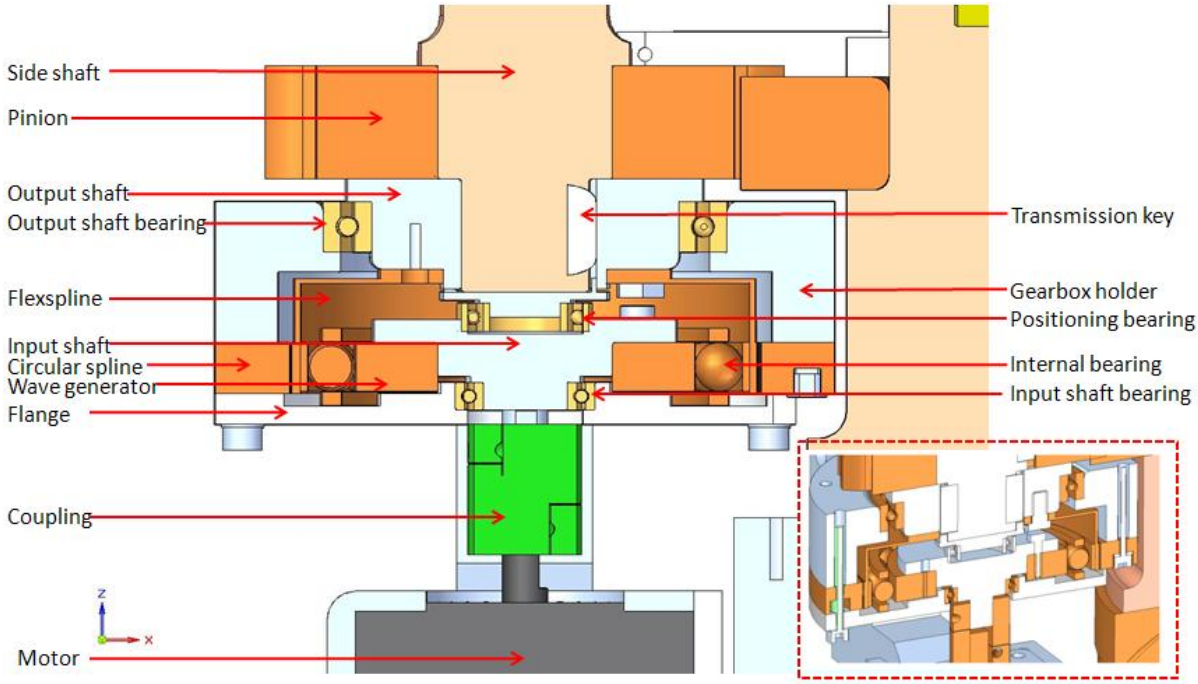

Figure 3.29 The design of the gearbox with multiple supporting components. The harmonic gearbox itself consists of the flexspline, the circular spline and the wave generator. It is driven by the stepper motor and supplies magnified torque to the side shaft.

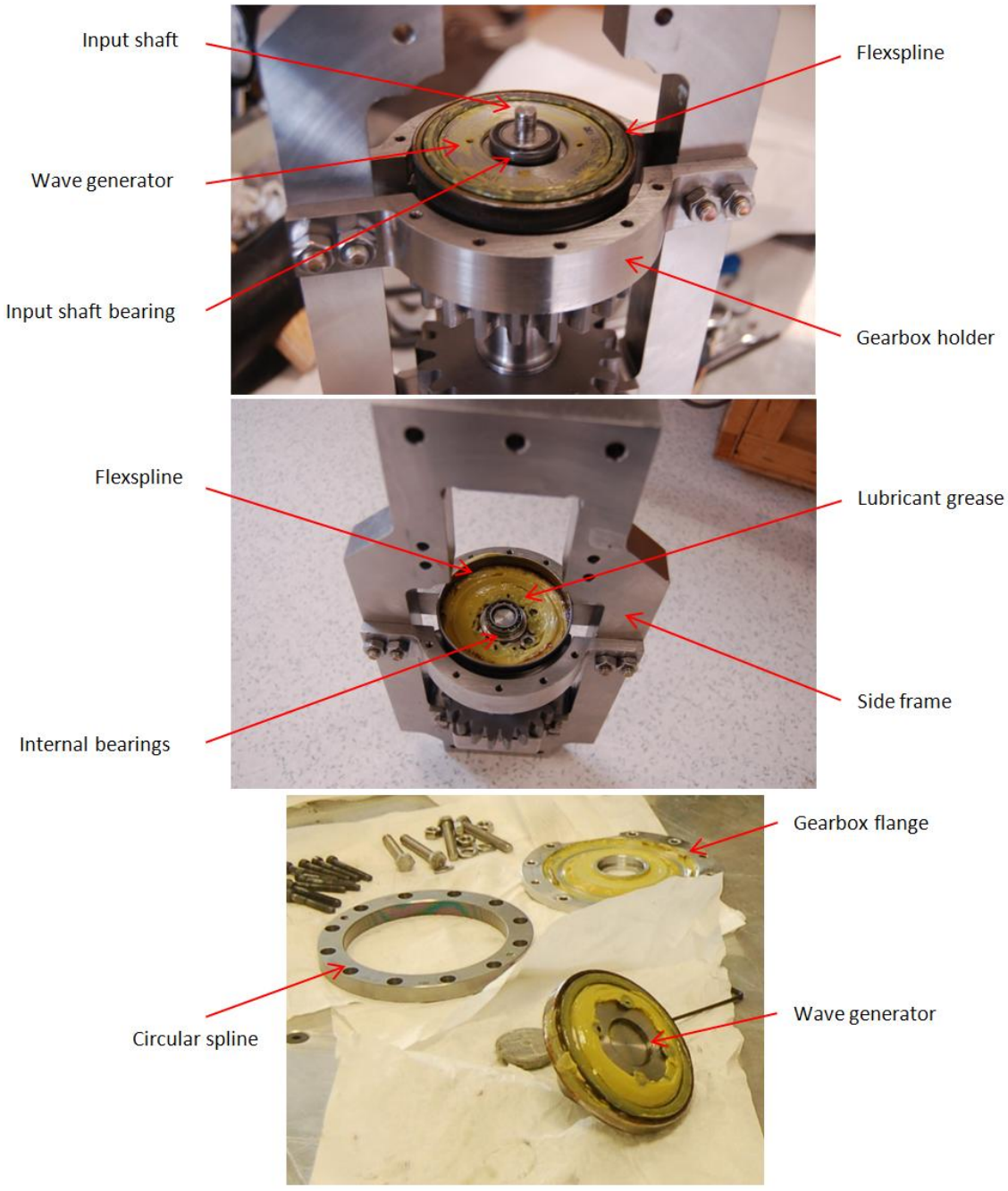

Figure 3.30 The main components of the gearbox stripped from the assembly.

3.3.10 Side Shaft

The side shaft is a single shaft with multiple stages for installing various components (Figure 3.31). There are the pinions, the gearbox output shaft piece, the positioning sleeve and other accessories such as bearings, seals and transmission keys.

On stage 1, the extension section is reserved for coupling to an optional optical encoder for position monitoring. On stage 2, a positioning sleeve and a ball bearing are installed as well as a seal on the upper end which covers the area from dust and also serves as a stop for the bearing. Stage 3 and stage 7 accommodate the top and bottom pinions. Each stage has a key slot and is subjected to resistant rotational moment of equal magnitude. Stage 4 and stage 6 are two axial stops for the pinions. Stage 5 is the middle section that is made with the diameter optimised to reduce the area blocking the scattered neutron beam. Stage 8 is used for coupling with the gearbox's output shaft piece. This section has two key slots at the opposed positions for power transmission and is subjected to the largest torsional torque.

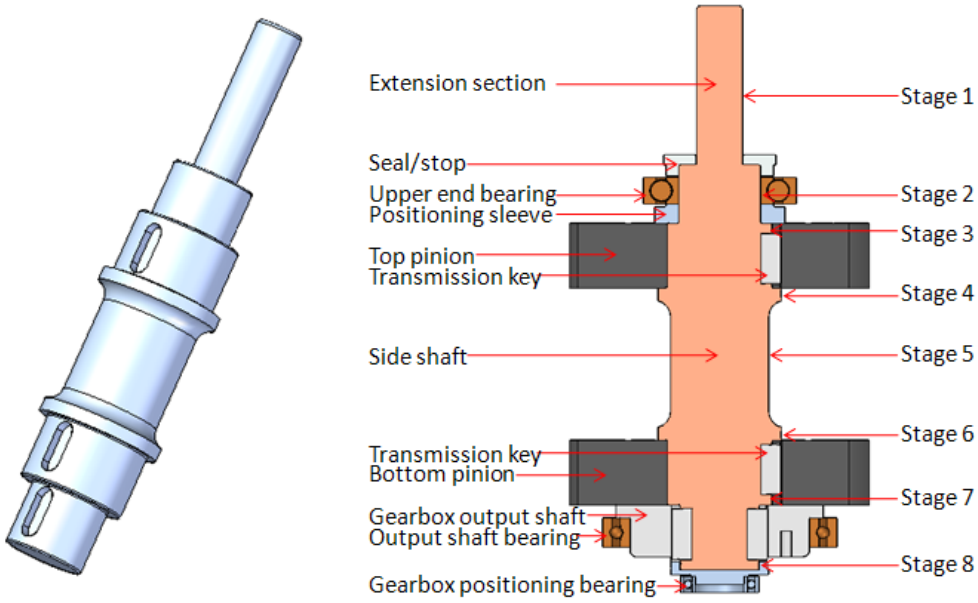

Figure 3.31 The design of the side shaft with multiple stages. It is 174 mm long with different diameters of individual stages.

The shaft was made of EN24 steel and was case-hardened in the engineering workshop. EN24 is a nickel-chromium-molybdenum steel with high strength and toughness commonly used in manufacturing of gear axles and high strength studs.

The shaft is 174 mm long and its maximum diameter is 30 mm. The detailed drawings with the diameters and lengths of each stage can be found in Appendix D. Below is a hand calculation of the loading conditions and resulting twisting angle and shearing stress for each stage. The load is mainly the drive moment T_d on stage 8, the two resistant moments T_{r3}, T_{r7} on stage 3 and 7. The axial load is neglected and it is assumed that the side shaft is static as the speed is very low.

$$T_d = T_{r3} + T_{r7} \tag{3.4}$$

T_d is in a direction opposite to that of T_{r3} and T_{r7}. It is assumed $T_{r3} = T_{r7}$.

For the static torsion of a shaft section, the relationship between the geometry, the torque T, the sectional deflection angle θ_s and shearing stress τ_r at radius r is:

$$\frac{T}{I} = \frac{G\theta_s}{L} = \frac{\tau_r}{r} \tag{3.5}$$

where I is the inertia of the section (for a circular shaft: $I = \frac{\pi D^4}{32}$), D is the diameter of the section, L is the length of the section and G is the shearing modulus, G=79 GPa.

Table 3.5 shows that the maximum shearing stress is only 82.1 MPa on stage 8 which sustains the largest moment with a small cross section. The maximum angular deflection is on stage 3 where the value is nearly 7 arc min. The difference in deflected angle between the two pinions (stage 3 and stage 7) is 2.7 arc min.

Stage	Length L (mm)	Diameter D (mm)	Moment T (Nm)	Sectional angular deflection θ_s (arc min)	Accumulative angular deflection θ_c (arc min)	Maximum shearing stress τ_{max} (MPa)
1	49	14	0	0.00	0	0.000
2	18	25	0	0.00	0	0.000
3*	20	32	T_{r3}=74.6	0.47	6.99	15.6
4	4	37.8	T_{r3}=74.6	0.06	6.52	7.0
5	39	30	T_{r3}=74.6	1.59	6.46	14.1
6	4	37.8	T_{r3}=74.6	0.06	4.87	7.0
7**	20	32	T_d =149.2	1.41	4.81	31.2
8***	20	24	T_d=149.2	3.40	3.40	82.1

Table 3.5 The stress and deformation of the shaft in the stages.

** The effective length is 10 mm as the key is acting in the middle of the section. The effective diameter is 29 mm.*

*** The effective moment is 74.6 Nm on a half of the section and 149.2 Nm on the other half of the section. The effective diameter is 29 mm.*

**** The effective length is 10 mm as the key is acting in the middle of the section. The effective diameter is 21 mm.*

3.4 Control, Electronics and Operations

This section describes the electronics and software system of the RV4 press. It includes the whole control diagram, the electronic system and the motor operation approach.

3.4.1 Holistic Control Diagram

Figure 3.32 is the system diagram indicating the control flow with schematics of the mechanical transmission.

The computers on the experimental platforms such as D9 or SXD exchange messages with the controller via a RS232 communication cable. Serial protocol is applied. When a rotation action is required for positioning the sample, commands can be sent to the controller for operation execution or status monitoring. When the controller is instructed, it uses its built-in driver to generate drive pulses to the motor via the motor cable. When the motor receives one or more pulses of voltage with sufficient current supply, it rotates a certain angle.

The output torque and speed by the stepper motor will, in sequence, be transmitted to the gearbox, the side shaft, the pinions, the gears, the central shaft and eventually the anvil assembly containing the sample. The process results in an increased drive torque and a reduced rotational speed. These are ideal rotational conditions for re-positioning a highly compressed sample.

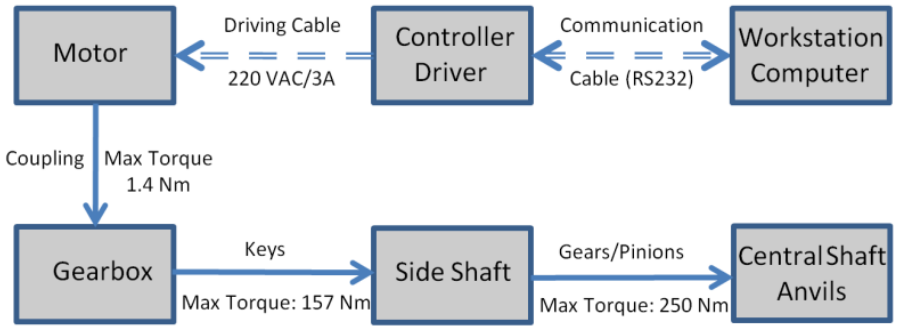

Figure 3.32 The system diagram of the control flow and the mechanical transmission.

3.4.2 Electronic System

The electronics for the RV4 press comprise mainly of the motor, the motor controller and the sensor that serves the controlling system. They are wired as shown in Figure 3.33.

3.4.2.1 Stepper motor

The stepper motor is driven and paced by pulsed power supplies. The required current supply for continuous operation is 3A. More details have been presented in Section 3.3.8.

3.4.2.2 The controller with built-in driver

The controller is a stand-alone task manager with stored programs. The commands mainly include three types, each with multiple functions. They are:

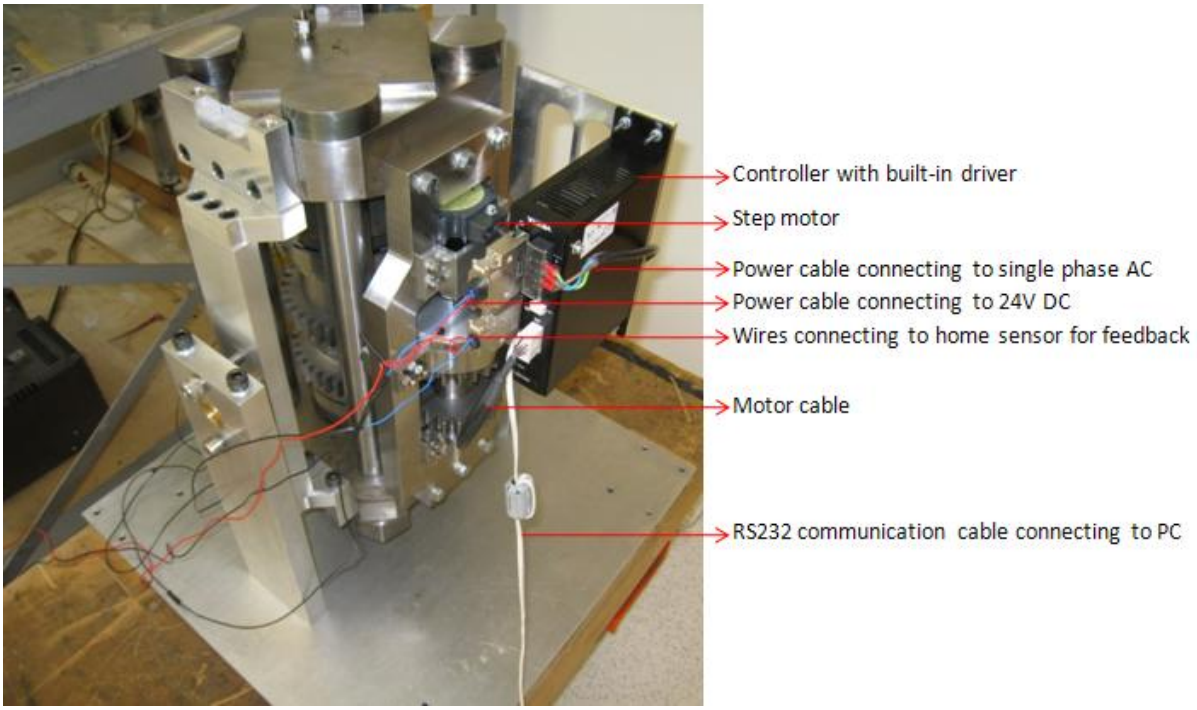

Figure 3.33 A picture of the electronic connections in the RV4. It consists of the stepper motor, the controller, the RS232 communication cable, the sensor and the power cables.

1) Monitor commands.

   A) Display functions (list, help, report, etc.)
   B) Parameter settings (starting speed, continuous speed, direction, etc.)
   C) Operation executions (absolute rotation action, relative move action, return home action, etc.)
   D) Program processing (copy or delete programs)
   E) Others, for instance the clear alarm.

2) Program editing commands.
   write or add new lines, delete or change existing lines

3) Programming commands.
   loop, end, if, wait, restart, alarm etc.

3.4.2.3 Home sensor

The mechanical switch manufactured by Honeywell Ltd. [76] (model: V15S05CZ015A01 [77]) is operating in constant-open manner and uses a roller lever for triggering to close the circuit. A small round-cap stud is installed on the bottom anvil support for triggering the switch when it passes by. This will generate and send a home signal to the controller.

The home sensor is for providing a positioning feedback to the control system. It serves as the home position for position definition and calibration. The reference of mechanical position alleviates the backlash-introduced positioning error by providing a home position and is further checked regularly during its operation to ensure that no loss of position has occurred.

3.4.3 Control and Operation

The total reduction ratio between the motor shaft and the anvils delivered via the gearbox and the gear/pinion mechanism is 800:3. When the motor supplies output with the resolution of 0.36˚ per step in the motor shaft, it is translated to only 0.00135˚ per step in the anvils. In terms of the speed, the RV4 is expected to provide rotation of the sample at low RPMs (between 0.2 rpm and 1 rpm). At the moment, a continuous operation speed of 360˚ per second for the stepper motor is found to be suitable for the RV4 press. This is 1000 pulse/second or 1000 Hz in the driver. It translates to 1.35˚ per second rotation in the anvils assembly and will make one complete turn in approximately 5 min. During the test, increased speeds up to 3000 Hz did not interrupt the operation.

The total resulting backlash of the mechanical system, resulting mainly from the meshing of the gear/pinion pairs, is found to be approximately 0.5˚ during online testing. The RV4 is operated in the same direction (i.e. only clockwise or only counter-clockwise 360˚ rotation without collision and problems with the hydraulic hosing twisting) in which case there is no backlash and a high precision positioning of the crystal can be achieved to within ±0.2˚. If the rotator is operated in both directions, corrections for backlash are made by the drive software.

Several programs developed to perform simple operations for the RV4 press are listed in Appendix G.

Chapter 4

Experimental Testing of the RV4

In the previous chapter, the general aspects and structural design of the rotational Paris-Edinburgh Press – the RV4 have been described. This chapter presents the results of the testing and use of the RV4 in the workshop and at large-scale neutron facilities, respectively. The process of testing and modifying the RV4 system involves a number of iterations. The difficulties encountered are partly expected and partly unexpected. With bold technical innovations, we managed to overcome the difficulties.

Section 4.1 describes the experiment with use of the 1st version of the RV4 system on the D9 single-crystal diffractometer at ILL.

Section 4.2 describes the technical problems encountered in the 1st version of the RV4 system and relevant mitigations. The corresponding testing and subsequent modifications we made led to the 2nd version of the RV4 system.

Section 4.3 describes the experiment and use of the 2nd version of the RV4 system on the single-crystal diffractometer SXD at ISIS.

4.1 Testing and Use of the 1st Version of the RV4 on D9

In late May 2009, the RV4 was assembled in the mechanical workshop of CSEC, Edinburgh, after half a year's manufacturing time. It was decided to ship it to ILL for testing on the D9 instrument as the beam time was scheduled in June 2009.

D9 is a monochromatic single-crystal diffractometer at the Institut Laue-Langevin (ILL) in Grenoble, France [22, 43, 45 and 46]. As described in Section 2.1.2.2, it is an ideal instrument for structural refinements beyond the determination of average atomic positions.

Figure 4.1 is a photo of the 1st version of the RV4 on the D9 instrument. The RV4 rests on the omega (ω) table which rotates the whole cell in horizontal plane. The RV4 itself rotates the anvil/sample assembly inside the frame relative to the tie rods.

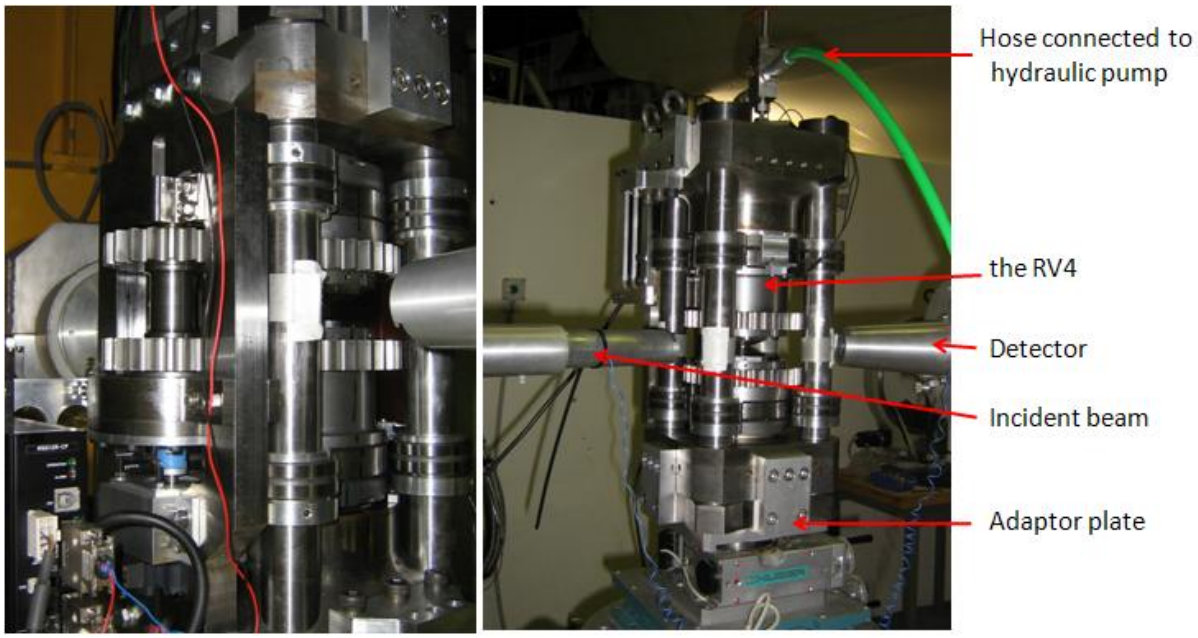

Figure 4.1 Pictures of the 1st version of the RV4 at the D9 instrument, ILL, France. The 1st version of the RV4 had mechanical spherical roller bearings for support of the central rotational shaft.

The test was scheduled for two days but due to earlier shutdown of the reactor the on-line test only lasted approximately 24 hours. The testing and the results are summarized below.

1) Mounting and alignment

It was checked at the initial stage that the RV4 was compatible with the experimental platform in terms of the hardware. The RV4 was mounted on the ω table by four adaptor plates (Figure 4.1). Some minor hardware changes were made, e.g. small inserts were added for height adjustment. Checks were also performed to ensure the alignment of the sample position to the beam to ensure that the height of the sample in the RV4 was suitable.

2) Electronics and software incorporation of the RV4 into the D9 instrument

ILL scientists and technicians wrote the controls of RV4 into the main control and measurement system – MAD. More programming work was yet to be carried out including incorporating the home sensor for position reference, making the positioning in parallel with other movements and sorting out occasional read error on position read function, etc.

3) Load capacity in rotation mode

The RV4 was able to rotate continuously with an applied load of ~20 tonnes. Above 20 tonnes the rotation could not be made continuous. Above 25 tonnes, the rotation could not be performed. At the time, possible solutions were considered to increase the target beyond 25 tonnes. These proposed measures were investigated after the RV4 was shipped back to Edinburgh. Section 4.2 discusses these issues in detail.

4) Testing of the quality of the single-crystal diffraction before and after the rotation under applied load.

A sample of squaric acid was ground into a disk with a volume of 3.5mm^3. It was glued into a modified SME gasket and loaded into the V4 cell with methanol:ethanol (4:1) solution as pressure-transmitting medium. Seven tonne load was applied to seal the gasket, and the cell was mounted and aligned on D9. The load was then increased to 20 tonnes which produced a pressure of approximately 0.6 GPa.

Overnight 52 reflections were collected using the omega table in normal beam geometry which allowed us to compare any induced strain in the crystal when using the rotation device. In the RV4 (1st version) eight needle bearings that were installed (on the tie rods) to restrict the anvil shaft tilting, but it still allowed a slight amount of

tilting. At the time we had no proof that this tilting was significant enough to move the reflections out of the detector area.

4.2 The 2nd Version of the RV4

After the testing of the first version on D9, two main technical problems were outstanding for mitigations and improvements.

1) Low load capacity.
2) Shaft misalignment and tilting.

With the structural modifications we made to solve the problems, the 1st version of the RV4 design was transformed into the second version. This section will describe the modification process.

4.2.1 Increasing Rotational Load Capacity

When the design started for the 1st version (Figure 4.2), the development strategy was to secure the integrity of the sample while improving the load capability. In the design process it was estimated that the average torque transmitted into the central shaft would be above 160 Nm which was sufficient to turn the spherical thrust roller bearings. Calculation and estimates of the transmission power and efficiency were listed in Table 3.1.

At the time of the completion of the 1st version, the RV4 test in laboratory and *in situ* (D9) found that the RV4 was able to rotate only if the applied load was less than 25 tonnes. To achieve a stable and continuous rotation only up to 20 tonnes could be applied.

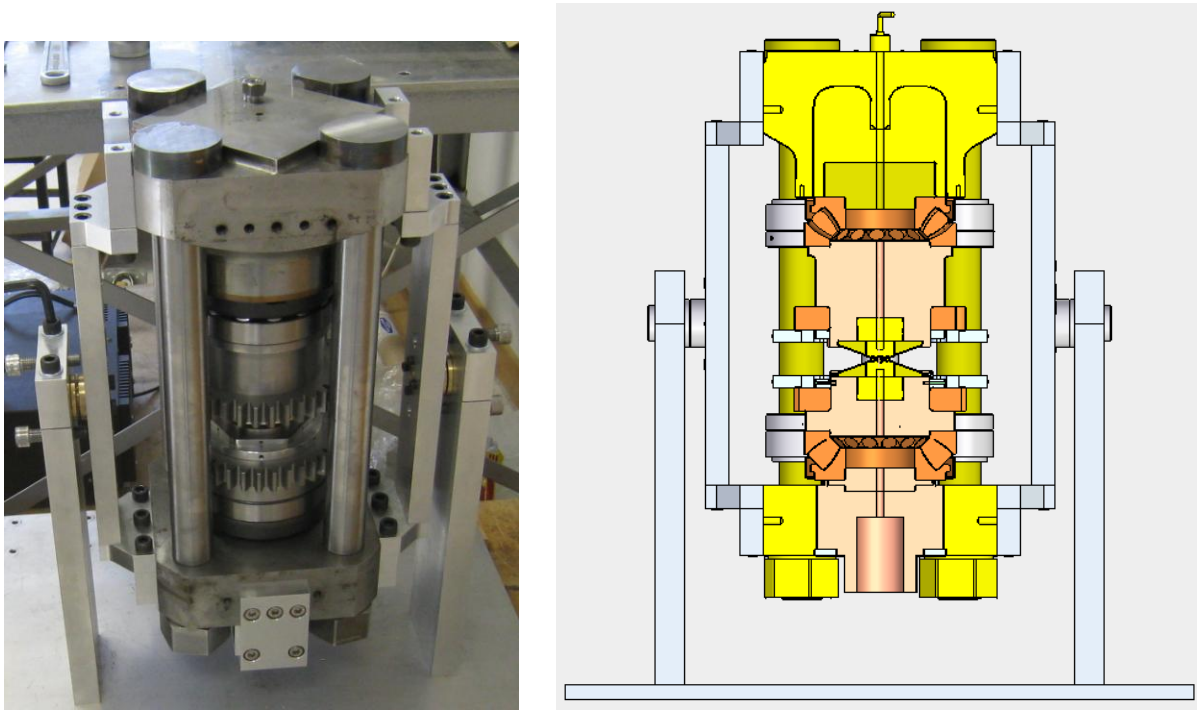

Figure 4.2 A picture and a sectional view of the 1st version of the RV4 design in an upside-down position. This position was used in the experiments on D9 and SXD.

4.2.1.1 The frictional resistance using spherical roller bearings

Naturally the focus of the loading capacity issue with the RV4 initially fell on the thrust bearings which may produce larger than expected frictional resistance when the axial load was applied. In the RV4 the thrust bearings of the central structure that is subjected to a large axial load is very critical to a successful rotation of the high-pressure anvil assembly. The adoption of the spherical roller bearings had rationales listed in the discussion on the options of the bearings is in Section 2.2.3.1.

It was found that the roller thrust bearings under the large axial load will have large friction between the bearing rollers and the bearing washers upon rotation. SKF 29412 was used in the roPEC apparatus where the different applied torques required for different gasket materials indicated that most torque was probably used to deform the sample [48]. Meanwhile the rotational HPXMT device used concentric low profile bearings and it was reported that the estimated frictional coefficient is 0.05 if grease lubricant was applied [51, 52]. The power torque for the rotation of the central shaft was calculated to be 745 Nm when the motor ran at a speed of 2000 rpm.

According to SKF official site [50, 53], the frictional moment can be calculated using the general formula:

$$M = 0.5\ \mu\ P\ d \qquad (4.1)$$

where

M = frictional moment in N.
μ = constant coefficient of friction for bearing; which is 0.0018 for spherical roller thrust bearings according to the SKF database.
P = equivalent dynamic bearing load, which is the axial load estimated at 915 kN in axial direction.
D = bore diameter, in the case of SKF 29412E, it is 0.06 m.

This results in a frictional moment of 50 Nm for either the cylindrical or spherical roller thrust bearings. In total, there is 100 Nm for two bearings. When the load is 150 tonnes, the total resistance is 150 Nm. This calculation however is the frictional resistance torque in dynamic operation and does not take into consideration the starting frictional torque of the rotation. The starting torque is normally of the same order of magnitude as the operational torque for plain roller bearings (e.g. SKF 89412TN), but is several times larger for tapered roller bearings (SKF 29412E). Furthermore, the actual friction varies significantly according to the running conditions, such as the temperature, the type of lubricant and the alignment of the rotation system.

In order to understand the reason of the unexpected high rotational resistance, two mechanical tests were carried out first in the workshop to measure the actual torque needed to turn the central shaft at rest.

4.2.1.2 Test 1 – torque wrench coupled to the side shaft

As it was physically impossible to install a torque meter on the central shaft, we measured the torque on the side shaft instead. The test configuration is illustrated in Figure 4.3. An adaptor with hexagonal profile replaced the harmonic gearbox and was connected to the bottom end of the side shaft. A torque wrench was engaged to the hex profile of the adaptor. The wrench had a minimum scale of 28 Nm and was rated to measure in a range up to 175 Nm.

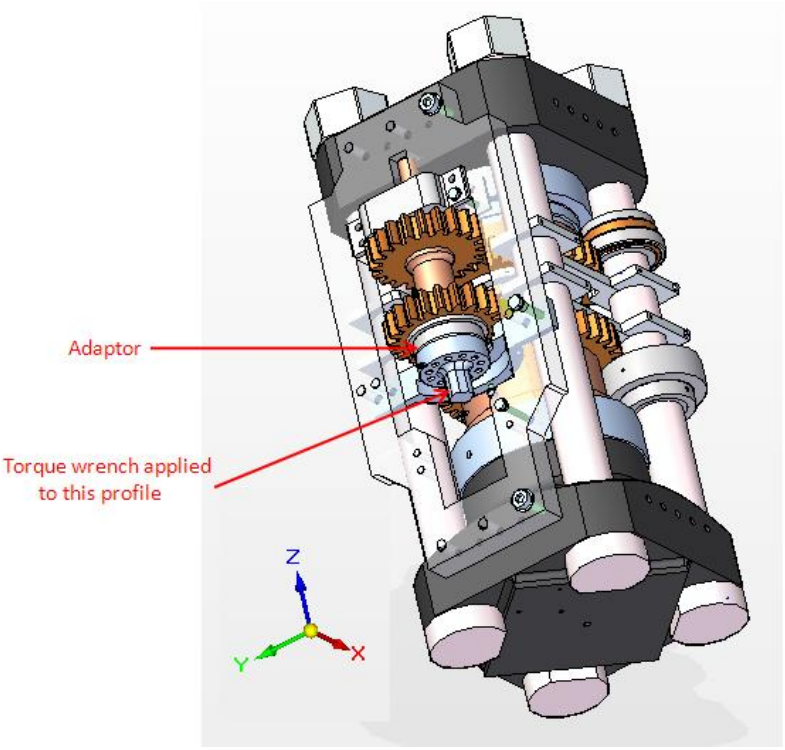

Figure 4.3 Illustration of the testing configuration with the torque wrench coupled to the side shaft via a hexagonal profile adaptor.

The tests showed that the wrench reading dropped significantly upon moving of the central shaft, which indicated a smaller rotational friction resistance compared to the starting friction resistance. The tests also showed that the resistance moments of the bearings varied as the turning directions changed (clockwise or counter-clockwise) when the applied axial load remained the same. The difference in the resistance when the direction switched was in the range of 10 – 20 Nm. Another finding was that the resistant moment normally would vary within a few Nm for a certain level of loading after reloading (to the same load). Two series of data were taken during two tests that followed the same procedures is included below in Table 4.1a and 4.1b. The torque readings in the wrench were collected in the first try of turning after loading increments.

Anvil axial load (tons)	Torque on wrench (Nm)	Equivalent central shaft torque (Nm)
11.8	<28	<46.7
14.2	-	-
16.6	100	166.7
18.9	118	196.7
21.3	126	210.0
23.7	134	223.3
26.0	140	233.3
28.4	146	243.3

Table 4.1a the 1st series of measurement data with the torque wrench coupled to the side shaft. Measurement records were taken on 6th June 2009.

Anvil axial load (tons)	Torque on wrench (Nm)	Equivalent central shaft torque (Nm)
4.7	<28	<42.0
7.1	40 (approximately)	60.0
9.4	60 (approximately)	90.0
11.8	80	112.0
14.2	96	144.0
16.6	115	172.5
18.9	120	180.0
21.3	124	186.0
23.7	132	198.0
26.0	140	210.0
28.4	146	219.0
30.8	154	231.0
33.1	160	240.0
35.5	166	249.0

Table 4.1b The 2nd series of measurement data with the torque wrench coupled to the side shaft. Measurement records were taken on 8th June 2009.

In the above tables, the central shaft torque was calculated using:

$$T_{central\ shaft} = T_{wrench} \times R_{gears} \times \eta_{gears} \qquad (4.2)$$

where $T_{central\ shaft}$ was the torque transmitted to the central shaft to turn the anvil assembly. T_{wrench} was the torque measured by the wrench. R_{gears} was the gear/pinion ratio (5:3). η_{gears} is the combined transmission efficiency of the gear/pinion pairs and the central shaft which was estimated to be 90%.

4.2.1.3 Test 2 – a bar coupled to the input shaft of the harmonic gearbox

As mentioned previously, the torque measurement with the torque wrench was limited to 28 – 175 Nm under an applied load of approximately 35 tonnes. In order to further understand the transmission system and estimate the torque needed to turn the central shaft under maximum applied load, a bar was coupled to the input shaft of the harmonic gearbox and turned by its far end by a force meter (Figure 4.4). The reading of the force meter was multiplied by the length of the bar (the arm length of a lever) and the product was effectively the input torque of the gearbox or the output of the motor coupling. The length of the bar was 100 mm.

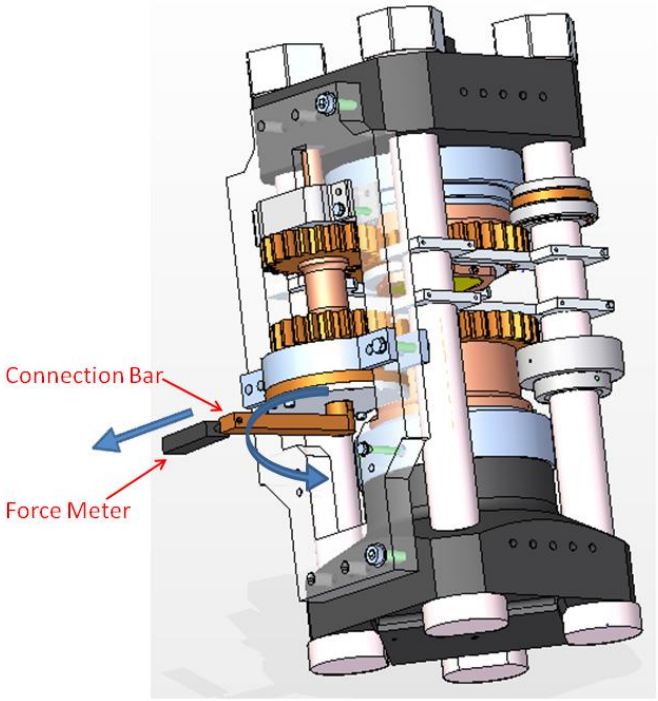

Figure 4.4 Illustration of the testing configurations with a bar coupled to the input shaft of the harmonic gearbox.

Two series of data were taken and included into the tables below:

Anvil load (tons)	Force (N)	Equivalent torque on the input end of the gearbox (Nm)	Equivalent output torque of the gearbox (Nm)	Equivalent transmitted central shaft torque (Nm)
0.1	0.9	0.09	9.4	14.0
6.1	5.0	0.50	5.2	78.0
12.1	8.0	0.80	83.2	124.8
18.0	7.5	0.75	78.0	117.0
24.3	11.0	1.10	114.4	171.6
30.0	15.5	1.55	161.2	241.8
35.5	15.0	1.50	156.0	234.0
41.0	24.5	2.45	254.8	382.2
47.1	35.0 (not stable)	3.50	364.0	546.0

Table 4.2a The 1st series of data with a force meter turning the input shaft of the gearbox. Measurement records were taken on 13th July 2009.

Anvil load (tons)	Force (N)	Equivalent torque on the input end of the gearbox (Nm)	Equivalent output torque of the gearbox (Nm)	Equivalent transmitted central shaft torque (Nm)
0.1	1.0	0.10	10.4	15.6
6.0	5.0	0.50	52.0	78.0
12.2	7.5	0.75	78.0	117.0
18.1	10.0	1.00	104.0	156.0
24.3	12.5	1.25	130.0	195.0
30.0	16.0	1.60	166.4	249.6
35.5	17.0	1.70	176.8	265.2
41.2	30.0	3.00	312.0	468.0

Table 4.2b The 2nd series of data with a force meter turning the input shaft of the gearbox. Measurements were taken on 14th July 2009.

In the above tables, the input torque of the gearbox was calculated using the formula below:

$$T_{input} = F \times L_{arm} \qquad (4.3)$$

where T_{input} was the torque produced by the turning force acting on the far end of the bar. F was the turning force when the central shaft started rotation. L_{arm} was the length of the bar which is 0.1 m.

The output torque of the gearbox was calculated using the formula below:

$$T_{ouput} = T_{input} \times R_{gearbox} \times \eta_{gearbox} \quad (4.4)$$

where T_{output} was the theoretical output torque of the gearbox. T_{input} was the input torque of the gearbox. $R_{gearbox}$ was the gearbox reduction ratio, 160:1. $\eta_{gearbox}$ was the combined transmission efficiency of the gearbox and the bar coupling [78]. $R_{gearbox}$=65% was used in the formula. The efficiency of the gearbox CSD-32-160-2A-GR alone was between 65% and 70% at 10°C and 500 rpm.

The equivalent torque transmitted to the central shaft was calculated using:

$$T_{central\ shaft} = T_{wrench} \times R_{gears} \times \eta_{gears} \quad (4.5)$$

where $T_{central\ shaft}$ was the torque transmitted to the central shaft to turn the anvil assembly. T_{wrench} was the measured torque in the wrench. R_{gears} was the gear/pinion ratio (5:3). It had no further discount on the efficiency after the gearbox. η_{gears} is the combined transmission efficiency of the gear/pinion pairs and the central shaft which was estimated to be 90%.

4.2.1.4 Summary of the tests and proposed mitigations

Two conclusions were drawn about the 1st version of the RV4 based on the test results:

- Conclusion 1:

  The primary difficulty in turning the central shaft under applied load was the large frictional resistance between the thrust bearings rollers and the washers. This meant the figure provided by SKF for general calculation in the initial design stage was far less than the actual starting friction resistance.

  The starting friction was nearly five times larger than the rotational friction expected at the initial design stage. On the other hand, the output and efficiency of the stepper motor, the couplings, the harmonic gearbox and the side shaft couplings was within the expected range. If the frictional resistance increased linearly when the applied load increased with the same gradient seen in the tests, the total frictional moment under an applied load of 100 tonnes would be around 1050 Nm.

- Conclusion 2:

  The friction was largely affected by the position and the alignment of the central shaft and transmission components, e.g. the pinions/gears, the bearings' rollers. An improvement to the supporting structure could possibly reduce the resistance. The amount of frictional moment that could be eliminated as a result was estimated to be up to 50 Nm. Lubrication between frictional contacts was also considered useful.

To overcome the problem, there were three options. The first two options focus on increasing the output torque. The third option focuses on reducing the resistant friction in the bearings.

- Option 1 – Increase the power with extra gears and larger gearboxes

  To increase the output torques of the RV4, some modifications were investigated for a design with a larger power generation and transmission. The suggested modifications were:

  - An extra small shaft directly coupled to the original stepper motor to increase the torque with another pair of spur gears. It could be installed next to the side shaft. With a gear ratio of 5:1, it could transmit 7 Nm to the input shaft of the harmonic gearbox compared.

  - Another gearbox with a larger torque capacity could replace the original unit. If a new model CSD-50-160-2A-GR was to be installed, it could output a torque of 730 Nm. This would then provide around 1100 Nm of torque to the central shaft.

  This option was not adopted as it involved significant modifications to the whole structure and could make the RV4 too big to fit into the vacuum tank on SXD.

- Option 2 – Increase the power with two motors and two gearboxes

  A two motor version of the RV4 was also considered for the purpose of providing extra torque to the system. It had two motors and two gearboxes. Both were identical products but would be installed at each end of the side shaft (Figure 4.5). This option was also not adopted as the RV4 with these modified structures would be very big. Besides the process could be very expensive and time consuming.

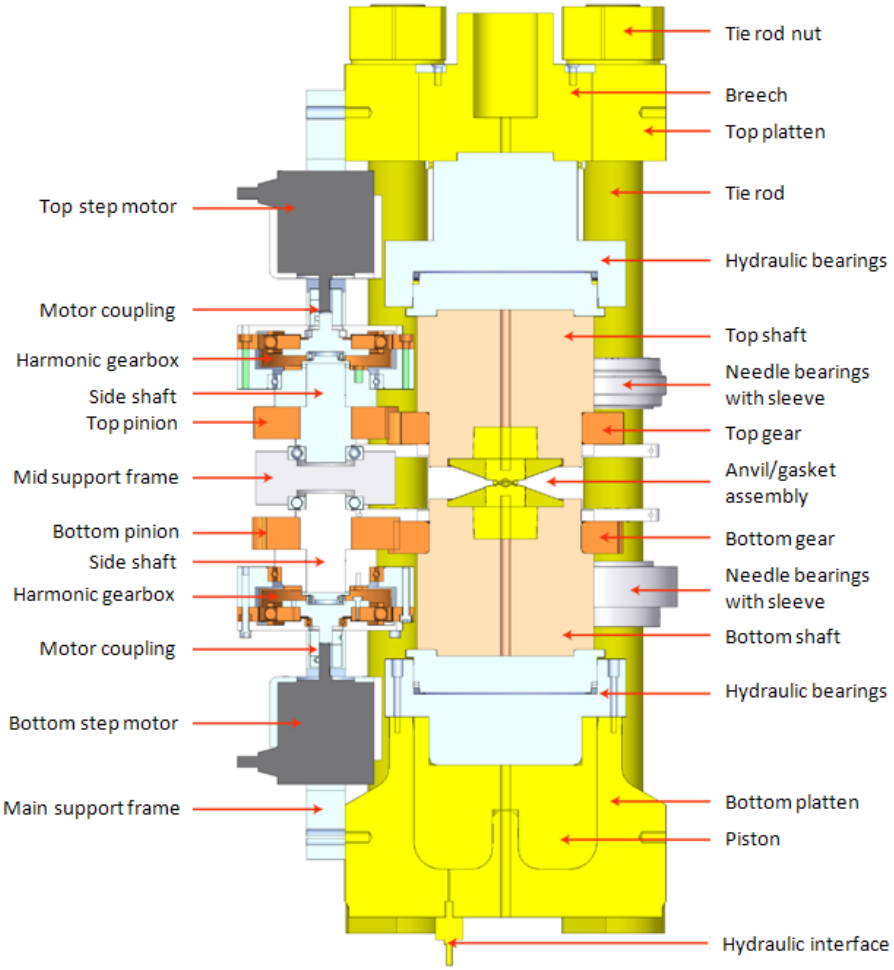

Figure 4.5 An optional design of the RV4 with two motors driving separate side shafts in order to increase rotational power to overcome the friction.

- Option 3 – a different design with hydraulic bearings

  This option was adopted as the modifications could be made without major structural changes in other part of the press. These subsequent changes have transformed the design of the RV4 from the first version into the second version (Figure 4.6).

  Initially a few measures towards the direction of reducing frictional resistance and power loss were:

- Using graphite as the thrust bearing lubricant.
- Re-lubrication of the gearbox to increase efficiency.
- Making new motor single-body coupling of stainless steel.

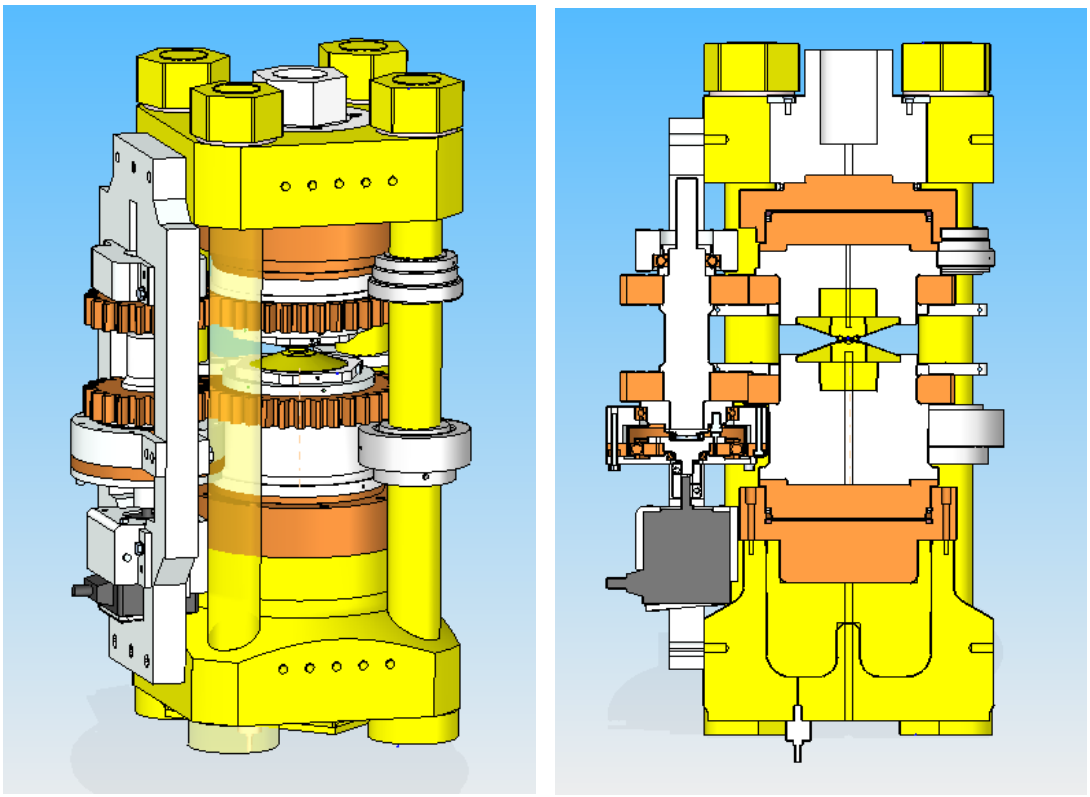

Figure 4.6 The 2nd version of the RV4 design with innovative hydraulic bearings

While the measures described above improved the friction and efficiency, the torque required to turn the rollers running on the bearing washer remained high. In an effort to reduce the frictional resistance significantly, a new type of hydraulic rotary bearings with an innovative and straightforward design has been developed. This was the major difference between the first version and second version of the RV4 design. Two sets of the hydraulic bearing were made. Each bearing had much smaller friction between two relatively slipping surfaces compared to mechanical roller bearings because there was a thin layer of lubricant applied between the slipping surfaces (design and analysis details in Section 3.3.5).

Significant amount of modification, manufacturing and testing work was carried out at the time to choose the hydraulic oil, the size and type of the sealing grub screw and the sealing ring material. Lubrication was applied to the piston and cylinder surfaces to help reduce the friction between the contact surfaces. The combination of a PTFE ring and a nylon ring were efficient in sealing the pressurized 100 MPa hydraulic oil in rotational condition. The PTFE exhibited good resistance to wear and low friction on the rotary sliding surface. The nylon ring provided supplementary sealing capability for the clearance gap between the rings and the cylinder bore surface. In contrast, sealing O rings made of rubber with different hardness ratings were also tested but they showed poor rotational sealing capability. They were squeezed into and caught in the gap between the piston and the cylinder. Upon stripping, the O rings showed some damage and were found unsuitable for use in the bearings.

To date, sets made of stainless steel have been verified by a laboratory test to rotate at above 100 tonnes in the RV4. The test showed that the frictional resistance was much less than that of spherical roller bearings.

The stainless steel bearings however showed very large deformation – 1 mm bending on the bottom surface of the piston – after being loaded to 150 tonnes in a test. The bearing cylinder and piston made of maraging steel were calculated to be capable to support more than 150 tonnes (Section 3.3.5). Two new sets of bearings made of maraging steel are being developed which are predicted to have better rotation performance.

4.2.2 Alignment Arrangements

In addition to the load capacity problem in the design of the 1st version, there was also an issue of misalignment in the central shaft mainly as a result of the relative slips between the bearing rollers and the housing washer. Although eight sets of needle bearings had been installed on the tie rods to support the central shaft, the issue still persisted. When driven by the gears, the two half shafts – referred to as the top shaft and bottom shaft – misalign horizontally and tilt vertically.

As illustrated in Figure 4.7, meshed teeth from the pinions and gears apply force F on the contact teeth surface. The force provides a power torque M’ that is needed in order to rotate the central shaft. However, at the same time it has a large force component F′ that pushes the central shaft to one side dependent on the direction of the rotation and the magnitude varied

with load. In the horizontal plane this undesirable force component F′ pushes the central shaft towards a tie rod (No. 3 in Figure 4.7) when the pinion rotates clockwise in a top view as is in Figure 4.7. As a result the whole shaft tends to shift from the target axis of rotation – the central line of the whole frame.

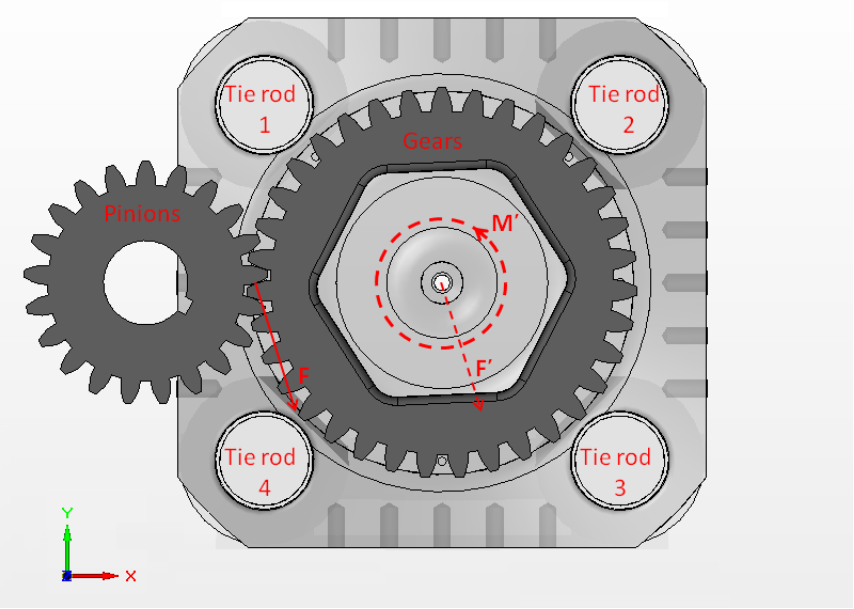

Figure 4.7 A demonstration of the force and moment that caused the horizontal misalignment. The action is driven by the meshed teeth contact force.

In a vertical view (Figure 4.8) this component F′ tends to tilt the central shaft into a slight '>' shape. The central shaft consists of the top and bottom shafts joining in the middle at the sample position. Each of the two shafts consists of multiple components such as the hydraulic bearing piston, the anvil support, the gear, the anvil and gasket rings etc. When the gears are turned by the pinions, the F′ component on each half is close to the 'tip' of the half shafts, i.e. to the anvils. They tilt around their root support – the cylinder of the hydraulic bearing which acts as a pin constraint and the 'tip' of the half shafts tends to shift towards the side that is opposite to the pinion side.

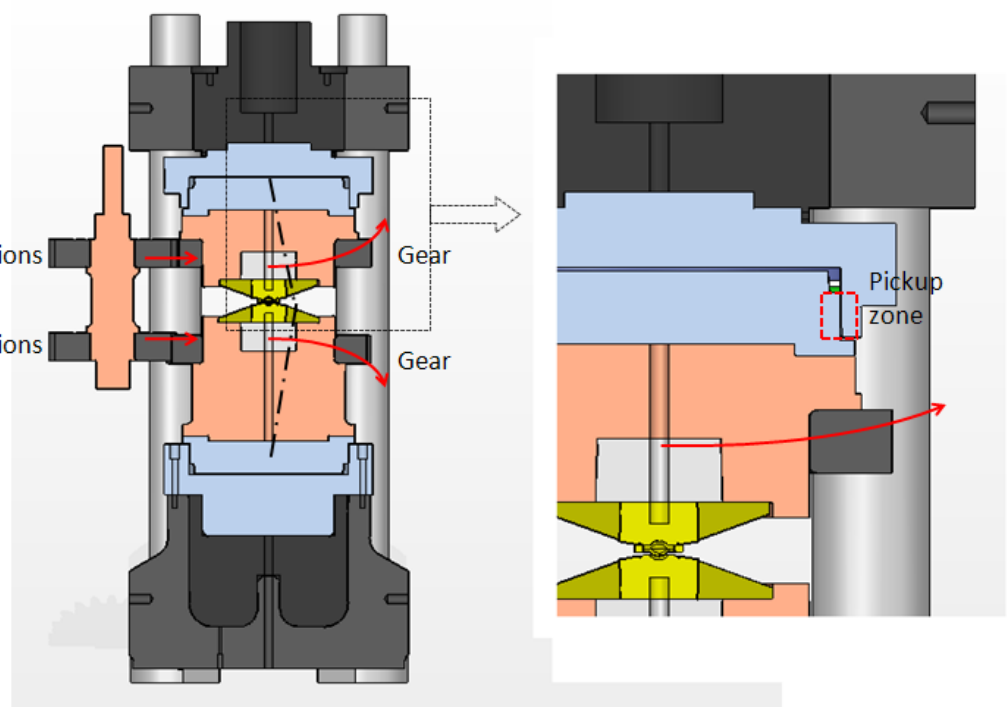

Figure 4.8 Vertical tilting due to meshing teeth force

In the radial direction, the positioning variance of the top and bottom shafts was measured near the gears during rotation with and without applied load. This was achieved by observing the deflection of a dial gauge with a minimum scale division of 0.01 mm (Figure 4.9). When the shafts rotated freely, they had a variance within ±0.12 mm. When the top and bottom shafts were loaded axially, they both tended to be pushed aside significantly by the pinions on the anvil end. The coupled shaft consequently proceeded with a radial variance between ±0.5 mm when it was running at 60 tonnes.

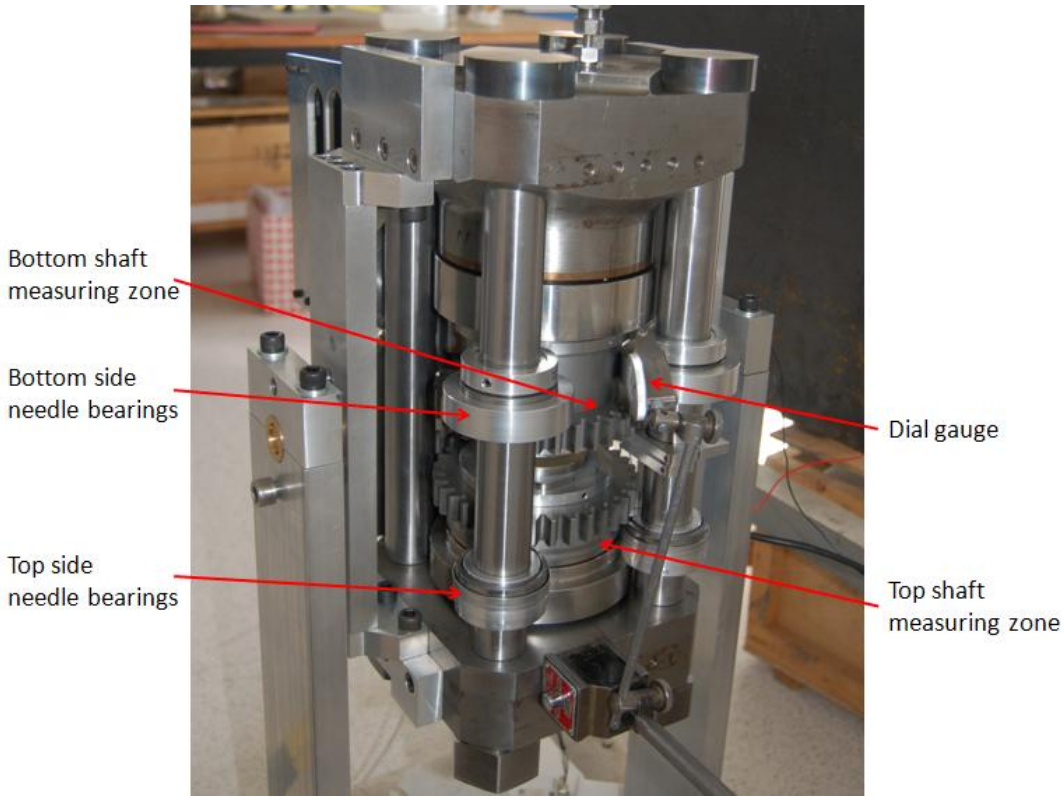

Figure 4.9 The configuration of the measurements of the alignment variance of the central shaft in radial direction using a dial gauge.

The misalignment produces unsteady rotation of the shafts. This unsteady rotation not only posed a danger of damaging the single-crystal samples, it also increased friction inside the hydraulic bearings as the bearing cylinder and piston surfaces rubbed against each other under radial force and formed a frictional metal-metal contact. Experiments showed scratches after a period of running under this condition. The zone where the bearing piston and cylinder surfaces picked up with each other is illustrated in the close-up view (Figure 4.8). In order to avoid the rubbing between the piston and the cylinder, the surfaces were machined to a higher finish quality and lubricant was applied to them. Most importantly, the clearance between the bearing piston and cylinder was carefully chosen. A larger clearance might avoid the surfaces picking up during rotation and thus reduce friction. However it might compromise the sealing properties of the seals. Two new hydraulic bearings are to be made of maraging steel as replacement to the current stainless steel ones. With tougher contact surfaces they are predicted to be more robust in preventing damage from surfaces rubbing.

As a major modification to eliminate misalignment and tilting, four enhanced needle roller bearings with sleeves (design details are described in Section 3.3.6) are mounted on the tie rods to counteract the side force from the pinions. Two of them are on the top side and the other two are on the bottom side of the mainframe of the press. They are precision machined and installed against the anvil support seats on the side opposite to the driving pinions (Figure 4.8). Thus the top and bottom shafts are constrained relative to the position of the four parallel tie rods. The cylindrical housings of the hydraulic bearings are also precisely located relative to the tie rods. By using these references the centres of the housings have relative misalignment less than 0.1mm upon assembly. This largely reduces radial positioning variance of the shaft to around ±0.2 mm during rotation operation under load. The needle bearing rollers of these constraints carry a large part of the force F' (Figure 4.7), reducing the normal force on the contact between the piston surface and the housing bore surface inside the hydraulic bearings and thus the friction resistance.

4.3 Testing and Use of the 2nd Version of the RV4 on SXD

After a series of structural modifications, the 2nd version of the RV4 was tested in the mechanical workshop of CSEC from December 2009 to March 2010. It performed well for loading up to just above 100 tonnes. In March 2010, it was shipped to the SXD instrument at ISIS (Rutherford Appleton Laboratory, Oxfordshire, UK) for neutron experiments.

When the press was used on SXD, it was mounted with the breech at the bottom of the support assembly on the SXD instrument. Shown in Figure 4.10 is the RV4 being lifted by the crane before being positioned into the vacuum tank on SXD. Shown in Figure 4.11 is a sectional view of the RV4 inside the vacuum tank (note the relative position of the RV4 to the tank).

When the breech is fully inserted into the top platen there is a 3 mm gap between the anvils for the gasket to be located. When the sample and gaskets are to be loaded into the cell, the breech can be withdrawn by 5 mm from its fully engaged position so that the hydraulic bearing and extended anvil support, with its anvil, are lowered, while the components on the other side remain in place supported by removable brackets mounted on the tie rods. With the breech withdrawn, a total gap of 8 mm between the top and bottom anvils is available for putting the gasket and sample in place and transferring pressure transmitting media into the sample space. Once the gasket assembly, sample and pressure-transmitting medium are inserted between the anvils, the breech can be screwed upward to its home position to close

the gap between the anvils, a load is then applied to seal the gasket assembly preventing loss of the pressure transmitting medium.

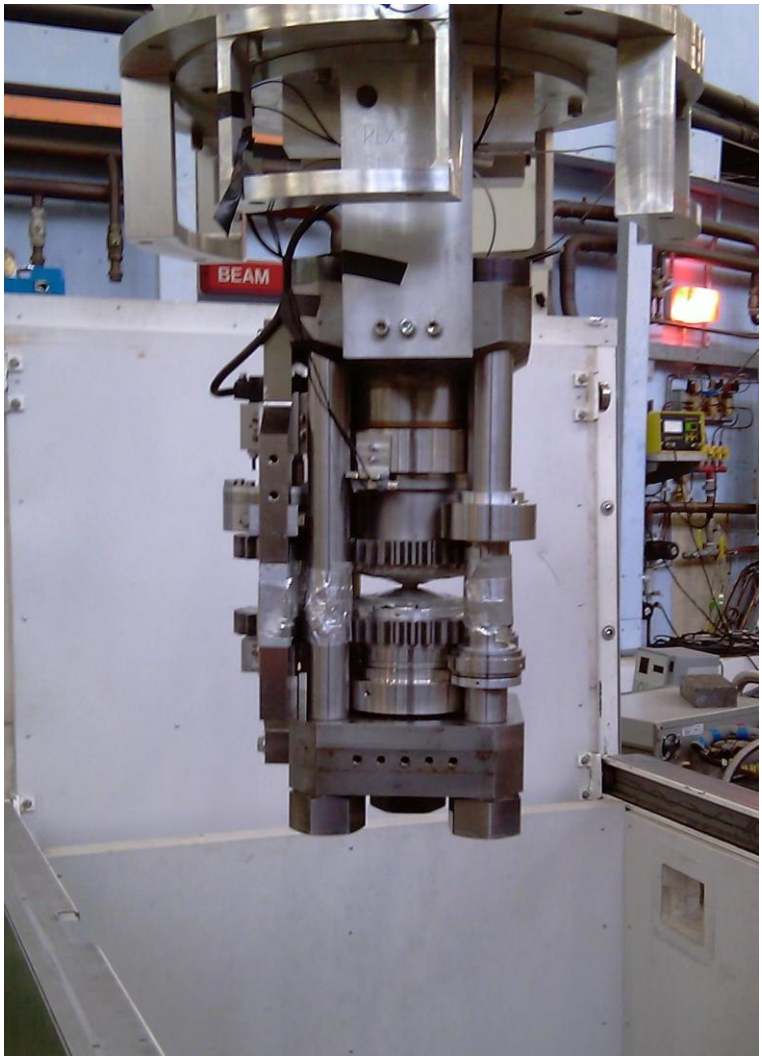

Figure 4.10 Photo of the RV4 being lifted in the air before being installed inside the vacuum tank on SXD instrument. In this position, the breech was at the bottom side of press.

In situ high-pressure neutron-scattering experiments were performed on a single crystal of germanium [38, 39]. The single-crystal diffractometer SXD at the ISIS pulsed neutron source was used [42, 44]. SXD utilizes polychromatic pulses of neutrons, and allows access to large volumes of reciprocal space by the Time-of-Flight (TOF) Laue technique.

The details of the sample loading and orientation process were the same as described by Bull *et al.* [41]. A pair of 20°-bevelled anvils was mounted in the RV4 press and modified encapsulated gaskets made of null-scattering TiZr alloy (67:33 molar ratio) were used. The sample used was a cylindrically shaped single crystal of germanium (see Bull *et al.* [27, 37 and 41]). The size of the crystal was approximately 3 mm in diameter and 1 mm in height. The crystal was mounted on the internal surface of a modified gasket and a deuterated methanol:ethanol mixture was used as a quasi-hydrostatic pressure medium. To reduce the background inherent from the anvils, gasket and press, the steel of the anvils and RV4 in the incident and diffracted beam path were covered with thin cadmium sheets. The beam size was defined further by the jaws of the SXD instrument itself. The configuration of the RV4 mounted on the SXD instrument is shown schematically in Figure 4.11. With the sample loaded into the gasket and the pressure medium placed in the sample chamber, the load in the press was increased in order to seal the gasket assembly and prevent the loss of the volatile pressure medium.

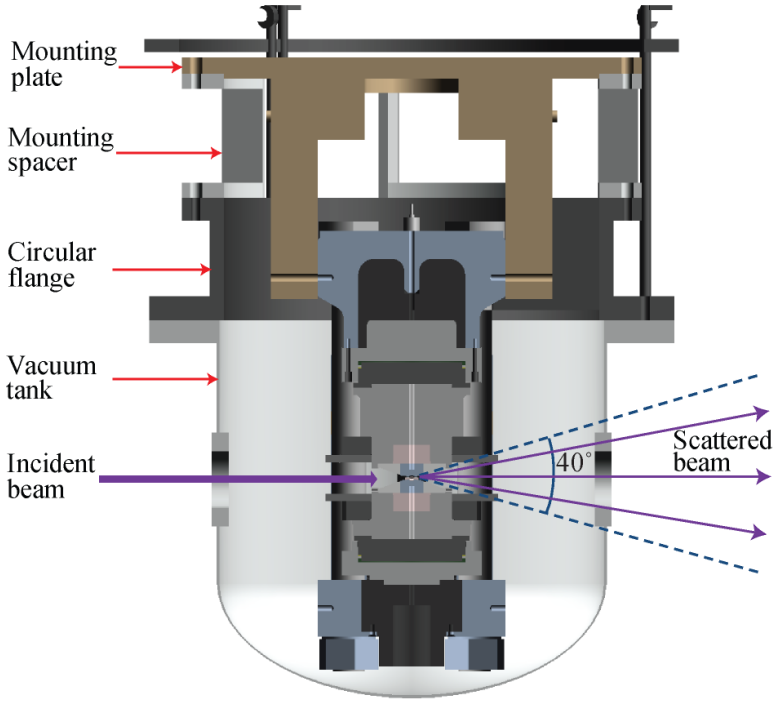

Figure 4.11 Cross-sectional view of the RV4 experimental setup at the SXD instrument, ISIS. The angular aperture was 40º as a pair of 20º bevelled anvils was utilized in the experiment to maximize access to reciprocal pace. Surrounding the set up are the six ZnS scintillator detectors centred on the equatorial plane of the instrument that can be accessed in high-pressure measurements [79].

The press assembly was mounted on SXD in an orientation which minimizes shadowing of the detector by the tie rods. With an applied load of 7 tonnes, the sample pressure was very close to ambient and a diffraction measurement was made to determine the sample's orientation. The hydraulic load on the piston was then sequentially increased. As each step increased the load by 10 tonnes, the changes in the diffraction patterns were observed. This was to monitor the generated sample pressure and any possible damage of the crystal at each step.

At 70 tonnes a sample pressure of ~6 GPa was achieved and a data set was collected for a period of approximately 6 hours. On completion of the data collection the bearings, the extended anvil supports, the anvils and the sample were rotated by 44.6 degrees, to bring previously inaccessible reflections out of the 'shadow' of the tie rods. Figure 4.12 shows the observed reflections from the horizontal h0l layer.

The reflections observed from the h0l layer of the crystal in the original position of the sample are shown as squares, and those observed after rotation are shown as circles (Figure 4.12). The substantially increased access to reciprocal space is clear. The reflections obtained after rotation were observed at positions predicted by the initial orientation matrix of the crystal, and reflections were unaltered in their shape and intensity. This indicates that a good quasi-hydrostatic environment was maintained during the loading and that there was no mismatch in rotation of the two anvils sufficient to cause any detectable shearing of the sample crystal.

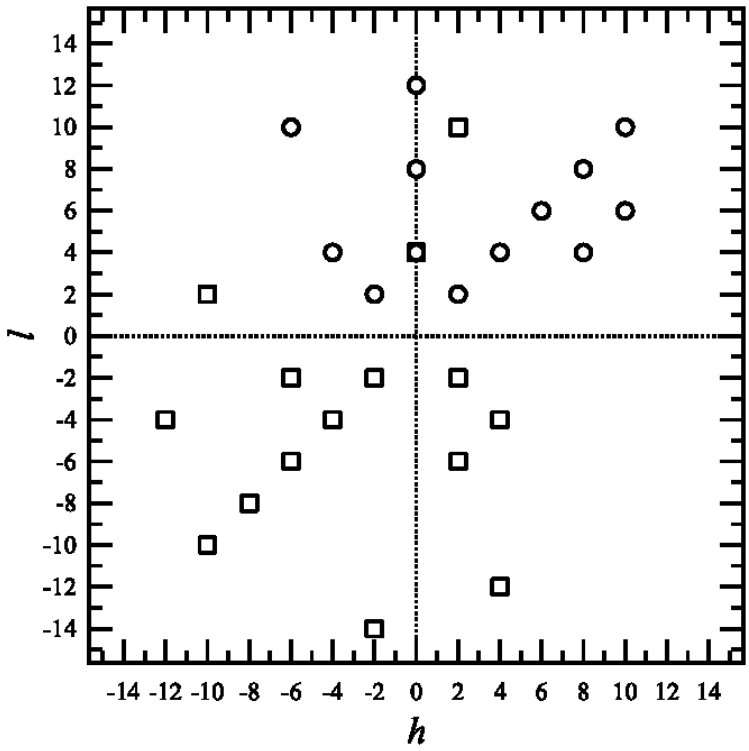

Figure 4.12 The map of h0l reflections observed during the SXD experiment on a single crystal of germanium at 70 tonnes in the RV4 (from [79]). The h and l Miller indices are shown along the x and y axes, respectively. The reflections in the original orientation of the crystal are shown as squares. The reflections observed from the same h0l layer after rotation of the crystal by 44.6 degrees are shown as circles. Note, 004 is the only reflection visible in both orientations of the sample.

Chapter 5

Finite Element Analysis of Double-toroidal Anvil

This chapter describes the numerical work on the mechanical performance of the double-toroidal anvils. These anvils reproducibly fail on the surface when the load applied to the anvil assembly approaches approximately 240 tonnes. The possibility of optimizing the anvil and gaskets to achieve higher pressure is also analysed.

Section 5.1 describes the background details of the work. The problem encountered in the experiments is explained and illustrated.

Section 5.2 describes the finite element model. The components of the modelling include the geometry, the materials' properties, and the load conditions. The description of the modelling also includes the analysis settings, such as the assumptions, the mesh and the calculation methods. This is followed by the explanation of the analytical procedure using this model and the validation process. Two major material properties – the plasticity of the gasket material TiZr and the modulus of the sample – crucial to the analysis are then determined.

Section 5.3 describes the results of the analysis. They include the direct model outputs such as the stress and deformation as well as the rationale based on these results to explain what is observed in experimental tests.

Section 5.4 describes the paths for optimizations of the existing anvil configuration in order to improve the mechanical performance of the anvil cell under very large applied load. Future work and some discussions on this issue are also included.

5.1 Background

The motivation for this analysis is a technical problem which has been encountered over the last few years when double-toroidal anvil cells experience failure on the anvils' surface when the applied load approaches 240 tonnes. The pressure produced in the sample by this load is close to 30 GPa.

So far a number of anvil failures have been encountered in laboratory high-pressure experiments. These toroidal anvils, including both single-toroidal and double-toroidal anvils, are routinely used for high-pressure neutron-diffraction experiments by my colleagues – a group of high-pressure crystallographers and engineers based in CSEC [17] and at ISIS [21].

Therefore, a complete investigation to look into how the anvil cell behaves under applied load can be beneficial in the following aspects:

- To find out the direct cause of the failure in the anvils and the mechanism of interaction between multiple components present in the cell.

- To look for the possible optimizations of the anvil and gaskets based on the above findings which may make it possible to achieve higher pressure.

- To provide reference to other studies investigating a similar problem. This is part of the vast efforts by the high-pressure researchers to improve similar opposed-anvil cells.

5.1.1 Single-toroidal Anvil

Single-toroidal anvils have two versions according to the angle of the taper on the surface: 7˚ or 20˚ (Figure 2.16). The 7˚ anvil is the standard version that was developed initially. The 20˚ version is a variant developed by C. L. Bull *et al.* [37] that gives greater angular aperture access for single-crystal neutron scattering on SXD. The geometries of the anvils are as shown in Figure 5.1. The assembly of the single-toroidal anvil cell with standard gaskets or encapsulated gaskets is shown in Figure 2.15.

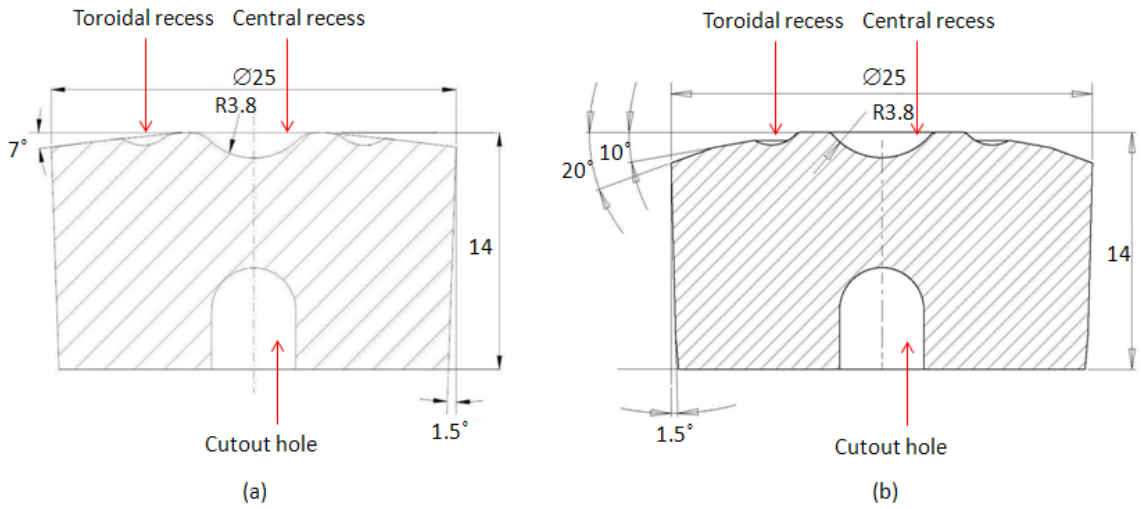

Figure 5.1 Cross-sectional view of the geometries of single-toroidal anvils with different taper angles: (a) is a 7° anvil; (b) is a 20° anvil (after [37]). On the top surface, there is a central recess and a toroidal groove. The central recess is relatively larger in space to allow for large-volume sample, compared to the toroidal groove. The toroidal groove is on the edge of the taper profile. It is made to provide hoop stress support in the radial direction for the highly-compressed and highly-deformed gaskets under applied load. At the bottom end of the anvils, a hole is created to allow neutron beams to go through.

Figure 5.2 Pictures of the single-toroidal anvils that broke under load on SXD and PEARL instruments at ISIS. Most of the failures are on the surface.

There are a number of high-pressure experiments that have been disrupted because of the mechanical failure in these anvils. Figure 5.2 shows some broken anvils that were used in neutron-diffraction experiments over the past few years on two instruments at ISIS: SXD [44] and PEARL [80]. Most of these failures occur on the top surface. Some of them failed with very small radial cracking that was only visible under microscope; some of them had visible chipping cracks on the contact surface with the gaskets and the damage can be small and localised, or large-scale cracks propagating through the volume of the anvil's body. Figure 5.3 shows pictures of the cracked single-toroidal anvils with a taper angle of $7°$ or $20°$.

5.1.2 Double-toroidal Anvil

The applications for various purposes have been driving the development of new or modified versions of toroidal anvils. One modification to the original toroidal profile is the addition of a second concentric toroidal groove around the central sample chamber known as the double-toroidal anvil [31]. It is designed to produce high pressure in the sample with extra radial support to the gaskets in compression. The geometry is shown in Figure 5.4.

With regard to the sample volume in neutron-diffraction experiments, a major problem with this type of experiment is the low flux of neutron sources, which requires the use of large samples. In order to collect sufficient diffraction data for full structural refinement in a reasonable amount of time, neutron scattering require single-crystal samples of at least 1 mm^3, and powder samples of 100 mm^3 [28]. Typically the sample volume for single-crystal diffraction measurements is 10 – 1000 mm^3 at ambient pressure [39, 40].

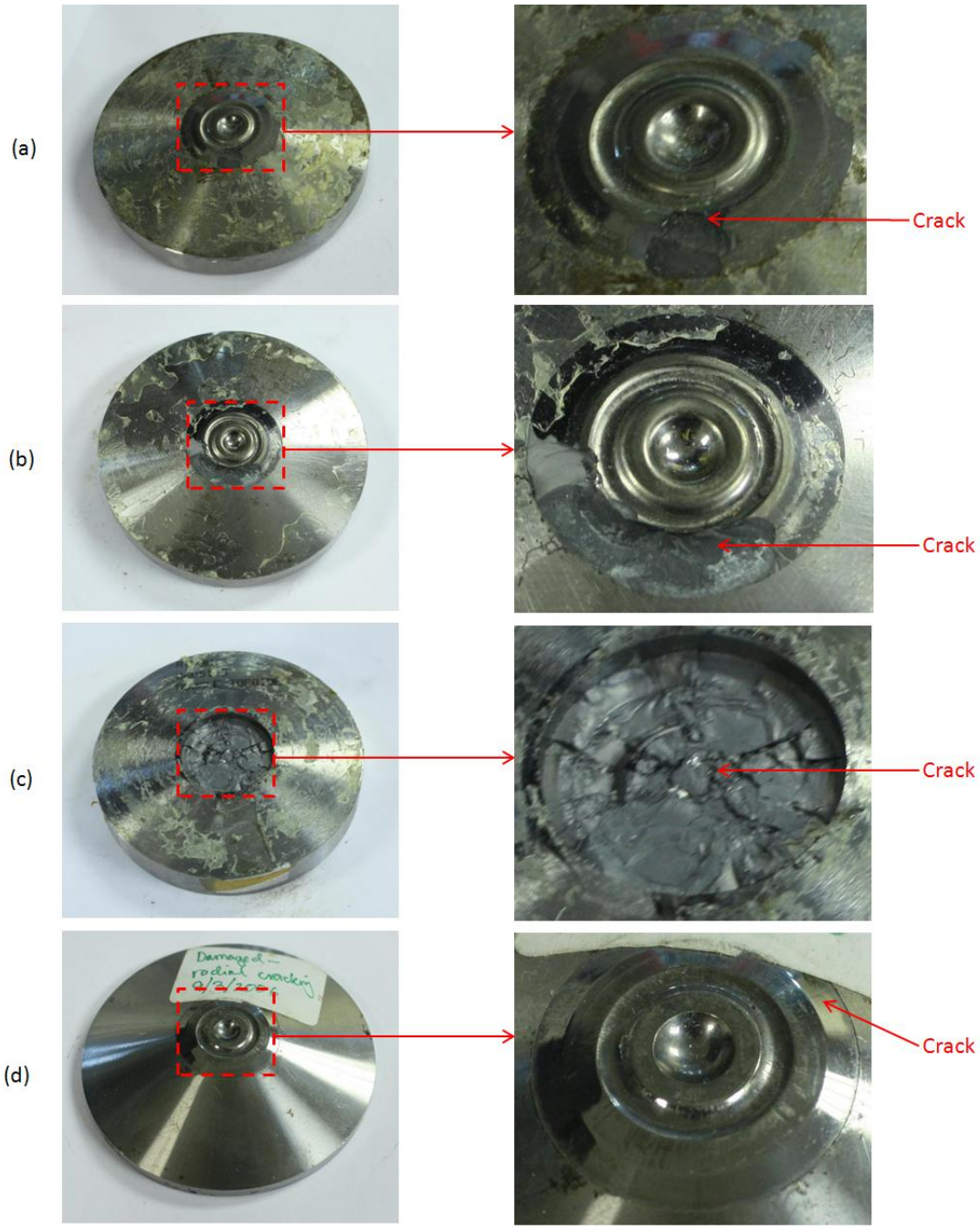

Figure 5.3 Broken single-toroidal anvils with close view of the cracks. (a), (b), (c) are 7º anvils with localised or large-scale cracks; (d) is a 20º anvil with cracks that are not visible to naked eyes.

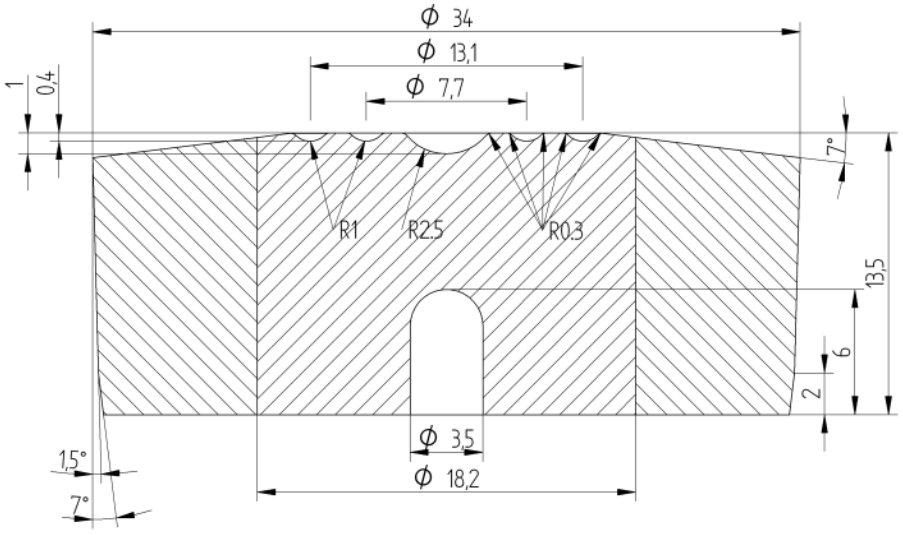

Figure 5.4 The geometry and key dimensions of the double-toroidal anvil (after [81]).

With a much larger sample, the pressure generated on the sample is limited. This limitation causes a serious problem in a number of fields of science, where neutron scattering studies of matter at much higher pressure could make important and unique contributions [28]. Currently double-toroidal anvils made of sintered diamonds are used in the Paris-Edinburgh press for neutron scattering experiments up to 30 GPa [4]. This is achieved on samples with a volume of ~35 mm^3 encapsulated by non SME gaskets. However, in the vicinity of this pressure the anvils fail as the surface and body of the anvils crack or fracture. Figure 5.5(a), (b) shows two of the double-toroidal anvils made of sintered diamond and tungsten carbide that cracked during high-pressure experiments. The binding rings outside the anvils are made of heat-treated maraging steel. Figure 5.5(c) shows two broken double-toroidal gasket assemblies with sample still encapsulated inside. The gaskets are made Titanium Zirconium alloy (67:33 molar ratio).

In order to achieve higher sample pressures with such large sample volumes, we carried out a comprehensive finite-element analysis to get insight into the mechanical performance of the anvils under load. This part of my PhD project investigates the causes of failure in the double-toroidal anvils and possible improvements that can be made in their design. ANSYS workbench is used as the platform of modelling, calculation and displaying the results.

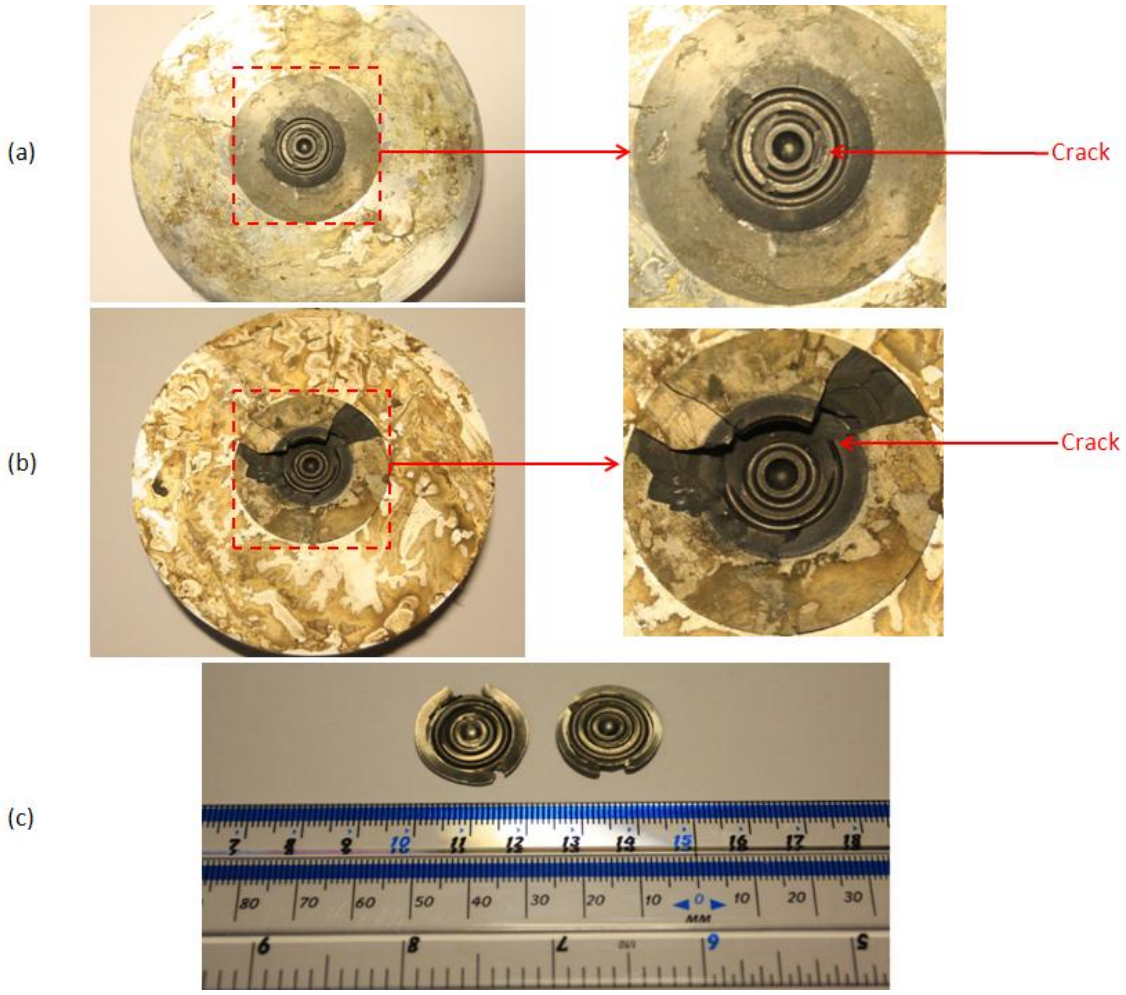

Figure 5.5 Photos of broken double-toroidal anvils and gasket assemblies. (a), (b) are two double-toroidal anvils with close-up views of the cracks; (c) are two broken gasket with a ruler for scale reference.

5.2 Finite Element Model

As described in Section 2.3, Finite Element Method (FEM) is a numerical technique that is now being used to routinely obtain numerical solutions to structural mechanics. FEA offers an effective simulation tool for structural design and optimization that minimize the resources required for commercial product development and scientific analysis of real-world problems. These automatic solutions tackle various problems and making the development

process less costly and more reliable. Finite Element Analysis has for decades been used for designing and modifying high-pressure devices. The Paris-Edinburgh press was designed and optimized by finite-element methods and new modifications and developments of toroidal anvils [37, 47] and diamond anvils (DAC) [58, 59, 62, 63, and 64] also utilise the technique.

In the finite element model we construct for the double-toroidal anvil cell, many factors are contributing to how effective and convincing the results are. These factors include the physical configurations of the geometry, the materials and the load conditions, as well as the analysis settings, such as the assumptions, the mesh and the calculation methods.

The process of the analysis with the model is as follows:

- Construct the model:
  The static structural model consists of multiple components and multiple parameters.

- Validate the model:
  There are two important material property parameters that are not available in publications and very difficult if not impossible to be determined by testing. These parameters are the plasticity of the gasket material and the elastic modulus of the sample. They are varied in the model to produce the data and compare with what is observed in experiments for best-fit match. This determines the parameters and thus validates the model.

- Produce mechanical performance results:
  Stress and deformation distributions are generated automatically. The data is then compared with strength data to analyse the failure cause of the anvils.

- Optimize the anvil:
  The potential modifications to the configurations are analysed to look for improvements in the performance of the cell and to attain higher pressures.

5.2.1 Model Configurations

The static-structural analysis we present is performed using ANSYS workbench [55] with mechanical meshing. The geometry is a configuration of two opposed double-toroidal anvils and five gasket pieces in which a powdered sample is encapsulated (Figure 5.6). The anvils are the hardest components in the device, obtained by machining commercially available tungsten carbide supported sintered diamond die blanks (D30-5913 by Diamond

Innovations) [82]. The die consists of two concentric portions which are integrally bonded together in the manufacturing process: the core die (A1, A2 in Figure 5.6a) made of polycrystalline diamond particles and the supporting ring (B1, B2) made of tungsten carbide. The toroidal profile is spark eroded into the blank die prior to final polishing of the surface.

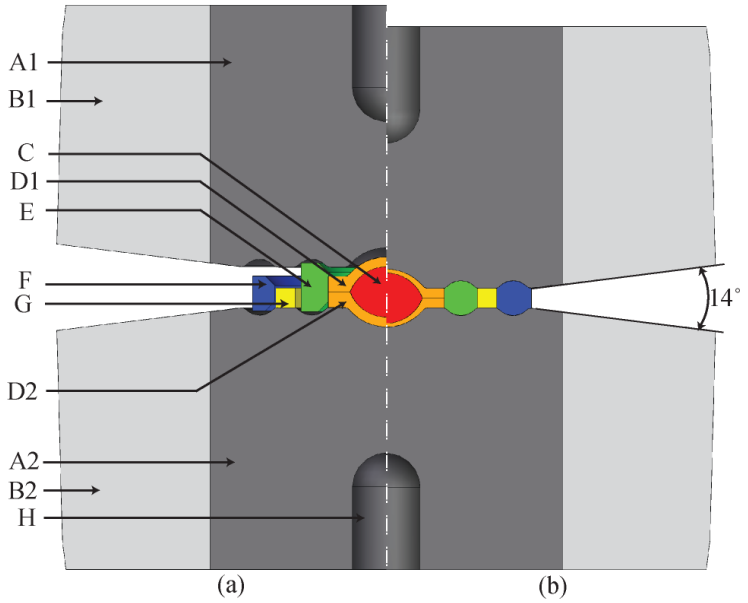

Figure 5.6 Schematic diagram showing the arrangement of the gaskets (a) before and (b) during loading used in the standard model.

***A1**, **A2**: Polycrystalline diamond (PCD) core portion of the anvils. PCD consists of randomly orientated micron size diamond crystals with extremely high diamond-to-diamond bonding and exhibits uniformly high, non-directional hardness and high resistance to failure [82]. Cobalt binder is used as the bonding agent.*

***B1**, **B2**: Tungsten carbide (WC) supporting ring of the anvils. They are integrally bonded to the diamond core and supported outside by maraging steel binding rings which initially provide a hoop tangential stress of 1 GPa and internal radial stress of 0.5 GPa.*

***C**: Powdered sample.*

***D1**, **D2, E, F and G**: Gaskets made of TiZr alloy (67:33 molar ratio). This deformable alloy has a low tensile strength and behaves plastically at high pressure.*

***H**: A blank hole of a diameter of 3.5 mm at the back of the anvils is machined to reduce the amount of material the incident beam of neutrons passes through before reaching the sample volume prior to diffraction.*

Between the anvils are the metallic gaskets (D1, D2, E, F, and G) machined from a null scattering TiZr (67:33 molar ratio) alloy which are pre-formed between the anvils at 5 tonnes prior to final stage of machining which allows them to fit perfectly into each other and also match the profile of the anvil's surface. When axial load is applied to the back surface of the anvils, they are brought together against the gaskets. The gaskets would then undergo significant plastic deformation – flatten and expand outward as soon as the stress exceeds its yield strength. Inside the gaskets, a powdered sample (C) (approximately 17 mm^3 in volume) is contained within the sample chamber. Surrounding the WC ring (B1, B2), there are two maraging steel binding rings (not shown) for radial support. Frictionless supports on the cylindrical surface in ANSYS are introduced to represent the binding effects provided by the steel rings.

The geometry of the anvil and gasket components has axial symmetry along their central axis and relative to the central plane and as a result only a quarter of the cross section is applied in the model using 2D axial-symmetric settings. Axial thrust load is applied to the top anvil against the stationary bottom anvil. The properties of the materials used in the model are listed in Table 5.1.

The difficulty associated with the simulation of the system is that there are a few unknown quantities. One of them is the frictional coefficient between the contact surfaces under high pressure. Some studies of the diamond anvil cell [64] have shown that the friction of contacts between the anvil and the gasket has no major impact. In our simulation of the double-toroidal anvil cell both perfectly cohesive (bonded) and frictional contacts between the anvil and the mating gaskets are analysed for comparison. Theoretically the frictional model should produce results that match the experimental data better than a bonded model which assumes no slipping between the gaskets and the anvils. In the frictional model, a range of gasket-anvil surface contact friction coefficients is considered. It is found that the results obtained when the frictional coefficient is between 0.2 and 0.5 are a close match to the gasket deformation observed in experiments while the solution does not converge when it is below 0.2. In the standard model we choose a frictional coefficient of 0.3.

Material	Strength (GPa)	Modulus (GPa)	Poisson's Ratio	Knoop Hardness (GPa)
PCD [82]	Compressive: 7.2	Elastic: 960	0.1	50
WC [68, 82]	Compressive: 5	Elastic: 680	0.24	13
TiZr [83]	Tensile: 0.64	Elastic: 85 Plastic: 3.5–85	0.3	-
Sample [84]	-	Elastic: 50–400	0.3	-

Table 5.1 The properties of the materials used in the standard model.

TiZr is a deformable null-scattering alloy with its modulus represented by a bilinear curve[6], which assumes that TiZr has two stages of linear strain-stress relationship. The first linear stage is elastic with Young's modulus; the second stage is plastic with a (smaller) plastic modulus. The values from 50 to 85 GPa were used as the plastic modulus in order to find a proper value by matching the simulated sample pressure–applied load pattern to that obtained in experiments. In the simulation, the sample's elastic modulus was varied from 50 to 400 GPa to explore its effect on the loading curve. The Young's modulus of the sample was estimated to be between 150 and 200 GPa when its pressure is around 30 GPa assuming ice is used [84].

5.2.2 Verifications of the Model

A range of values describing sample properties and nonlinear properties for gasket materials have been explored in the model. To verify the model, a simulation has been conducted with thrust load, sample pressure and gasket deformation being chosen as the key quantities for matching those obtained from experiments.

5.2.2.1 Validation of TiZr plasticity

The relationships between the sample pressure and the axially applied load are plotted in Figures 5.7 and 5.8. Of all the materials, the properties of the gasket (TiZr) and the sample significantly affect the pressure–load behaviour. The experimental pressure–load data is

[6] In bilinear method, two straight lines are used to characterize the elastic-plastic behaviour (stress-strain relationship) of the material under load.

determined by comparing the load applied in the press and the diffraction pattern, and determining the sample pressure using equation of state of sodium chloride. A range of plastic and elastic moduli of the two have been investigated by the simulation. Simulation results indicate other factors, e.g. the moduli of the polycrystalline diamond (PCD) and tungsten carbide (WC), have limited effect on the sample pressure attained under a certain applied load. This is due to the fact that the anvils are much more rigid compared to the gasket and sample materials.

In other similar analysis [58, 59 and 63] the ductile gasket materials are treated either as elastic or as plastic. In contrast, we characterize TiZr with bilinear isotropic hardening behaviour which includes an elastic modulus $\boldsymbol{E_1}$ and a plastic modulus $\boldsymbol{E_2}$ (Figure 5.9). $\boldsymbol{E_1}$ has been determined experimentally to be 85 GPa [83]. $\boldsymbol{E_2}$ is varied in the range from 3.5 GPa to its maximum possible value of nearly 85 GPa. In the model the slight increase in its modulus at very high pressure and the effect of work hardening during pre-indentation is neglected. As illustrated in Figure 5.7, the pressure–load behaviour shows the sample pressure varies from 10.3 GPa to 38.6 GPa as $\boldsymbol{E_2}$ changes from 85 GPa to 3.5 GPa respectively for an applied load of 240 tonnes. The smaller $\boldsymbol{E_2}$ is applied, the greater sample pressure is produced. As the modulus $\boldsymbol{E_2}$ decreases below 3.5 GPa, the gaskets become too compressible to sustain the thrust, and the solution does not converge for the model as constrained. $\boldsymbol{E_2}$ = 5 GPa gives the best match to the experimental pressure load behaviour which has a maximum sample pressure of 30.1 GPa generated at 240 tonnes (175 GPa is used as the elastic modulus of the sample and justified in Section 5.2.2.2). The gasket deformation derived from the simulation matches that obtained from experiments. The gaskets are flattened with the thickness of gasket G (Figure 5.6) axially decreasing by 0.32mm (or 32%), and in radial direction gaskets D1 and D2 increasing in diameter from 15 mm to around 20 mm.

5.2.2.2 Validation of sample modulus

The elastic modulus of the sample is known to be pressure-dependent. For deuterated ice (D_2O), the modulus is approximated to be 175 GPa when it is pressurized to 30 GPa using linear extension to the measurement data available in [84]. Figure 5.8 shows the pressure–load behaviour as the sample modulus is varied from 50 to 400 GPa. It shows that the higher the sample modulus, the higher the sample pressure achieved. The experimental data set is best matched by the results of a simulation for a sample with the elastic modulus of 175 GPa.

We have therefore established a model that reproduces the pressure–load behaviour and gasket deformation data observed in experiments. This model is based on the assumptions

detailed above and is used for investigating the stress distribution in the anvils. The model uses 5 GPa as the gasket's plastic modulus and 175 GPa as the sample's elastic modulus.

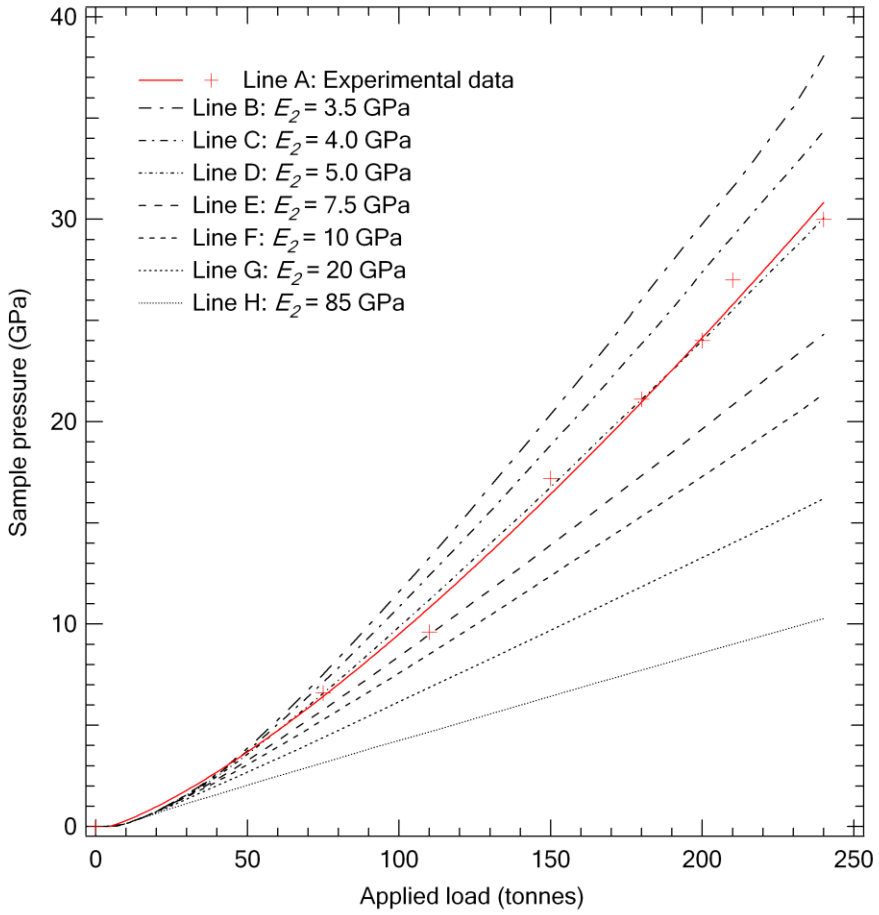

Figure 5.7 Pressure–load behaviour derived from simulations with different plastic modulus values for TiZr. Line A: experimental data; Lines B, C, D, E, F, G, H: simulations where the plastic modulus of TiZr ***E_2*** *is assumed to be 3.5, 4.0, 5.0, 7.5, 10, 20 and 85 GPa, respectively. The simulation is carried out in a 2D model on the assumption that elastic modulus of sample is 175 GPa.*

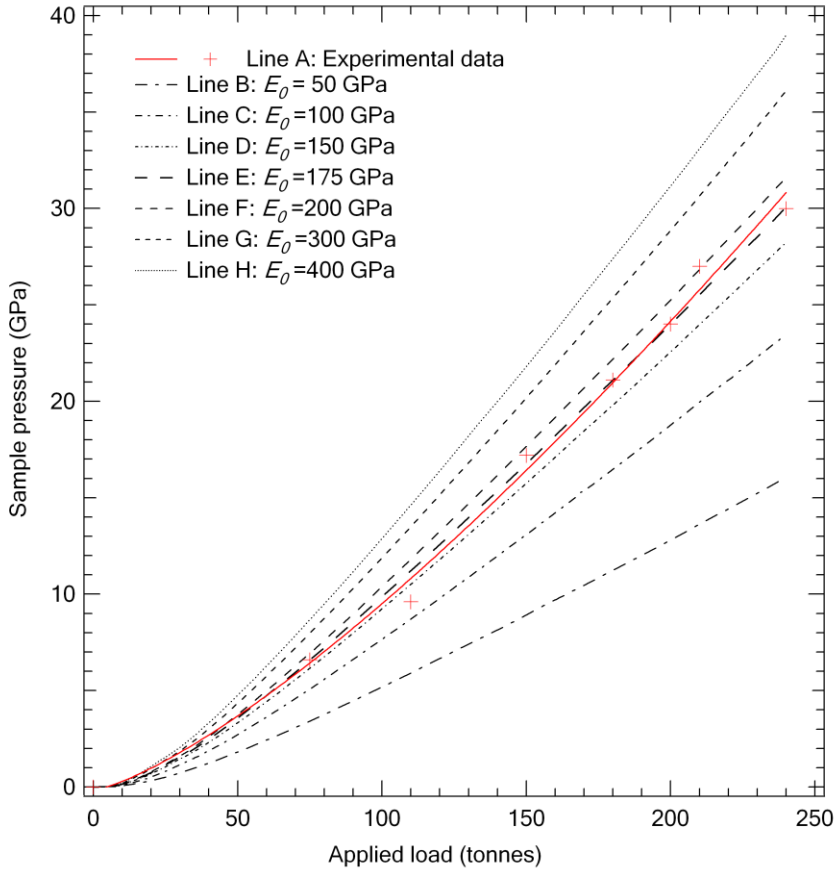

Figure 5.8 Pressure–load behaviour determined experimentally and from simulations with different elastic modulus settings for sample. Line A: experiment; Line B, C, D, E, F, G and H: simulations with the sample modulus $\boldsymbol{E_0}$ *set as 50, 100, 150, 175, 200, 300 and 400 GPa, respectively. The simulation is carried out in a 2D model provided that plastic modulus of TiZr is 5 GPa.*

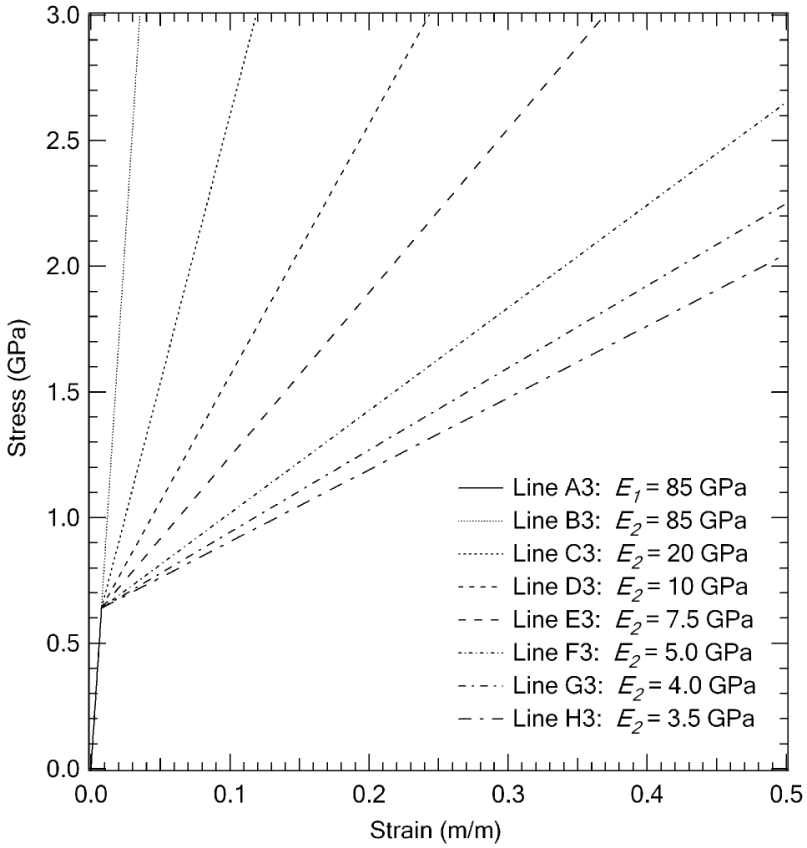

Figure 5.9 Properties of gasket material TiZr by bilinear isotropic hardening. Line A is E_1 *− the modulus of TiZr at the elastic stage: 85 GPa; Lines B, C, D, E, F, G, H result from different values of* E_2 *− the modulus of TiZr in the plastic mode: 3.5, 4.0, 5.0, 7.5, 10, 20 and 85 GPa, respectively.*

5.3 Modelling Results and Failure Analysis

5.3.1 Maximum Principal Stress and Shear Stress

Figure 5.10 shows the maximum principal and shear stress on the anvil's surface under an applied load of 240 tonnes as a function of the radial distance from the centre of the anvil. When its value is positive, the maximum principal stress indicates the tensile stress along the anvil's surface. The curve has a peak value of 7.4 GPa at position B while local peak values are 2.4 GPa and 4.9 GPa around positions A and C respectively. The shear stress curve fluctuates with the three peaks being 8.7 GPa at position A, 8.9 GPa at position B and 5.6

GPa at position C. Figure 5.10 also shows that the surface of the anvil is partly subjected to compressive stress, which can be above 10 GPa. This is believed to be non-critical and the reason is detailed in Section 5.3.2. Figure 5.11 shows the maximum principal and shear stress in the deformed gaskets, the sample and the portion of the anvil near the top surface under an applied load of 240 tonnes.

This information is crucial as in many studies these two types of stress were found to be the causes of failure or used as a criterion for anvil performance in diamond anvil cell [58, 59, 60, 61 and 62]. The diamond anvils fail because of plastic deformation when shear stress reaches a maximum at some point in a material [59, 63] or because of brittle failure which tensile stress contributes significantly to [61, 62]. The ceramic-like PCD dies have a compressive strength of 7.2 GPa [82] and a tensile strength of around 3 GPa at ambient pressure [62, 84]. Both of these values become larger under compression [86] but their exact values at high pressure are unknown. Unknown is also the value for the shear strength of the PCD at ambient or high-pressure. However, for brittle materials such as cast iron, the shear strength is approximately 1.3 times its tensile strength [87]. This ratio is assumed and used for the PCD material.

The tensile stress present at position B is the most likely cause of the repeated failure encountered in experiments. In the simulation, the maximum tensile stress is 7.4 GPa at position B while the peak shear stress is 8.9 GPa at position A. In comparison, the shear stress is less critical than the tensile stress. If we apply 8.9 GPa as the shear strength of the PCD, then its tensile strength would be only 6.85 GPa (given a ratio of 1.3 between the shear strength and tensile strength), below the maximum tensile stress 7.4 GPa. This means that the anvils will fail because of the tensile stress well before the shear stress reaches the shear strength and 7.4 GPa is probably the tensile strength of the PCD material when it is compressed to the range of pressure seen in the experiments.

Also, this is in agreement with experimental observations. As can been seen from Figure 5.12 the failed anvils and gaskets show damage mostly occurring at positions B and C inside the toroidal recesses instead of the sample chamber. The damage at position C can occur right after the failure at position B which results in radial stress concentration at position C. The maximum principal stress and shear stress in the anvil body is given in Figure 8 where it shows that there is a concentration of basal tensions near the centre of the recess at the back of the anvil – position D.

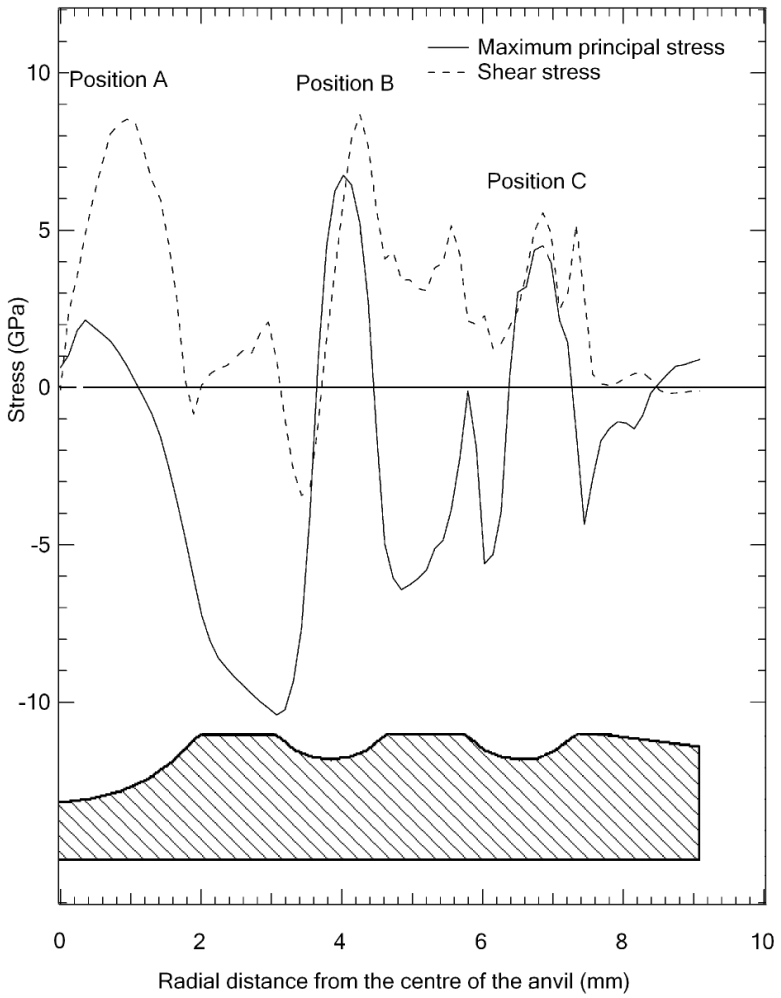

Figure 5.10 Distribution of maximum principal stress and shear stress on the double-toroidal anvil surface. The stress is tensile when its value is positive and compressive when negative. Half of an anvil face is shown as a result of the anvils' axial symmetry (axis: along 0 mm). Positions A, B and C are critical locations where a peak of maximum principal stress and shear stress appear. They correspond to positions A, B, C on the anvil surface in Figure 5.11, 5.12 and 5.13.

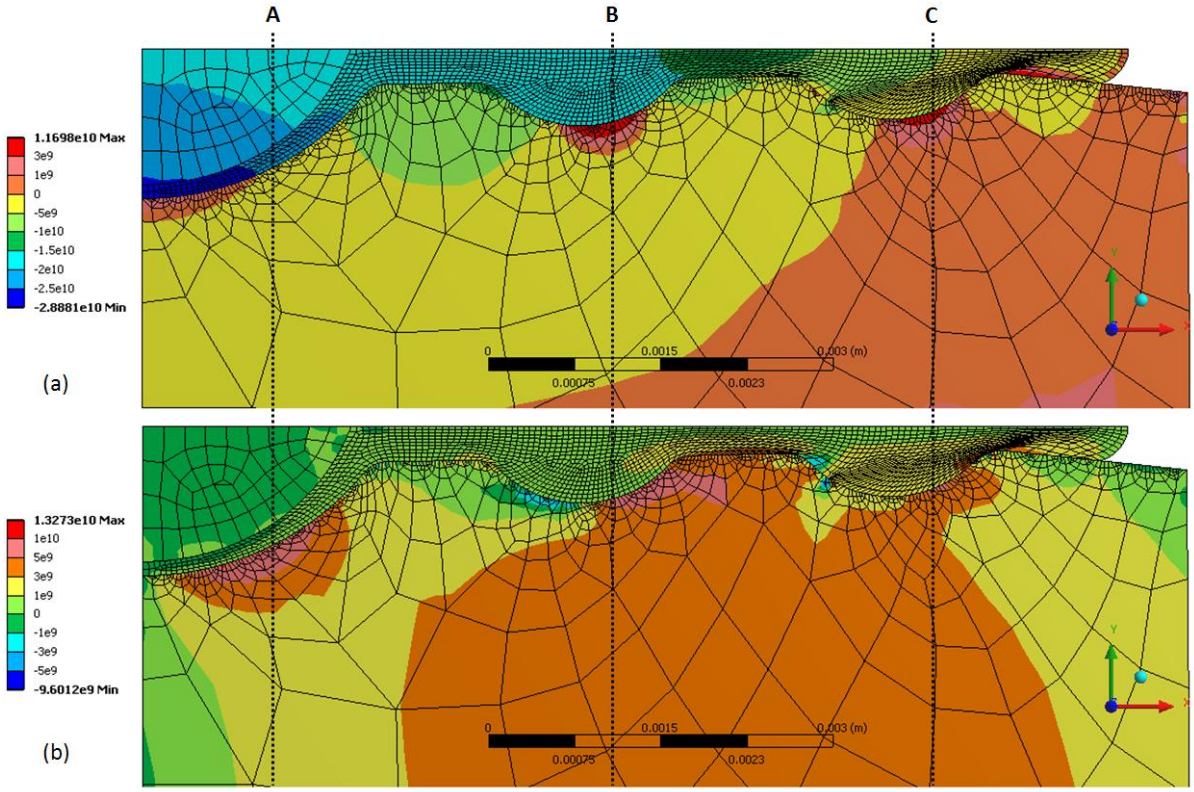

Figure 5.11 Cross-sectional view of the distribution of maximum principal stress and shear stress on the double-toroidal anvil body near the surface under 240 tonnes (in colour). The meshes on the anvil, the gasket and the sample are also shown.

(a) Distribution of maximum principal stress;

(b) Distribution of shear stress.

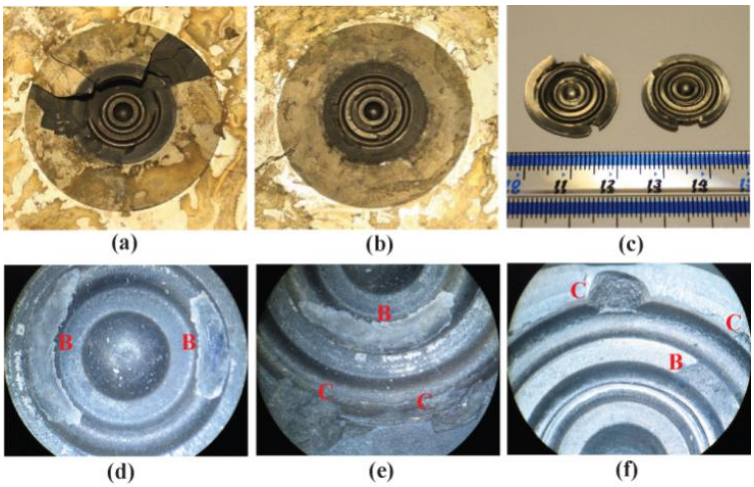

Figure 5.12 Detailed views of broken double-toroidal anvils and deformed gaskets after loading to approximately 240 tonnes. (a), (b) are two broken anvils. (d), (e) are magnified views of chipping and breakages on the face of the anvil in (b). (c), (f) are normal view and microscopic view of deformed gaskets respectively.

5.3.2 Normal Stress

The simulated distribution of axial normal stress, radial normal stress and hoop normal stress in the anvil body are shown in Figure 5.13e and f. It shows that most part of the anvil body is subjected to compressive stress. In the axial direction, compressive vertical stress concentrates around the centre of the sample chamber resulting in sample compression and increased sample pressure. As a result, there is a maximum axial compressive stress of 32.1 GPa at the centre of the anvil surface and a large part of the body of the anvil around the central axis is beyond its compressive strength at ambient pressure (7.2 GPa). The magnitude of the axial compressive stress is also well above the compressive stress of ~10 GPa seen in Figure 5.10. However, these compressive stresses are not considered to be the cause of the anvil failure. Previous experiments showed that the anvils did not fail in the body and in the centre of the surface where the high compressive stress existed. This can be explained by the massive support principal [33, 56]. In a device with massive support, the critical portion (of the device) that is highly compressed is well supported and contained by the surrounding materials. In this case, the material in the critical portion can sustain compressive stress much higher than the compressive strength of the material and will not fail, even if the material may undergo plastic deformation.

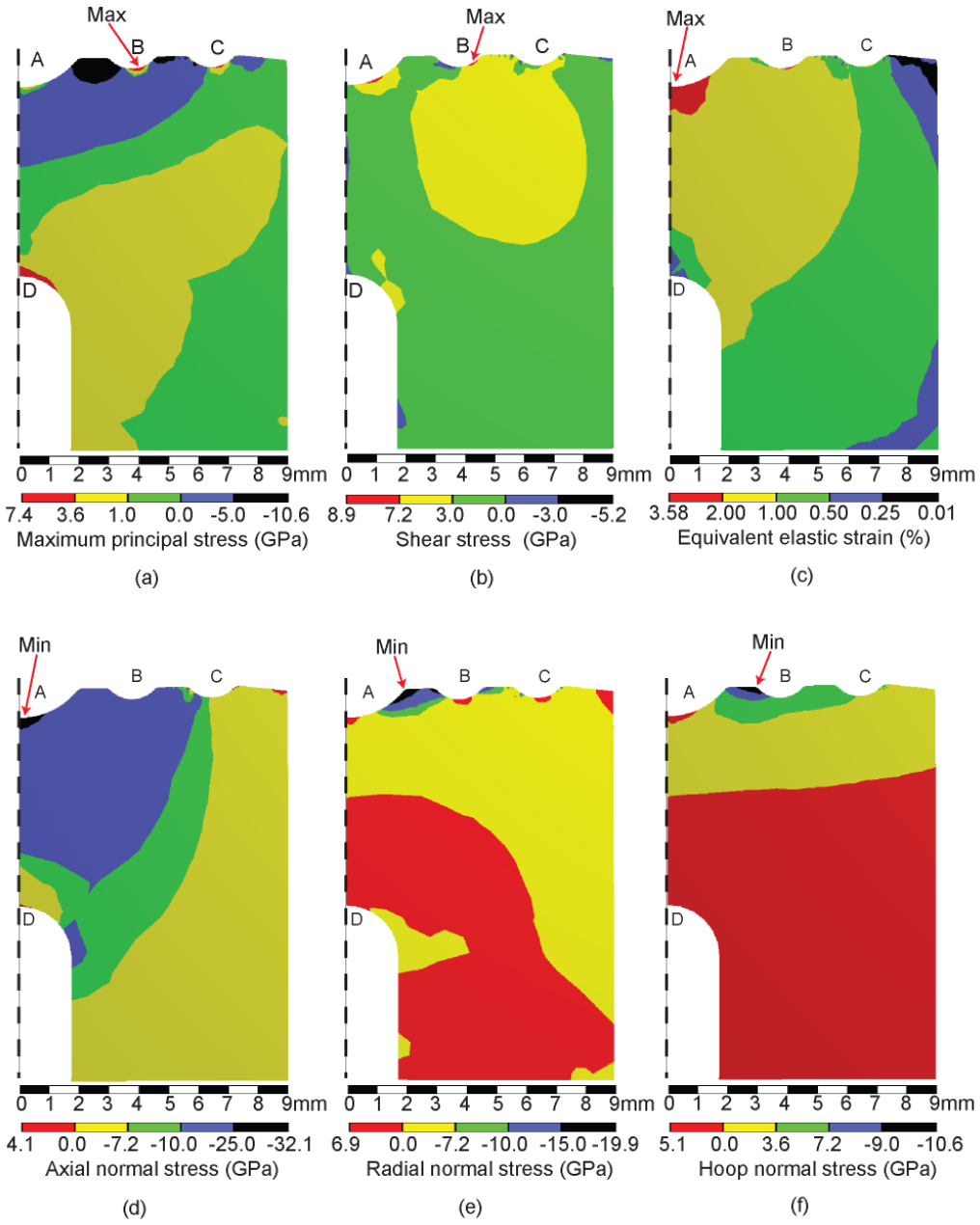

Figure 5.13 Half cross-sectional view of the distribution of maximal principal stress, shear stress, elastic strain and normal stress in the anvil body under an applied load of 240 tonnes. (a) Maximal principal stress; (b) shear stress; (c) equivalent elastic strain; (d) axial normal stress; (e) radial normal stress; (f) hoop normal stress. The colours indicate different stress magnitudes as shown in the individual keys. The stress is tensile when its value is positive and compressive when negative. The PCD anvil is treated elastically below and above its strength. The slight increase in elastic modulus at high pressure is neglected here.

In the double-toroidal anvil, the plastically deformed region can be seen to extend to the bottom of the outer toroid (position C); while the remainder of the anvil body remains stable. As the anvils are well supported by surrounding components, the critical point for the anvil body to fail as a result of excessive axial compression would be when the recessed hole at the back of the anvil (position D) is subjected to stress beyond its strength. In the radial direction, stress beyond 7.2 GPa only exists in limited areas on the anvil surface. The resulting hoop stress is also significantly less.

5.3.3 Strains and Deformation

Elastic strain is up to 3.58% at the centre of the anvil surface (Figure 5.13c) and in general decreases along the radius and when the depth increases. As a result of the large axial thrust, the general anvil face becomes concave, showing a "cupping" trend, that is, the central portion near the sample chamber sinks while rest relatively rises and bends inward.

5.4 Conclusions and Optimization

In the present study by use of finite element analysis we have been able to determine, stress, strain and stress gradients within double-toroidal profile anvils. This information is not accessible experimentally and has been used to investigate the mechanism of failure at high load. It shows that failures occur at raised locations along the anvil surface, mainly as a result of excessive tensile stress and these critical locations with a concentration of tensile stress are closely related to the gasket/sample material properties and anvils' geometry. For this reason, a further study has been performed in order to understand what improvements can be made to allow us to eventually obtain higher sample pressure.

Figure 5.14 is a plot of the sample pressure generated under an applied load of 240 tonnes as the gasket and sample properties are varied. The sample pressure is generally determined by the relative 'hardness' of the two materials. Intuitively, when 'relatively' soft gaskets plastically flow aside under load, the sample is subject to the majority of the load and its pressure increases. When the gaskets are hard enough to significantly share the thrust load, the sample is compressed to a lower pressure. The standard model generates 30.1 GPa at location O while the sample pressure reaches 48.7 GPa at location P where the gasket's plastic modulus is 3.5 GPa and sample modulus is 400 GPa. The FEA solution does not converge when the gasket modulus is below 3.5 GPa and the sample modulus is 50 GPa within a reasonable time with current simulation settings. When the increase in tensile stress

and shear stress is taken into account, it is possible to increase the maximum generated sample pressure from 30.1 to 33.6 GPa by altering material properties. At Q when the gasket modulus is 4 GPa and the sample modulus is 200 GPa, the sample pressure is 33.6 GPa under an applied load of 215 tonnes with the maximum tensile stress and shear stress below 7.4 and 9.6 GPa (1.3 times of its tensile strength) respectively.

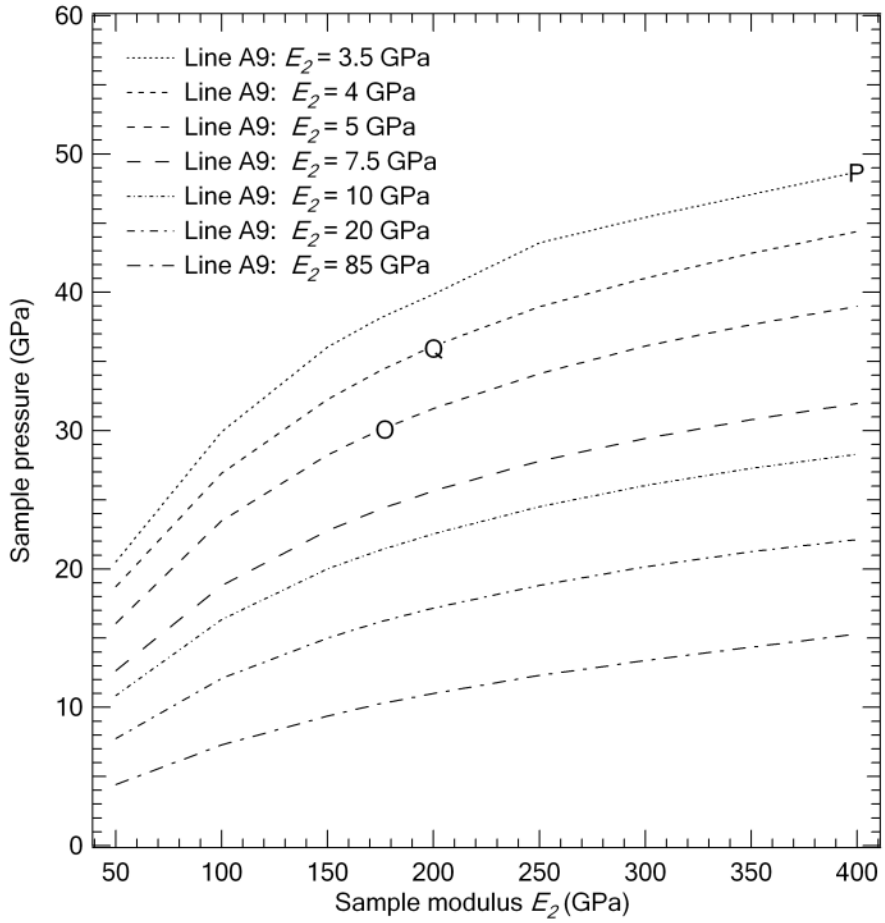

Figure 5.14 Sample pressure under applied load of 240 tonnes as a result of varied combination of sample modulus and gasket plastic modulus. The simulation shows that an increased sample pressure can be achieved with higher sample modulus and lower gasket material plastic modulus. O indicates the location of the standard model setting. P shows the location of the highest sample pressure achievable in the relevant simulation domains if the anvils do not fail as a result of excess stress. Q is the location where the highest pressure can be achieved under 215 tonnes load with the maximum tensile and shear stress less than 7.4 and 9.6 GPa respectively.

Besides, adapting the anvil geometry would be an alternative approach to optimise the gasket geometry. A sample pressure of 35.6 GPa can be produced with the maximum tensile stress and shear stress below 7.4 and 9.6 GPa respectively if a minor modification is performed to the anvil face, reducing the radius of the inner toroid by 10% as shown in Figure 5.15. However, to achieve an optimal anvil profile requires much more work to be done and a comprehensive analysis is needed in the future.

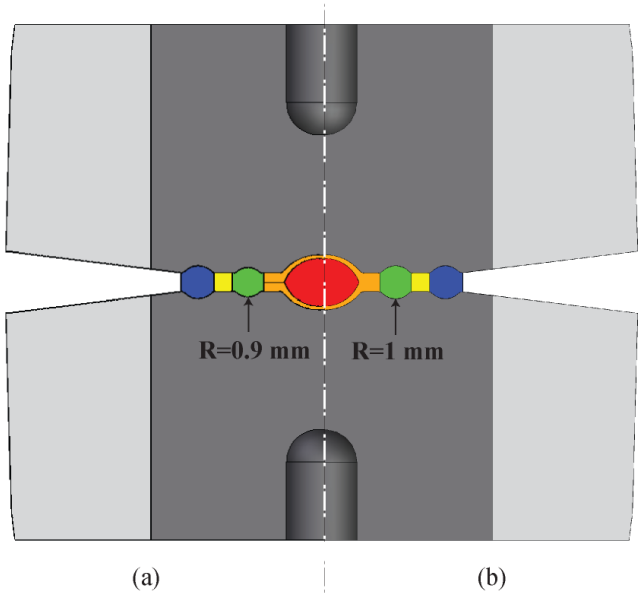

Figure 5.15 A side-by-side comparison of optimized and original anvil/gasket assembly. (a) The left half of the assembly with optimized anvils. The radius of the inner toroid is reduced from 1.0 mm to 0.9 mm; (b) The right half of the assembly of original anvils and gaskets.

To this end, we have performed a comprehensive finite element analysis (FEA) of these anvils combined with TiZr gaskets. The analysis investigates the failure mechanism of the anvils in previous experiments and demonstrates the effects of the geometries and material properties of the anvils and gaskets on their mechanical performance. It is found that for a typical configuration of the anvils and gaskets with a pressure of 30 GPa under applied load of approximately 240 tonnes, a maximum tensile stress of 7.4 GPa is present on the bevel in the outer groove while a maximum compressive axial stress of 23.8 GPa exists on the central recess. The tensile stress is a critical contribution factor to the anvil failure. Anvils and gasket/sample materials are simulated for optimizations in order to minimize the stress concentration. The assumptions made and other considerations are also discussed.

Chapter 6

Conclusions and Future Developments

This chapter provides an overview of the work done during this project and draws some final conclusions as to the achieved results. It also explores future directions in the instrumentation development for neutron scattering at high-pressure.

Section 6.1 is an overview of the content of this thesis which summarises the main progress to date. The summary covers the development of the RV4 system and the FEA analysis of the double-toroidal anvil cells.

Section 6.2 is a look into the future. The potential developments based on the current progress are considered. The RV4 has other potential applications and also can be further developed in terms of the load capacity and positioning precision. The methodology of the FE analysis developed for the double toroidal anvils is valuable for future engineering improvements of this and other high pressure cells.

6.1 Summary

High pressure is a powerful tool for probing magnetic and structural properties of materials and neutron scattering provides and insight into the nature of interactions at microscopic level. However, experimental neutron studies require a relatively large volume of sample which results in rather large presses being used. One of the most commonly used high-pressure devices used in neutron-diffraction experiments is the Paris-Edinburgh press. However, there are some limitations imposed by the design of the press and the cell. My project was focused on resolving two of them:

- The restriction on the accessible reciprocal space of the Paris-Edinburgh press imposed by the tie-rods of the mainframe.

- The pressure limit of the current design of the double-toroidal anvils at the load of 240 tonnes.

6.1.1 The Development of the Rotational RV4 System

One intrinsic disadvantage associated with the design of the standard Paris-Edinburgh press is its limited aperture access. The tie rods of the load frame significantly obstruct reciprocal space for single-crystal diffraction and inelastic techniques at pulsed and constant wavelength sources. In order to solve this problem we developed a new rotational system – the RV4. The purpose of the device is to rotate the anvils at a high load in a controlled fashion so that neutron data can be collected from the sample at particular angles.

The RV4 system with rotational module is presented in this thesis complete with its design and the description of its use at large-scale neutron facilities. The portable device is primarily designed for performing high-pressure *in situ* experiments on the large-volume single-crystal samples using neutron scattering instruments SXD (ISIS) and D9 (ILL). To satisfy the design brief, its general specifications are customised in terms of the load capacity, compatible anvil types, size & weight aspects, rotational dynamics, positioning precision, etc.

The RV4 system consists of the RV4 press, the hydraulic pumping module, the electronic control module and an assembly stand. The RV4 press is developed based on the standard V4 variant of Paris-Edinburgh press and has the central structure that incorporates a main frame and rotational support mechanism, and the side structure on which the power supply

and gearing mechanism are mounted. The overall configuration of the system allows both static and dynamic operations for high-pressure experiments.

A number of technical challenges had to be overcome in the design process. One of the problems was caused by the significant friction in the commercially available thrust roller bearings at loads above 25 tonnes. To resolve this issue a set of custom-designed hydraulic bearings has been developed. In these bearings a thin layer of oil separates the two parts that can rotate with respect to each other. The other issue was related to the tilting and misalignment of the central shaft. This was rectified by introducing the enhanced anvil support.

The RV4 system was tested in mechanical workshop and used online at large-scale facilities. The RV4 was tested on the single-crystal diffractometer D9 and incorporated into the control system of the instrument. With the current configurations the RV4 press has been successfully used at the load of 60 tonnes at the pulsed neutron source. In the latest mechanical testing in the workshop, it was able to rotate under applied load of 100 tonnes. The work to improve the performance of the RV4 system to extend its load capacity and stability is continuing.

6.1.2 The Mechanical Analysis of the Double-toroidal Anvil Cell

Anvil failure has been an issue that hindered very high pressure generation in various cells. The anvil analysis described here is an effort to understand the mechanism responsible for the failure of the double-toroidal-profile anvils machined from sintered diamond dies when the sample pressure is close to 30 GPa.

In order to find out the direct cause of the failure in the anvils and the mechanism of interaction between multiple components present in the system, a comprehensive finite element analysis (FEA) of this anvil and gasket assembly has been carried out. ANSYS Workbench was used as the platform for modelling, calculation and display of the results.

In the multi-component model, a series of parameters is set up to represent the physical configuration and the loading conditions in the double-toroidal anvil cell. Two key material properties not known experimentally have been narrowed down to a certain range and then validated based on the load – pressure relationship and the deformation data statistics available from the experimental data. This is a novel approach to the models in which one or

several materials' properties are not known at extreme conditions. It can be applied in conducting the FEA modelling of future designs.

Based on the FEA model the analysis investigates the failure mechanism of the anvils in previous experiments. It is found that for a typical configuration under applied load of approximately 240 tonnes, a maximum tensile stress of 7.4 GPa is present on the bevel in the inner groove. According to the current available strength data of the anvil this is the critical contribution to the failure. It causes dominant damage to the integrity of the anvil. Besides it is revealed that there is also a high (though not critical) level of shear stress existing in the anvil's surfaces.

In addition to simulating the loading process and the failure mode, the analysis also looks at possible optimizations of the anvil and gaskets based on the above findings which can make it possible to achieve higher pressure. Modified anvils and gasket/sample materials are also simulated in order to minimize the stress concentration in the critical area.

6.2 A Look into the Future

Though the objectives of my research programme have been achieved, most of the work presented in this thesis is in its infancy. Yet, it holds a great promise for the future.

The prospects of the RV4 system being used for single-crystal neutron-diffraction experiments and other experiments are excellent.

- The RV4 system has been tested to be suitable for high-pressure experiments on both D9 and SXD with large-volume single-crystal samples. It will be shipped to the instruments for future neutron experiments when the beam time is scheduled.

- For similar applications where a complete or larger reciprocal space coverage is required or rotating the sample through 360 degrees, such as in tomography experiments, is beneficial, the RV4 system would be a good option to consider (with optional customisations).

- The current RV4 system is used at ambient temperature. In places where a lower temperature or higher temperature is required, verification work would be necessary as well as modifications in terms of the materials and/or structures used.

Certain modifications or upgrades in hardware of the RV4 system would potentially increase the loading capacity, improve the stability and repeatability of the rotational operation under applied load and increase the positioning precision of the rotation. Some of them are already under way.

- Extending the loading capacity. The loading capacity is the major target in the development of the RV4 device. This is currently limited by the input power from the motor and the resistance in the hydraulic bearings as well as the efficiencies in the transmission components. A two motor combined with two gearboxes version of the RV4 system has been considered. The design would require some preliminary testing to prove its technical feasibility. It is based on use of the current high pressure hydraulic bearings for thrust support, although other options may be looked at as the alternatives.

- Improving stability and repeatability of the rotational operation under load. The CSEC group and the mechanical workshop are making efforts to make the rotation more stable and smooth. One activity that is underway is to replace the existing hydraulic thrust bearings with those made of maraging steel. Other complementary techniques, for instance, installing more rigid structures to support and align the central shaft, using alternative lubricants in the transmission components such as the hydraulic bearings and the gearbox are being considered or tried.

- Enhancing positioning precision. In order to position the sample more precisely, an optical encoder could be added to obtain a high resolution in position detection. Currently only a simple mechanical switch is operated as a home position reference. A feedback from the encoder would enhance the monitoring of the sample position. It can be used to adjust the sample positioning during the experiment. With an instant read of the precise position information the rotation control scheme would be flexible and secure.

  An optional version of the RV4 with the encoder is available with the encoder from BOMH [70]. The BOMH 58S1P05C encoder is an absolute multi-turn encoder with SSI I/O connection. It uses optical sensing with a resolution of 18 bit/turn. The shaft diameter is 12 mm and the mounting depth is 46 mm. Its size is compact and it is possible to accommodate it in the space at the top end of the side structure frame and it is designed to couple to the top end of the side shaft (Figure 6.1).

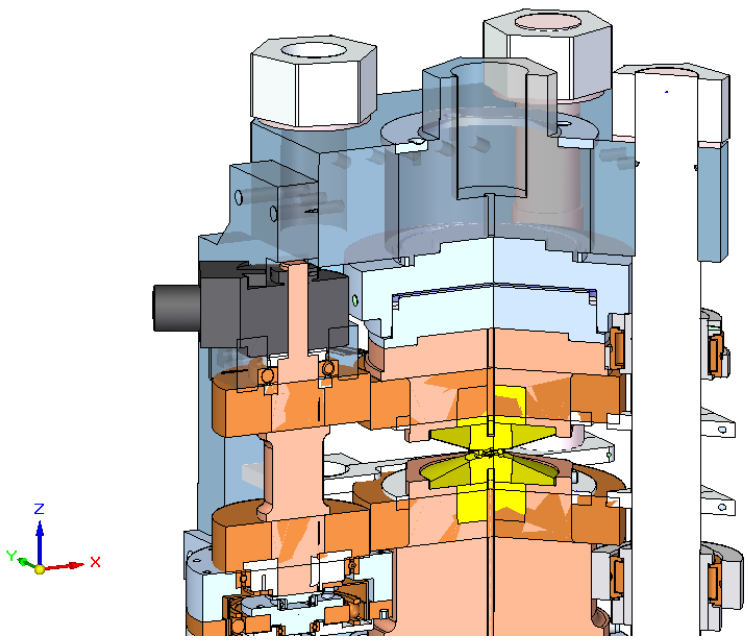

Figure 6.1 The fragment of the design of the RV4 with an optical encoder (in black). The space is reserved at the top end of the side shaft.

The FEA simulation and mechanical analysis of the double-toroidal anvil cell is also a promising piece of research that promises to open more interesting avenues of experimental work in future.

- Attaining higher pressure on large-volume sample. So far 30 GPa is the highest pressure that can be achieved on large-volume samples using the double-toroidal anvils. To reach pressure in excess of this figure, new geometries and anvil shapes are being developed as well as a more powerful but compact ram. It is beyond doubt that this would extend accurate neutron-diffraction studies up to the ultra-high-pressure range where fully refinable patterns with very fine resolution are the ultimate goal.

- Providing reference for other studies of similar problems. Although there are several publications using Finite-Element method for mechanical analysis of high-pressure cells, none focuses on toroidal anvils. The current modelling method and results

provide valuable assessment of the materials' properties at high pressure and can give back-to-back comparison in future efforts to analyse similar configurations or improve current configuration with novel materials with superior properties.

Bibliography

1. **High-pressure crystallography**, A. Katrusiak, *Acta Cryst.* **A64**, 135-148 (2008).

2. **CRC handbook of chemistry and physics (87th ed.)**, D. R. Lide, 14-13 (2006-2007). Web-site: http://hbcpnetbase.com/

3. **Water storage in the mantle**, T. J. Ahrens, *Nature* **342**, 122 (1989).

4. **Neutron powder diffraction at pressures beyond 25 GPa**, S. Klotz *et al.*, *Appl. Phys. Lett.* **66**, 1735 (1995).

5. **Thermal conductivity in the mantle**, European Synchrotron Radiation Facility (ESRF) website. Web-site: http://www.esrf.eu/AboutUs/Applications/earth-science/thermal-conductivity-mantle

6. **Ultimate metastable solubility of boron in diamond: synthesis of superhard diamond-like BC^5**, V. L. Solozhenko *et al.*, *Phys. Rev. Lett.* **102,** 015506 (2009).

7. **Electronic and magnetic phase diagram of β-$Fe_{1.01}$Se with superconductivity at 36.7 K under pressure**, S. Medvedev *et al.*, *Nature Materials* **8**, 630-633 (2009).

8. **Superconductivity up to 29 K in SrFe2As2 and BaFe2As2 at high pressures**, P. L. Alireza *et al.*, *J. Phys.: Condens. Matter* **21**, 012208 (2009).

9. **Direct observation of a pressure-induced metal-to-semiconductor transition in lithium**, T. Matsuoka *et al.*, *Nature* **458**, 186-189 (2009).

10. **Effect of pressure on the iron arsenide superconductor LixFeAs (x = 0.8, 1.0, 1.1)**, S. J. Zhang *et al.*, *Phys. Rev. B* **80**, 014506 (2009).

11. **Advances in high-pressure biophysics: status and prospects of macromolecular crystallography**, R. Fourme *et al.*, *Annu. Rev. of Biophys.* **38**, 153-171 (2009).

12. **Structural rigidity of a large cavity-containing protein revealed by high-pressure crystallography**, M. D. Collins *et al.*, *J. of Mol. Biol.* **367**, 752-763 (2007).

13. **The influence of high hydrostatic pressure on structure, function and assembly of proteins and protein complexes**, M. Gross *et al.*, *Eur J Biochem.* **221**, 617-30 (1994).

14. **Deep sea microbiology**, H. W. Jannasch *et al.*, Annu. *Rev. Microbiol.* **38**, 487-514 (1984).

15. **Protein structure and dynamics at high pressure**, K. Heremans *et al.*, *Biochimica et Biophysica Acta (BBA)* **1386**, 353-370 (1998).

16. **Commercial high-pressure processed products marketed in Japan, Europe and the United States**, the Ohio State University High Pressure Food Processing Lab. Web-site: http://grad.fst.ohio-state.edu/hpp/products.html

17. **Extreme Conditions Physics and Centre for Science at Extreme Conditions (CSEC)**, University of Edinburgh. Web-sites:
http://www2.ph.ed.ac.uk/cmatter/extreme.html
http://www.csec.ed.ac.uk/

18. **Diamond anvil cell and high-pressure physical investigations**, A. Jayaraman, Rev. *Mod. Phys.* **55**, 65-108 (1983).

19. **Diagnostic system of the Lawrence Livermore National Laboratory two-stage light gas gun**, A. C. Mitchell *et al.*, *Rev. Sci. Instrum.* **52**, 347-359 (1981).

20. **Research highlight: A laser look inside planet**s, K. Walter, Lawrence Livermore National Laboratory. Web-site: https://str.llnl.gov/June09/smith.html

21. **ISIS - A world centre for neutrons and muons**, ISIS website. Web-site:
http://www.isis.stfc.ac.uk/index.html

22. **ILL - Welcome to the Institut Laue-Langevin**, ILL website. Web-site:
http://www.ill.eu/

23. ***In situ* x-ray study of thermal expansion and phase transition of iron at multimegabar pressure**, L. S. Dubrovinsky *et al.*, *Rev. Lett.* **84**, 1720-1723 (2000).

24. **Evidence of a fcc-hcp transition in aluminum at multimegabar pressure**, Y. Akahama *et al.*, *Phys. Rev. Lett.* **96**, 045505 (2006).

25. **Putting the squeeze on energetic materials - structural characterisation of a high-pressure phase of CL-20**, beamline case study website of Diamond - the synchrotron light source. Web-site:
http://www.diamond.ac.uk/Home/Beamlines/I15/casestudies/Energetic-materials.html

26. **Java applet simulation of x-ray diffraction patterns for the Laue method (transmission or backreflection mode)**, S. Weber. Web-site: http://www.ccp14.ac.uk/ccp/web-mirrors/weber/~weber/JAVA/jlaue/jlaue.html

27. **Low-temperature neutron single-crystal diffraction studies of samples grown at high pressure**, C. L. Bull *et al.*, *High Press. Res.* **29**, 644-648 (2009).

28. **Neutron powder diffraction above 10 GPa**, J. M. Besson *et al.*, *Physica B* **180-181**, 907-910 (1992).

29. **Equation of state of lithium deuteride from neutron diffraction under high pressure**, J. M. Besson *et al.*, *Phys. Rev. B* **45**, 2613-2619 (1992).

30. **Variation of interatomic distances in ice VIII to 10 GPa**, J. M. Besson*et al.*, *Phys. Rev. B* **49**, 12540-12550 (1994).

31. **New developments in neutron-scattering methods under high pressure with the Paris-Edinburgh cells**, J. M. Besson *et al.*, *Physica B* **213-214**, 31-36 (1995).

32. **High pressure neutron diffraction using the Paris-Edinburgh Cell: Experimental possibilities and future prospects**, S. Klotz *et al.*, *High Press. Res.* **14**, 249-255 (1996).

33. **The coagulation of albumen by pressure**, P. W. Bridgman, *Proc. Amer. Acad. Arts Sci.* **81**, 165 (1952).

34. **Device of toroid type for high pressure generation**, L. G. Khvostantsev *et al.*, *High Temp. High Press.* **9** 637-639 (1977).

35. **Large-volume high-pressure devices for physical investigations**, L. G. Khvostantsev *et al.*, *High Press. Res.* **24**, 371-383(2004).

36. **Polaris - medium resolution powder diffraction**, ISIS website. Web-site: http://www.isis.stfc.ac.uk/instruments/polaris/

37. **Toroidal anvils for single-crystal neutron studies,** C. L. Bull *et al.*, *High Press. Res.* **25,** 229- 231 (2005).

38. **High-pressure ultrasonic setup using the Paris-Edinburgh press: elastic properties of single-crystalline germanium up to 6 GPa**, M. l. Gauthier *et al.*, *Rev. Sci. Instrum.* **74**, 3712-3716 (2003)**.**

39. **Phonon dispersion measurements at high pressures to 7 GPa by inelastic neutron scattering**, S. Klotz *et al.*, *Appl. Phys. Lett.* **66**, 1557 (1995).

40. **Inelastic neutron scattering to very high pressures**, S. Klotz *et al.*, *Hyperfine Interactions* **128**, 245-254 (2000).

41. **Time-of-flight single-crystal neutron diffraction to 10 GPa and above**, C. L. Bull *et al.*, *High Press. Res.* **29**, 780-791 (2009).

42. **High-pressure single-crystal neutron diffraction to 10 GPa by angle-dispersive techniques**, C. L. Bull *et al.*, *J. of Appl. Cryst.* **44**, 831–838 (2011).

43. **SXD - the single-crystal diffractometer at the ISIS Spallation Neutron Source**, D. A. Keen *et al.*, *J. of Appl. Cryst.* **39** 714-722 (2006).

44. **SXD - single-crystal diffractometer**, ISIS website. Web-site: http://www.isis.stfc.ac.uk/instruments/sxd/

45. **Hot neutron four-circle diffractometer D9**, a user guide to a standard single-crystal diffraction experiment on D9. Web-site: http://www.ill.eu/instruments-support/instruments-groups/instruments/d9/

46. **D9 - Hot neutron four-circle diffractometer**, ILL website. Web-site: http://www.ill.eu/instruments-support/instruments-groups/instruments/d9/

47. **A new type of compact large-capacity press for neutron and x-ray scattering**, S. Klotz *et al.*, *High Press. Res.* **24**, 219-223 (2004).

48. **A portable high-pressure stress cell based on the V7 Paris-Edinburgh apparatus, high pressure research**, G. D. Bromiley *et al.*, *High Press. Res.* **29**, 306-316 (2009).

49. **Harmonic Drive AG – the manufacturer of the Harmonic Drive™ gearbox**. Web-site: http://www.harmonicdrive.de/

50. **Spherical thrust roller bearings model 29412E**, the manufacturer is SKF. Web-site: http://www.skf.com/

51. **High-pressure x-ray tomography microscope: Synchrotron computed microtomography at high pressure and temperature**, Y. Wang *et al.*, *Rev. Sci. Instrum.* **76**, 073709 (2005).

52. **Volumetric properties of magnesium silicate glasses and supercooled liquid at high pressure by x-ray microtomography**, C. E. Lesher *et al.*, *Phys. Earth Planet. Int.* **174**, 292-301 (2009).

53. **Pressure distribution in solid samples compressed by toroidal anvils**, S. Klotz *et al.*, *High Press. Res.* **26**, 277-282 (2006).

54. **Cylindrical thrust roller bearings model 89412TN**, the manufacturer is SKF. Web-site: http://www.skf.com/

55. **ANSYS, Inc.** Web-site: http://www.ansys.com/

56. **Principle of massive support in the opposed anvil high pressure apparatus**, M. Yousuf *et al., PRAMANA - J. of Phys.* **18**, 1-15 (1982).

57. **Attainment of near-hydrostatic compression conditions using the Paris-Edinburgh cell**, W. G. Marshall *et al., J. Appl. Cryst.* **35**, 122-125 (2002).

58. **Stress analysis of a beveled diamond anvil**, M. S. Bruno *et al., Rev. Sci. Instrum.* **55**, 940-943 (1984).

59. **Finite element design of diamond anvils**, W. C. Moss *et al., Appl. Phys. Lett.* **50**, 25-27 (1987).

60. **Theory of the gasket in diamond anvil highpressure cells**, D. J. Dunstan, *Rev. Sci. Instrum.* **60**, 3789 (1989).

61. **A computer-aided design study of the behaviour of diamond anvils under stress**, D. M. Adams *et al., J. Phys. D: Appl. Phys.* **15**, 1609 (1982).

62. **Optimization of diamond anvil cell performance by finite element analysis**, D. M. Adams *et al., Measurement Science and Technology* **4**, 422-430 (1993).

63. **Finite element analysis of the diamond anvil cell: achieving 4.6 Mbar**, W. C. Moss *et al., Appl. Phys. Lett.* **48**, 1258-1260 (1986).

64. **Finite-Element modelling of diamond deformation at multimegabar pressures**, S. Merkel *et al., Appl. Phys. Lett.* **74**, 656-658 (1999).

65. **Large elastoplastic strains and the stressed state of a deformable gasket in high pressure equipment with diamond anvils**, V. I. Levitas *et al., Strength of Materials* **28**, 221-227 (1996).

66. **Stress distribution in deformable gaskets of toroidal high pressure equipment**, V. I. Levitas *et al., Sverkhtverdye Materialy* **5**, 7-11 (1983).

67. **Simulation of pressure distribution in a pyrophyllite high-pressure cell by finite-element analysis**, R. Li *et al., High Press. Res.* **27**, 249-257(2007).

68. **Finite-element analysis on performance and shear stress of cemented tungsten carbide anvils used in the China-type cubic-anvil high-pressure apparatus**, Q. G. Han *et al., High Press. Res.* **29**, 457-465 (2009).

69. **FEM study on a double-beveled anvil and its application to synthetic diamonds**, Q. G .Han *et al.*, *High Press. Res.* **29**, 449-456 (2009).

70. **BOMH - the supplier of the BOMH SSI Encoder**. Web-site: http://sensor.baumer.com/productnavigator/scripts/index.php

71. **HPC Gears Ltd. – the manufacturer of the spur gears and pinions**. Web-site: http://www.hpcgears.com/

72. **M. G. 63 - the manufacturer of Paris-Edinburgh press**. Web-site: http://www.mg63.com/

73. **Aubert & Duval - the supplier of maraging steel 819AW.** Web-site: http://www.aubertduval.com/

74. **Oriental Motor Corp. - the manufacturer of the AC stepper motor model AS66ACEP**. Web-site: http://www.orientalmotor.com/

75. **Animation of harmonic gearbox working principal**, Wikipedia. Web-site: http://en.wikipedia.org/wiki/Harmonic_drive

76. **Honeywell – the manufacturer of the micro-switch**. Web-site: http://honeywell.com/Pages/Home.aspx

77. **RS – the on-line supplier of the micro-switch**. Web-site: http://uk.rs-online.com

78. **User manual of harmonic gearbox CSD-32-160-2A-GR**. Web-site: http://www.harmonicdrive.de/

79. **A rotator for single-crystal neutron diffraction at high pressure**, J. Fang *et al.*, *Rev. Sci. Instrum.* **81**, 113901 (2010).

80. **PEARL- high pressure powder diffractometer**, ISIS website. Web-site: http://www.isis.stfc.ac.uk/instruments/pearl/

81. **Drawings of the double toroidal anvils**, C. L. Bull and S. Klotz (private communication).

82. **Compax diamond die blanks**, commercial product manual from the manufacturer - Diamond Innovations. Web-site: http://www.diamondinnovations.com/en/Pages/home.aspx

83. **Safety Report - Titanium/Zirconium null matrix alloy**, Rob Done, Rutherford Appleton Laboratory (RAL), internal safety report.

84. **High-pressure elastic properties of the VI and VII phase of ice in dense H_2O and D_2O**, H. Shimizu *et al.*, *Phys. Rev. B* **53**, 6107-6110 (1996).

85. **Tensile strength data PCD diamond die from a supplier**. Web-site: http://www.jinpingwiredie.com/2.htm

86. **High pressure experimental methods.** M. Eremets. Oxford Science Publications (1996).

87. **Machine design Theory and Practice, Machinery's Handbook (27th ed.)**, A. D. Deutschman *et al.*, MacMillan Publishing Co. Inc. (1975)

Appendix

Appendix A: The Layout and Drawing of the V4 Variant of Paris-Edinburgh Press

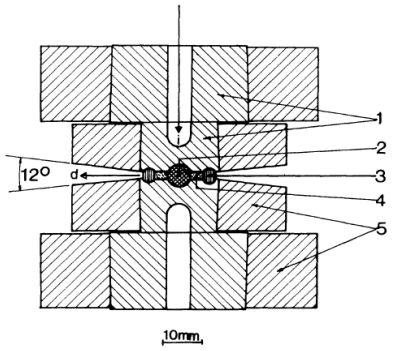

FIG. 1. Cross section of high-pressure anvils and sample volume. (1) Tungsten carbide anvils and anvil seats. The 6-mm-diam hole reduces the incident neutron absorption. (2) Sample space. The sample space is typically a 6-mm-diam spheroid. Pellets of the sample powder (^{7}LiD in the present case) are precompressed under ~1.2 GPa with the required amount of the calibrant (NaCl) to reach adequate compactness before the run. (3) Toroidal gasket. Soft beryllium copper gaskets are machined to the correct section, then shaped by compression in their grooves, and finally aged at 320 °C to full hardness (42 RC). (4) Pyrophyllite gaskets 1–2 mm in thickness depending on the final pressure. (5) Maraging steel rings are heat-treated to full hardness (52 HRC) and the tungsten carbide cores are pushed in, on a 1.5° angle, to the maximum tensile strength of the steel at the carbide-steel face (1600 MPa). The incident neutron beam (i) is precollimated by a 6-mm-diam B_4C collimator. The diffracted beam (d) can be collected over a 12° angle in 2θ: 90°±6°. The faces and sides of the anvil binding rings are coated with gadolinium oxide paint.

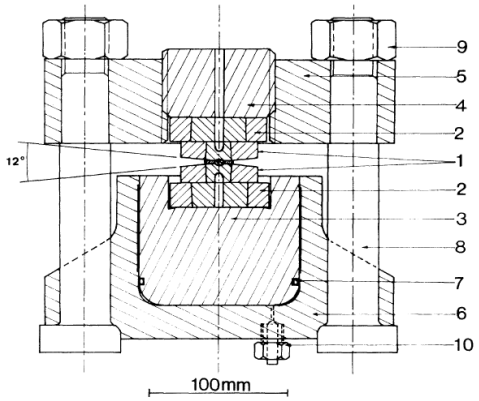

FIG. 2. Cross-sectional sketch of the 2.5-MN press. (1) Anvils and sample assembly. (2) Anvil seats and supporting rings. (3) Main piston (35 NCD 16 steel—52 HRC), 100 cm^2 in diameter to provide a ~2.5-MN thrust under 250 MPa oil pressure. (4) Front breech (same material) has two functions: to make assembling of the sample and anvils possible without disassembling the tie rods, and to provide a flat resting surface for the seats by being mechanically decoupled through the thread from the plate (5) which bends outwards under load. (5) Top plate [same steel as (3)]. (6) Hydraulic ram [same material as (3)]. Its unusual shape has been calculated (Ref. 20) to provide compensation of strains and negligible deformation under load at the level of the gasket (7) and of guide ring (top of piston). (7) Neoprene O ring. This is leak tight to well above 200 MPa because the diameter of the oil chamber (6) does not vary under pressure. (8) Tie rods. Marval 18 maraging steel (51 HRC—tensile strength: 1800 MPa). (9) Retaining nuts [same metal as (8)]. (10) Hydraulic oil inlet connected to a 280-MPa pump.

The layout and component descriptions of the standard V4 Paris-Edinburgh press and toroidal anvil cell (from [28])

Appendix B: A Full List of the Components in the RV4 and their Materials

S/N	Part Name	NO.	Material	Note
1	Tie Rod Nuts	4	819AW	*MG63*
2	Tie Rod Washers	4	819AW	*MG63*
3	Breech Centring Ring	1	Bronze	*MG63*
4	Top Platen	1	819AW	*MG63*
5	Breech	1	819AW	*Modified in workshop*
6	Tie Rods	4	819AW	*Extended version, MG63*
7	Spherical Thrust Bearings	2	N/A	*SKF 29412E*
8	Top Shaft	1	819AW	*MG63*
9	Gears	2	EN36	*HPC Gear Ltd.*
10	WC Supporting Die	2	WC	*MG63*
11	Mounting Collar Big	4	Al	
12	Mounting Collar Small	8	Al	
13	Gear Position Ring	2	Al	
14	Anvil Binding Ring	2	819AW	*Modified version, MG63*
15	Anvil	2	WC	*MG63*
16	Gasket	2	TiZr	
17	Gasket Ring	1	TiZr	
18	Bottom Shaft	1	819AW	*MG63*
19	Sensor Body	1	N/A	*Honeywell V15T16-CC100A01*
20	Sensor Tappet	1	Al	
21	Sensor Base2	1	Al	
22	Sensor Base	1	Al	
23	Bottom Backing Plate	1	819AW	*MG63*
24	Piston	1	819AW	*MG63*
25	Bottom Platen	1	819AW	*MG63*
26	Hydraulic Interface	1	N/A	*Enerpac*
27	Side Supporting Base	1	Stainless Steel	
28	Side Alignment Bearing Housing	1	Stainless Steel	
29	Side Bearing Seal	1	Al	
30	Side Deep Groove Bearings	1	N/A	*SKF 16005*
31	Side Top Position Sleeve	1	Brass	
32	Pinions	2	EN36	*HPC Gear Ltd.*
33	Pinions Keys	2	BS46	KK6-16
34	Side Shaft	1	EN24	*Yield Strength=654MPa*
35	Side Gearbox Connection	1	EN24	*Yield Strength=654MPa*
36	Side Gearbox Key	2	BS46	KK6-16
37	Side Deep Groove Bearings3	1	N/A	*SKF 61811-2RS*
38	Side Gearbox Base	2	Stainless Steel	
39	Side Gearbox	1	N/A	*Harmonic Drive CSD32-160-2A-GR-Stardard*

40	Side Motor Connection	1	Stainless Steel	
41	Side Deep Groove Bearings2	1	N/A	*SKF 61803-2RS*
42	Side Gearbox Flange	1	Al	
43	Side Motor Couplings	1	Stainless steel	*20-*$\emptyset 8 \times \emptyset 8$
44	Side Motor Base Assembly	1	Al	
45	Side Motor	1	N/A	*Oriental MotorAS66ACEP including FC04W5 & controller*
46	Hydraulic Bearing Cylinder	2	Stainless Steel/ WC	*One for top end, one for bottom end. Maraging steel to be made*
47	Hydraulic Bearing Piston	2	Stainless steel/ WC	*One for top end, one for bottom end. Maraging steel to be made*
48	Hydraulic bearing PTFE rings	2	PTFE	*Teflon*
49	Hydraulic bearing nylon rings 2	2	Nylon	
50	Side Encoder	1	N/A	Bei Ideacod
51	Spacer with holding arm	1	Stainless steel	
Assembly Stand				
52	Frame Long Arm	4	Al	
53	Frame Short Arm	4	Al	
54	Frame Short Leg	2	Al	
55	Frame Long Leg Head	2	Al	
56	Frame Long Leg Rotator	2	Brass	
57	Frame Long Leg Stator	2	Brass	
58	Frame Long Leg	2	Al	
59	Frame Eyebolt	4	N/A	RS Components Ltd. M10
60	Frame Bottom Platen	1	Al	
61	Frame Sling	2	N/A	round lifting sling,2m, 1 ton pull
62	Frame Shackle	4	N/A	RS Galvanisedsteel Bowshackle
63	Frame Castor	4	N/A	Revvo TS3 075 PT03
Minor Consumables				
64	Loctite 5203 LowStrength Sealant	1	Glue	50 ml
65	Loctite 243	1	Glue	50 ml

Appendix C: Technical Specifications of Single-crystal diffractometers – SXD and D9

1) Technical specification of the SXD [42, 44]

Beamline	S3
Moderator	Ambient water, poisoned at 2 cm
Incident wavelenghts	0.2 – 10 Å
Sin θ/λ	0.03 - 2.5$Å^{-1}$
Resolution	Δd/d ~ 0.5% (backscattering) - 1% (90 degrees)
Sample position	8.3 m from moderator
Beam size at sample	< 15 mm diameter
Sample size	Dependent on scattering characteristics and unit cell size, at least 1 mm^3 and typically 100 mm^3
Data collection time	Typically 1 - 2 hours per crystal orientation
Position-sensitive detectors	Eleven 64 x 64 pixel optically encoded ZnS scintillators each with 192 × 192 mm^2 active area and 3 × 3 mm^2 resolution
Detector positions (centre)	L2 = 0.225 m in equatorial plane at longitude = ±37.5 °, ±90 °, ±142.5 °; L2 = 0.27 m at latitude = 45 °, longitude = 0 °, ±90 °, 180 °; L2 = 0.28 m at latitude = -90 °, longitude = 0 °.
Diffractometer motion	w rotation available on vacuum tank, cryostat and furnace.
Sample environment	Standard sample environments plus the following SXD specific items: Liquid He Orange cryostat (1.5 – 300 K) Displex cooler (12 – 300 K) Furnace (300 – 1200 K) Cryostat with 3He dilution insert: 300 mK – 300 K and omega rotation

Data acquisition and analysis	Windows PC. Labview based instrument control software. Analysis program SXD2001 for initial data visualisation, reduction to structure factors including data corrections, fully corrected volumes in reciprocal space. Supported structure refinement packages: SHELX, GSAS, FULLPROF

2) Detector location and coverage in SXD

Detector labels correspond to those indicated in Figure 3; longitude, latitude and L2 are the scattering angle, angle out of the equatorial plane of the instrument and secondary flight path distance of the central pixel of each detector, respectively [42, 44].

Detector	Longitude (°)	Latitude (˚)	L2 (mm)
1	142.5	0.0	225
2	90.0	0.0	225
3	37.5	0.0	225
4	-37.5	0.0	225
5	-90.0	0.0	225
6	-142.5	0.0	225
7	90.0	-45.0	270
8	0.0	-45.0	270
9	-90.0	-45.0	270
10	180.0	-45.0	270
11	0.0	-90.0	280

3) Technical Specifications of D9 [45, 46]

Monochromator	Cu (2 2 0) in transmission geometry
Wavelength	Accessible from 0.3 to 0.9 Å
Four-circle angle ranges	$5 < 2\theta < 120^{\circ}$, $-34 < 2\theta < 48^{\circ}$, $80 < 2\theta < 200^{\circ}$, $-179 < 2\theta < 179^{\circ}$
Lifting counter angle range	$-12.5 < 2\theta < 25^{\circ}$
Detector	Resolution: 32×32 pixels Pixel size: 2 mm × 2 mm or 0.25˚ × 0.25˚ Area: 64 mm^2
Distance setup	Hot source – monochromator: 10 m (partly in vacuum) Monochromator – sample distance 2.29 m Sample – detector distance 49 cm
Visible size of hot source	Vertical: 15 cm Horizontal: 5 cm
Sample size	Maximum: 50 mm^3 Minimum: 1 mm^3 Generally from 5 – 25 mm^3
Beam size	6 mm × 6 mm

Appendix D: Drawings of Key Components Manufactured in the Workshop

A majority of these parts are manufactured by the technicians in the Mechanical Workshop of the School of Physics and Astronomy.

Component List:

1) Top Hydraulic Bearing Cylindrical Housing
2) Bottom Hydraulic Bearing Cylindrical Housing
3) Top and Bottom Hydraulic Bearing Piston
4) Side Shaft
5) Transmission Gear
6) Transmission Pinion
7) Top Anvil Support
8) Bottom Anvil Support

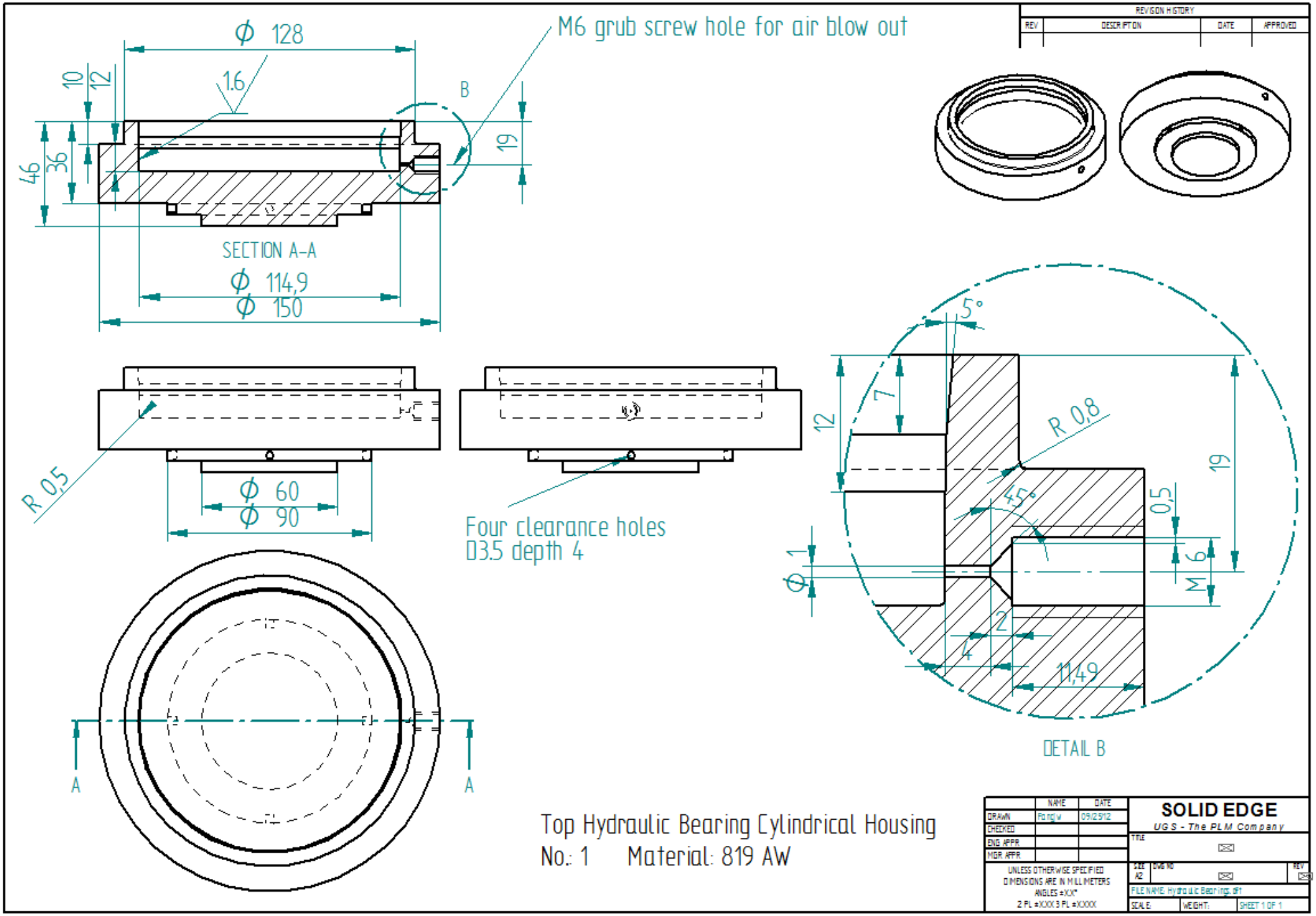
REVISION HISTORY
REV
DESCRIPTION
DATE
APPROVED
M6 grub screw hole for air blow out
Φ 128
1.6
10
12
46
36
19
B
SECTION A-A
Φ 114,9
Φ 150
R 0,5
Φ 60
Φ 90
Four clearance holes
D3.5 depth 4
5°
7
12
R 0,8
19
45°
0,5
Φ 1
M 6
2
4
11,49
DETAIL B
A
A
Top Hydraulic Bearing Cylindrical Housing
No.: 1 Material: 819 AW
NAME
DATE
DRAWN
Rongw
09/2/512
CHECKED
ENG APPR.
MGR APPR.
UNLESS OTHERWISE SPECIFIED
DIMENSIONS ARE IN MILLIMETERS
ANGLES ±XX°
2 PL ±XXX 3 PL ±XXXX
SOLID EDGE
UGS - The PLM Company
TITLE
SIZE
A2
DWG NO
REV
FILE NAME: Hydraulic Bearing.dft
SCALE:
WEIGHT:
SHEET 1 OF 1

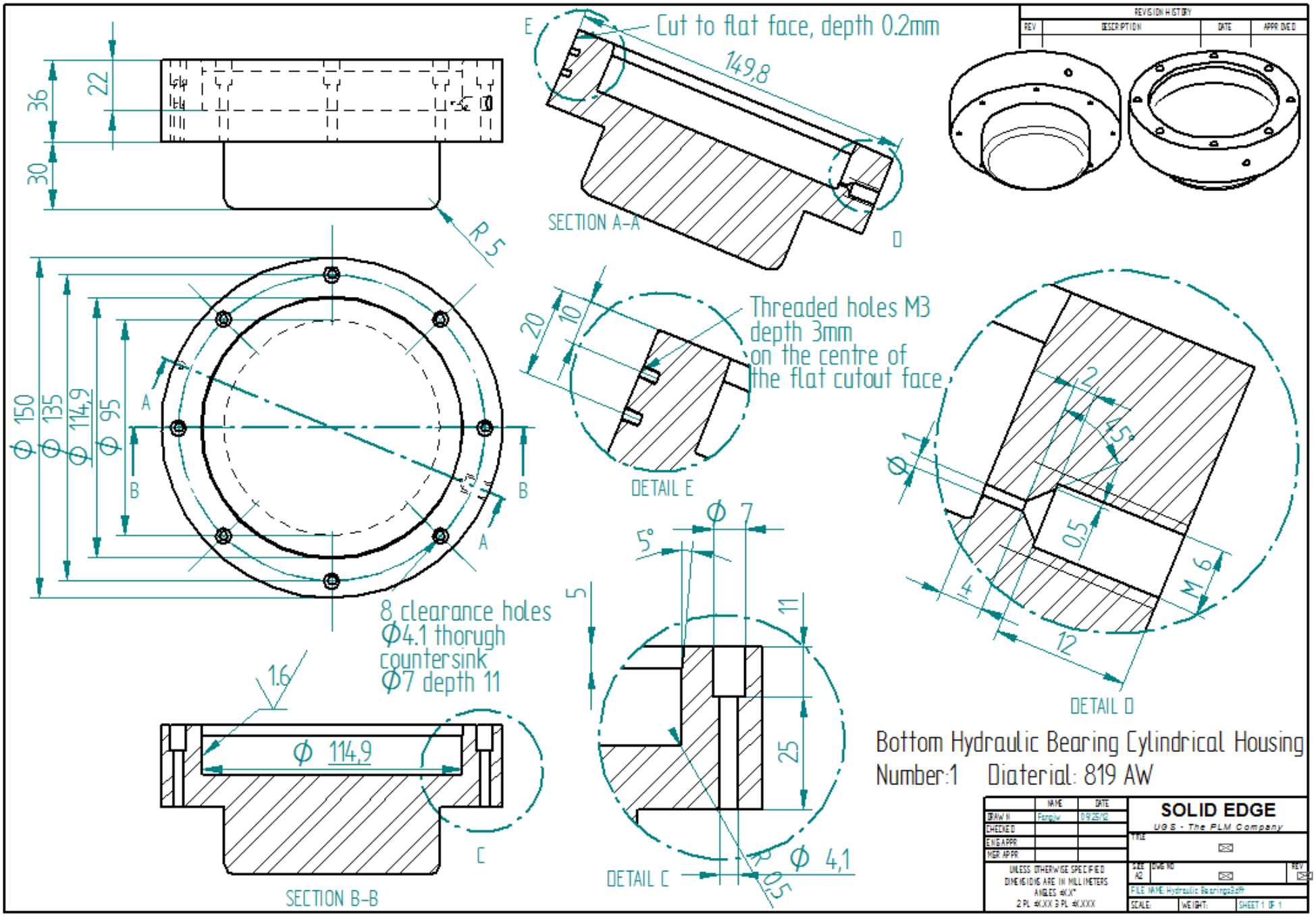
Cut to flat face, depth 0.2mm
149,8
E
D
SECTION A–A
22
36
30
R 5
Φ 150
Φ 135
Φ 114,9
Φ 95
A
B
Threaded holes M3
depth 3mm
on the centre of
the flat cutout face
20
10
DETAIL E
8 clearance holes
Φ4.1 thorugh
countersink
Φ7 depth 11
Φ 7
5°
5
11
25
R 0,5
Φ 4,1
DETAIL C
2
45°
Φ 1
0,5
M 6
4
12
DETAIL D
1.6
Φ 114,9
C
SECTION B–B
Bottom Hydraulic Bearing Cylindrical Housing
Number:1 Diaterial: 819 AW
REVISION HISTORY
REV
DESCRIPTION
DATE
APPROVED
NAME
DATE
DRAWN
Fenglv
09/25/12
CHECKED
ENG APPR.
MGR APPR.
UNLESS OTHERWISE SPECIFIED
DIMENSIONS ARE IN MILLIMETERS
ANGLES ±X°
2 PL ±X.XX 3 PL ±X.XXX
SOLID EDGE
UGS - The PLM Company
TITLE
SIZE
A2
DWG NO
REV
FILE NAME: Hydraulic Bearings3dft
SCALE:
WEIGHT:
SHEET 1 OF 1

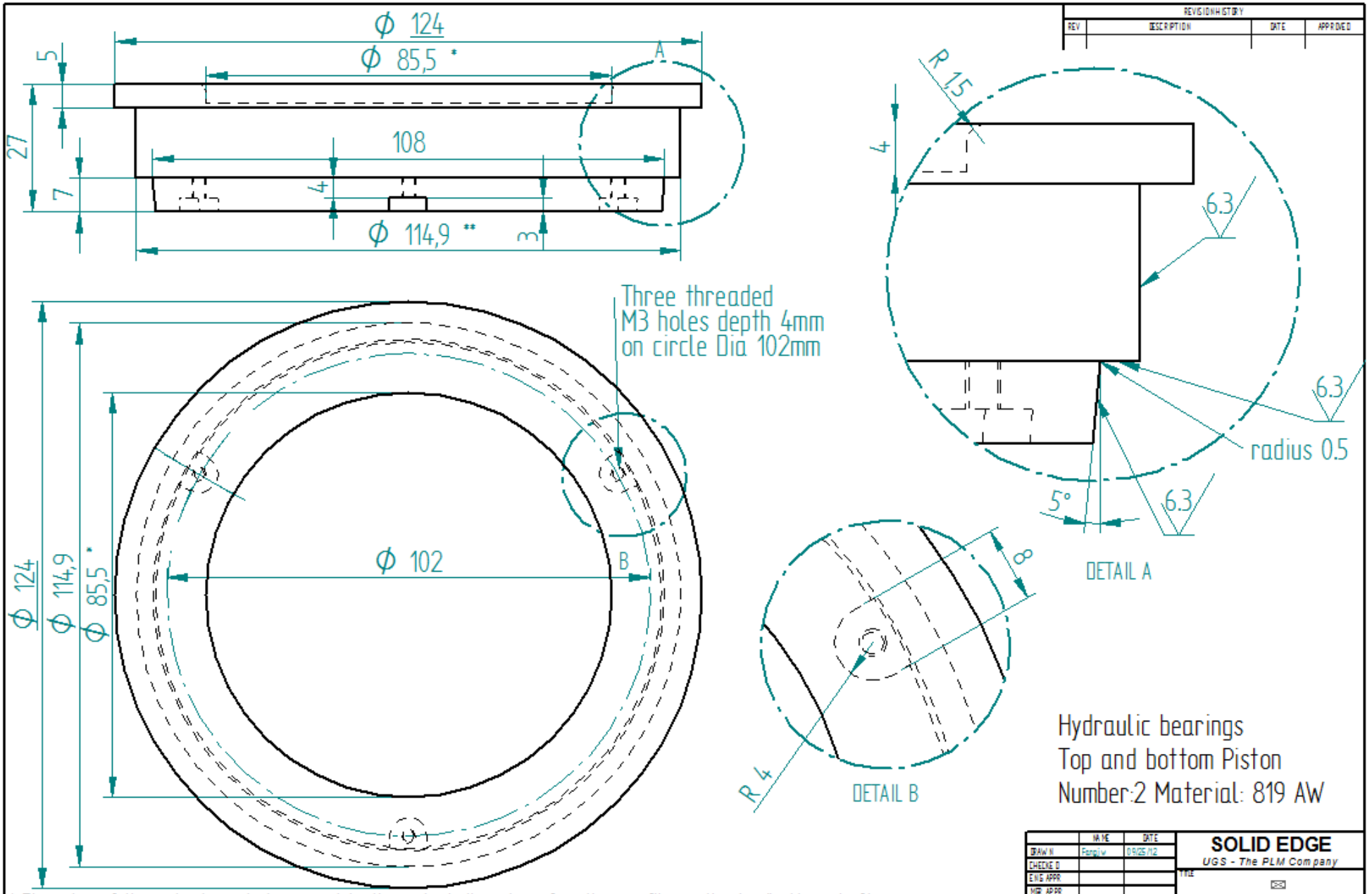

* Diameter of the cutout needs to accord to the actual diameter of mating profile on the top/bottom shaft

** OD of the piston needs to be carefully determined to allow proper clearance between piston & cylinder

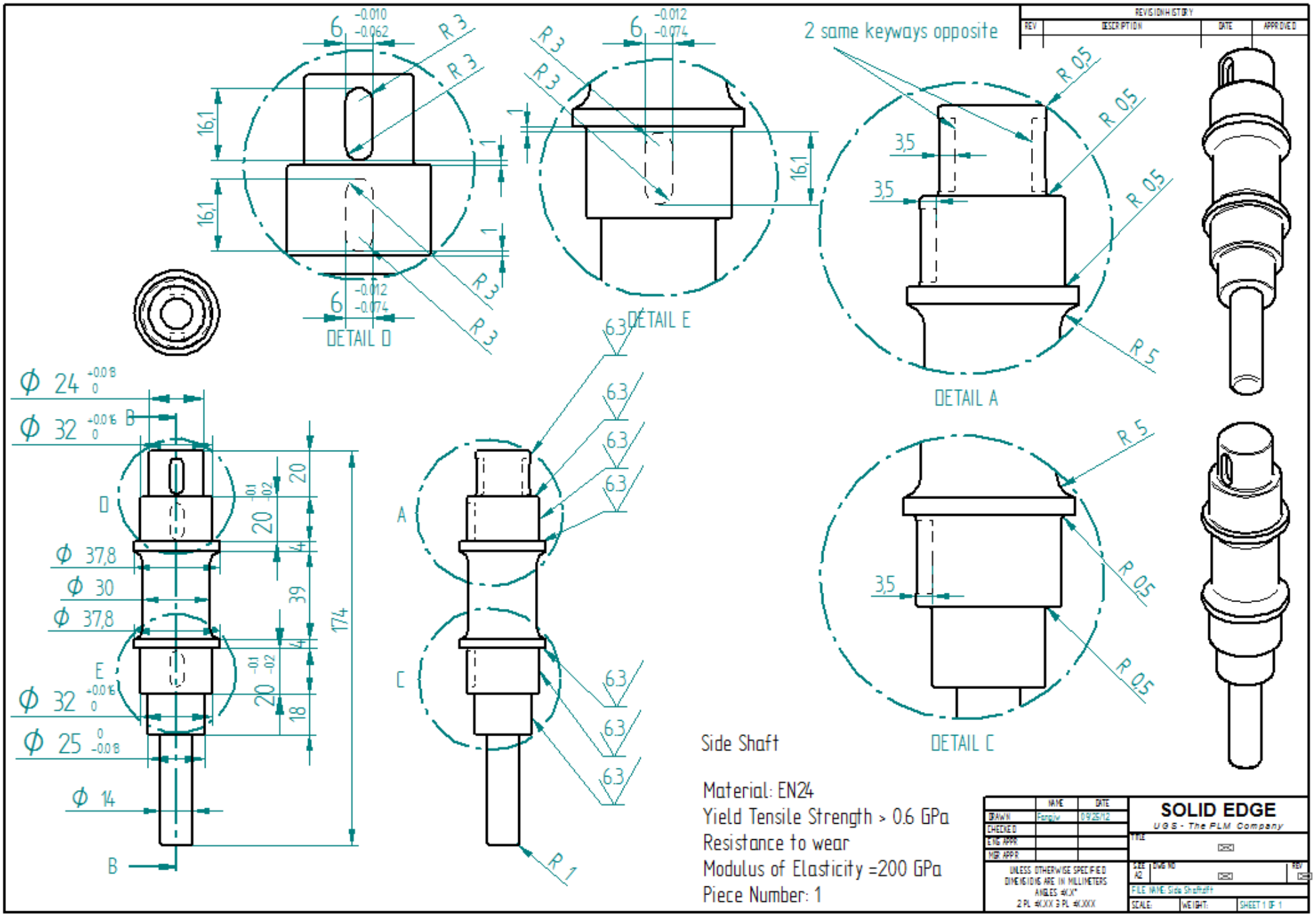
REVISION HISTORY
REV
DESCRIPTION
DATE
APPROVED
2 same keyways opposite
DETAIL D
DETAIL E
DETAIL A
DETAIL C
Side Shaft
Material: EN24
Yield Tensile Strength > 0.6 GPa
Resistance to wear
Modulus of Elasticity =200 GPa
Piece Number: 1
SOLID EDGE
UGS - The PLM Company
UNLESS OTHERWISE SPECIFIED
DIMENSIONS ARE IN MILLIMETERS
ANGLES ±X.X°
2 PL ±X.XX 3 PL ±X.XXX
DRAWN
Pangiv
09/25/12
CHECKED
ENG APPR
MGR APPR
SIZE
A2
DWG NO
REV
FILE NAME: Side Shaft.prt
SCALE:
WEIGHT:
SHEET 1 OF 1

REVISION HISTORY			
REV	DESCRIPTION	DATE	APPROVED

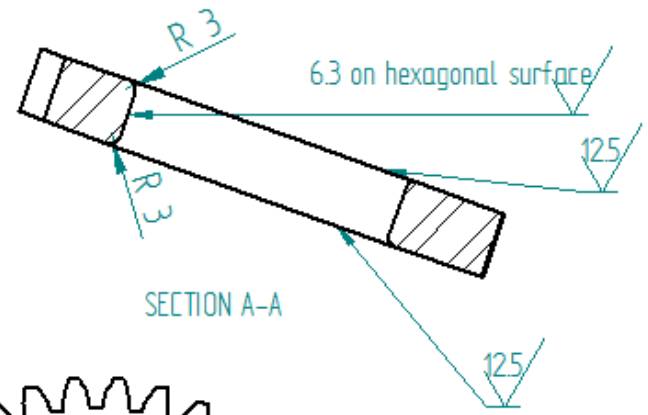

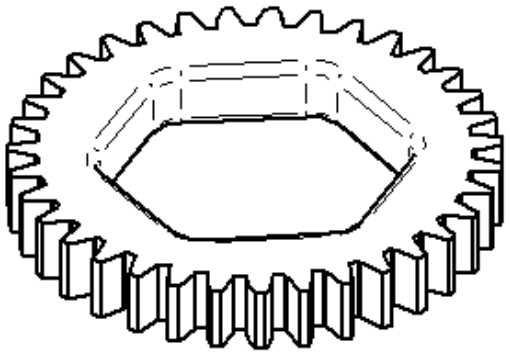

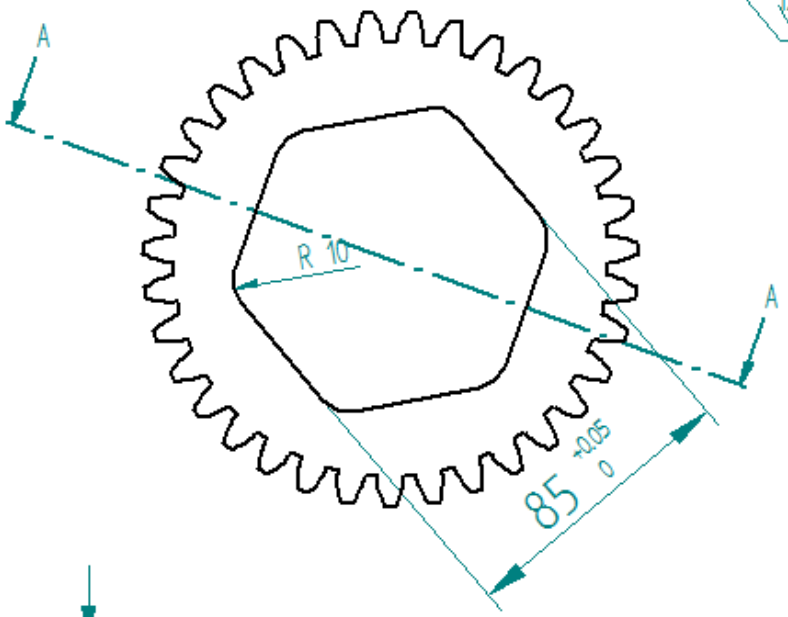

Gears for central shafts

Involute Spur Gear
Material: EN36
Height: 20mm
Pitch Diameter: 140mm
Module: 4mm
Tooth Number:35
Torque Load: 127.32 Nm
Mating Pinion Tooth Number: 21
Gear Rate: 1.667

	NAME	DATE
DRAWN	Fergov	09/25/12
CHECKED		
ENG APPR.		
MFG APPR.		

UNLESS OTHERWISE SPECIFIED
DIMENSIONS ARE IN MILLIMETERS
ANGLES ±0.X°
2 PL ±0.XX 3 PL ±0.XXX

SOLID EDGE
UGS - The PLM Company

TITLE: Gear1

SIZE: A2 | DWG NO: | REV:

FILE NAME: Gear1.dft

SCALE: | WEIGHT: | SHEET 1 OF 1

REVISION HISTORY			
REV	DESCRIPTION	DATE	APPROVED

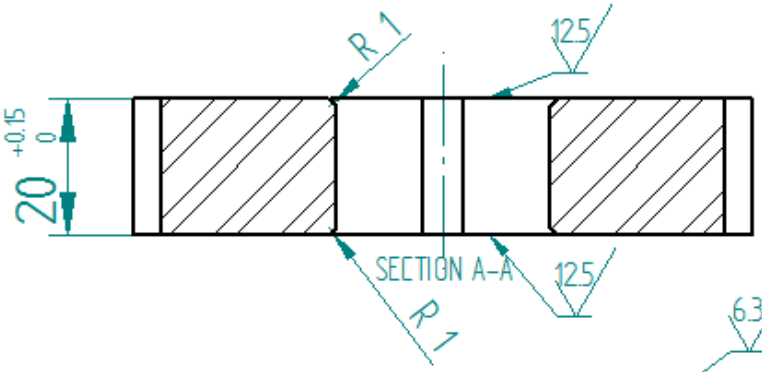

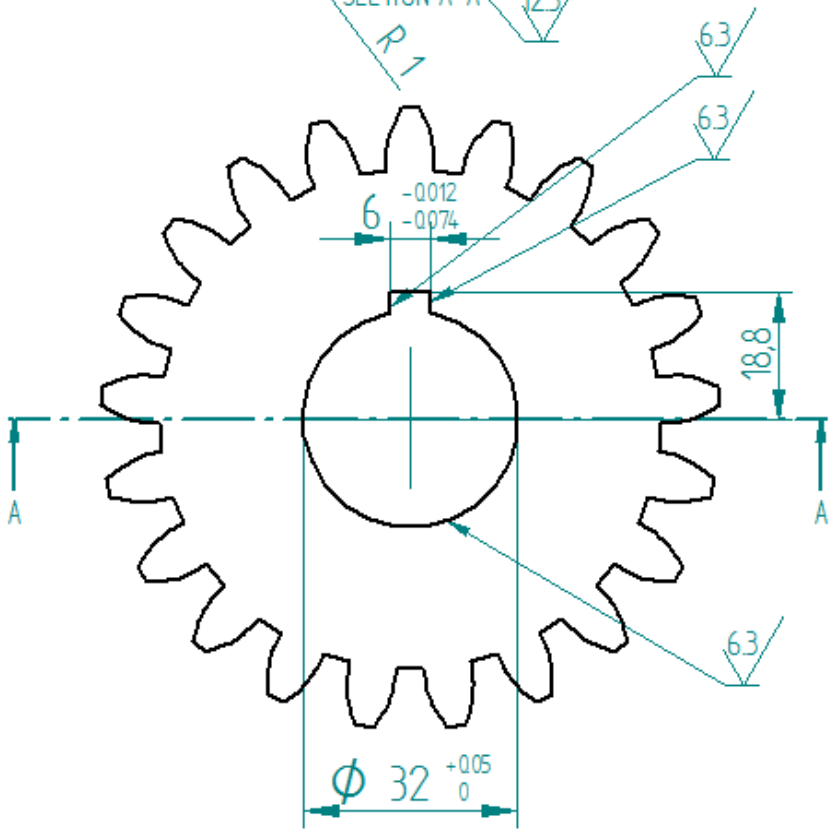

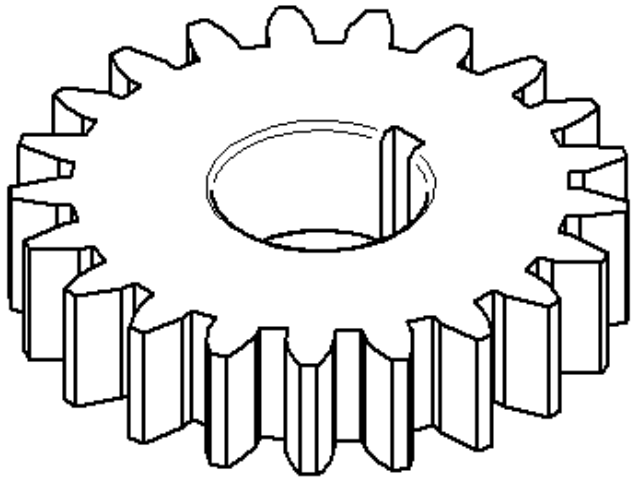

Side Pinions

Involute Spur Gear
Material: EN36
Height: 20mm
Pitch Diameter:84 mm
Module: 4mm
Tooth Number: 21
Torque Load: 127.32 Nm
Mating Gear Tooth Number: 35
Gear Rate: 1.667

	NAME	DATE
DRAWN	Fergav	09/25/12
CHECKED		
ENG APPR.		
MFG APPR.		

UNLESS OTHERWISE SPECIFIED
DIMENSIONS ARE IN MILLIMETERS
ANGLES ±0.X°
2 PL ±0.XX 3 PL ±0.XXX

SOLID EDGE
UGS - The PLM Company

TITLE: Side Pinion1

SIZE A2 | DWG NO | REV

FILE NAME: Side Pinion1.dft

SCALE: | WEIGHT: | SHEET 1 OF 1

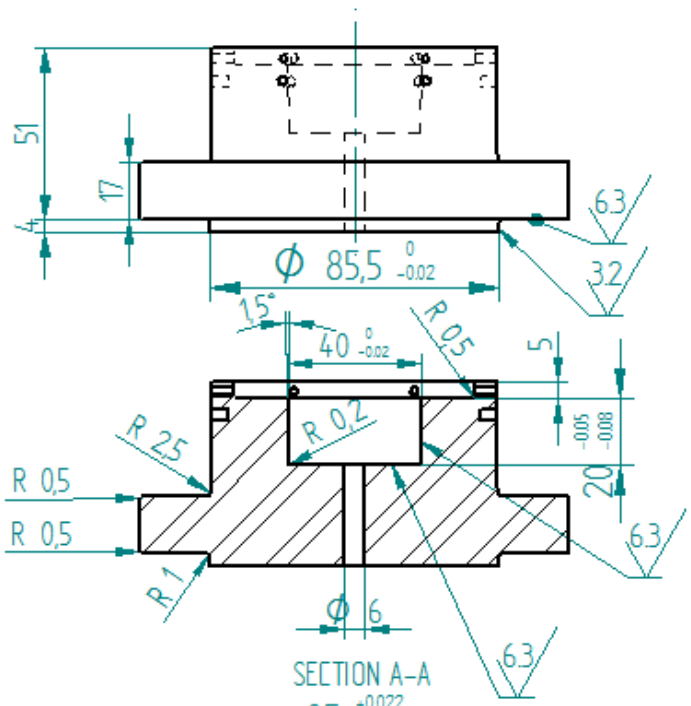

SECTION A-A

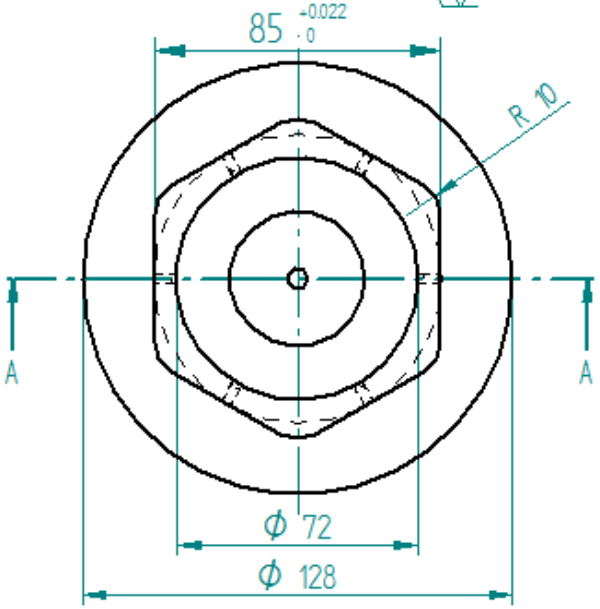

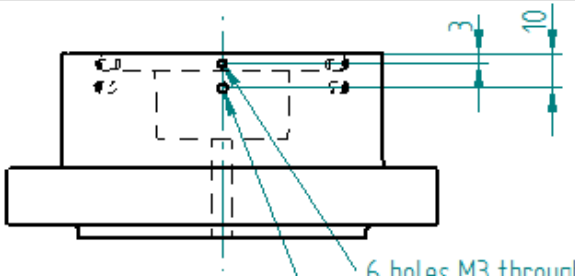

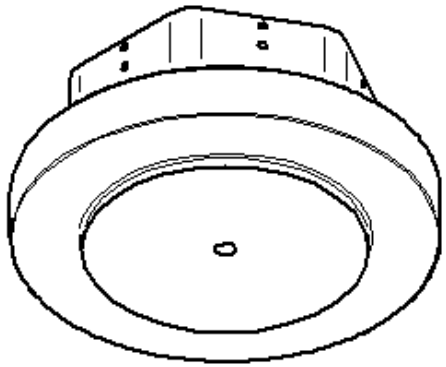

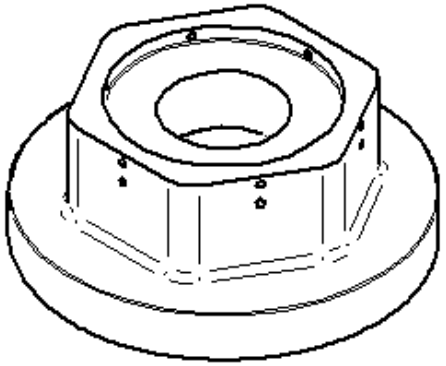

Top Anvil Support
Material: 819 AW
Piece Number: 1
Heat Treatment: 1.8GPa

REVISION HISTORY			
REV	DESCRIPTION	DATE	APPROVED

	NAME	DATE
DRAWN	Pangiw	09/25/12
CHECKED		
ENG APPR.		
MFG APPR.		

UNLESS OTHERWISE SPECIFIED
DIMENSIONS ARE IN MILLIMETERS
ANGLES ±X°
2 PL ±X.XX 3 PL ±X.XXX

SOLID EDGE
UGS - The PLM Company

TITLE: Top Shaft

SIZE	DWG NO	REV
A2		

FILE NAME: Top Shaft.dft

SCALE:	WEIGHT:	SHEET 1 OF 1

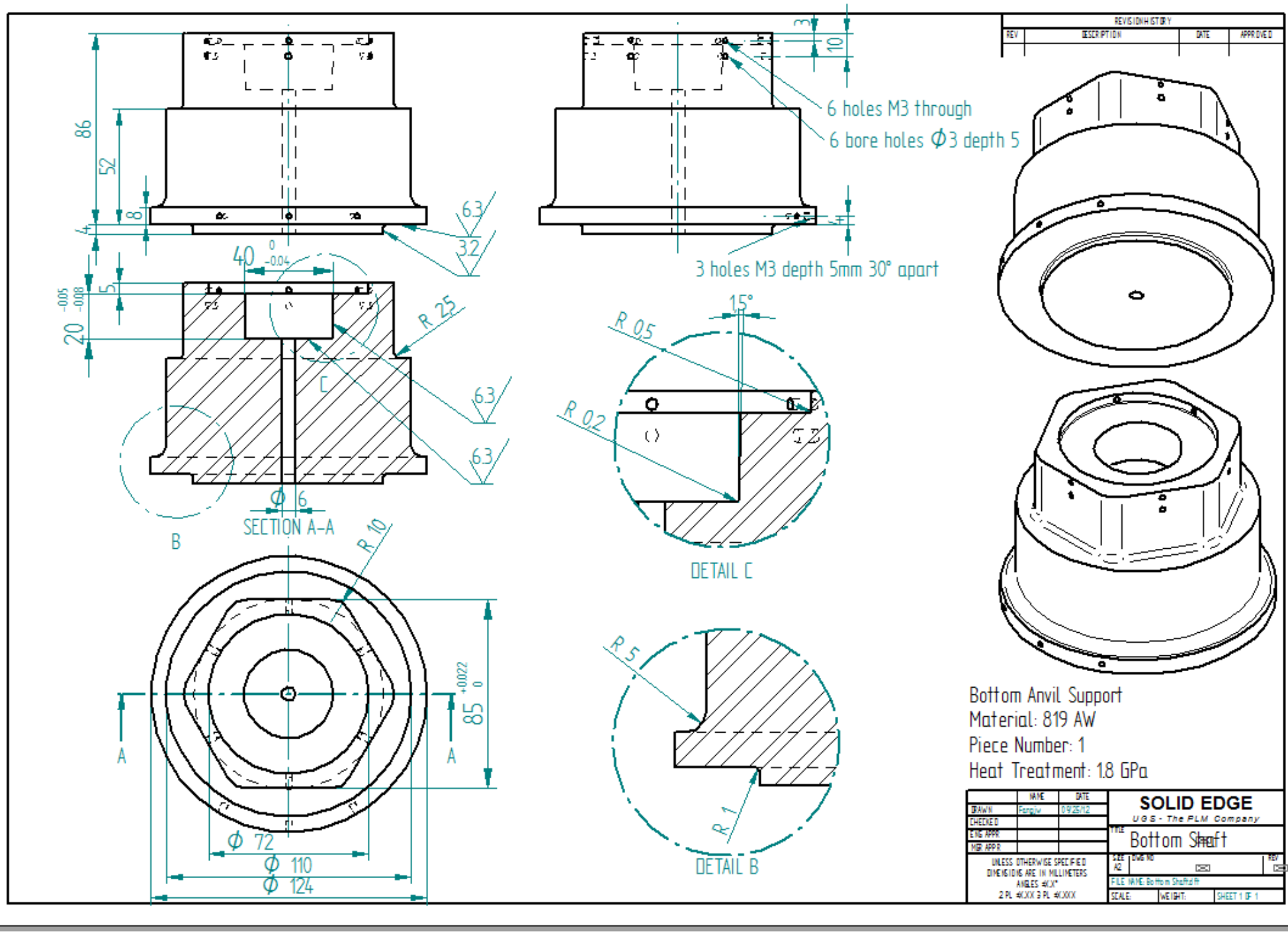
REVISION HISTORY
REV
DESCRIPTION
DATE
APPROVED
86
52
8
4
6.3
32
40 0 -0.04
5 -0.05 -0.08
20
R 25
C
6.3
6.3
Φ 6
SECTION A-A
B
R 10
85 +0.0022 0
A
A
Φ 72
Φ 110
Φ 124
3
10
6 holes M3 through
6 bore holes Φ3 depth 5
3 holes M3 depth 5mm 30° apart
15°
R 0.5
R 0.2
DETAIL C
R 5
R 1
DETAIL B
Bottom Anvil Support
Material: 819 AW
Piece Number: 1
Heat Treatment: 1.8 GPa
NAME
DATE
DRAWN
Fangjiv
09/25/12
CHECKED
ENG APPR.
MFG APPR.
UNLESS OTHERWISE SPECIFIED
DIMENSIONS ARE IN MILLIMETERS
ANGLES ±X°
2 PL ±X.XX 3 PL ±X.XXX
SOLID EDGE
UGS - The PLM Company
TITLE
Bottom Shaft
SIZE
A2
DWG NO
REV
FILE NAME: Bottom Shaft.dft
SCALE:
WEIGHT:
SHEET 1 OF 1

Appendix E: User Manual for Striping and Assembling the RV4 system

How to strip and build the Rotator

Note:

* The Rotator can be separated into the following four sub structures:

The rotator central structure (frame with sample assembly), the side structure (side plate with the motor), the electrical module, the assembly stand (on the trolley)

* * 'bottom' and 'top' in the following text refer to the position of the Rotator when it is in normal position. The **normal position** is such that the breech is on the top side, the hydraulic ram on the bottom side. While loading, the Rotator is placed up-side-down in a **reverse position**. On the horizontal position, the Rotator is places horizontally. All these positions require tightening of the screws on the assembly stand to make sure the Rotator would not spin and hurt you.

1.1 Strip the sample/gaskets after loading sample

1) Open the valve of the pump and release the pressure.
2) Strip the electrical module. (see **Section 1.3**)
3) Remove the side plate as a whole and place the Rotator in **reverse position**.
4) Mount two brackets on the tie rods to hold the bottom shaft tight in place, stopping it from moving in the axial direction.
5) Unscrew the breech by 5 mm. Allow a gap of 5 mm between the gaskets when the top shaft falls after the breech.
6) Remove the gaskets using tweezers.
7) Unscrew the tiny screws fixing the anvils and remove the anvils.
8) Put in the test die between the top and bottom shafts. The die has a 0.5mm step to help locate its position in the hole of the shaft.
9) Screw in the breech, in order to push the hydraulic piston back to initial position in the ram. Will need to make sure the valve of the pump is open. Once the piston is pushed back in position, slide the brackets on the tie rods accordingly to hold the shafts in position.

1.2 Rebuild the Rotator after striping the sample/gaskets

1) Strip the sample/gaskets (see above **Section 1.1**)
2) Align the teeth of top and bottom gears on the top and bottom shafts. (following the marks on the gears, will need to release the breech a little bit)
3) Depending on what to do next.
   If to test the Rotator with the test die, will need to
   a) Remove the brackets on the tie rods.
   b) Mount the side plate, mating the gears and pinions (might need to release the breech a little bit, while turning the breech will need to keep the teeth of top and bottom gears well aligned)
   c) Rebuild the electrical module.

   If to reload the sample, will need to
   a) Mount the side plate, mating the gears and pinions (might need to release the breech a little bit, while turning the breech will need to keep the teeth of top and bottom gears well aligned). Before mounting the side plate, carefully treat the positions of the brackets on the tie rods to make sure they can hold the shafts in place but won't interfere with the side plate. See if they are easy to be stripped when the side plate is mounted, allowing some room to unscrew them.
   b) Rebuild the electrical module. (optional, can be done at step g, see **Section 1.4**)
   c) Release the breech by 5 mm and remove the test die.
   d) Install the anvils. Hold one anvil and insert it into the hole of the bottom shaft (which is on the top side now), make sure it is fully pushed (upward) to the bottom of the hole in the shaft before fixing one or two tiny screws to hold it in place. Mark the screws fixing the anvil for easier stripping later on. Put in the other anvil on the top shaft (which is on the bottom side now), push and fix it in the same way.
   e) If old sample and gaskets are to be used, use tweezers to put them in between the anvils. Align them in the centre. Turn the breech in and tight. Notice the mark on the side of the hydraulic bearings and the face of the top platen; align the lines to be sure that the breech is fully in position.
      If new sample and gaskets are to be used, need to follow strict loading procedure which largely depends on experimental context. After the procedure, the breech needs to be fully screwed in with the pump putting a pre-load on the gaskets.
   f) Remove the brackets.
   g) Rebuild the electrical module. (see **section 1.4**, if it is not done yet)

1.3 Stripping the electrical module

1) Turn off the power supply of the motor controller and the DC power converter.
2) Disconnect the communication wire between computer and motor controller, the connector is on the controller side.
3) Disconnect the power cable between motor controller and the motor, the connector is on the controller side.
4) If the position sensor (micro mechanical switch) is installed, strip it on the bottom shaft.
5) Unscrew two black screws mounting the controller bracket to the side plate and remove the controller bracket with the controller on it. Put it aside.

1.4 Setting up the electrical module

1) Screw two black screws, fixing the controller bracket to the side of the side plate
2) Connect the power cable between motor controller and the motor, the connector is on the controller side.
3) Connect the communication wire between computer and motor controller, the connector is on the controller side. There is another connector on the computer side which has 9 pins.
   The wire needs to be carefully treated (e.g. cover it with tapes) on the floor as it can be a trip hazard.
4) Turn on the power supply of the motor controller and the DC power converter.
5) Dismount the spade crimps on the DC converter. Turn on the output to check the output voltage is 24 V. Turn off the converter output. Remount the crimps on the output studs of the converter. Turn on the output.
6) Electrical module is done. Ready to use the HyperTerminal to control the motor.

1.5 Strip the hydraulic bearings

1) Strip the sample/gaskets (see **Section 1.1**)
2) Strip the pump. Seal the oil interface on the bottom platen. Clean the oil left on the bottom platen during the operation.
3) Remove the brackets mounted on the two tie rods with the needle bearings on them. Install the brackets on the two tie rods on the opposite side to hold the shafts. The brackets will be such that it holds the bottom shaft (on the top side now) tight in position.
4) Release the screws on the needle bearings stands which fix the stands to the tie rods (not the screws that fix the needle bearings on the stands.), so that the stands can slide on the tie rods.
5) Remove the two tie rods which have the needle bearings on them. Hold and take away the needle bearings stands which will fall while the tie rods are being removed.
6) Release the breech by 5 mm and remove the test die.

7) Remove the brackets fixing the top shaft (which is on the bottom side now). Lift and remove the top shaft. Screw the breech back.
8) Place the Rotator on **normal position** (with the bottom shaft on the bottom side). Tighten the screws on the assembly stand in case the Rotator spin while operation.
9) Remove the brackets on the tie rods that fix the bottom shaft. Lift and remove the bottom shaft. Unscrew 12 screws to remove the bottom hydraulic bearings.
10) Spin the Rotator to **reverse position** (with the top hydraulic bearing on the bottom side). Tighten the screws on the assembly stand in case the Rotator spin while operation.
11) Unscrew 4 small screws under the top hydraulic bearing that fix it to the breech. Will need long Allen key to do the job (might need to turn breech a little bit to allow easier access of the screws). Remove the bottom hydraulic bearings.

1.6 Rebuild the hydraulic bearings.

1) After procedure described in **Section 1.5.**
2) Carefully check if the hydraulic bearings' air-blow-out grub screw is tightly screwed in.
3) Place the frame of the Rotator in the **reverse position**. With two tie rods near the side plate (the side plate is not installed yet) on it and two tie rods for mounting needle bearings removed.
4) Put in the top hydraulic bearing; adjust it to be at the centre of the breech/frame using four pieces of round plates to fill the gap between the side of it and the tie rods. Tighten the four tiny screws uniformly underneath to fix it in position.
5) Spin the rotator to be in the **normal position**. Install the bottom hydraulic bearing, need to slide it straight into the long cylinder in the bottom platen carefully. 12 screws are to be screwed in with some room to allow the piston pop up while loading of pressure. Normally it will be such that the top surface of the screw cap is levered with the hydraulic bearing's top surface.
6) Place the bottom shaft on the bottom hydraulic bearing. Fix its position using brackets on the tie rods near the side plate (the side plate is not installed yet). Hold and stop it from falling.
7) Spin the rotator to the **reverse position**. Install the top shaft and fix it with brackets on the tie rods.
8) Install the two spare tie rods together with four needle bearings (two big ones on the bottom shaft side, two small ones on the top shaft side). Need to slide the tie rods through the bottom platen first, then the stands of the big bearings and small bearings (there are two sides of the bearings stand, make sure that the needle bearings side are close to the gears), and finally the top platen. Tighten the tie rods with the tie rod nuts.
9) One the tie rods are fixed, adjust the position of the needle bearings to be around 1 mm off the face of gears and fix the bearing stands tightly on the tie rods with the screws on it.
10) Connect the pump.

11) Install the sample/gaskets and side plate, electrical module (see **Section 1.2**).

1.7 Start a test

After building of the Rotator

1) Check if the breech is tight and in right position
2) Check if the tie rods nuts are tight.
3) Check if all brackets are removed from the tie rods.
4) Check if any oil leakage near the hydraulic bearings and the pump connector, also monitor this during loading process.
5) Check if personnel are behind shielding before loading.
6) Try low speed operation first.
7) Do not increase/release the load during rotation operation.

Appendix F: Strength Calculation for the Gears and Pinions

UNIVERSITY OF EDINBURGH

PAGE 1 OF 2

FAX

HPC Gears Ltd
Manufacturer and stockist of
Gear transmission products.
Unit 14, Foxwood Industrial Park
Foxwood Road, Chesterfield,
Derbyshire, S41 9RN ENGLAND
TEL: +44(0)1246 268080
FAX; +44(0) 1246 260003
E-mail; sales@hpcgears.com

FAX NO. 01316 517049

ATTENTION OF: JUNWEI FANG.

FROM: PAUL BERRY, TECHNICAL DEPARTMENT

DATE: 15/7/08.

REF 4 MOD 21T DRIVER GEAR 25mm FACE WIDTH
4 MOD 35T DRIVEN GEAR 25mm FACE WIDTH
ABOVE MADE IN EN36 CASE HARDENED
INPUT TORQUE 76.4NM
INPUT SPEED 2RPM
HOURS PAY DUTY = 2 HOURS

ABOVE GEARS IN EN36 CASE HARDENED WILL TRANSMIT THE ABOVE STATED TORQUE
PLEASE SEEL CALC SHEET

REGARDS PAUL.

Calculation Fax from the supplier – HPC Gears Ltd. [71]. Page 1 of 2

JUNIWEI RANG. TORQUE CHECK. PAGE 1 OF 2

GEAR SIZE	DP PITCH 4 mod.	NO OF TEETH. 21	PCD" 3.307		
MATING GEAR No OF TEETH	35	PCD" 5.511	FACE WIDTH" .984"	MATERIAL EN36 CH	
MATING GEAR MATERIAL	EN36 CH	RUNNING TIME HRS/DAY	2 HRS	MOTOR KW	
RPM IN 2	OUT 1.2	TORQUE. INPUT 76.4 NM	676.1 lbsins		
ALLOWABLE TANGENTIAL LOAD AT PITCH RADIUS			408.89 lbs		

CALCULATIONS :-

RATIO 1.666 – 1

FOR WEAR $\frac{Xc \; Z \; Sc \; F}{k}$ lbs

21 $\frac{1.55 \quad 1.77 \quad 11000 \quad .984}{4.387}$ 6769

35 $\frac{1.75 \quad 1.77 \quad 11000 \quad .984}{4.387}$ 7642

FOR STRENGTH $\frac{Yb \; Y \; Sb \; F}{DP}$ lbs

21 $\frac{.875 \quad .66 \quad 50000 \quad .984}{6.35}$ 4474

35 $\frac{.92 \quad .585 \quad 50000 \quad .984}{6.35}$ 4169

CONCLUSION :- ABOVE WILL TRANSMIT THE REQUIRED TORQUE

APPLICATION :-

Appendix G: Motor Control Programs for the Positioning Maneuvers in the RV4 system

Three programs developed to perform simple operations of the RV4 press. They are stored on the motor controller.

1) Seeking mechanical home position

(1)TA=100	*The acceleration time is set to 100 msec.*
(2)TD=100	*The deceleration time is set to 100 msec.*
(3) VS=200	*The starting speed is set to 500 Hz.*
(4) DIRINV=0	*The clockwise direction is refined as positive direction.*
(5) VR=1000	*The operating speed is set to 1,000 Hz.*
(6) MGHP	*Mechancial home seeking operation is executed in positive direction. If MGHN is used, negative direction is used – that is counter-clockwise here.*
(7) CALL HOMED	*Ensure homing operation is complete.*

Note: This program requests the motor to rotate in clockwise direction until it is triggered by external mechanical sensor.

2) Rotating in incremental positioning mode

(1)TA=100	*The acceleration time is set to 100 msec.*
(2)TD=100	*The deceleration time is set to 100 msec.*
(3) VS=200	*The starting speed is set to 500 Hz.*
(4) DIRINV=0	*The clockwise direction is refined as positive direction.*

(5) DIS=10000 *The number of steps is set to 10,000.*

(6) VR=1000 *The operating speed is set to 1,000 Hz.*

(7) MI *Incremental positioning operation is executed.*

Note: This program requests the motor to rotate clockwise from its current position 10 revolutions, equivalent to 13.5° in the anvil. Each pulse output in the motor is 0.36° in the motor shaft. The total reduction ratio between the motor shaft and the anvil shaft is 800:3.

3) Rotating in absolute positioning mode

(1)TA=100 *The acceleration time is set to 100 msec.*

(2)TD=100 *The deceleration time is set to 100 msec.*

(3) VS=200 *The starting speed is set to 500 Hz.*

(4) DIRINV=0 *The clockwise direction is refined as positive direction.*

(5) PC= 20,000 *The number of steps is set to 10,000*

(6) VR=1000 *The operating speed is set to 1,000 Hz.*

(7) MA *Incremental positioning operation is executed.*

Note: Once the home position (Position Counter =0) is established. This program can be used to request the motor to rotate clockwise UNTIL it arrives at the absolute position where Position Counter = 20,000.

List of Figures

List of Tables

Publications

A rotator for single-crystal neutron diffraction at high pressure, J. Fang, *et al.* Rev. Sci. Instrum. **81**, 113901 (2010).

Finite element analysis of the double-toroidal anvils for high pressure research, J. Fang, *et al.* Rev. Sci. Instrum. Vol. 83, 2012: 093902 (2012).